Total Synthesis of the Reported Structure of Stresgenin B, its Structural Elucidation Using DFT Calculations, and Visible-Light-Mediated Functionalizations of Electron-Deficient Olefins

by

Wei Chuen Chan

B.Sc (Honors), Nanyang Technological University, Singapore, 2012

Submitted to the Graduate Faculty of the

Dietrich School of Arts and Sciences in partial fulfillment

of the requirements for the degree of

Doctor of Philosophy

University of Pittsburgh

2020

UNIVERSITY OF PITTSBURGH

DIETRICH SCHOOL OF ARTS AND SCIENCES

This dissertation was presented

by

Wei Chuen Chan

It was defended on

March 9, 2020

and approved by

Paul E. Floreancig, Professor and Director of Graduate Studies, Department of Chemistry

Peter Wipf, Distinguished University Professor, Department of Chemistry

Jeffrey L. Brodsky, Professor and Chair of Biological Sciences, Department of Biological Sciences

Dissertation Advisor: Kazunori Koide, Professor, Department of Chemistry

Total Synthesis of the Reported Structure of Stresgenin B, its Structural Elucidation Using DFT Calculations, and Visible Light Mediated Functionalizations of Electron Deficient Olefins

Wei Chuen Chan, PhD

University of Pittsburgh, 2020

The first chapter outlines the synthesis of the reported structure of stresgenin B. Stresgenin B was reported to be small molecule inhibitor of heat shock proteins (HSPs). Toward this pursuit, two synthetic routes were investigated. In the first route leading to the undesired diastereomer, the key reaction was a Pummerer rearrangement. In the second route, a neighboring-group directed diastereoselective cyanation is critical for the construction of the fully substituted α-amidoketal. A late-stage cerium-mediated alkynylation or Peterson olefination is also crucial in installing the exocyclic olefin. Lastly, computational studies were employed to elucidate the correct structure of stresgenin B. Density Function Theory (DFT) calculations were used to predict the proton (^{1}H) and carbon (^{13}C) nuclear magnetic resonance (NMR) of plausible candidate structures.

In the second chapter, a visible light mediated C–H functionalization of ethers using electron-deficient olefins is reported. 1,3-Dioxolane and 1,3-benzodioxole are suitable reacting partners. A radical-chain mechanism is proposed and corroborated by various experimental proof. DFT calculations suggested that C–H abstraction is the rate-determining step. During the course of the mechanistic studies, α-bromomalonate and α-bromoester were found to be competent radical initiators.

Table of Contents

List of Tables

List of Figures

List of Schemes

List of Abbreviations

Å .... angstrom (10^{-10} meter)

Ac .... acetyl

aq .... aqueous

BHT................ butylated hydroxytoluene

BINAP............ (2,2'-bis(diphenylphosphino)-1,1'-binaphthyl

BINOL .... 1,1'-bi-2-naphthol

BPE .... 1,2-bis((2,5)-diphenylphospholano)ethane

Boc .... *t*-butyloxycarbonyl

Bn .... benzyl

Bz .... benzoyl

Bu   butyl

calcd .... calculated

CCDC .... Cambridge Crystallographic Data Centre

CDI .... carbonyldiimidazole

CSA .... 10-camphorsulfonic acid

Cy .... cyclohexyl

d...................... days

DABCO .... 1,4-diazabicyclo[2.2.2]octane

DBU .... 1,8-diazabicyclo[5.4.0]undec-7-ene

DCE................ 1,2-dichloroethane

DEPT.............. distortionless enhancement by polarization transfer (NMR method)

DFT………… density functional theory

DHP................ 3,4-dihydro-2*H*-pyran

DMA .... dimethylacetamide

DMAP 4-dimethylaminopyridine

DMF .... dimethylformamide

DMP .... Dess-Martin periodinane

DMSO .... dimethylsulfoxide

ee .... enantiomeric excess

equiv .... equivalents

EC_{50} .... effective concentration for 50% inhibition

Et .... ethyl

ESI-TOF.................. electrospray ionization

US FDA................ United States Food and Drug Administration

HFIP .... hexafluoroisopropanol

HMBC .... heteronuclear multiple bond correlation (NMR method)

HPLC .... high performance liquid chromatography

HRMS .... high resolution mass spectrometry

HSF ………… heat shock factor

HSP ………… heat shock protein

HSR ………… heat shock response

HSQC .... heteronuclear single quantum coherence spectroscopy (NMR method)

Hz .... hertz

IR.................... infrared

M .... molar (mole per liter, concentration unit)

m-CPBA .... *meta*-chloroperbenzoic acid

Me .... methyl

min .... minutes

mp .... melting point

Ms .... mesyl; methanesulfonyl

MS .... mass spectrometry

NBS .... *N*-bromosuccinimide

NMO .... *N*-methylmorpholine-*N*-oxide

NMR .... nuclear magnetic resonance

NOESY .... nuclear Overhauser effect spectroscopy (NMR method)

NR………….. no reaction

PCC .... pyridinium chlorochromate

PPTS .... pyridinium *p*-toluenesulfonate

Ph .... phenyl

PMB ………… *p*-methoxyphenyl (4-methoxybenzyl)

PMP ………… *p*-methoxyphenyl (4-methoxyphenyl)

R_f .... retardation factor

rt .... room temperature

RSM .... recovered starting material

SuFEx………. sulfur(VI) fluoride exchange

$t_{1/2}$ .... half life

t .... tertiary

THF .... tetrahydrofuran

THP ………… tetrahydropyran

TLC .... thin layer chromatography

Ts.................... toluenesulfonyl

UV .... ultraviolet

VSF…………. vinyl sulfonylfluoride (ethylene sulfonylfluoride)

Acknowledgements

First and foremost, I thank God for seeing me through the past seven years in the United States. Although there is no language barrier, cultural differences among other matters made doing research in a foreign land extra challenging. I also thank my PhD advisor Prof. Kazunori Koide for accepting me in his lab in 2014, and thereafter for trusting and giving me a large degree of freedom to pursue several of my own ideas in the laboratory. I should note that most of my ideas/hypotheses failed to work. I also want to thank Prof. Peter Wipf and Prof. Paul Floreancig for agreeing to be on my dissertation committee. Prof. Jeffrey Brodsky is also gratefully acknowledged for agreeing to be my external committee member. I thank all of them for being so accommodating with all the scheduling required for my comprehensive exam and PhD defense. I also thank Prof. Peng Liu for teaching and giving me useful advice on computational chemistry.

Seven years is a long duration and I had the privilege to interact with some of Koide group previous and current members. Tomoya, Basu, Robert Bressin, Dianne Pham, James Burrows, Paul Markaj, Adriana Gambino, Ivanna Pohorilets, Jacob Beard, Miho Naruse, Brittany Klootwyk, Filippo Gentile are some of those people. I also want to specifically thank Adriana, Alex, Ivanna, Jacob, Julia, Paul, Rob, and Shogo for proofreading sections of my dissertation drafts. I wish to mention that any remaining typographical errors are my own.

I also thank the very helpful and supportive facilities directors. Dr. Steve Geib is the one with whom I have most interactions (I was fortunate to have obtained a decent number of X-ray quality crystals over the last 6 years); Dr. Bhaskar Godugu who would always try to provide analysis of my last minute HRMS samples; Dr. Damodaran Achary who gave me advices on VT-NMR and other miscellaneous questions that I have had over the last few years.

Finally, I thank my parents, sister and brother-in-law, and my absolutely adorable niece and two nephews for their love. I am also very grateful for the friends and brethren from Singapore, Canada, and the United States. I thank all my brethren from Calvary Jurong B-P church and Providence R-P church. Specifically, I thank Chi Sin and Valerie Tang, Hee Yin Ooi, auntie May Eng and uncle Willie, Kenny Neo and his family, Lilee Yick, Keene Chen, uncle Phillip and auntie Atchima, Weng Ngai and Jocelyn Lam, Dr. Nicole Loy, Samantha Seah, Isaac, Rebecca, and Anna-Joy Ong, Bendick Ong, the Liang family, Lionel Leong, Nicholas Ballard and his family, Luke Dinkledine and his family, Sergei and his family, Calvin McCarter and his family, Mark Brown, Nate and Leigh Olivieri, Wally, Rob Keenan and his family, Barbara Friend, Hautzeng and his family, Steve and Julie Bradley, Mike Labutta, Jim MacFarland and his family, Adriana and her mother, Don and Becky Krieger, Matt and Michelle McKnight, and others I would not be able to mention here. I thank them for their constant support and occasional nudge to keep me going. I believe the PhD journey (especially in a foreign land) is to a large extent a test of perseverance and resilience; support from other people is absolutely essential.

Soli Deo Gloria

To my family

<center>**1.0 Total Synthesis of the Reported Structure of Stresgenin B**</center>

<center>**1.1 Introduction**</center>

1.1.1 Heat Shock Proteins and its Role in Cancer

Heat shock proteins (HSPs), first discovered in 1962, are intracellular proteins that exist in every organism (ca.5% of total intracellular proteins) and are produced at higher levels (15% or more) when exposed to stressful conditions such as heat shock. There exists a total of 10 families of HSPs, classified by their molecular weights (e.g., members from HSP90 have molecular weights of ca.90 kDa). Although initially defined as stress-responsive proteins, HSPs have since been characterized as "molecular chaperone", i.e., proteins that are capable of binding and thereby modifying the structures and interactions of the other proteins/peptides.[2]

HSPs are essential for normal cell survival, and these proteins are reported to be involved in several cellular pathways and processes. However, HSPs are also over-expressed in cancer and essential for tumor development. The major role of HSPs in cancer is their chaperone duties; in the context of cancer cells, they stabilize active functions of over-expressed and mutated oncogenes. Therefore, over-expression of HSPs in cancerous cells has been implicated in the development, proliferation, and survival of these cells.[2-11]

HSP70 contains two major functional domains, the C-terminal peptide binding domain and the N-terminal ATPase domain.[1,12] HSP70 can bind to unfolded client proteins, including oncoproteins, at the C-terminal. Upon N-terminal ATP binding and hydrolysis, the folded client is released from the C-terminal. The two domains are mutually allosteric controlled: ATPase activity

<center>1</center>

is triggered upon protein binding and ATP binding triggers client release. HSP90 contains an additional major functional domain called the middle domain. The middle domain is for binding to co-chaperones such as Aha1. Like many other chaperones, HSP70 and HSP90 require co-chaperones to amplify rates of client association and ATPase activity. The smaller HSP27 does not have a co-chaperone but relies on the activities of HSP70 and HSP90. Within the cell, HSP27's clients are passed on to HSP70-co-chaperone complexes, and then to HSP90 complexes, releasing a functional folded client protein. The larger HSP110 primarily functions to a large extent as a co-chaperon to HSP70.

There are three known heat shock factors (HSF1, 2, and 4), and HSF1 has been identified to be the most important concerning cellular responses to stress in humans.[9-11] Under non-stress conditions, HSF1 exists as an inactive monomer localized in the cytoplasm of a cell. In the context of cancerous cells, the conditions within the tumor micro-environment are ideal for promoting a stress response. HSF1 responds by undergoing trimerization and phosphorylation. Translocalization to the nucleus and subsequent binding to DNA at the heat shock elements (HSEs) activate the transcription of HSPs. Therefore, HSF1 is responsible for the biosynthesis (or biogenesis) of HSPs in cells.[1] For example, Dai et al. recently reported that HSF1 is associated with poor survival in patients with gastric cancer. The authors also found a correlation between elevated HSF1 expression and larger tumor size. Additionally, Kaplan-Meier and Cox proportional hazard analyses indicated that elevated HSF1 expression showed worse overall survival and recurrence-free survival.

There are two main types of HSPs synthesized in response to stress. The first type includes HSP27, HSP70, and HSP90, which interact directly with the surfaces of unfolded proteins.[1] The

second type of HSPs (e.g., HSP60) assemble into complexes that resemble folding chambers. These act as a privileged environment that is favorable for restoring active protein conformations.[1]

Shown below are examples of the HSP90 inhibitors that were in clinical trials (Figure 1). Among these examples, XL888 and PU-H71 are currently still in clinical trials (both phase 1b, http://clinicaltrials.gov).
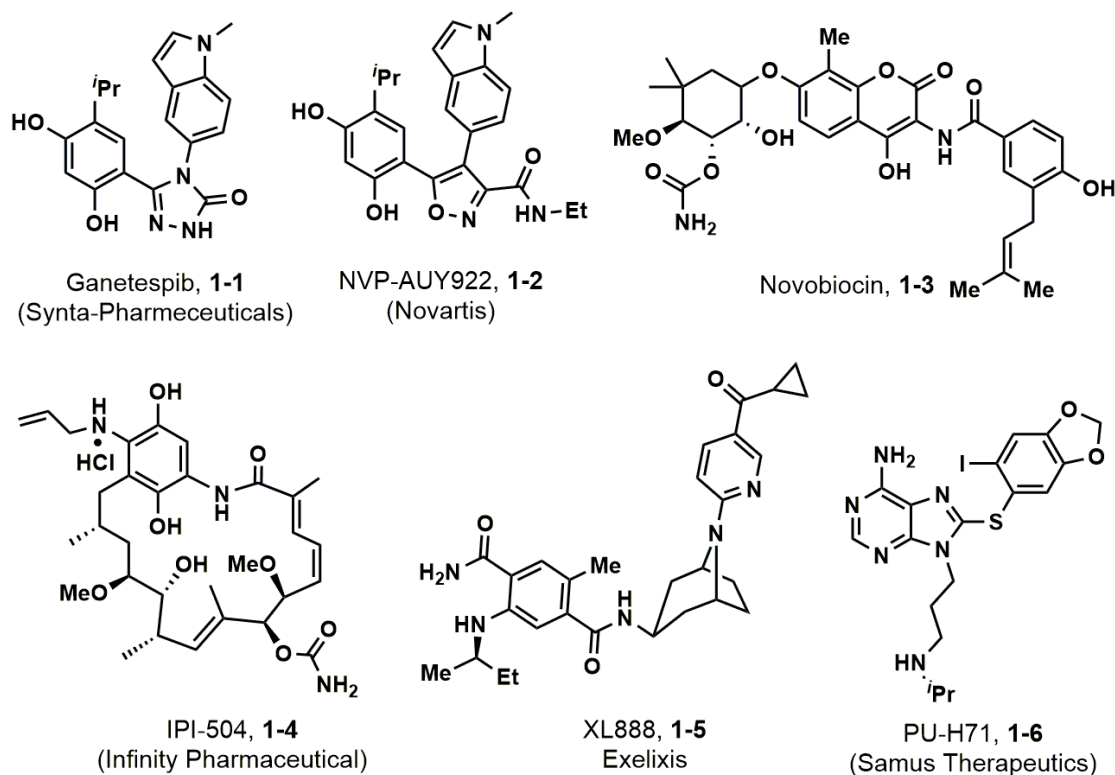
Figure 1. Examples of HSP90 inhibitors

Small molecules such as 17-AAG (not shown), or its less toxic derivative IPI-504, ganetespib, and AUY922 are examples of HSP90 N-terminal ligands. These inhibitors function by binding to the ATP binding site, which is necessary for client association and dissociation. This mode of inhibition triggers a heat shock response (HSR) and the biosynthesis of inducible HSP27,

HSP40, and HSP70. This likely hampers the progress of HSP90 inhibitors in clinical applications.[13] C-terminal inhibitors (e.g., Novobiocin) and modulators have also been reported. Importantly, it was reported that C-terminal ligands did not trigger the HSR characteristic of N-terminal inhibitors. McAlpine et al. reported a series of C-terminal modulators that bind between the N-terminal and middle domain of HSP90, preventing the binding of cochaperones that interact at the C-terminal.[13]

1.1.2 Isolation and Initial Biological Studies of Stresgenin B

In 1999, Akagawa et al. reported the isolation and characterization of stresgenin B.[14] The authors used three sequential screening assays to eventually identify stresgenin B. Stresgenin B was also found to be selective in inhibition of the HS-Luc expression and was 4.9 times more potent than quercetin (IC_{50} 7.0 μM versus 34 μM). Additionally, exposure of cells to stresgenin B only during heat stress (42 ℃, 90 min) inhibited the thermotolerance acquisition of Chinese Hamster Ovary (CHO) cells, which is expected of its inhibition of heat-induced HSP70 synthesis. Lastly, stresgenin B showed modest cytotoxicity toward various neoplastic cell lines (Table 1). Although the mechanism for the inhibition of heat-induced HSP70 synthesis is unknown, the authors believed that stresgenin B would be advantageous over quercetin B as an inhibitor due to its greater potency and improved water solubility (solubility data were not reported).

Table 1. Cytotoxocity of stresgenin B

Cell lines	IC$_{50}$ (µM)
K562	2.6
PC6	6.3
HT1080	13.7
HT29	5.9
MCF7	19.5
MKN28	5.6

The authors used HRMS, 1D and 2D NMR, and UV-Vis spectroscopic methods to determine the proposed structure of stresgenin B (Table 2).[14,15] TLC analysis of stresgenin B was negative toward ninhydrin (amines) and 2,4-dinitrophenylhydrazine (unhindered carbonyls). The molecular formula was determined using HRMS (FAB). The authors observed a λ_{max} of 275 nm in the UV spectrum, suggesting the presence of an unsaturated ester moiety. Unfortunately, the Woodward-Fisher rule was not discussed to further facilitate the structural determination base on the UV spectrum.

Table 2. Physsical and chemical properties of stresgenin B

Appearance	white powder
Solubility	MeOH, $CHCl_3$ and acetone
Melting Point (°C)	183–184
$[\alpha]_D^{25}$ (c 0.157, MeOH)	–12.6
Molecular Formula	$C_{11}H_{13}NO_5$
HRMS (FAB) m/z	Calcd: 240.0872; Found: 240.0875
UV $\lambda_{max}^{MeOH}(\varepsilon)$	275 (25, 800)
IR $\nu_{max}^{KBr}(cm^{-1})$	3429, 1716, 1593, 1439, 1197, 1064, 551

Analysis of the NMR spectroscopic data suggested the presence of one methyl group, one methoxy group, two oxymethine carbons, four olefin carbons, two carbonyl carbons, and a quaternary carbon in the molecule. Based on 1D and 2D NMR spectroscopic data, the authors determined the connectivity to be shown in Table 3.

Table 3. HMBC correlation

Protons	Correlation	Proposed structure
-CO$_2$CH$_3$	C1	
H2	C1, C4, C7	
H4	C6	
H5	C3, C7	
H6	C7	
H3'	C2', C1'	
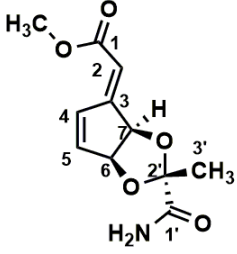
Lastly, the authors used NOESY correlation to determine the relative stereochemistry in the molecule. According to the authors, the geometry of the exocyclic olefin is *E* due to the correlation between the ester OCH$_3$ and the α-olefinic C–H. Correlation between CH$_3$ (of dioxolane) and exocyclic olefin C–H suggested that the CH$_3$ should be on the concave face of the bicycle.
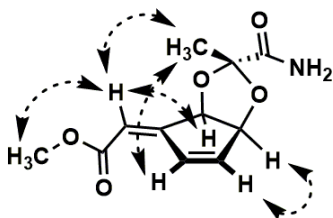
Figure 2. NOESY correlations

1.1.3 Examples of Asymmetric Acetal and Ketal Formation

There have been several reports of asymmetric acetal formation. Some examples include the use of Pd-catalyzed intermolecular hydroalkoxylation of alkoxyallenes,[16-17] Pd-catalyzed coupling of allylic alcohols with vinyl ethers,[18] substrate-controlled hetero-Diels-Alder reaction,[19] and stereoselective acetalization of chromium tricarbonyl-bound benzaldehydes.[20] Chiral phosphoric acid catalyzed reactions have received a tremendous amount of attention, some of which include the asymmetric formation of acetals.[21-27]

List et al. reported the first catalytic asymmetric acetalization of 1,2- and 1,3-diols **1-7** with aldehydes **1-8**, forming a series of enantioenriched acetals **1-10** (Scheme 1, top).[27-28] The work relied on the use of chiral imidodiphosphoric acids, which are stronger Brønsted acids than phosphoric acids. These acids have extremely sterically demanding chiral environment allowing high enantioselectivity to be obtained.[29] However, there still exists the limitation of substrate scope generality – specificity in terms of both diols and aldehydes was a requirement for good asymmetric induction in several cases. The intermolecular variant of diols and ketones has also not been achieved yet. Chiral confined imidodiphosphoric acid **1-12** was then used to catalyze the formation of spiroketals of varying ring sizes (Scheme 1, bottom).[29]
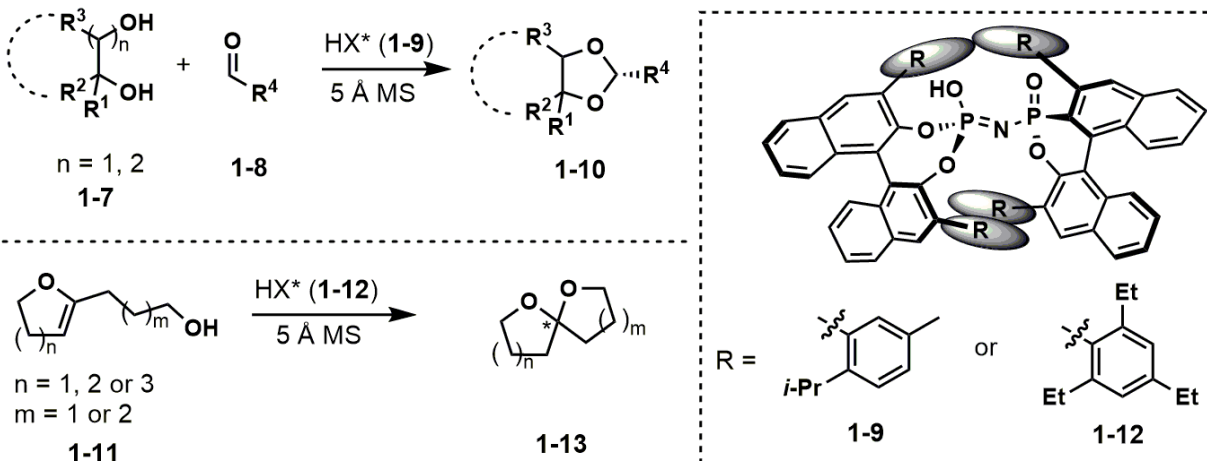
Scheme 1. Catalytic asymmetric synthesis of acetals and ketals using chiral confined Brønsted acid

1.1.4 Examples of Natural Products Containing 1,3-Dioxolane

A literature survey revealed that several natural products contain 1,3-dioxolane motifs. Specifically, these results mostly contain the 2,2-disubstituted-1,3-dioxolane (Figure 3). The substitutions at the C-2 position are mostly alkyl substituents part of a cyclic scaffold. Palytoxin,[30] pinnatoxins[31], the pteriatoxins,[32] dioxasampsone A,[33] frontalins,[34] amberketal,[35] austalides,[36] chuktabularins,[37] isogosterones,[38] loukacinols,[39] Riesling acetal,[40] and brevicomins[41] are some examples of the many natural products that contain 2,2-substituted-1,3-dioxolane fused as a dioxabicyclo[3.2.1]octane or dioxabicyclo[2.2.1]heptane framework. In these examples, the stereodetermining step was not the ketalization; the stereochemistry was instead governed by having stereochemically well-defined tethers.
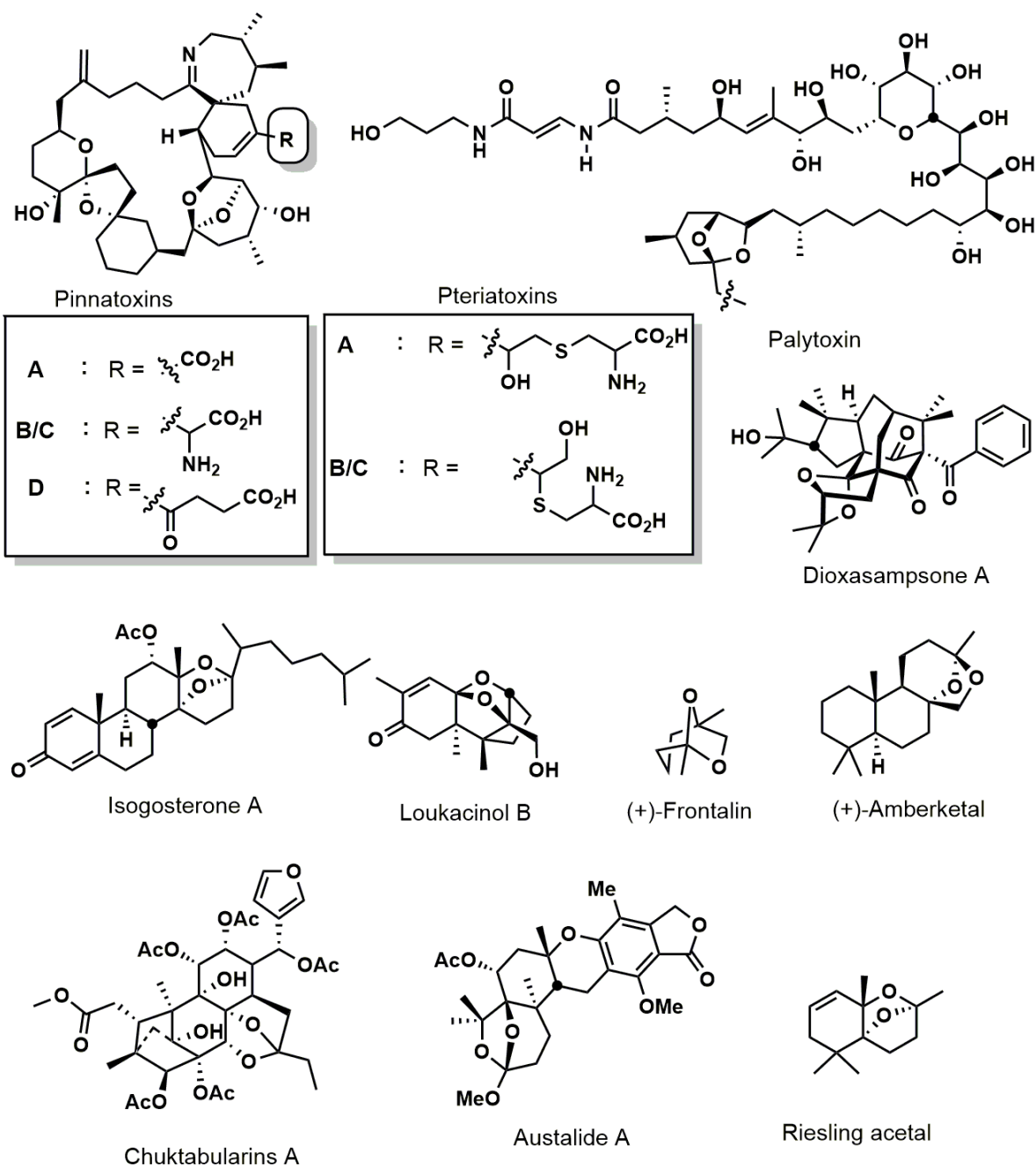
Figure 3. Examples of natural products containing 2,2-disubstituted-1,3-dioxolanes

1.1.5 The Structurally Similar Dioxolamycin

Results from literature search yielded only a single example of natural product containing a 1,3-dioxolane substituted at C-2 with an alkyl and an electron-withdrawing carbamoyl (amide) functionality (Figure 5).[42] This molecule shows significant structural resemblance to stresgenin B.
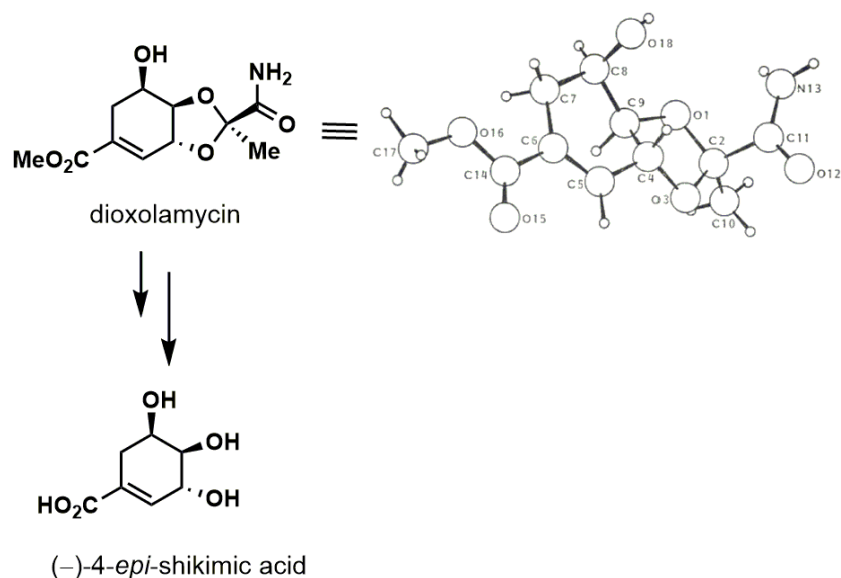
Figure 4. Structure of dioxolamycin and its hydrolysis

The structural assignment was confirmed by X-ray analysis. To determine the absolute configuration of dioxolamycin, the natural product was hydrolyzed under acidic conditions, yielding a product with an optical rotation of $[\alpha]_D^{23} = -72$ (solvent and concentration was not reported), compared to the literature value of $[\alpha]_D^{23} = -93$ (c 0.9, H_2O) for (−)-4-epi-shikimic acid.[43] The authors concluded the absolute configuration of dioxolamycin as shown (Figure 5). Reaction conditions for the hydrolysis of dioxolamycin to (−)-4-epi-shikimic acid was not reported.

1.1.6 Examples of Cyclopent-2-en-1-ylidene Syntheses

The motif consisting of an exocyclic α,β-unsaturated ester of a cyclopentene ring, i.e., cyclopent-2-en-1-ylidene, has received some attention for its construction. Burke *et al.* utilized an interesting desymmetrization of meso-diols to give brevicomin (Scheme 2).[41c] Diol **1-14** was converted to a mixture of three ketals. Diene **1-15** was then desymmetrized via ring-closing metathesis to give **1-19**. Subsequent hydrogenation gave brevicomin in 87% yield.
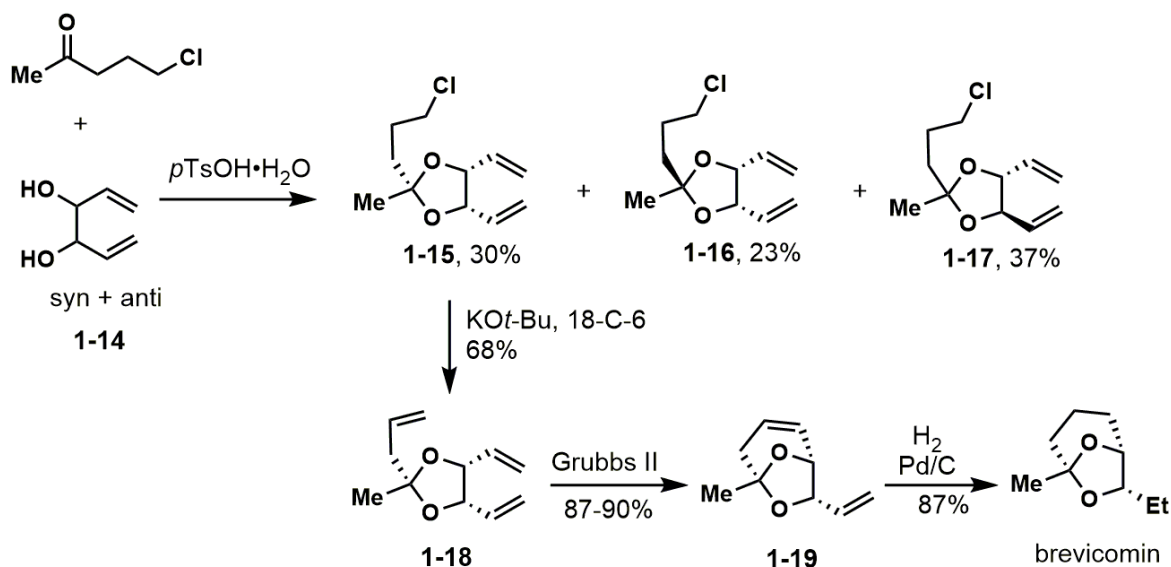
Scheme 2. Desymmetrization of meso-diol using ring-closing metathesis

Oh et al. reported the use of the versatile allenynecarboxylate **1-20** under Pd-catalysis in a divergent manner, yielding different cyclic olefins.[44] The substrate scope included a single example of ethyl cyclopent-2-en-1-ylidene **1-21** motif in 64% yield (Scheme 3).
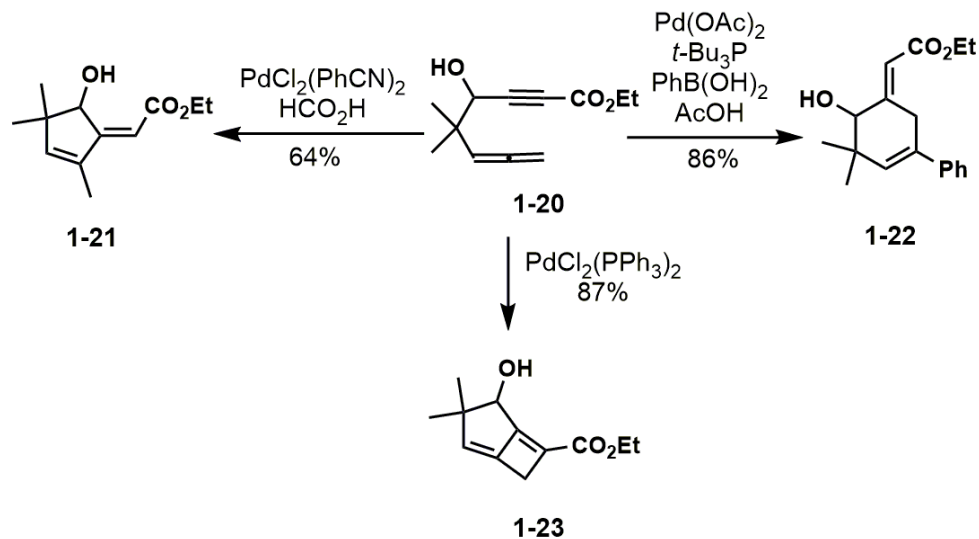
Scheme 3. Pd-catalyzed chemodivergent cyclizations of allenyne carboxylate

Egorov et al. reported a direct Wittig olefination on the relatively strained trichlorinated cyclopentenone **1-24** to afford exocyclic α,β-unsaturated ester **1-25** in 98% yield (Scheme 5).[45] Novák et al. reported the syntheses of cyclopent-2-en-1-ylidene esters using either Peterson or HWE olefination of cyclopentenones **1-26**, giving low to moderate yields **1-29E** (33-42%) and **1-29Z** (17-26%).[46]
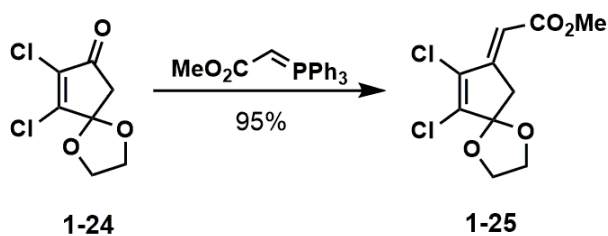
Scheme 4. Wittig olefination of chlorinated cyclopentenone
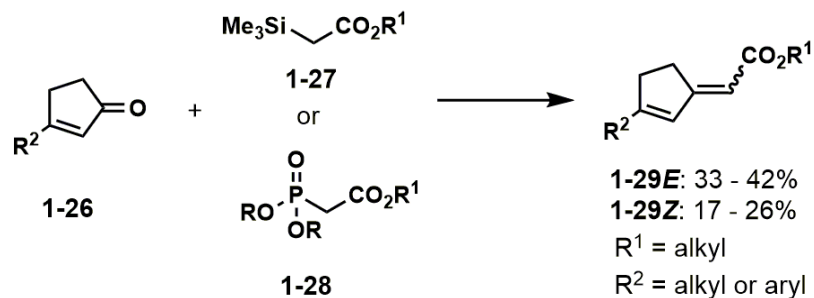
Scheme 5. Direct Peterson or HWE olefination of substituted cyclopentenones

West et al. reported the vinylogous Nazarov cyclizations of dienones **1-31** to afford cyclopent-2-en-1-ylidene esters and amides **1-32** (Scheme 6). The authors noted that the syntheses of substrates **1-31** were challenging because starting materials **1-30** were unreactive toward standard olefination protocols. Eventually the authors used an alkynylation/vanadium-catalyzed Meyer–Schuster rearrangement[47a] sequence, which furnished **1-31**.[47b,c]
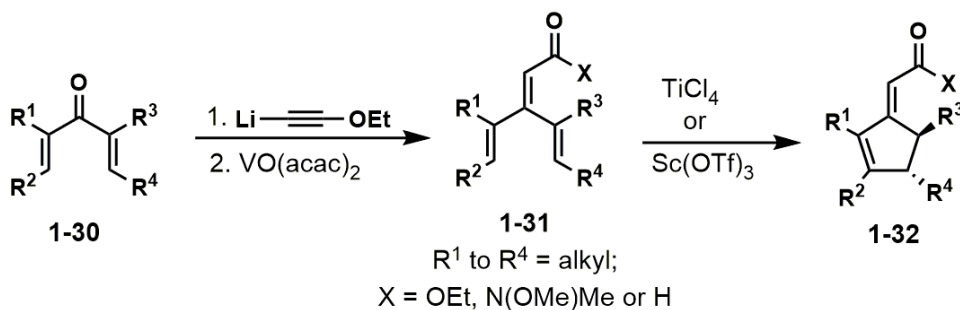
Scheme 6. Vinylogous Nazarov cyclization

Lautens and Bryan developed an intermolecular Suzuki–intramolecular Heck cascade to generate inden-1-ylidene esters **1-34** from dibromide **1-33**.[48] The authors designed their substrates to exploit the *syn*-stereospecificity of both olefin insertion and β-hydride elimination to control the stereochemistry of the olefin in the products **1-34** (Scheme 7).
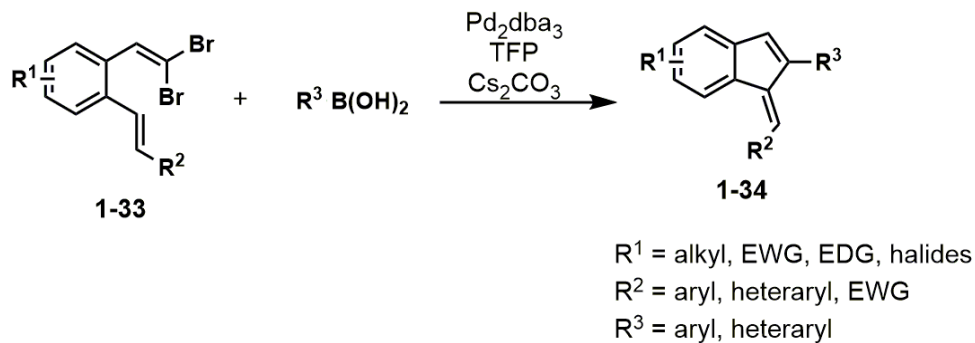
Scheme 7. Pd-catalyzed Suzuki-Heck cascade reaction to generate indenes

1.1.7 Synthetic Efforts Toward Zaragozic Acids and Synthesis of of (±)-7-Episordidin

Although there are no natural products that contain a dioxolane substituted with an electron-withdrawing group at C-2, a related 1,3-dioxane moiety had appeared in synthetic intermediates during total syntheses. In their synthetic efforts toward zaragozic acids, Wardrop et al. encountered C-2 EWG-substituted dioxanes (where EWG = ester or amide) as synthetic intermediates.[49] According to the authors, direct acetalization of 1,3-propanediol **1-35** with α-ketoester **1-37** afforded 1,3-dioxane **1-39** in a moderate yield of 61%. A slight increase of the complexity of the substrates shuts down the reaction between **1-36** and **1-38** completely (Scheme 7, top). The authors used a slightly round-about route that accessed 1,3-dioxane **1-44** in three steps with a 73% overall yield. To achieve this, **1-41** was first converted to the semi-stable orthoester **1-42** followed by Sn-catalyzed cyanation to cyanoketal **1-43**. Treatment with alkaline H_2O_2 afforded the desired amide functionality in **1-44**. The amide was subjected to methanolysis conditions, then hydrolyzed and acidified to the carboxylic acid **1-45** in 73% yield (two steps). Acid **1-45** was activated as the acid chloride and converted to the diazo compound **1-46**. Rh-carbenoid C–H insertion afforded the desired oxabicycle **1-47**.
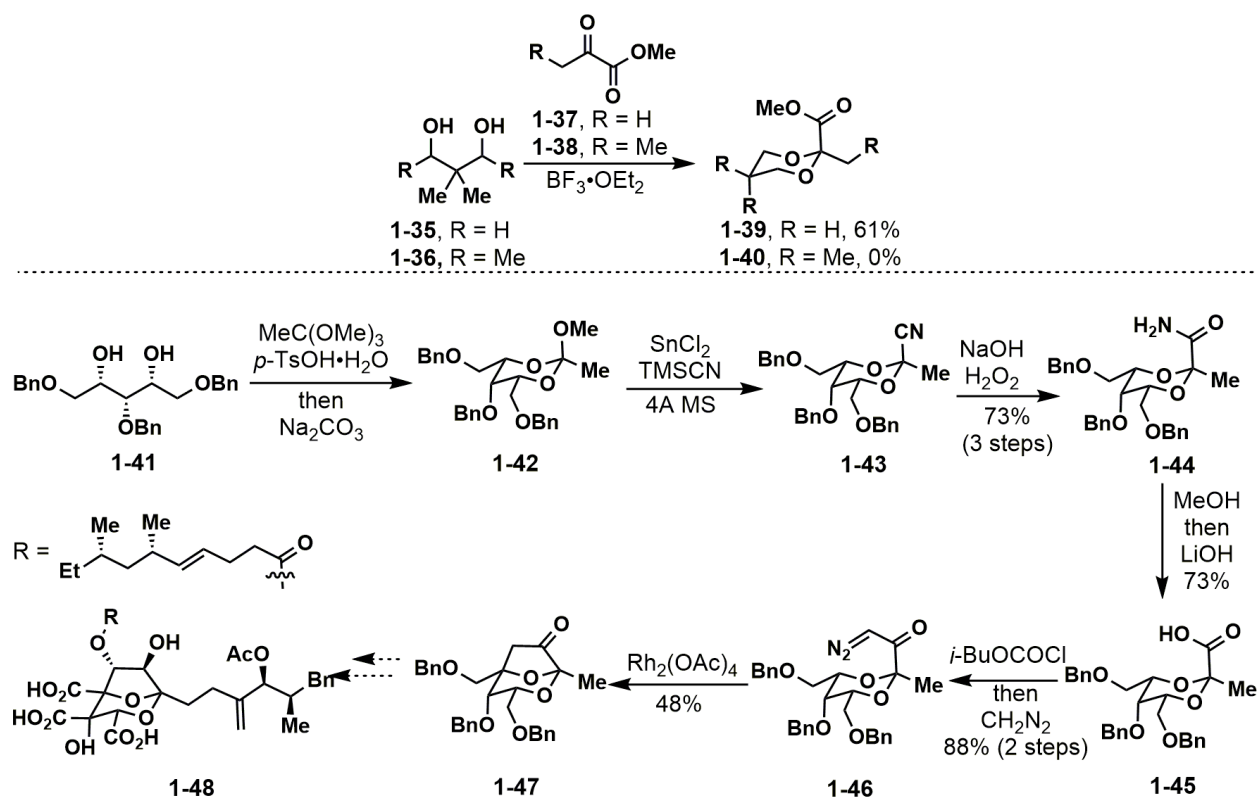
Scheme 8. Synthesis of (±)-7-episordidin

Using a similar strategy, Wardrop et al. accessed the cyanoketal intermediate from the corresponding pentane-2,4-diol (99%, 2 steps).[50] Alkaline H_2O_2 hydrolysis afforded amide **1-52** in 91% yield; conversion to the acid **1-53** via methanolysis and hydrolysis was achieved in 97% and 98% yields, respectively. Diazo compound **1-54** was formed in 96% yield over two steps. Rh(II)-catalyzed C–H insertion provided bicyclic ketone **1-55** in 58% yield. Four additional steps converted ketone **1-55** to (±)-7-episordidin. The synthetic efforts toward and synthesis of zaragozic acids exemplified the challenges in direct construction of C-2 EWG-substituted dioxanes.[49-51]
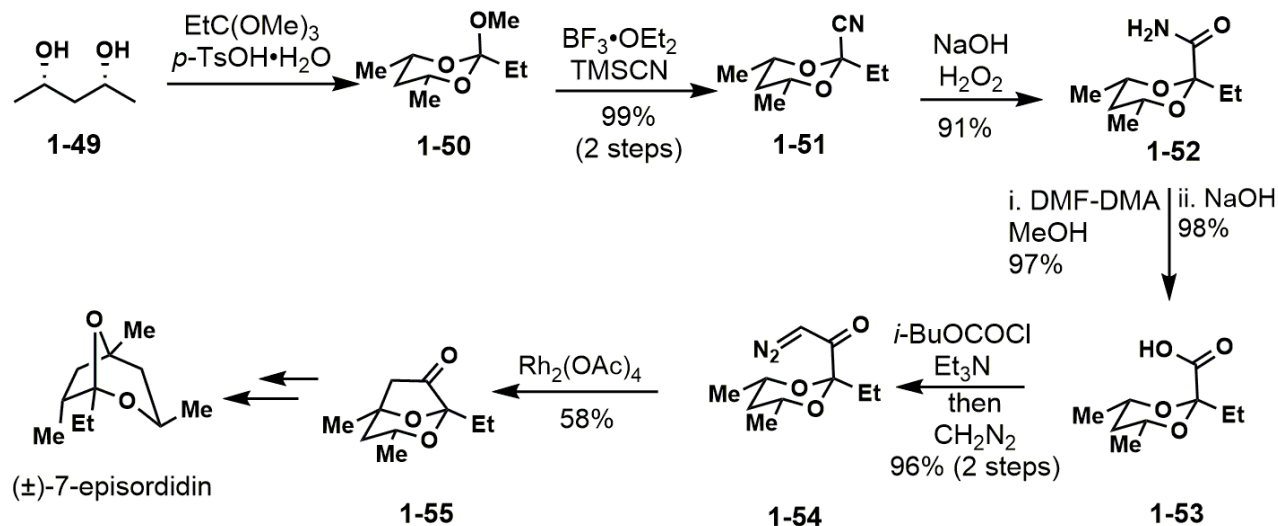
Scheme 9. Total synthesis of (±)-7-episordidin

1.1.8 Previous Work in the Koide Group

We envision that the inhibition of expression of HSPs by a small molecule such as stresgenin B would have great potential in bypassing the problem of the inducible synthesis of HSP70.[12] As mentioned, it was reported that stresgenin B exhibited 4.9 times greater potency than quercetin.[14] Although the micromolar potency of stresgenin B is not impressive, we envision that this molecule would serve as a platform for the design of more potent analogs. It is also of great interest to investigate the mode of action of stresgenin B and whether it is similar to that of quercetin. The selectivity of this molecule toward cancer cells over normal cells has not been reported.

The initial effort toward stresgenin B started from alkynal **1-56** (Scheme 10). Grignard vinylation gave propargylic alcohol **1-57** in 78% yield. Protection with dihydropyran gave ether **1-58** in quantitative yield. Methanolysis of the TMS group yielded the terminal alkyne **1-59** in 77% yield. A methoxycarbonyl group was installed using methyl chloroformate to give **1-60** in quantitative yield. Removal of the THP protecting group gave **1-61** in 73% yield. Another

Grignard vinylation gave triene **1-62** in 85% yield. Ring-closing metathesis with Grubbs II catalyst afforded cyclopentene **1-63** in 41% yield.
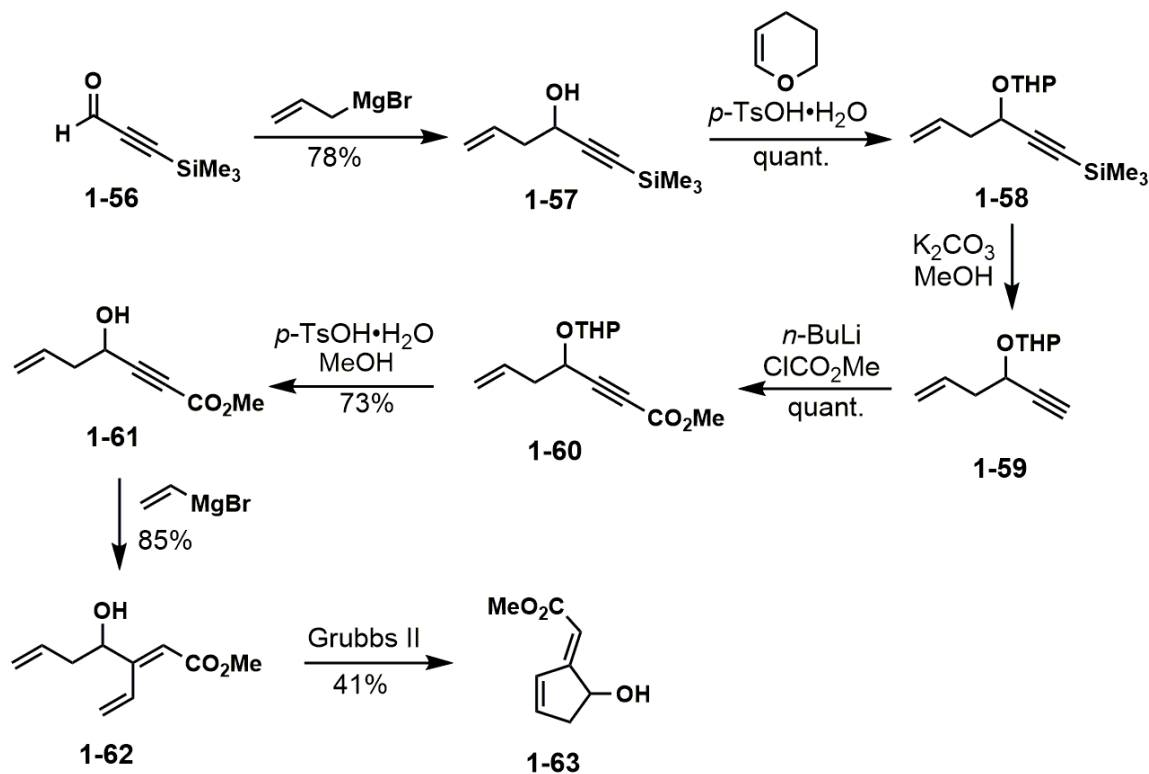
Scheme 10. Initial efforts toward reported structure of stresgenin B

The synthesis was stalled at this juncture; the envisioned allylic C–H oxidation was unsuccessful (Scheme 11). When cyclopentenol **1-63** was subjected to classical Riley oxidation conditions (SeO$_2$/TBHP), no reaction was observed. Treating **1-63** with the Pd-catalyzed allylic C–H oxidation developed by White et al.[52-54] also did not produce any desired diol **1-64** (Scheme 11, top). A possible solution was envisioned, namely to perform the required allylic C–H oxidation followed by RCM. Thus, the C–H oxidation of triene **1-65** was tested and did give desired oxidized product **1-66**, albeit in low yield of 15% (Scheme 11, bottom).

18
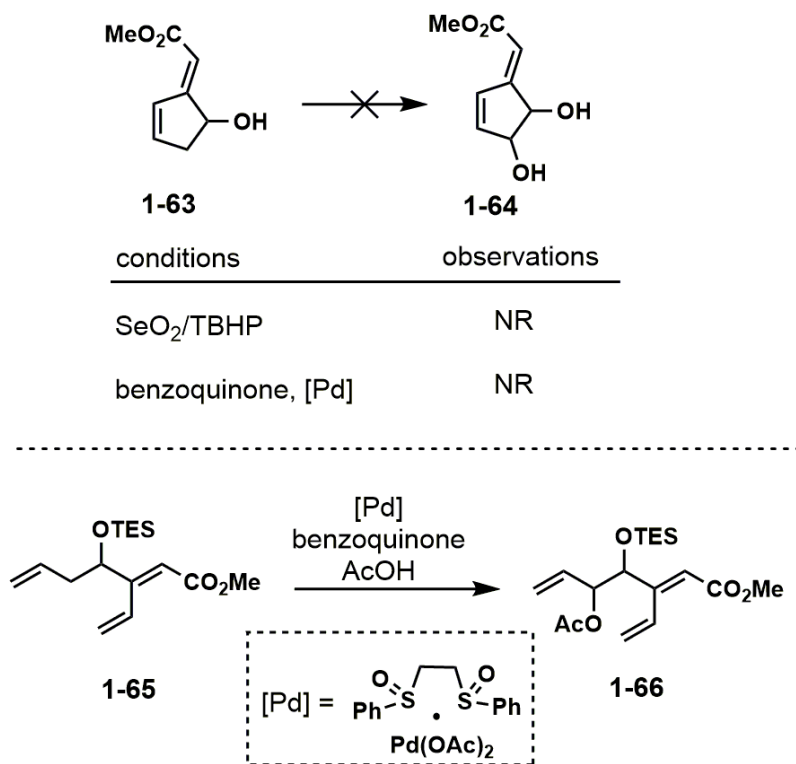
Scheme 11. Attempted allylic oxidations

To address the question of stresgenin B's absolute configuration, a chiral pool strategy[55] was adopted. D-Ribose was chosen as the chiral starting material (Scheme 12). Additionally, this strategy was promising because it would avoid the need to develop or optimize reaction conditions for late stage oxidations (see Scheme 11). Using a two-step literature sequence,[56] D-ribose was converted to diol **1-68**. Aldehyde **1-69** was formed by oxidative cleavage and a non-selective vinylation afforded allylic alcohol **1-70** in 42% combined yield. The 1:1 diastereomeric mixture of alcohols **1-70** was benzylated in 94% total yield, and deprotection of the acetal yielded diol **1-72** in 88% combined yield. Ketal formation with thiophenylacetone **1-73** gave **1-74** as a mixture of four diastereomers in 74% combined yield. Separation of the diastereomers was tedious, and as such **1-74** was used as a mixture for subsequent steps. A four-step sequence involving oxidation to **1-75**, Pummerer rearrangement[57] to **1-76**, Pinnick oxidation[58] to **1-77**, and amidation gave a

1:1:1:1 mixture of amide **1-78** (combined yield = 46% over four steps). A portion of the desired diastereomer was used in DDQ deprotection.

The deprotection to form **1-79** was challenging and several trials only led to a low yield of 27%. Furthermore, efforts to perform RCM on **1-79** required more than 0.50 equiv of the nitro-Grela catalyst[59] for low conversions, although it was later found that the actual cause for this was likely due to phenol contamination (see results and discussion of this chapter). Performing RCM on **1-78** did give the cyclized alkene **1-80** in 42% yield, still requiring 0.50 equiv of the nitro-Grela catalyst. The stereochemical configuration of the benzyloxy substituent was assigned by NOESY experiments.
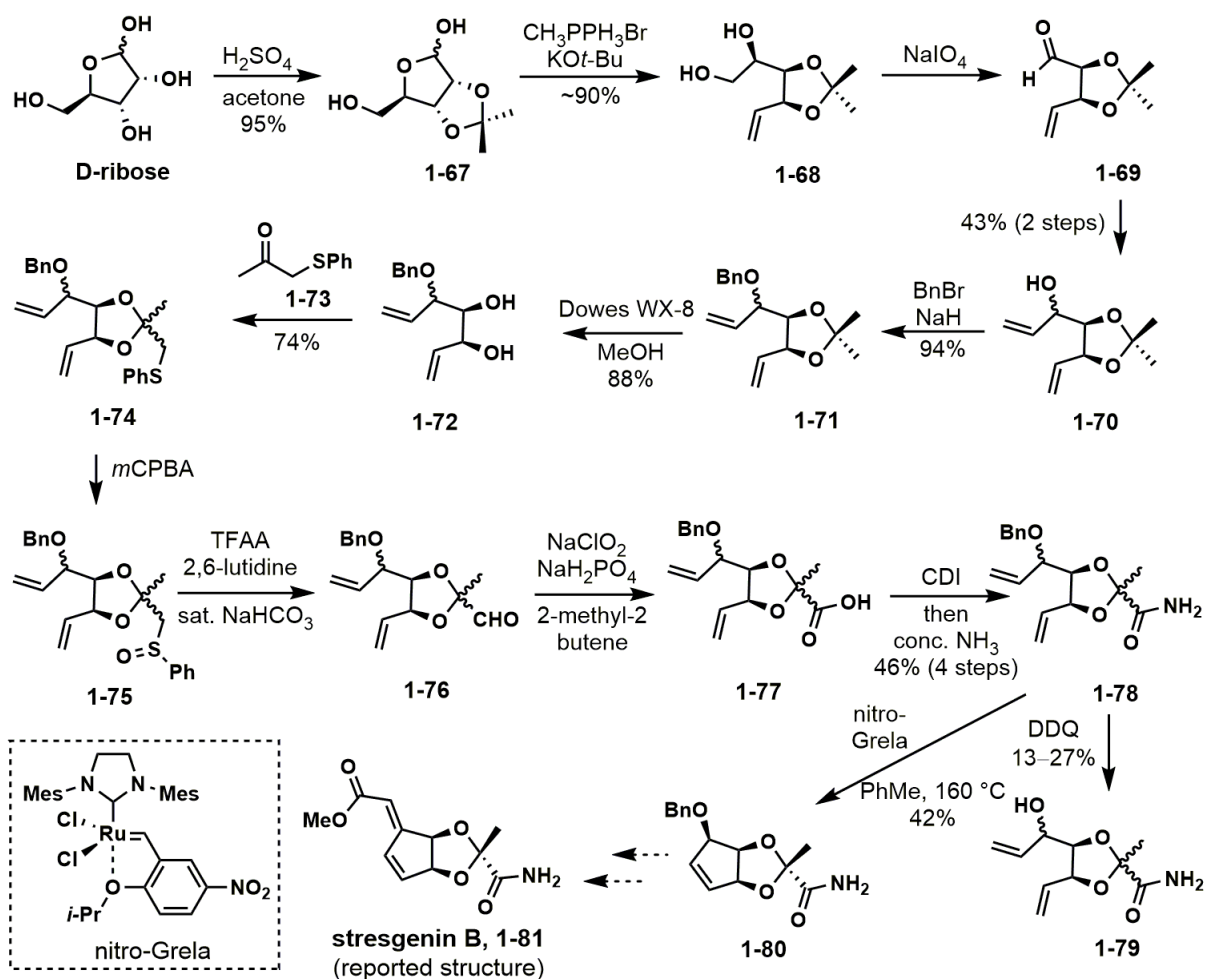
Scheme 12. Previous synthetic efforts toward stresgenin B

At this juncture, the project was stalled once again. The challenges in the debenzylation and the high ruthenium catalyst loadings to cyclize **1-79** made it nearly impossible to move forward. Nonetheless, sufficient amounts of a diastereomer of **1-79** could be obtained and converted to **1-84**. Earlier model studies had given some promising results in a HWE reaction of cyclopentenone **1-82** to give **1-84** (Scheme 13). A similar HWE reaction of cyclopentenone **1-85** gave no reaction; the Wittig reaction with ylide **1-86** afforded a complex reaction mixture. However, milligram quantities of **1-87** could be isolated and submitted for X-ray analysis. The X-ray structure confirmed the stereochemical configuration of **1-87**. Deprotection of model substrate

21

1-84 temporarily afforded **1-88,** which was too unstable, presumably toward oligomerizations. This marked the end of the synthetic pursuits undertaken by previous members of the Koide group.
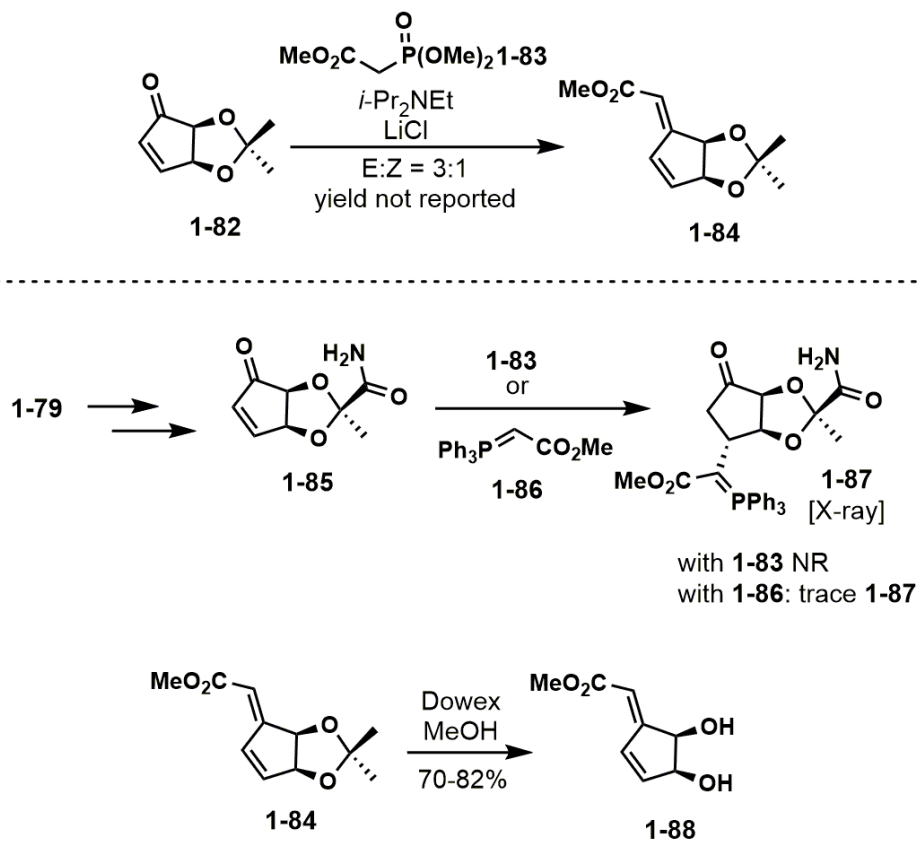
Scheme 13. Olefination attempts on model substrate and late-stage intermediate

1.2 Results and Discussion

A significant portion of this chapter was published as: Chan, W. C. & Koide, K. *Org. Lett.* **2018**, *20*, 7798-7802.

1.2.1 Retrosynthetic Analysis for this Project

Upon taking over the project for stresgenin B, there were a few issues we planned to address. The adoption of a chiral pool strategy was to address the absolute configuration question. The strategy, however, was not properly executed to realize its full potential. Specifically, the removal of stereochemical information by oxidative cleavage; as it turns out, this stereochemical information is critical for stereoselectively installing the ketal (*vide infra*). Next, we wondered whether there are literature precedents for a one-carbon homologation of a diol (e.g., **1-68**) to an allylic alcohol (e.g., **1-70**). Thirdly, a practical problem that arose was the formation of complex diastereomeric mixtures that would be tedious and time-consuming to purify (**1-74** and **1-78**). Fourthly, debenzylation conditions or a new protecting group needed to be identified. We also wanted to lower the ruthenium catalyst loadings for RCM. Finally, an alternative strategy was necessary to install the exocyclic olefin.

To further confirm that direct olefination strategy is not viable, preliminary tests in this project showed that Julia,[60-62] Reformatsky,[63,64] or Peterson olefinations[65] caused degradation of the starting material (Scheme 14, **1-89** → **1-81**). It was hypothesized that enone **1-89** was too sterically demanding for a direct olefination. A literature survey revealed that the 1,4-addition of phosphonate **1-83** onto acyclic enones (e.g., *trans*-chalcone)[67], cyclopentenone[68] and cyclohexanone[68] is known. Thus, we envisioned a two-step indirect approach. A sterically unhindered acetylide could constitute the requisite two-carbon, and subsequent Meyer-Schuster rearrangement of **1-90** might give the exocyclic olefin **1-81**.

The cyclopentene ring could be formed by an RCM-oxidation sequence from diene **1-91** (Scheme 14). The cyanoketal moiety of **1-91** can be installed by a neighboring-group-controlled cyanation of oxocarbenium ion **1-92**. A one-carbon homologation would be used to convert diol

1-68 to allylic alcohol **1-70** – to avoid oxidative cleavage and to retain the stereochemical information at C-3 in **1-92**. We hypothesized that the stereogenic center at C-3 might influence the ketal formation. D-Ribose was still deemed a suitable chiral pool substrate for the total synthesis pursuit.
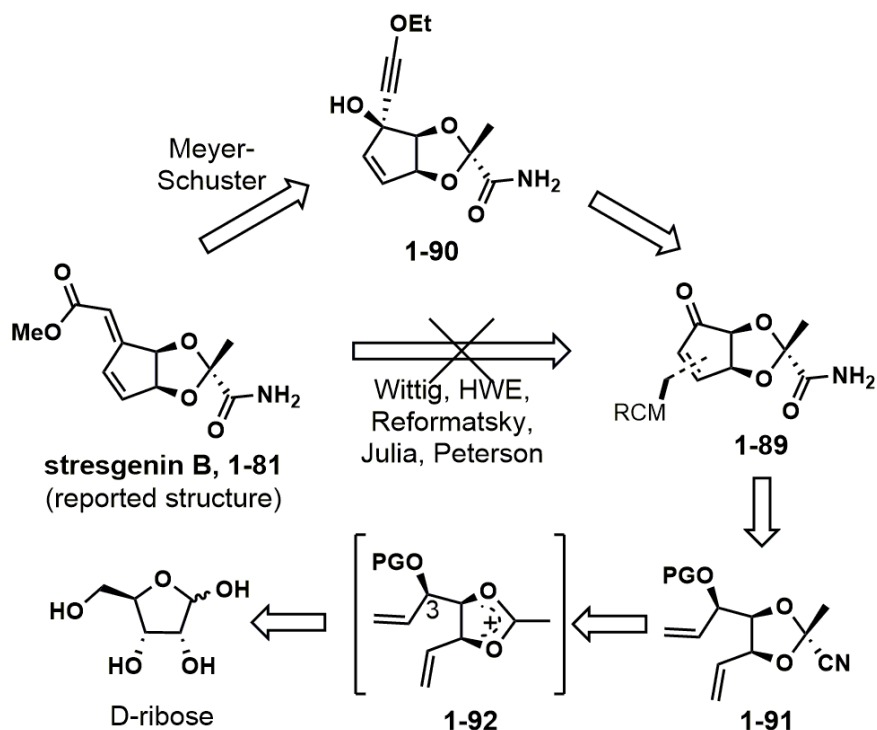
Scheme 14. Retrosynthetic analysis

1.2.2 First Generation Synthesis Featuring a Pummerer Rearrangement

The known epoxide **1-93** was prepared in three steps from D-ribose in 53% overall yield (Scheme 15).[56] The epoxide was then homologated,[69-70] the product of which was subjected to protecting group manipulations to give diols **1-94** and **1-95** in 60% and 62% yield over three steps, respectively. Similar to the observations by Wardrop et al.,[49-51] the direct construction of the α-

amidodioxolane functionality is also challenging for our system. The direct condensation with various α-ketoamide or α-ketoester was unsuccessful. Usually no reaction could be observed. After much exploration, we returned to α-(phenylthio)acetone **1-96** that had been previously employed in the Koide group. Additionally, analogs **1-97** and **1-98** were also synthesized. The combination of diol **1-94** and ketone **1-96** under acidic conditions gave a moderate diastereoselectivity of ca. 4.9:1; **1-97** and **1-98** were better ketones for greater diastereoselectivity. Although it was interesting to note that varying the substituents on the (arylthio)acetone **1-96** to **1-98** affected the diastereoselectivity, the reason for the selectivity was not clear at this stage.
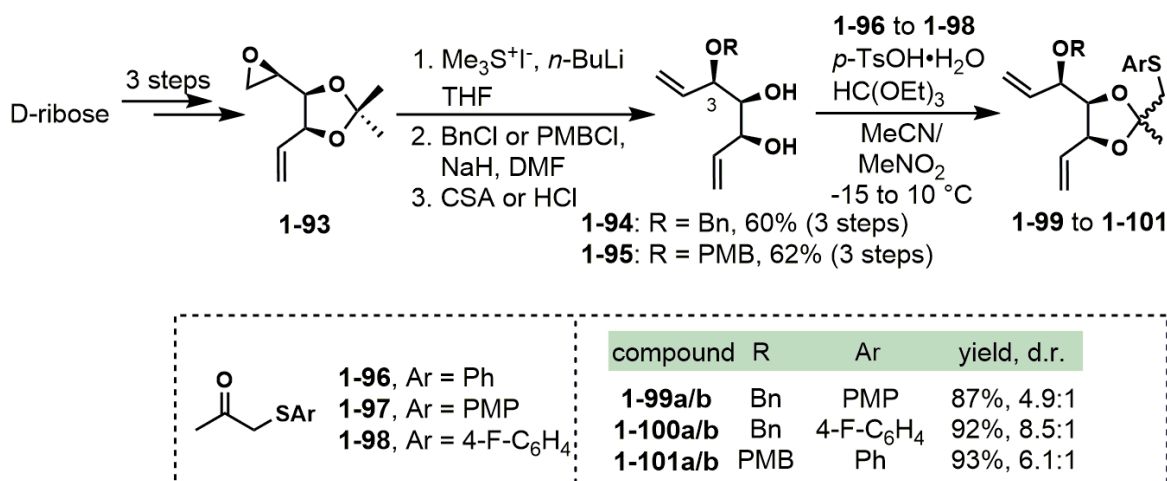
Scheme 15. First generation route leading to ketals with sulfide handles

compound	R	Ar	yield, d.r.
1-99a/b	Bn	PMP	87%, 4.9:1
1-100a/b	Bn	4-F-C$_6$H$_4$	92%, 8.5:1
1-101a/b	PMB	Ph	93%, 6.1:1

Because it was the first time that the ketal (**1-99** to **1-101**) was formed stereoselectively, there was little basis for predicting the major stereoisomer of this reaction. We chose to move forward with the synthetic scheme although we were uncertain regarding the stereochemical outcome of the ketal formation (Scheme 16). Thus, ketal **1-101** was selected because facile late-stage PMB deprotection was anticipated. The oxidation of sulfide **1-101** to sulfoxide **1-102**, its

Pummerer rearrangement[57] to aldehyde **1-103**, Pinnick oxidation[58] to acid **1-104**, and finally amidation afforded amides **1-105a** and **1-105b**. The minor product **1-105a** was crystalline, and X-ray analysis revealed it to be the desired isomer. This unfortunately indicated that ketal formation afforded the undesired diastereomer as the major product. This shows that the stereogenic center at C-3 indeed has an influence on the stereoselectivity of ketal formation, but it was not yet clear how this center governs stereoselectivity and how this influence could be reversed.
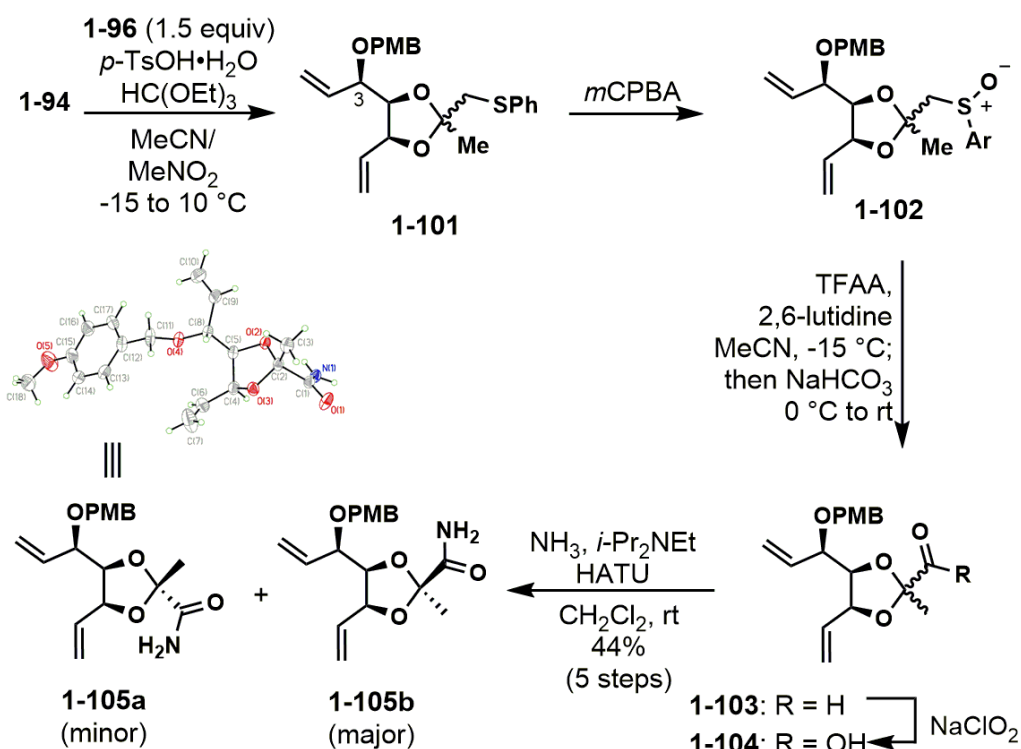
Scheme 16. First generation route leading to undesired diastereomer

The ketal formation step was revisited (Table 1). The dr improved with an electron-poor aromatic group on (phenylthiol)acetone (Table 4, entry 2 vs 4). The electronics of the protecting group (benzyl in **1-94** vs *p*-methoxybenzyl in **1-95**) appeared to have no effect on the dr.

26

Table 4. Effects of protecting groups on diastereoselectivity

R = Bn, **1-94**
R = PMB, **1-95**
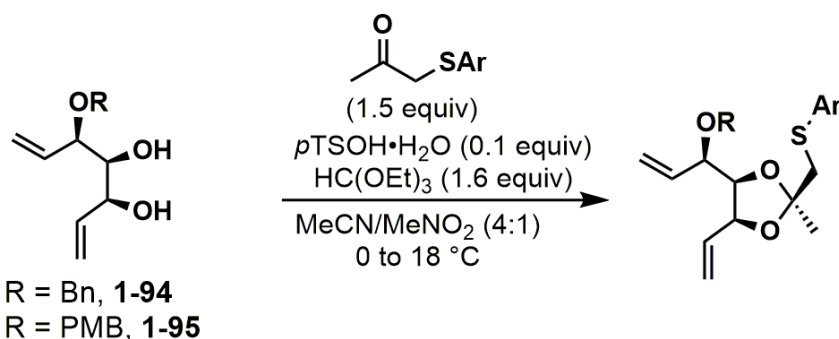
entry	R	Ar	yield[a] (d.r.)	entry	R	Ar	yield[a] (d.r.)
1	Bn	Ph	80%, 5.4:1	5	PMB	Ph	79%, 5.5:1
2	Bn	$4\text{-FC}_6\text{H}_4$	86%, 5.7:1	6	PMB	$4\text{-FC}_6\text{H}_4$	79%, 5.8:1
3	Bn	$3\text{-FC}_6\text{H}_4$	77%, 8.1:1	7	PMB	$3\text{-FC}_6\text{H}_4$	75%, 7.6:1
4	Bn	$3,4\text{-(MeO)}_2\text{C}_6\text{H}_3$	83%, 3.6:1	8	PMB	$3,4\text{-(OMe)}_2\text{C}_6\text{H}_3$	81%, 3.7:1

[a]Determined by ^{1}H NMR using mesitylene as external standard, combined yields of both diastereomers

Both electrostatic and $\pi{-}\pi$ interactions[71-75] might be involved in controlling the stereoselectivity. Oxocarbenium ion **1-107b** (Figure 6) might be more sterically sensitive due to $A^{1,3}$ strain,[76] preventing the benzyl group from approaching the oxocarbenium species, compromising the electrostatic stabilization. An electron-rich R group, such as PMB in **1-95**, should exert stronger electrostatic attraction but is presumably counterbalanced by weaker $\pi{-}\pi$ interactions. It was surmised that the T-shaped configuration[71-75] might be more conformationally compatible with **1-107**.
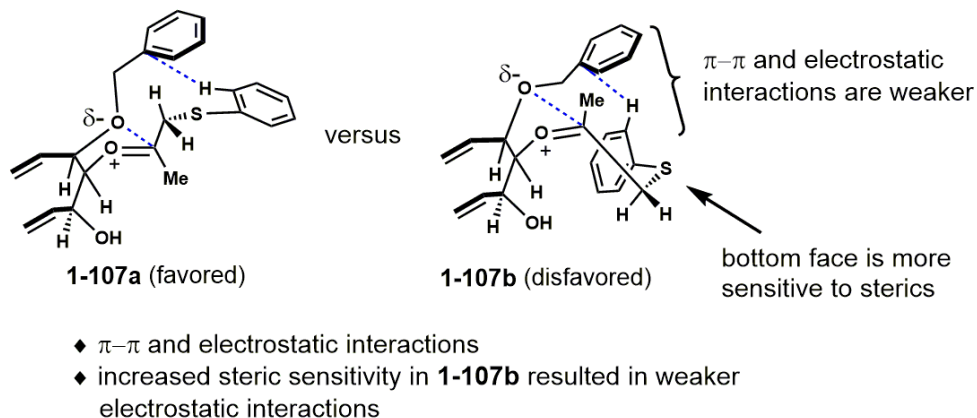
Figure 5. Rationalization of diastereoselective thioketal formation

Attempts to equilibrate **1-99** to a 1:1 mixture were unsuccessful (Scheme 17); deketalization was observed when a stronger Lewis acid (e.g., BF$_3$·OEt$_2$) was used. Attempts to rescreen conditions from diol **1-94** also did not yield favorable results.
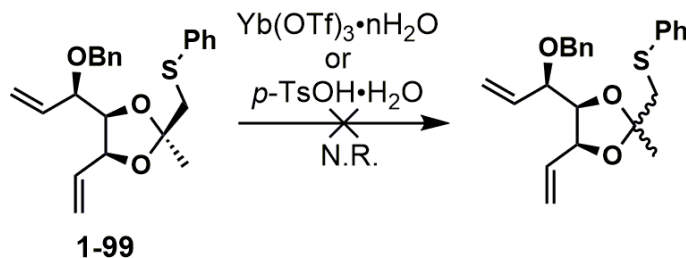
Scheme 17. Attempts to reverse diastereoselectivity

The last interesting observation in the first route was the unexpected lactonization of the primary amide **1-108** under storage conditions as shown in Scheme 18. Chromatographed allylic alcohol **1-108** (neat, 1-dram vial, no special precautions) was stored in a −20 °C freezer. It was discovered that upon two weeks of storage, part of the material was converted to bicyclic lactone **1-109**. The lactone was chromatographically purified and characterized by ^{1}H, ^{13}C, HMBC,

HMQC, and HRMS. Additionally, the identity of lactone **1-109** was confirmed by its facile conversion back to the primary amide **1-108** by aminolysis with concentrated aqueous NH$_3$. This was actually the first hint of the stereochemical outcome in Scheme 16 before an X-ray crystal was obtained.
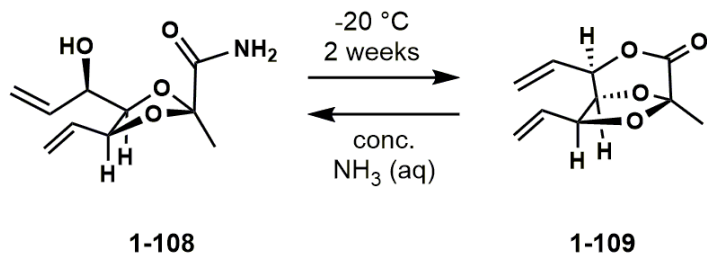
Scheme 18. Unexpected lactonization

1.2.3 Second Generation Synthesis Featuring a Diastereoselective Cyanation

Although the presence of stereochemical information at C-3 of **1-94** did indeed influence the stereoselectivity of ketal formation, it was not the desired outcome. A different strategy was pursued to enable the formation of the dioxolane with the desired diastereoselectivity (Table 5 and Scheme 19). It was strategized that a benzyloxy substituent at C-3 (Table 5) might undergo neighboring-group participation in a *cyclic* oxocarbenium ion. There are related precedents from the groups of Molander[77] and Woerpel[78-83] that suggested the feasibility of this strategy. First reported by Mukaiyama[84] was the use of Ph$_3$CBF$_4$ to generate similar cyclic oxocarbenium ions. Due to the presence of oxidation-labile protecting groups, the requisite oxocarbenium ion **1-92** was planned to be generated via an orthoester. Diol **1-94** was treated with MeC(OMe)$_3$ under acidic conditions, and the resulting orthoester **1-110** was directly treated with TMSCN and BF$_3$·OEt$_2$ to afford cyanoketal **1-112** via oxocarbenium ion **1-111** (Table 5 and Scheme 19). Other Lewis acids

generally proved to be inferior (entries 1−4 and 6−8). TiCl$_4$ afforded a higher dr (entry 5), but difficulties in work-up rendered in unsuitable for scale-ups.

Table 5. Optimization of cyanation conditions[a]
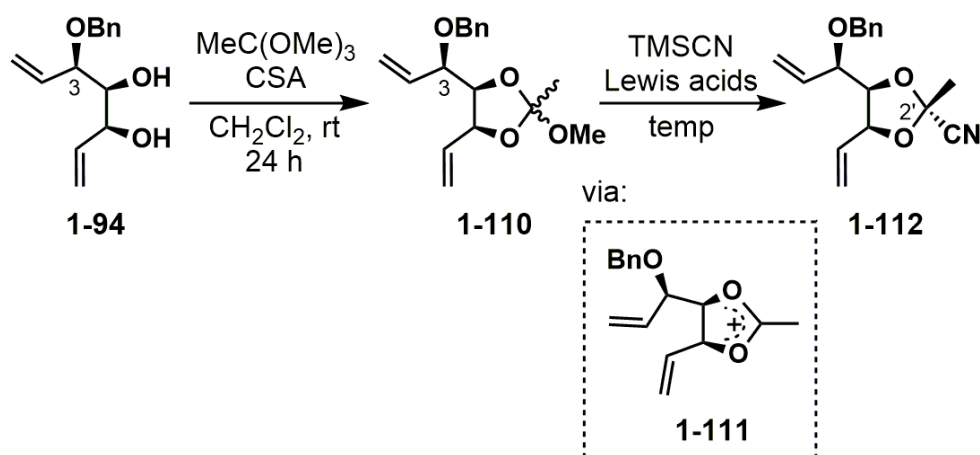
entry	Lewis acid (equiv)	temp (°C)	yield (d.r.)[b]
1	n-Bu$_2$BOTf (1.5)	25	decomposed
2	Sc(OTf)$_3$ (0.20)	25	16% (7.1:1)
3	TiCl$_4$ (1.5)	25	15% (6.9:1)
4	Yb(OTf)$_3 \cdot n$H$_2$O (0.20)	25	decomposed
5	TiCl$_4$ (1.5)	−78	76% (12:1)
6	AlCl$_3$ (1.5)	−78	trace (n.d.)[c]
7	Et$_2$AlCl (1.5)	−78	30% (14:1)
8	SnCl$_4$ (1.5)	−78	35% (8:1)
9	BF$_3 \cdot$OEt$_2$ (1.5)	−78	91% (8.2:1)
10	BF$_3 \cdot$OEt$_2$ (1.5)	−78 to −20	97% (9:1)[d]

[a]Typical reaction conditions: 8 (0.10 mmol, 1 equiv), MeC(OMe)$_3$ (0.15 mmol, 1.5 equiv), CSA (0.0050 mmol, 0.05 equiv), DCM, rt, then TMSCN (4.0 equiv), Lewis acid (x equiv). [b]Determined by ^{1}H NMR analysis using mesitylene as external standard, [c]n.d. = not determined. [d]50 mmol scale, combined isolated yield of diastereomers.
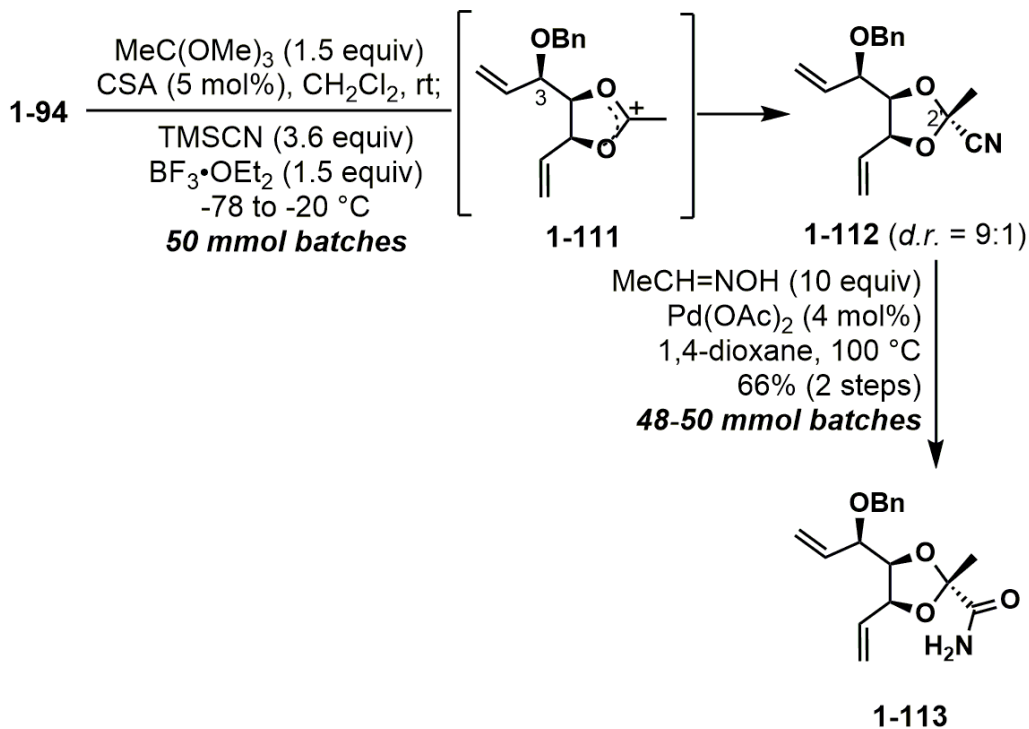
Scheme 19. Second generation synthetic route

DFT calculations were undertaken to further understand the factors governing the stereoselectivity of cyanation. Two transition states were located, **1-113a** and **1-113b** (Scheme 20a). The distance of 3.16 or 3.30 Å between the benzyl ether oxygen and the oxocarbenium ion suggests that it is a noncovalent interaction, not a formal neighboring-group participation as proposed in a related work.[77] The difference in energies of the transition states is probably due to a combination of electrostatics and sterics. In **1-114b**, the benzyl ether is further away from the oxocarbenium ion to accommodate the incoming nucleophile, thereby weakening the electrostatic interaction. In **114-a,** it is obvious that oxocarbenium ion is more stabilized by the benzyloxy oxygen (3.16 Å in **1-114a** vs 3.30 Å in **1-114b**). The stereochemical model is initially inspired by reports from Woerpel et al. on alkoxy-directed/accelerated nucleophilic additions to furanylacetal-derived oxocarbeniums.[78-83] However, it should be noted that this may be the first example of the

use of neighboring-group stabilization as a stereocontrolling factor in a dioxolane derivative synthesis.
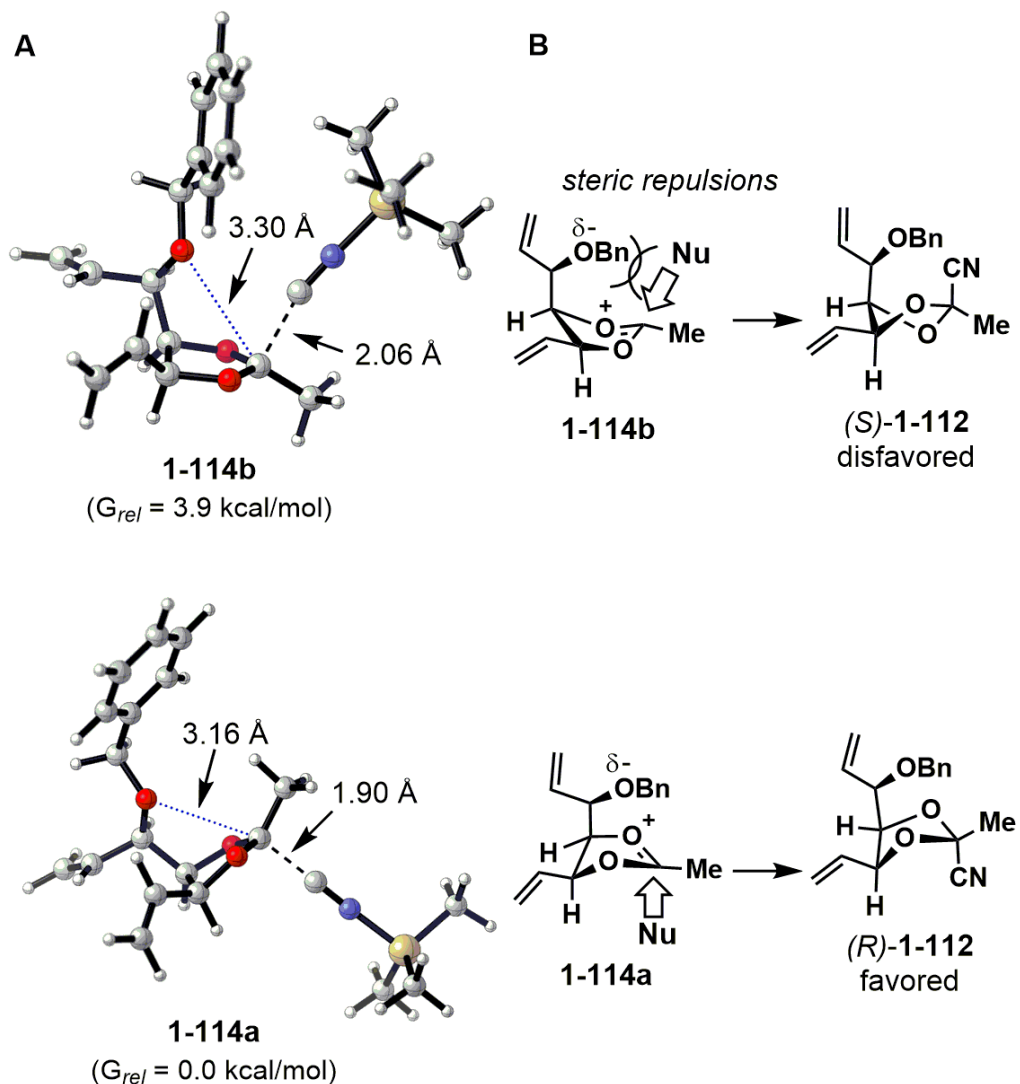
Scheme 20. Stereochemical model for cyanation

The conversion of the (R)-nitrile **1-112** to primary amide **1-113** (Scheme 19) met with difficulties because of the dioxolane ring opening under widely used reaction conditions, such as alkaline H_2O_2[49-51] and Parkins' catalyst, $[PtH\{(PMe_2O)_2H\}(PMe_2OH)]$.[85-86] After some trials, it

was discovered that an anhydrous hydration methodology developed by Chang and Lee using Wilkinson's catalyst, $(Ph_3P)_3RhCl$,[87-88] provided trace amounts of desired **1-113**. Screening of transition-metal catalysts revealed that $Pd(OAc)_2$ to be the catalyst of choice. During the course of this project, Naka et al. reported Pd(II) catalyzed transfer hydration of cyanohydrins to α-hydroxyamides.[89-92] As evident from Naka's papers, this robust and scalable transformation (up to 50 mmol in our case) may find broader applications for the conversion of nitriles to primary amides in complex molecules syntheses.[89]

Based on Chang and Lee,[87] and Naka's papers,[89-92] it is proposed that Pd(II) promotes the dehydration of acetaldoxime and the concomitant hydration of nitrile **1-112** (Scheme 21)**.** Pd(II) possibly activates nitrile **1-112** toward nucleophilic attack by acetaldoxime. Pd-complex **1-115** may undergo ligand exchange to form **1-116** that has Pd bound to both oxime and nitrile. Nucleophilic attack of the oxime on nitrile gives palladacycle **1-117**. The Rh variant had been proposed by Chang and Lee.[87] Tautomerization and ligand dissociation gave acetonitrile and amide **1-113**. Acetonitrile co-product can re-enter the catalytic cycle, reacting with the second equivalent of acetaldoxime, forming acetamide as a by-product.
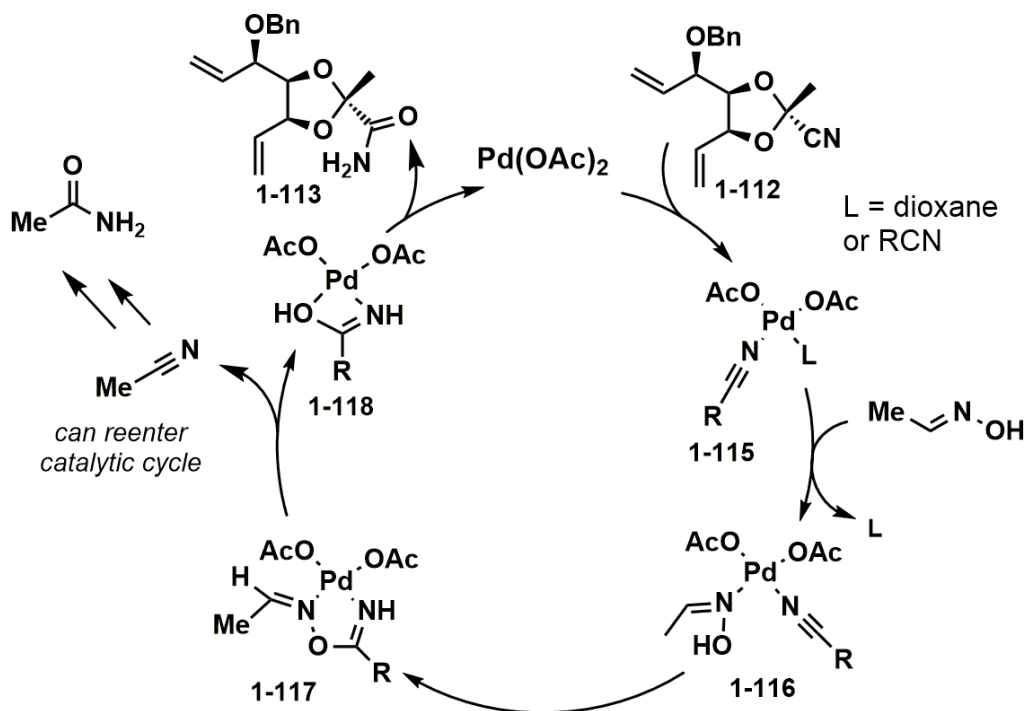
Scheme 21. Proposed catalytic cycle for transfer hydration

With **1-113** in hand, the next step was to forge the cyclopentenone moiety (Scheme 22). As previously found, debenzylation with DDQ was problematic. Oxidative deprotection with DDQ required excess oxidant, long reaction times, and irreproducible low yields (see the Experimental section for conditions tested). Reductive cleavage with Na/liq. NH₃ afforded the desired allylic alcohol in small-scale test reactions but was found to be not scalable. Unlike previous efforts in the Koide group, the experiences with the RCM step (**1-114** → **1-115**) had been surprisingly efficient. During the course of finding a deprotecting condition for **1-113**, different batches of **1-114** had been accumulated for RCM. It was realized that phenolic co-products formed from the reduction of DDQ could not be fully removed by aqueous extraction. Furthermore, **1-114** is water-soluble, rendering aqueous workup to be unsuitable. ¹H NMR analysis alone would give the false conclusion that **1-114** was sufficiently pure for the next step. Nonetheless, the ¹³C NMR spectrum

indicated that **1-114** was far from being pure. Even visual inspection of **1-114** (usually orange-brown viscous oil) should suggest to the experimentalist that the material was insufficiently pure for RCM.

Removal of excess phenolic co-product necessitates decolorization with charcoal followed by careful filtration through a pad of basic Al_2O_3 and occasionally a further filtration through solid $NaHCO_3$ to yield **1-114** as a pale-yellow oil. A sample of **1-114** thus obtained underwent RCM easily with usually ca.1 mol% nitro-Grela catalyst.[59] Although this purification protocol gave pure **1-114**, the yield was irreproducible. Varying amounts of highly polar **1-114** were often lost during the extensive filtrations.

Finally, it was found that the rarely employed combination of $BF_3 \cdot OEt_2$ and EtSH afforded the desired allylic alcohol **1-114** in 64% yield (Scheme 22).[93] With this method, **1-114** could be reproducibly formed (up to 64% yield). Furthermore, enough material was accumulated such that a scale-up of RCM could be performed using low ruthenium catalyst loadings. Ensuing oxidation could be performed in a one-pot fashion using MnO_2 to give **1-89** in 84% yield.
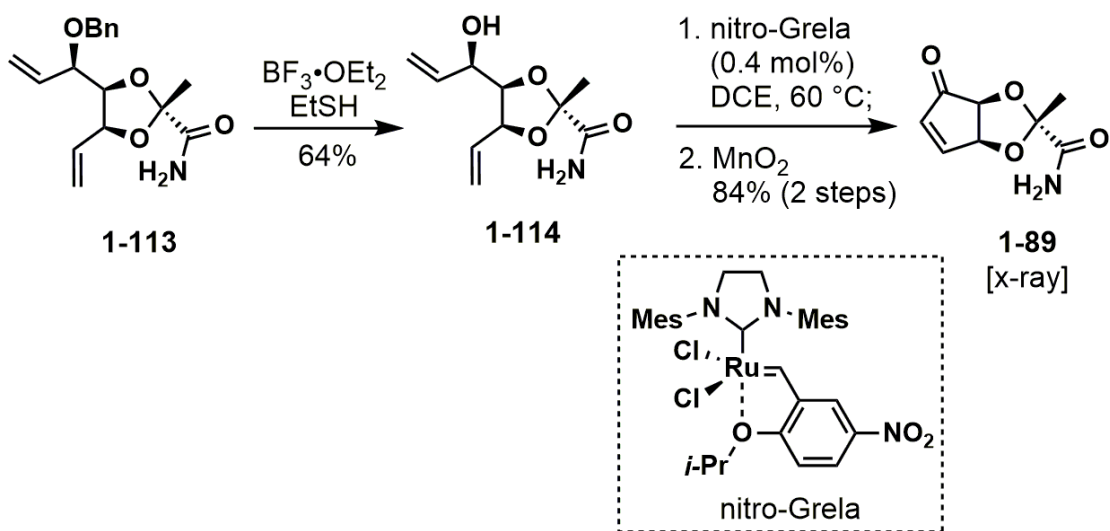
Scheme 22. Toward enone **1-89**

It was hypothesized that a hard and sterically unhindered metal acetylide might preferentially undergo 1,2-addition with **1-89** (Scheme 23).[94-96] Thus, propargylic alcohol **1-90** was obtained as a single diastereomer in 59% isolated yield. **1-90** underwent a smooth Meyer−Schuster rearrangement[98-99] in excess MeOH to give the reported structure (**1-81a**) and its Z isomer (**1-81b**), albeit with modest E/Z selectivity (Scheme 23). It should be mentioned that no ethoxy ester was observed in the Meyer-Schuster rearrangement.
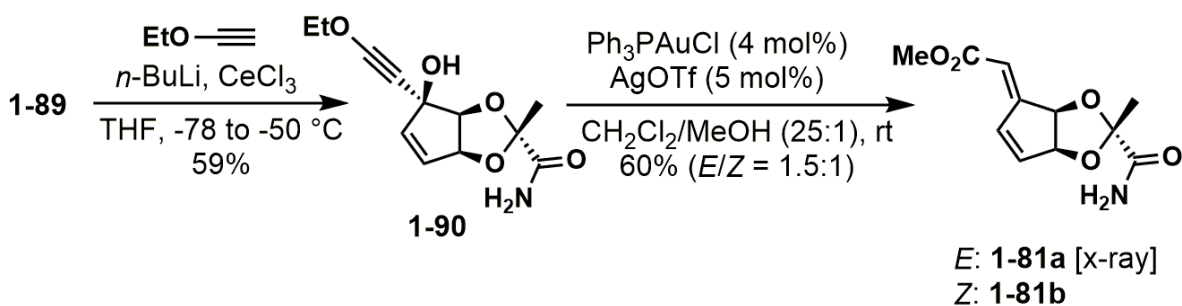
Scheme 23. End-game of total synthesis

Mechanistically, Au(I) activates the alkyne **1-90** toward nucleophilic attack by MeOH (Scheme 24).[98-99] The highly reactive enol ether **1-91** undergoes dehydrative deauration to form the enol allene **1-92** that can be readily trapped by a second equivalent of MeOH. Trapping of the putative oxocarbenium **1-93**/**1-94** gives the desired rearrangement product **1-81**/**1-82**. Treatment of the methoxy product with an alcoholic solvent under the reaction conditions did not result in trans-esterification.

Scheme 24. Plausible mechanism for Meyer-Schuster rearrangment/transesterification

More conveniently, it was found that Ce-mediated[94-96] Peterson olefination of enone **1-89** could directly afford **1-81a** and **1-81b** in 40% combined yield (unoptimized, Scheme 25). The structure of **1-81a** was unambiguously confirmed by X-ray analysis. It should be noted that Peterson olefination in the absence of CeCl$_3$ failed to afford any desired product. Although unique benefits of organocerium chemistry (such as alkylation/alkynylation of enolizable or hindered ketones) were already known,[94-96] this might be the first example of a direct olefin formation using an organocerium enolate.

Scheme 25. Cerium-mediated Peterson olefination

1.3 Structural Elucidation of the Real Structure of Stresgenin B

1.3.1 Comparison of NMR Spectroscopic Data

The ^{1}H and ^{13}C NMR spectra of both **1-81a** and **1-81b** do not match those reported for stresgenin B.[14] There are also discrepancies in the original assignment of ^{1}H and ^{13}C NMR data. In particular, ^{13}C NMR spectrum of **1-81a** shows significant differences for the chemical shifts of C2–C5, with differences ranging from 4.5 to 26.0 ppm (Table 6). These differences cannot be accounted by mere stereochemical mis-assignments (i.e., epimers, diastereomers). Furthermore, the coupling constant reported for the olefin C-H's was 9.7 Hz while those of **1-81a** and **1-81b** were 6.0 and 5.6 Hz, respectively. Based on literature surveys and observations with disubstituted cyclopentene systems, the endocyclic olefin has signature coupling constants of 5.0–6.0 Hz. These strongly suggest the natural product contains a ring structure other than a cyclopentene.
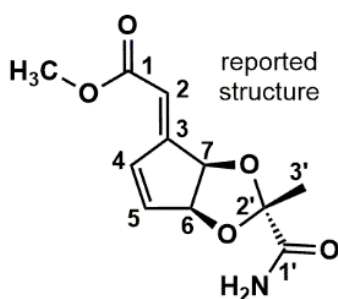
Table 6. Comparison of NMR spectroscopic data

position	Natural δ_C	Synthetic δ_C	Natural δ_H (mult, J (Hz))	Synthetic δ_H (mult, J (Hz))
C-1	164.5	166.4	--	--
C-2	136.2	115.2	7.43 (br)	6.02 (s)
C-3	130.0	156.0	--	--
C-4	124.4	141.5	6.43 (ddd, J = 9.7, 1.8, 1.8 Hz)	7.39 (d, J = 5.6 Hz)
C-5	129.1	133.6	6.56 (d, J = 9.7 Hz)	6.49 (dd, J = 6.0, 1.6 Hz)
C-6	80.9	82.5	4.42 (m)	5.20 (dd, J = 5.6, 2.0 Hz)
C-7	79.2	80.3	4.46 (m)	5.02 (d, J = 5.6 Hz)
C-1'	172.1	173.1	--	--
C-2'	109.8	109.0	--	--
C-3'	22.9	23.4	1.66 (s)	1.57 (s)
O-CH$_3$	52.2	51.5	3.79 (s)	3.76 (s)
NH$_2$	--	--	not reported	6.45, 5.87 (br)

1.3.2 DFT Calculations of the NMR of the Reported Structure

With irreconcilable differences in the spectroscopic data, we resorted to using DFT calculations.. At the outset of this computational effort, a computational method had to be determined. Based on the recommendations by Tantillo et al.,[103] four methods of reasonable computational cost and reported accuracies were chosen. Although these methods were considered to be "high accuracy methods" based on their performances on a test set of molecules, it was not clear whether the method would perform equally well for stresgenin-type structures. Assuming the real structure of stresgenin B is similar to that of the reported structure **1-81,** the chosen methods were first tested on **1-81**.

The calculated ^{1}H and ^{13}C NMR chemical shifts for **1-81** were compared to its experimental chemical shifts (Table 7), and the most accurate method was chosen for further calculations. Based on benchmark studies,[103a] root-mean-square-deviations (RMSDs) of calculated ^{1}H chemical shift below 0.1 ppm was considered highly accurate; the RMSDs for ^{13}C are more variable but must be below 3 ppm to be considered accurate. Based on these benchmarks, the mPW1PW91 functional (single-point NMR calculations, implicit solvation with chloroform) and B3LYP functional (gas phase geometry optimizations) showed the best performance. (see the SI for other methods that were tested on **1-81**.

Table 7. Testing accuracy of DFT method on reported structure

	conformer1 (57.5%)	conformer2 (22.9%)	conformer3 (19.6%)	average	expt	absolute deviation
OCH$_3$	50.78	50.68	50.68	50.7	51.5	0.8
C1	166.60	166.60	165.98	166.5	166.4	0.1
C2	112.45	112.67	115.01	113.0	115.2	2.2
C3	158.84	162.53	156.30	159.2	156.0	3.2
C4	132.87	134.69	133.05	133.3	133.6	0.3
C5	147.01	147.84	146.56	147.1	141.5	5.6
C6	82.79	83.75	82.87	83.0	82.5	0.5
C7	79.94	80.67	80.55	80.2	80.3	0.1
C3'	22.09	22.26	22.02	22.1	23.4	1.3
C2'	109.55	111.06	109.49	109.9	109.0	0.9
C1'	170.22	167.56	170.16	169.6	173.1	3.5
					MAD =	1.7

Upon inspection of the ^{13}C NMR spectroscopic data of synthetic versus natural material, it was found that the large differences are mainly from C-2 to C-5. Thus, a six-membered ring was speculated to be part of the real structure. Two possible constitutional isomers **CS1** and **CS2** (Table 8) were envisioned. The calculated chemical shifts for C-2 to C-5 supported the possibility of a conjugated cyclohexadiene motif. Changing the position of the methoxy carbonyl substituent afforded better results for C-2 to C-5 with **CS2** over **CS1**. Therefore, subsequent efforts were focussed on constitutional isomer **CS2**. For the constitutional isomer **CS2**, there exists 2^3 stereoisomers, four of which are NMR-distinguishable diastereomers, corresponding to **CS2**–**CS5**. We also note that for **CS5**, the ^{13}C NMR chemical shift for C-3 still has an absolute deviation of 5.0 ppm. Similar overestimations were also observed for the reported structure (see Table 7, chemical shift for C-5). It appears that this method systematically overestimates carbons conjugated (β and δ carbons) to an electron-withdrawing group.

Diastereomeric structure **CS3** gave larger MAD and RMSD than **CS2.** The chemical shifts for C-6, C-7 and C-2' of **CS2** and **CS3** still exhibited large deviations. It was thus considered whether the dioxolane ring could be trans-fused to the cyclohexadiene (**CS4** and **CS5**). To our knowledge, there is no literature precedence for dioxolane trans-fused to a cyclohexadiene. The closest resemblance is dioxolamycin (see Figure 5), which is equipped with a cyclohexene ring and may be less strained. Despite the lack of literature support, the calculated NMR data of **CS5** exhibit the lowest MAD and RMSD (^{13}C NMR: MAD = 1.6 and RMSD = 2.2; ^{1}H NMR, MAD = 0.10 and RMSD = 0.12, see the Experimental section).

42

Table 8. Comparison of calculated ^{13}C NMR
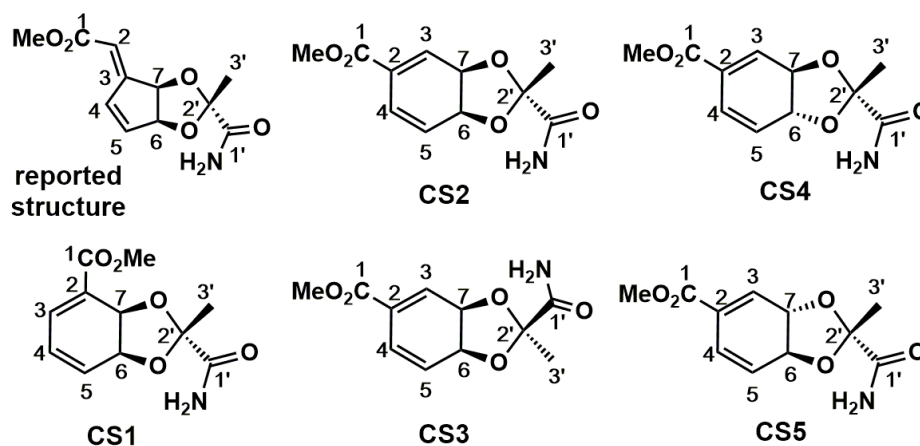
position	natural	CS1	CS2	CS3	CS4	CS5
O-CH$_3$	52.2	51.2	51.6	51.4	51.4	51.3
C-1	164.5	166.1	164.2	164.5	164.1	163.8
C-2	130.0	123.3	126.7	125.9	129.0	129.0
C-3	136.2	138.7	137.6	140.4	141.8	141.2
C-4	124.4	120.4	122.8	126.1	131.0	124.4
C-5	129.1	139.8	125.7	125.2	131.2	131.6
C-6	79.2	74.0	69.8	70.0	78.6	78.9
C-7	80.9	68.4	71.2	73.6	80.4	80.1
C-3'	22.1	21.6	21.2	20.3	20.7	21.1
C-2'	109.8	102.1	101.8	104.3	110.8	110.9
C-1'	172.1	169.3	170.1	168.2	175.9	168.3
MAD[a]	-	5.0	3.7	3.9	2.2	1.6

| RMSD[b] | - | 6.2 | 5.1 | 4.7 | 3.0 | 2.2 |

Moreover, it is reasoned that a trans-fused bicycle might be less susceptible to aromatization. The Akagawa group used the UV-vis spectrum of stresgenin B with a peak at 275 nm as a basis for the presence of a fully conjugated dienoate.[14] However, Figure 5 of the original patent[15] does not show such a peak. The structure of **CS5** does not support their NOESY correlations. Specifically, the authors reported NOE correlation between the methoxy group and C2–H; they assigned this olefin proton to the peak at 7.43 ppm, which is likely a mis-assignment. The peak at 7.43 ppm must be due to an olefin C–H conjugated to the ester. If **CS5** is the correct structure, the reported correlation would refer to the ester CH_3 and C3–H. However, our calculated average distance between the methoxy group and C3–H (conformer 1 of **CS5**, see Experimental secion **3.2.2.2**) is approximately 4.27 Å, suggesting that the NOE enhancement might be relatively weak.

The authors also reported NOE correlations between the dioxolane methyl group and the peaks at 7.43 and 6.43 ppm; none of our candidate structures can account for these correlations. At this point, without access to the original NOESY experiment data, it is not possible to determine whether these NOE enhancements are significant. While DFT calculations support the chemical structure of **CS5** as the natural product, other constitutional isomers and diastereomers cannot be fully excluded at this stage.

1.4 Conclusion

In conclusion, the total synthesis of the reported structure of stresgenin B **1-81** was completed. The synthetic route features a one-pot neighboring-group-directed diastereoselective cyanation. DFT calculations suggested that the directing effect stems from non-bonding interactions between benzyloxy group and electrophilic oxocarbenium ion **1-111**. A Pd-catalyzed transfer hydration of nitrile **1-112** was also employed. This transformation has been used by other groups in total synthesis and hydration of unstable cyanohydrins.[88-92] The challenging exocyclic olefin could be installed by either an alkynylation–Meyer-Schuster sequence or a Ce-mediated direct Peterson olefination. Both olefination methods allowed **1-81** to be formed as a mixture of E/Z isomers, and X-ray analysis confirmed the reported structure **1-81a**. Computations of ^{1}H and ^{13}C NMR spectra of candidate structures gave a plausible structure, **CS5**, for stresgenin B.

2.0 Hydroalkylation of Electron-Deficient Olefins via the Radical Chain Mechanism –

Experimental and Theoretical Investigations

2.1 Introduction

2.1.1 Introduction to Radical Chain Chemistry

The concept of radical chemistry is taught from an early stage of organic chemistry. Free radical halogenation of alkanes is a chapter found in most undergraduate organic chemistry textbooks.[106] It is well-established that the halogenation of alkanes operates via a radical chain mechanism. This classical example of a radical chain process, however, is rarely employed as a synthetic strategy in modern synthetic chemistry. In recent years, radical reactions operative via a radical chain mechanism typically involve a combination of AIBN (azobis(isobutyronitrile) or Et_3B/O_2 with a tin-based reagent.[107-117]

A generalized mechanism for AIBN as radical initiators is shown in Scheme 26a. Under heating or UV irradiation, homolysis of AIBN, **2-1**, occurs to form radical **2-2**. This radical species then abstracts a hydrogen from R_3SnH to generate nitrile **2-3** and $R_3Sn\cdot$. The trialkyltin radical species reacts with the radical acceptor **2-4** to form the alkyl radical **2-5**. The carbon-centered radical can undergoes a hydrogen abstraction from remaining R_3SnH to regenerate the tin radical $R_3Sn\bullet$, propagating the radical chain.

A generalized mechanism for Et_3B and O_2 is shown in Scheme 26b. Et_3B undergoes autooxidation with O_2 (usually in the form of air at $-78\ ^{\circ}C$) to generate peroxyborane **2-7** and ethyl radicals, which propagate the chain process.

a)

Initiation:

AIBN, **2-1** →(hν or Δ) 2 × **2-2** + N$_2$

Propagation:

2-2 + R$_3$SnH → **2-3** + R$_3$Sn•

R$_3$Sn• + **2-4** → **2-5**

2-5 + R$_3$SnH → **2-6** + R$_3$Sn•

b)

Initiation:

Et$_3$B + O$_2$ → Et$_2$BOO• + Et•
2-7

Propagation:

Et• + O$_2$ → EtOO•
2-8

EtOO• + Et$_3$B → EtOOBEt$_2$ + Et•
2-8 **2-9**
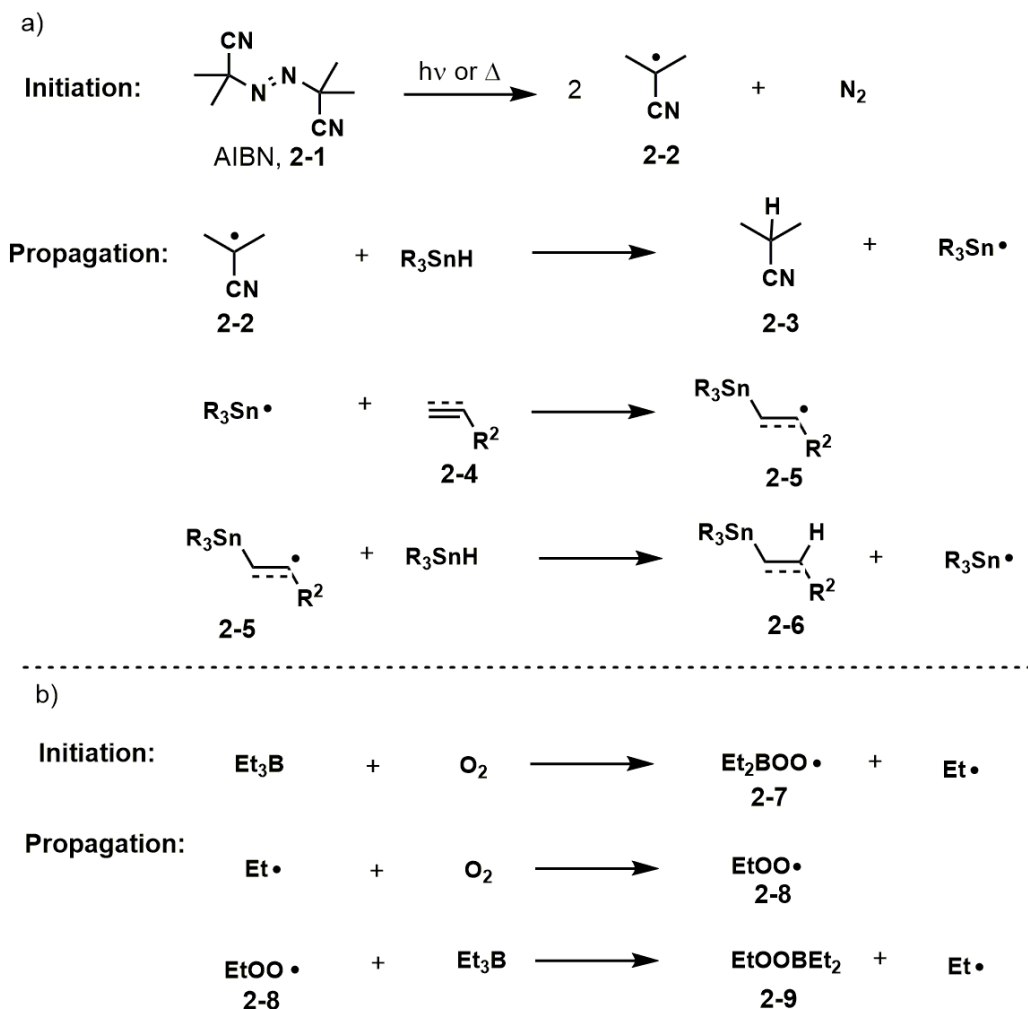
Scheme 26. a) Radical chain mechanism for hydrostannation of olefins and alkynes. b) Radical chain initiated by Et$_3$B/O$_2$

In general, synthetic strategies operative via a radical chain process has been largely limited to the use of AIBN or Et$_3$B/O$_2$ as radical initiators. Additionally, these synthetic reactions usually involve the use of toxic tin reagents. The latter is especially significant regarding the limitation of substrate scope as typically the radical donor must possess a necessarily weak X–H bond to allow hydrogen abstraction by a carbon-centered radical (*vide infra*).

2.1.2 Background to Modern Photochemistry

While the use of heat or UV light to accomplish radical chemistry is well-established, there might be potential reevaluation established chemistry using visible light.[118-121] To this end, varying combinations of photocatalyst, transition-metal cocatalyst, redox reagent(s), and hydrogen donors have been employed.

Photocatalysts can be further classified as organic or transition-metal based.[122] Common examples of organic photocatalysts are acridinium salts, benzophenones, phenylglyoxylic acid, pyrylium salts, and thioxanthones. In the second class, polypyridyl-Ru(II) and Ir(III) are most commonly employed[122,123] with more recent, chromium-[125,126] and cerium-based[127-130] photocatalysts emeringas inexpensive alternatives to Ir(III) catalysts. Furthermore, Ir(III)/Ni(II) dual catalytic systems[131] are also popular for the additional synthetic possibilities they provide to synthetic chemists. Redox reagents such as tertiary amines or redox-active esters are required for redox quenching and catalysts' turnovers. Hantzsch esters and thiols are commonly used hydrogen donors found in the literature.[122-124]

Mechanistically (Scheme 27),[122] ground state S_0 photocatalyst (PC) undergoes excitation in the presence of light to the first excited single excited state S_1, which undergoes rapid intersystem crossing to the more stable triplet state T_1. This T_1 state is commonly denoted PC* (e.g., Ru*, Ir*, etc.) in the literature. The excited photocatalyst is sufficiently long-lived due to a spin-forbidden decay to the ground state and can face two possible pathways, redox quenching or energy transfer. In redox quenching, PC* may undergo oxidative quenching, i.e., $(PC^n)^* \rightarrow PC^{n+1}$, and the oxidized PC, PC^{n+1}, would require a terminal reductant for turnover (i.e., $PC^{n+1} \rightarrow PC^n$). If PC* undergoes reductive quenching, i.e., $(PC^n)^* \rightarrow PC^{n-1}$, a terminal oxidant is required for the turnover ($PC^{n-1} \rightarrow PC^n$).
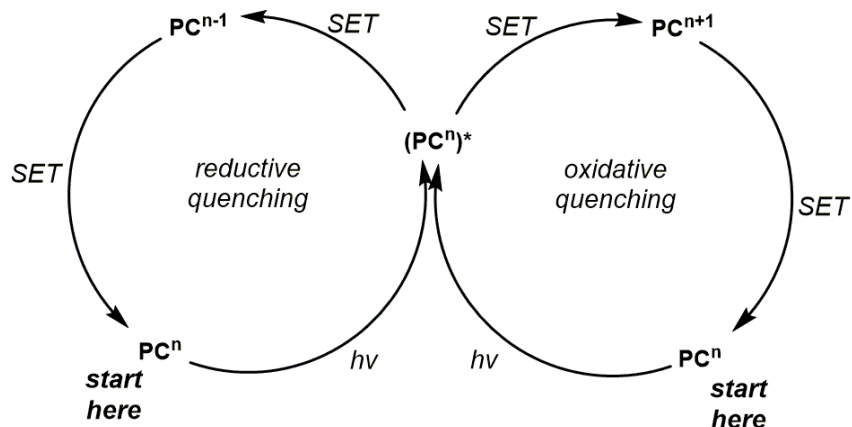
Scheme 27. General photocatalytic cycles for oxidative and reductive quenchings (SET = single electron transfer, PC photocatalyst)

In energy transfer, **PC*** can undergo triplet-to-triplet energy transfer, in which **PC*** decays from T_1 to S_0 while exciting an organic molecule **A** from S_0 to T_1 (Scheme 28). The excited **A*** can undergo subsequent reactions. Energy transfers are net redox neutral, and no redox reagent is required for catalyst turnovers.
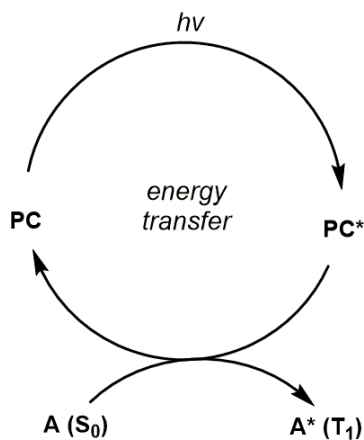
Scheme 28. General photocatalytic cycle for energy transfer

2.1.3 C–H Functionalizations of Ethers

Analogous to Sn–H, C–H abstractions have been designed and implemented in the repertoire of synthetic chemistry. In particular, C–H abstractions of activated substrates such as tertiary amines and ethers have been reported.[122] The thus formed α-amino or α-alkoxy radicals are nucleophilic and can add to electrophilic olefins or undergo cross-coupling reactions. The majority of these examples operate via closed catalytic cycles, presumably due to the innate challenge in cleaving the C–H bond; examples of radical chain C–H functionalizations usually involve formation of strong X–H bonds in the propagation steps.

2.1.3.1 Transition-Metal Catalyzed C–H Functionalizations of Ethers with Arylboronic

Acids (Lei)

In 2013, Lei et al. reported a Ni-catalyzed C–H arylation of ethereal substrates **2-10**. Common ethers such as tetrahydrofurans, 1,4-dioxanes, and 1,3-benzodioxoles were coupled with arylboronic acids **2-11** to form arylated ethers **2-12** (Scheme 29).[132]
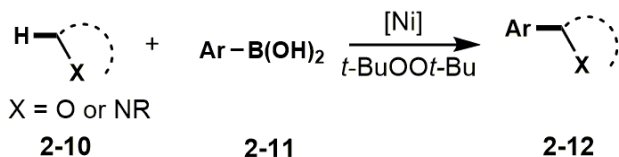
Scheme 29. C–H arylation of ethers with boronic acids

Mechanistically, it was proposed that di-*t*-butylperoxide (*t*-BuOO*t*-Bu) undergoes Ni-catalyzed homolysis (Scheme 30, path A). The thus formed *t*-butoxy radical abstracts the α-C–H of an ether, e.g., THF, **2-12**, forming the oxyalkyl radical **2-13**. This radical can undergo single

electron oxidation to form the more stable oxocarbenium ion **2-14**. The oxocarbenium ion is then

trapped by pronucleophile arylboronic acids **2-11** to give arylated ether **2-15**. Alternatively (path

B), the authors proposed the addition of aryl radical to **2-14** to form radical cation **2-16**.

Subsequently, **2-16** abstracts a hydrogen atom from THF to give product **2-15**.
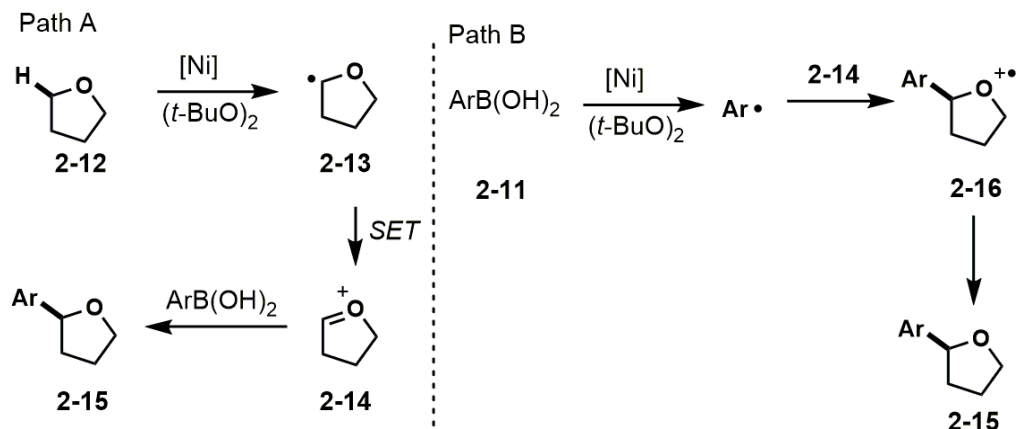
Scheme 30. Proposed mechanisms for Ni-catalyzed C–H arylation of ethers

2.1.3.2 Photoredox Minisci Reaction (MacMillan and Jin)

In 2015, MacMillan and Jin reported the first photoredox Minisci reaction (Scheme 31).[133] A

variety of pyridines and isoquinolines were coupled with ethers **2-18** to form useful

pharmocophores **2-19**.
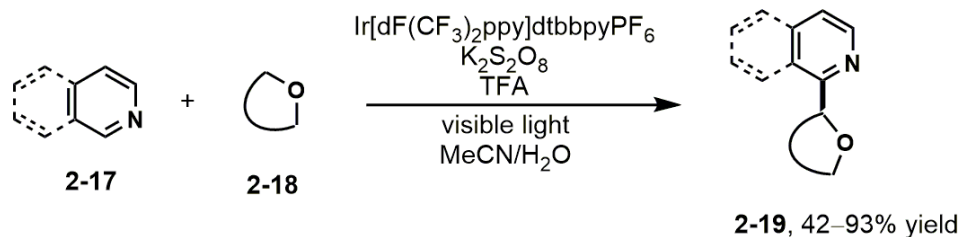
Scheme 31. Photoredox Minisci reaction

Mechanistically (Scheme 32), it involves the formation of oxygen-centered sulfate radical anion via single electron transfer from Ir(III)* to persulfate $S_2O_8^{2-}$ to form sulfonate ions SO_4^{2-} and sulfate radical anion $SO_4^{\bullet-}$. The sulfate radical anion then abstracts the α-C–H from an ether, such as tetrahydropyran (THP) **2-20**. The resulting THP radical **2-21** adds to the TFA-activated *N*-heteroarene **2-22**, forming radical cation **2-23**. Finally, proton transfer to give **2-24** and a single-electron oxidation yields the Minisci product **2-25**.
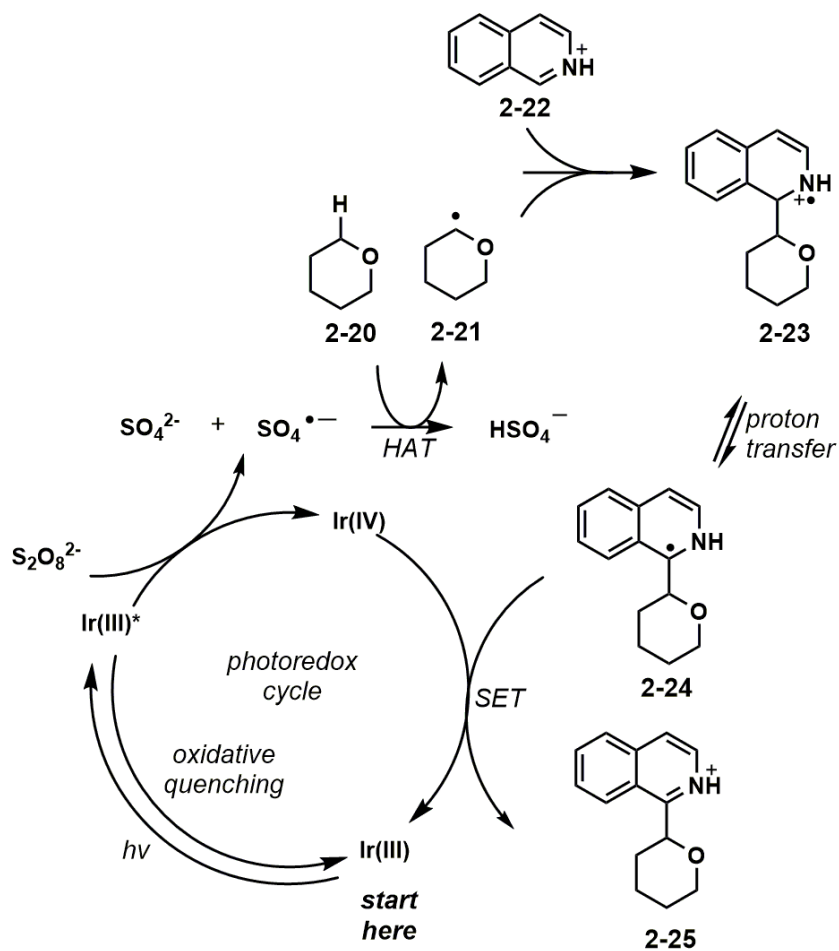
Scheme 32. Proposed mechanism for photoredox Minisci reaction

52

2.1.3.3 Photoredox Cross-Couplings of *N*-heteroaryl Chlorides with 1,3-Dioxolanes (Doyle)

Doyle et al. reported Ir(III)/Ni(II) dual catalysis to functionalize 1,3-dioxolane with (*N*-hetero)aryl chlorides (Scheme 33).[134] A Ni(III) species **2-26** was postulated as the key intermediate. The arylated dioxolanes **2-27** were deprotected with dilute HCl to afford the (*N*-hetero)aryl aldehydes **2-28**.
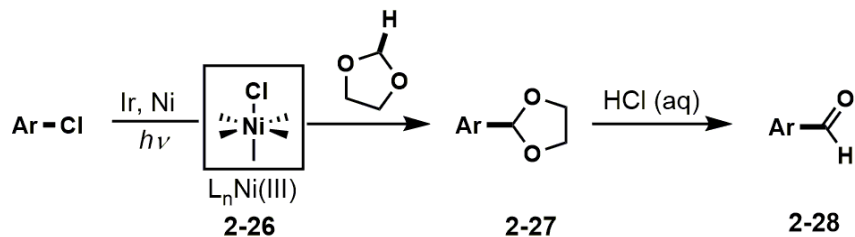
Scheme 33. Ir/Ni Co-catalyzed formal hydroformylation of (*N*-hetero)aryl chlorides
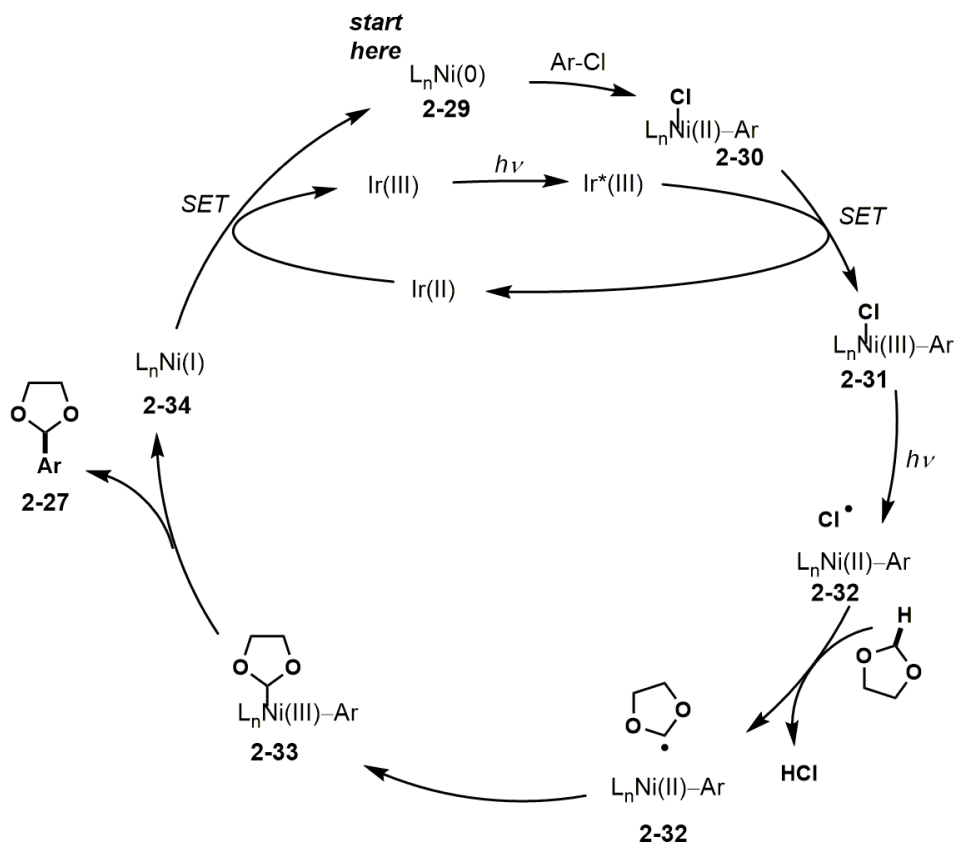
Scheme 34. Proposed Ir/Ni dual catalytic cycles

53

Mechanistically (Scheme 34), Ar-Cl undergoes an oxidative addition with Ni(0) **2-29** to form aryl Ni(II) **2-30**, which undergoes a single electron transfer with Ir*(III) to form aryl Ni(III) **2-31**. Under light irradiation conditions, photolysis occurs to form chlorine radical and aryl Ni(II) **2-32**. The chlorine radical abstracts a hydrogen atom from dioxolane to form dioxolanyl radical. The thus formed dioxolan-2-yl radical can recoordinate to form aryl Ni(III) **2-33**. Subsequent reductive elimination gives the product **2-27** and Ni(I) **2-34**. Ir(II) then reduces **2-34** back to **2-29**, closing both the Ni and Ir cycles. A noted problem, however, is the presence of two activated C–H bonds (C2–H vs C4–H), that can be abstracted by a chlorine radical. In some cases, a mixture of regioisomers were formed. Nonetheless, a one-pot procedure was devised to selectively convert the C2 isomer to the aldehyde **2-28**.

2.1.3.4 Thermal Minisci Reaction with 1,3,5-trioxanes (Yeung and Angeles)

In 2018, Yeung and Angeles reported a thermal variant (Scheme 35) of MacMillan and Jin's work.[133, 135] Additionally, 1,3,5-trioxane (5.0 equiv) could be used to replace 1,3-dioxolane (solvent). In this work, it was found that a transition-metal catalyst was not required for the reaction. During the optimization studies, the authors also found that visible light alone can promote the desired reaction to moderate yields. Due to the Lewis basicity of the nitrogen, a strong Lewis acid was necessary for deprotection to give **2-37**.
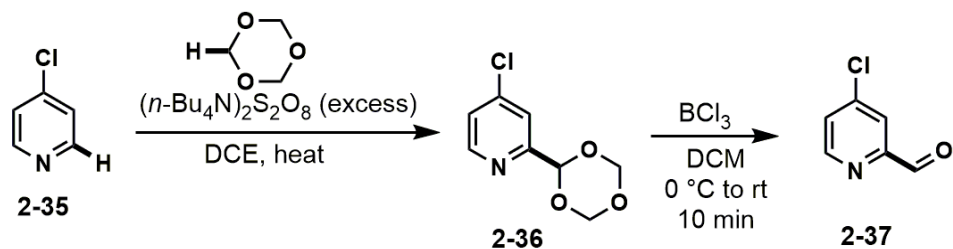
Scheme 35. Thermal Minisci reaction

Similar to MacMillan and Jin's report,[133] a persulfate oxidant was used in excess – in this case an organic soluble persulfate was employed. The radical anion $SO_4^{\cdot-}$ is formed under thermal conditions and abstracts the activated C–H bond of trioxane (Scheme 36). Trioxanyl radical **2-38** adds to the *N*-heteroarene (TFA not required, cf. Scheme 32) to give **2-39**. Nitrogen-centered radical **2-39** can undergo a spin-center shift to give *C*-centered radical **2-40**. Final oxidation/rearomatization gives product **2-41** (Scheme 36). The use of elevated temperature (60 ℃) promoted formation of $SO_4^{\cdot-}$ and addition of **2-38** to neutral *N*-heteroarenes.
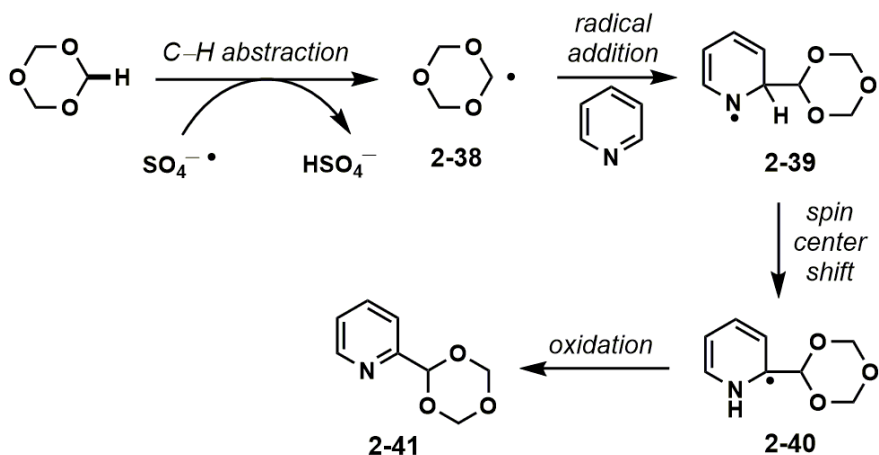
Scheme 36. Proposed mechanism for thermal Minisci reaction with trioxane

2.1.3.5 Photoredox C–H Functionalization (Wu and Meggers)

Wu et al. reported an Eosin Y-catalyzed hydrofunctionalization of a variety of electron-deficient olefins (Scheme 37).[136] Their work had a broad substrate scope with regards to C–H donors **2-42** and radical acceptors **2-43**. However, the reaction needs *both* light and heat, presumably to facilitate the cleavage of the C–H bonds.
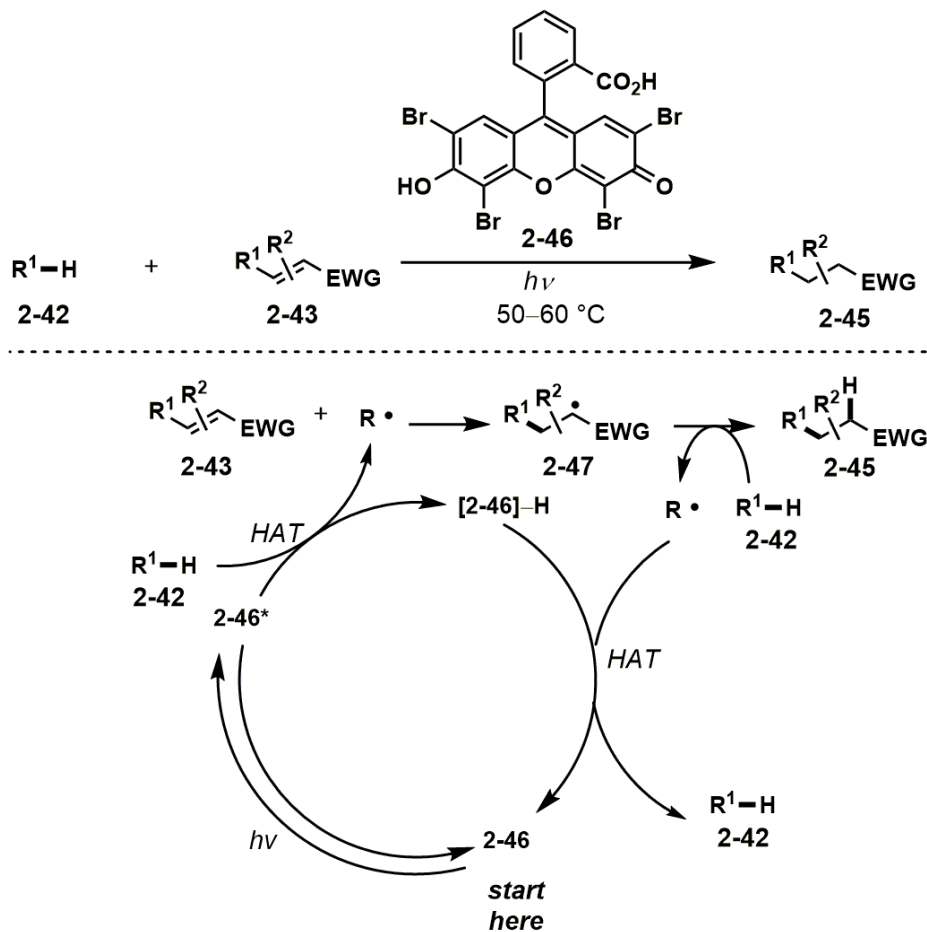
Scheme 37. Eosin Y catalyzed hydroalkylation of electron-deficient olefins

It is interesting to note that in Wu's work, the photocatalyst **2-46** undergoes direct hydrogen atom transfer (HAT). Under visible light irradiation, **2-46** is excited to triplet species **2-46***, which abstracts a hydrogen from **2-42**. The resulting R· then adds to electron-deficient olefins **2-43** to

give *C*-centered radical **2-47**. At this point, **2-47** is proposed to abstract a hydrogen from a second molecule of **2-42**. Newly formed R· is responsible for regenerating photocatalyst **2-46** and closing the catalytic cycle. Based on the authors' mechanistic studies, a radical-chain process was ruled out.

Following that, Meggers and Wu combined **2-46** with a chiral Rh(III) catalyst **2-47** (previously reported by Meggers et al.) for the enantioselective hydroformylation of electron-deficient olefins (Scheme 38).[137] The olefin acceptors **2-49** can be easily prepared from the corresponding acyl chlorides and 3,5-dimethylpyrazole. Importantly, the saturated acyl pyrazole **2-50** can be displaced under mild conditions without eroding the enantioselectivity.
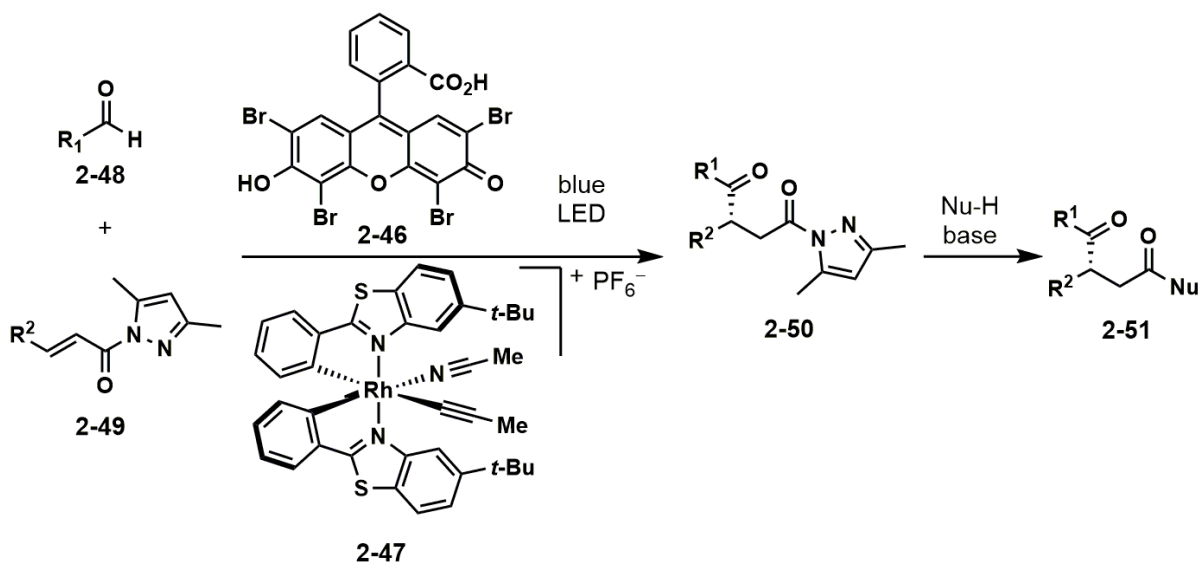
Scheme 38. Enantioselective photoredox synthesis of 1,4-dicarbonyls

2.1.3.6 Formal Hydroformylation of Cinnamic Acids with 1,3-Dioxolanes (Ooi)

During the course of our study, Ooi et al. reported the radical addition of dioxolan-2-yl radicals to cinnamic acids (Scheme 39).[138] The authors tentatively proposed a SET mechanism, in which thioxanthone **2-53**, upon excitation, undergoes SET with dioxolane to form a relatively acidic

radical cation **2-55** (pKa = 1.4 in MeCN). Proton transfer gives dioxolanyl radical that undergoes conjugate addition to cinnamic acids to form α-carbonyl radical **2-56**. Subsequent SET to the enolate **2-57** and proton transfer would afford product **2-54** and close the catalytic cycle. The authors also stated that neither a HAT (i.e., direct C–H abstraction by **2-53***) could not be ruled out at this stage.[139-144]
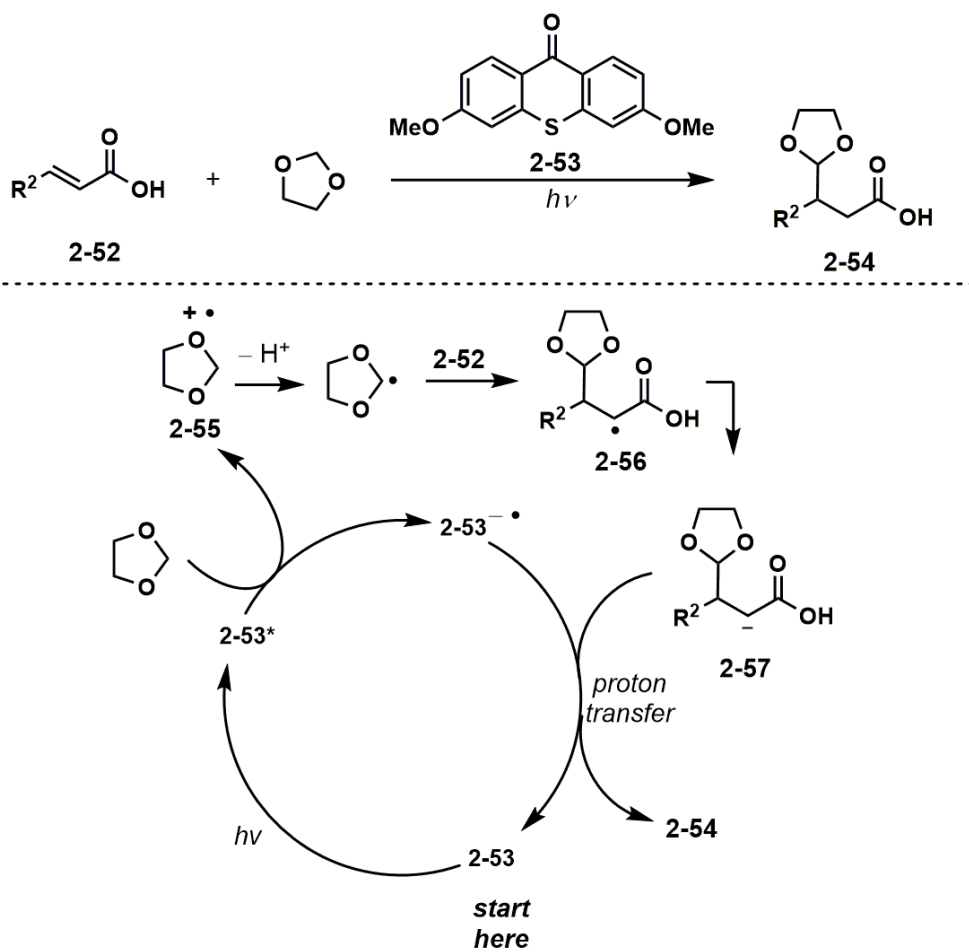
Scheme 39. Hydroalkylation of cinnamic acids with 1,3-dioxolane

2.1.3.7 C–H Functionalization via Uranyl Photocatalysis (Ravelli)

Ravelli et al. also reported a direct C–H abstraction from **2-58**, reacting with malononitriles **2-59** (Scheme 40). Uranium(VI) salt **2-60** was reported to be a competent photocatalyst that undergoes direct C–H abstractions from alkanes.[145] The authors proposed that **2-60*** directly abstracts a hydrogen from alkanes, generating alkyl radicals which were trapped by **2-59**. α-Malonyl radical **2-62** undergoes SET and proton transfer to close the catalytic cycle and afford product **2-61**.
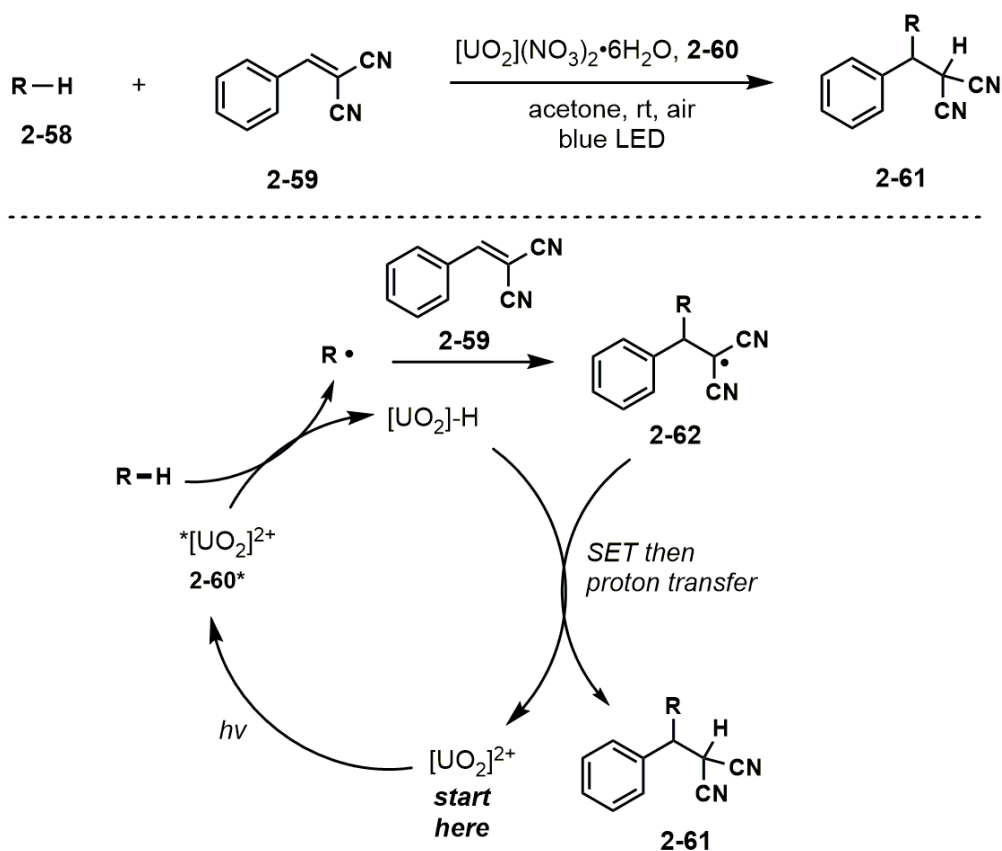
Scheme 40. Uranyl catalyzed hydroalkylation with unactivated $C(sp^3)$–H donors

2.1.3.8 Photoredox Formal Hydroformylation of Acrylamides with 1,3-Dioxolanes (Su)

Su et al. designed a catalytic cascade triggered by the nucleophilic addition of dioxolanyl radicals to acrylamides **2-63** (Scheme 41).[146] Examples of suitable substrates required the β-position to be unsubstituted. The products can be deprotected under mild-acidic conditions to unmask the free aldehydes **2-66**. Mechanistically, upon dioxolanyl addition, the *C*-centered radical **2-64** is expected to be electrophilic, thus, substrates were designed with electron-rich aryl tethers as radical traps.
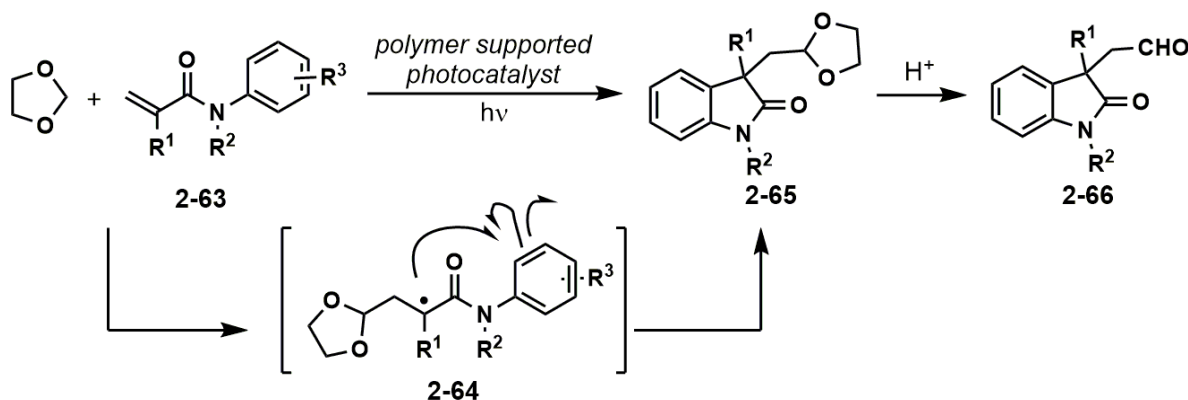
Scheme 41. Photoredox radical cascade to form indolines

2.1.3.9 Visible-Light Mediated Formylation of Imines (Gong and Lu)

Gong and Lu reported the addition of dioxolanyl radicals to imines. α-trifluoro- (**2-67**) and α-ethoxycarbonyl imines (formed in situ from **2-70** and **2-71**) (Scheme 42).[147-148] Noteworthily, the reactions were proposed to operate via radical chain mechanisms. The key feature of the reactions is likely the formations of *N*-centered radicals **2-68** and **2-72**, which would undergo exergonic C–H abstractions to form stronger N–H bonds.
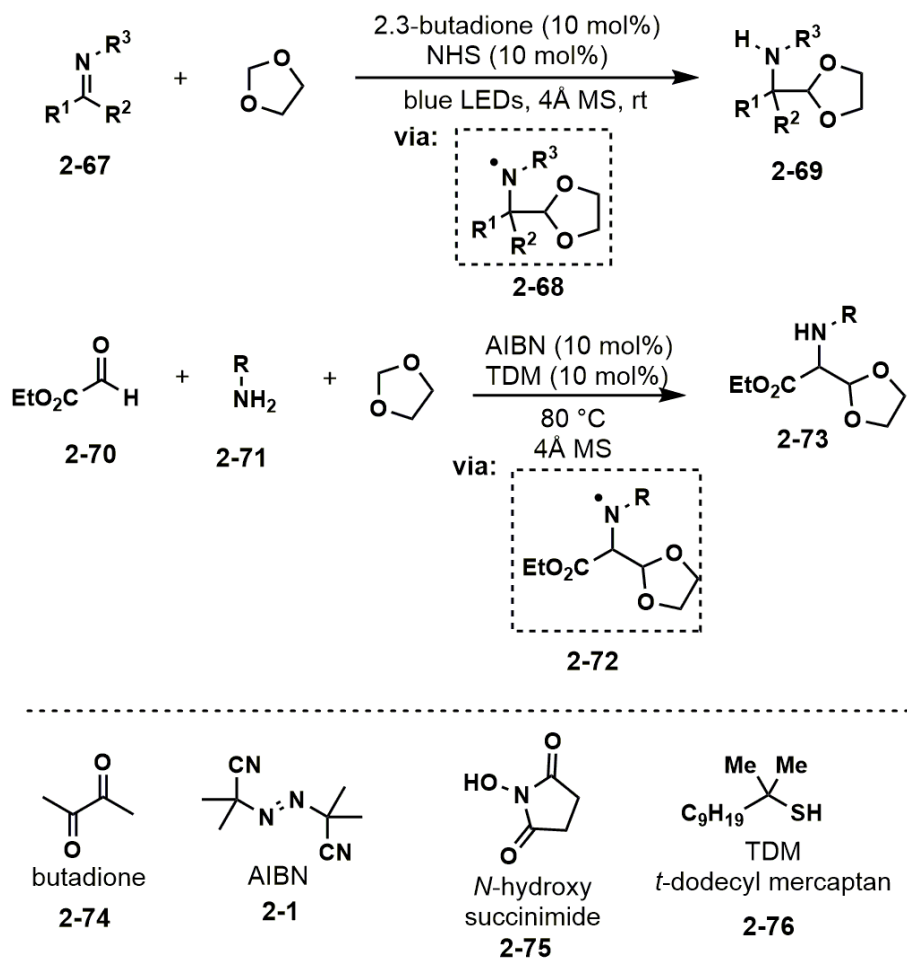
Scheme 42. Dioxolane addition to imines via a radical chain mechanism

2.1.3.10 Hydroalkylations of Vinyl Sulfonylfluorides (Liao)

Liao et al. reported the synthesis of hydroalkylated sulfonylfluorides using redox-active esters (RAEs) as the alkylating agents (Scheme 43).[149] The RAEs were synthesized form the corresponding carboxylic acids, and 1°, 2°, and 3° alkyl radicals could be added to vinyl sulfonylfluoride **2-78**. Mechanistically, upon SET, RAE **2-77** undergoes concomitant decarboxylation to generate alkyl radical **2-82**. Conjugate addition to electrophilic **2-78** gives radical **2-83**, which abstracts a hydrogen from Hantzsch ester **2-80**. Radical **2-85** then undergoes SET and proton transfer to close the catalytic cycle and form pyridine **2-87** and product **2-79**.
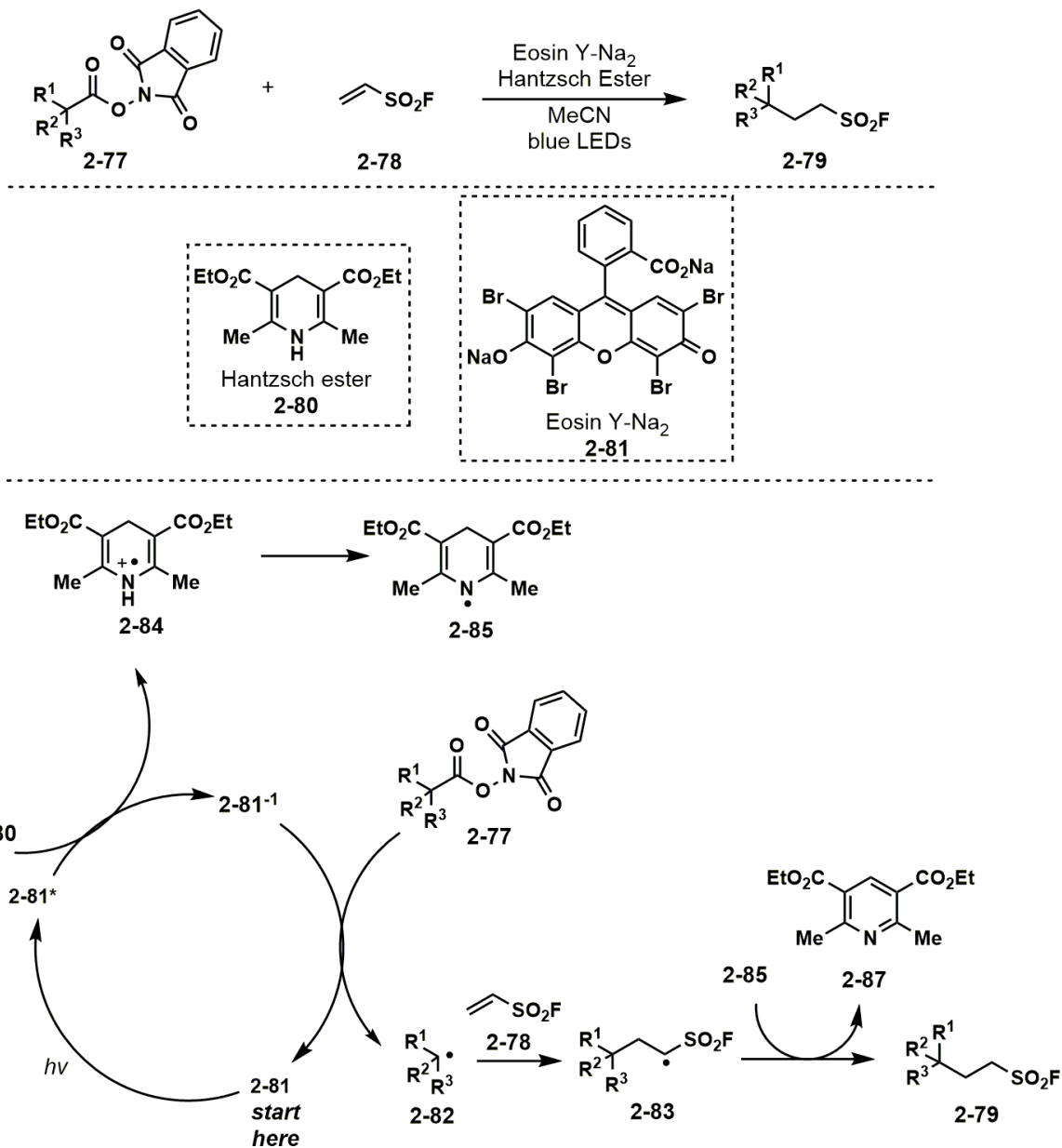
Scheme 43. Photoredox hydroalkylation of vinyl sulfonylfluoride

2.1.4 Background for Xanthones and Chromones

Xanthones are privileged scaffolds with many examples of natural products containing this scaffold.[150-153] The simplest member of the family is the tricyclic natural product named xanthone (**2-86**), with other variably substituted xanthones being commercially available. Briefly, xanthone

natural products can be classified based on their oxidation states and substitution pattern (Figure 6). Namely, dihydro- (**2-87** and **2-88**), tetrahydro (**2-89** and **2-90**), and hexahydroxanthones (**2-91**) refer to the differentially oxidized *C*-ring of tricyclic xanthones. Beyond that, xanthones also undergo homo- and heterodimerization to form a large variety of dimeric natural products.[152]

xanthone, **2-86**   dihydroxanthone, **2-87**   dihydroxanthone, **2-88**

tetrahydroxanthone, **2-89**   tetrahydroxanthone, **2-90**   hexahydroxanthone, **2-91**
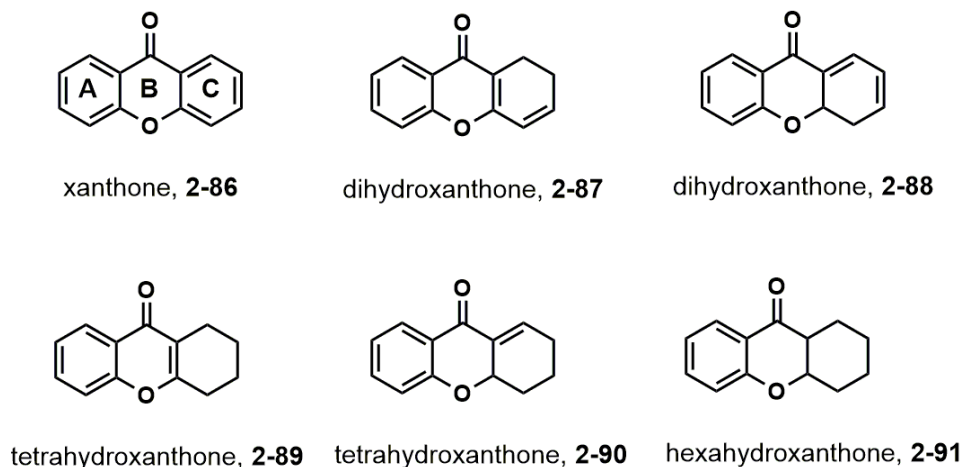
Figure 6. Generic classification of xanthones

The parnafungins belong to a subclass of heterodimeric xanthones (Figure 7); of interest is the biological activity of the parnafungins.[154] It is the Koide group's longstanding interest in studying small molecules that have interesting biological activities.[155] Parish et al.[154] used the Candida albicans Fitness Test (CaFT), a whole-cell screening platform to profile crude fermentation extracts for novel natural products that exhibit antifungal activity. The CaFT profile obtained from one of the extracts showed to affect mRNA 3'-cleavage and polyadenylation. It is proposed that mRNA processing is the molecular target for the antifungal activity. To date, there have only been two papers documenting synthetic studies toward parnafungins.[156-157]
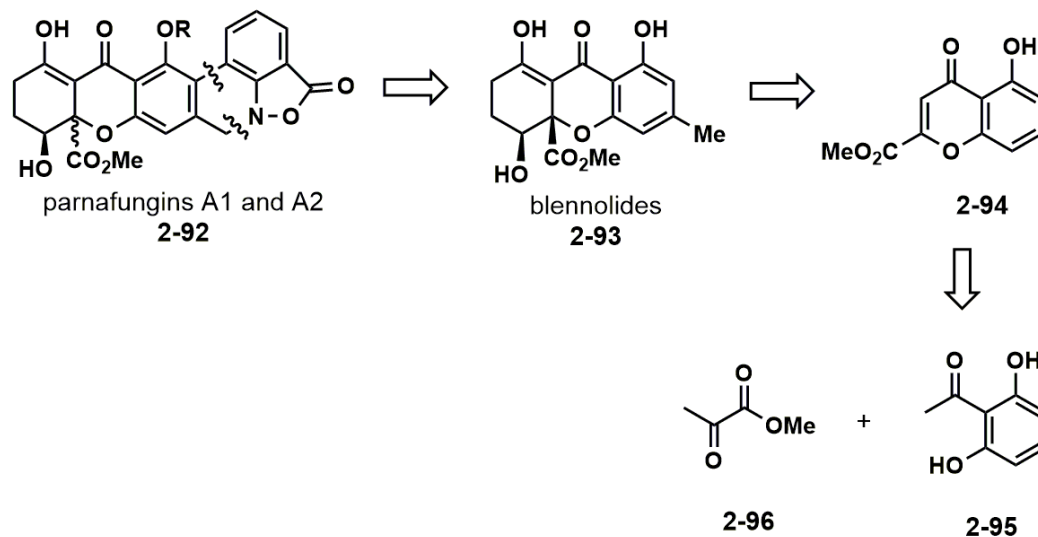
Figure 7. Retrosynthetic analysis of parnafungins

Inspired by the proposed biosynthesis of xanthone paranfungins,[154-157] the retrosynthetic route involved blennolides as synthetic intermediates (Figure 7). Previously, Porco et al. reported an elegant method to access blennolides en route to secalonic acids (Figure 8).[158-161] In their method, they relied on nucleophilic addition of siloxyfuran **2-98** to the electrophilic pyrylium **2-97**. The electrophile was synthesized by pre-treating chromone **2-94** with stoichiometric amounts of R_2SiCl_2. Chromone could be synthesized from commercially available acetophenone **2-95** and α-ketoester **2-96** (Figure 7). This strategy easily assembled all the requisite carbon atoms for the blennolide skeleton. To our knowledge, this is the most efficient strategy in accessing the blennolides.[152]
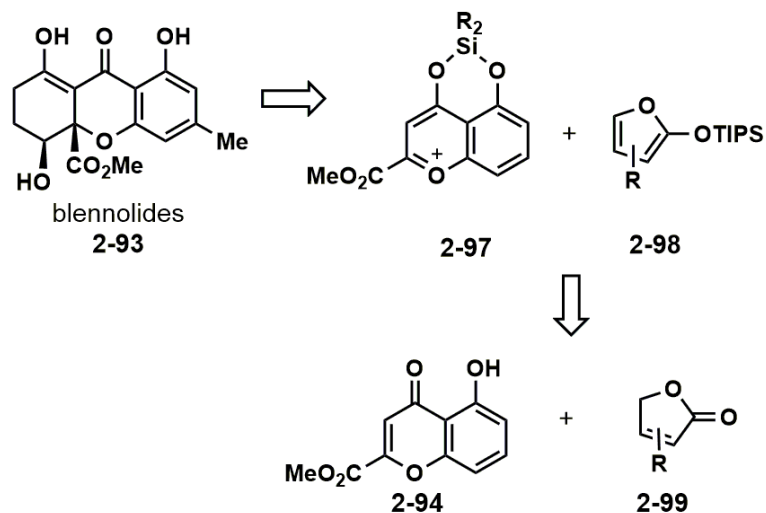
Figure 8. Retrosynthetic analysis of blennolides by Porco et al.

Retrosynthetically, it is attractive to access blennolides via chromones. There is a variety of substituted chromones commercially available. Non-commercial substituted chromones can also be readily prepared from inexpensive acetophenones and α-ketoesters. There are some literature precedents for the functionalization of simple chromones, mostly unsubstituted at C-2. However, to our knowledge, few methods are developed in the context of a total synthesis. Hence, we aimed to develop a new method to functionalize chromones for the total syntheses of xanthone natural products.

2.2 Results and Discussion

2.2.1 Efforts to Develop a New Method to Functionalize Chromones

In the literature, only chromones substituted at the C-3 position with an electron-withdrawing group underwent Diels-Alder or formal cycloadditions.[162-164] One might assume chromones without additional activation at the C-3 position is not sufficiently reactive for Diels-Alder reaction. Based on the retrosynthetic analysis, C-2-substituted chromones are more useful for the synthesis of parnafungins **2-92**. It was unknown whether chromone substituted with an electron-withdrawing group at the C-2 position would influence its Diels-Alder reactivity. Therefore, chromone **2-94** and siloxydiene **2-100** were chosen as reacting partners (Scheme 44). Instead of using the more electron-rich Danishefsky's diene, siloxydiene **2-100** was chosen because of its oxidation state. If successful, subsequent redox manipulations would be more straightforward.

Under most conditions tested, **2-100** proved to be too unstable while **2-94** was inert. For example, when a mixture of **2-94** and **2-100** was heated in mesitylene to 200 ˚C (with catalytic BHT) overnight, **2-94** could be recovered intact (Scheme 44).
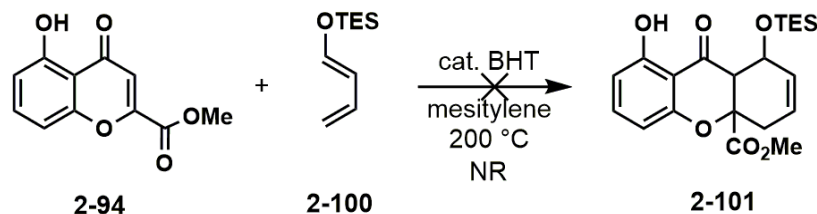
Scheme 44. Attempted intermolecular Diels-Alder reaction

The next step was to investigate the feasibility of the intramolecular variant (Scheme 45). Furanyl ester **2-102** was designed as the substrate. If the intramolecular Diels-Alder furan (IMDAF) is successful, the tricyclic skeleton would be assembled in addition to having two "oxidized" carbons in the *C*-ring. When furanyl ester **2-102** was first subjected to the Diels-Alder reaction under thermal conditions, there was no apparent reaction observed. We speculated that the lack of reactivity might be due to the reversibility of the reaction. We then hypothesized that the Thorpe-Ingold effect[165-166] could be used to override the reversibility issue (Scheme 45, bottom). Thus, *gem*-dimethyl ester **2-103** was designed as the substrate and probed computationally. DFT calculations suggested that adding *gem*-dimethyl groups to the ester tether does lower the barrier for the forward reaction. However, the barrier for the reverse reaction is still significantly lower. Furthermore, it was realized that *gem*-disubstituted esters were synthetically impractical. It was found that the ester **2-103** was unstable due to the hydrolysis of the tertiary furanyl ester.
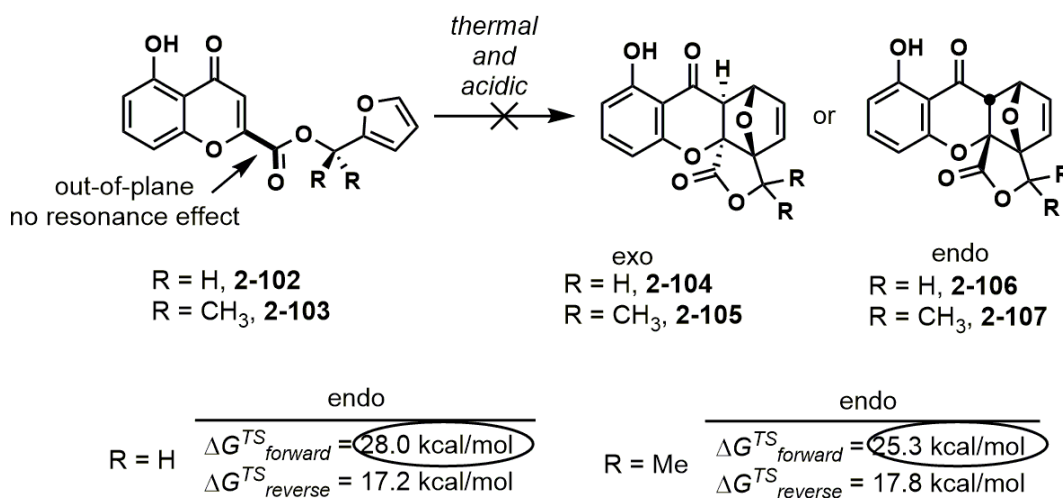
Scheme 45. DFT calculations of intramolecular Diels-Alder with furan (IMDAF)

After several failed attempts, we wondered whether C–H functionalization could be used to functionalize chromones (Scheme 46).[167] Although C–H functionalization of unsubstituted chromones have been reported,[168] those of C–2 substituted chromones are not known. Besides, there are some literature examples in which an ester could act as a weak coordinating group,[169] directing transition-metal catalyzed C–H functionalizations. Several conditions were screened for a reaction between chromone **2-94** and *t*-butyl acrylate **2-108**. However, no reaction was observed in the screenings.
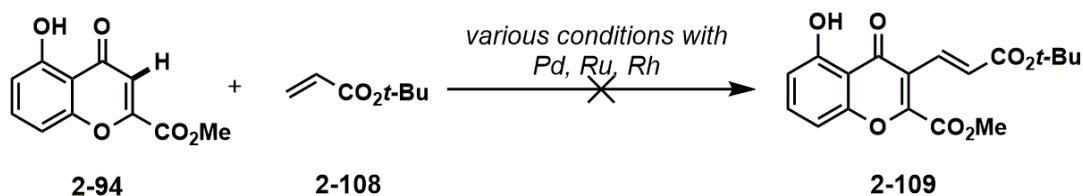
Scheme 46. Attempted C–H functionalization of C-2 substituted chromone

2.2.1.1 Exploration of Radical Chemistry and Preliminary Findings with Chromone

When logical disconnections based on polarities failed to work, or when cycloadditions are limited by a HOMO-LUMO mismatch, perhaps radical strategy can shine new light to the issue.[170] The radical chemistry between ethers and chromone was examined. With the initial aim of developing a method toward total synthesis, an oxidative functionalization of chromone was envisioned (Scheme 47). The unsaturated product is the desired product as it can allow a second functionalization at the β-position.
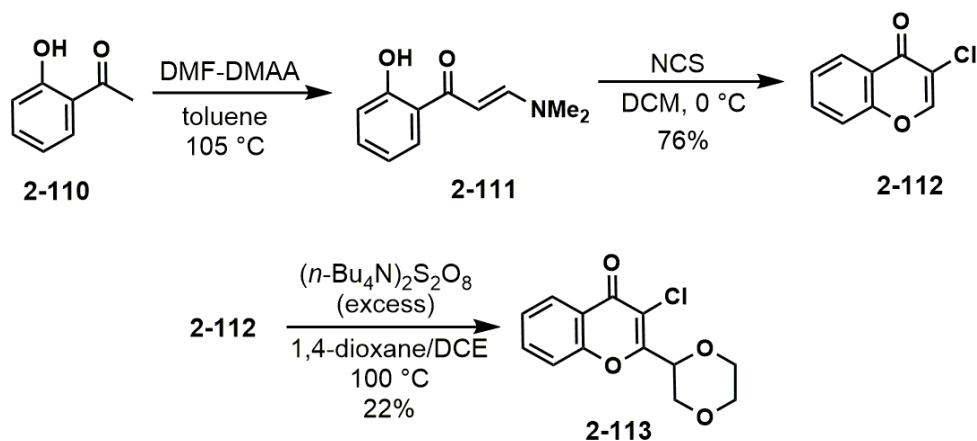
Scheme 47. Radical functionalization of chromone

As a proof of concept, a mixture of chromone and 1,4-dioxane in DCE was heated with excess $(n\text{-Bu}_4\text{N})_2\text{S}_2\text{O}_8$ in a sealed vial at 100 ℃. 1,4-Dioxane was chosen initially because it has only one activated C–H to be abstracted. Known 3-chlorochromone was prepared as a substrate. The chloride handle was installed with the plan of subsequent transition-metal-catalyzed cross-couplings. Heating **2-112** in the solvent mixture gave a complex mixture, and the desired product **2-113** was formed in only 22% isolated yield (Scheme 47).

The focus was turned toward generating radicals using visible light. Based on literature survey (Sections 2.1.3.1 to 2.1.3.10),[133-147] the inexpensive 1,3-dioxolane ($107/L from ACROS Organic) was chosen as both the reagent and solvent. Additionally, chromone was further simplified to unsubstituted **2-114**. It was found that undesired saturated ketone **2-115** was formed as the major product (Scheme 48). Efforts to achieve an "oxidative alkylation" of chromone in excess of oxidant was unsuccessful (based on TLC analysis).

69
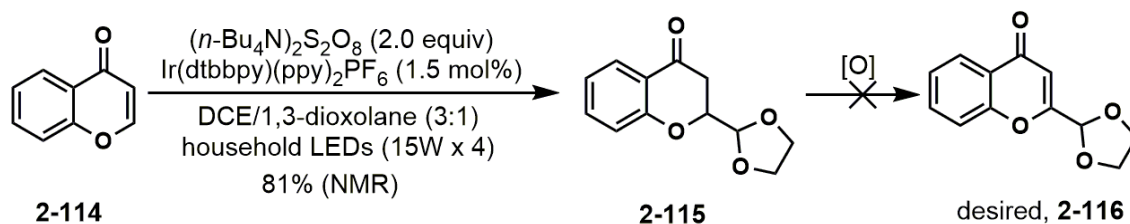
Scheme 48. Initial result of dioxolane addition

When the reaction was tested on an initially desired synthon **2-94**, there was no reaction observed. Protecting the phenolic group as acetate **2-117** did not restore reactivity (Scheme 49). Because 1,4-addition was the dominant outcome and the newly found reaction could not be applied to the initial goal, a new question was asked: could this chemistry be generalized toward other electron-deficient olefins?
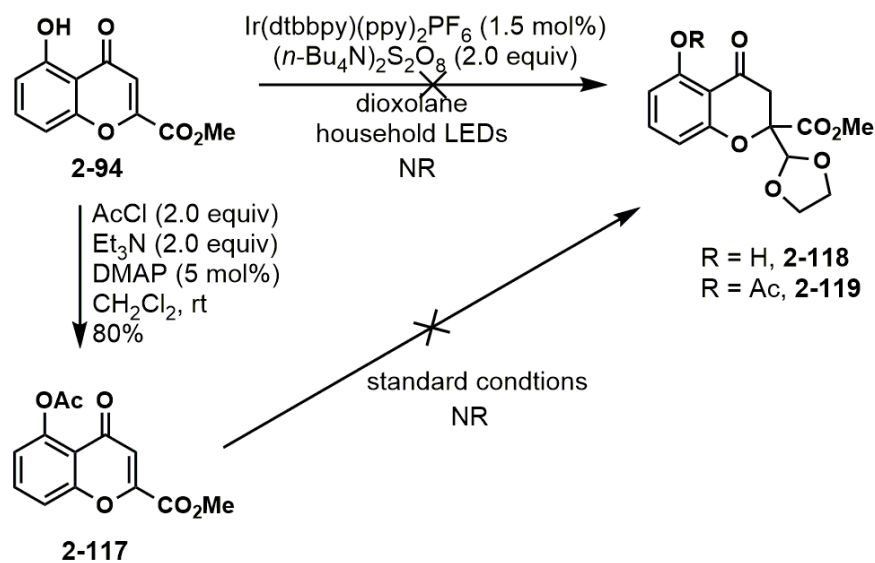
Scheme 49. Attempted dioxolane addition to C-2 substituted chromone

2.2.2 Optimization of Reaction Conditions Using *trans*-Chalcone as Radical Acceptor

With the question in mind, the commercially available *trans*-chalcone **2-120** was first chosen as the substrate for reaction optimization (Table 9).[71-75] It was envisioned that the thus formed products would be masked 1,4-dicarbonyls and useful for downstream functionalizations. Extensive screenings were performed but *trans*-chalcone proved to be an unsuitable substrate. In many cases, complete consumption of chalcone was observed, but the product was formed in low to moderate yields. Furthermore, the yields of the reaction were also irreproducible. In a single case, an NMR yield of 80% was observed (Table 9 entry 10). However, the joy was short-lived as it proved to be irreproducible upon several subsequent repetitions (entries 10 vs 11). Additives and different sources of light were also tested with no success.

Table 9. Representative screening conditions for chalcone
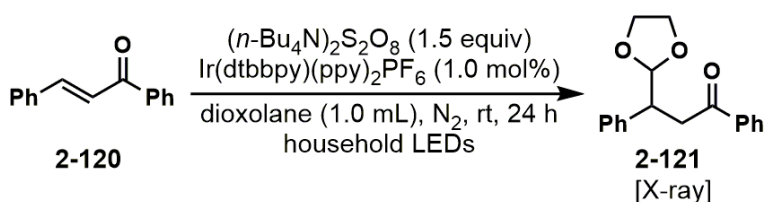
entry	changes from standard	yield[a]
1	none	43% (33%)
2	1.5 mL dioxolane	59%
3	2.0 equiv [O]	53%
4	1.0 equiv [O], 1.5 mL dioxolane	63%
5	2.0 mL dioxolane	62%
6	1.0 equiv [O], 2.0 mL dioxolane	60%
7	1.0 equiv [O}, 2.5 mL dioxolane	56%
8	Ir(ppy)$_3$ (1.0 mol%), i-Pr$_2$NEt (1.5 equiv)	20%
9	Ir[dF(ppy)]$_3$ (1.0 mol%)	63%
10	Ir[dF(CF$_3$)ppy]$_2$(dtbbpy)PF$_6$ (1.0 mol%)	80%
11	repeat entry 10	55%

[a]Determined by ^{1}H NMR spectroscopic analysis using mesitylene as external standard

2.2.3 Optimization of Reaction Conditions Using Benzylidenemalonate as Radical Acceptor

Since the postulated 1,3-dioxolanyl radical was expected to be nucleophilic,[171] it was hypothesized that increasing the electrophilicity of the radical acceptors might increase the reaction efficiency. β-Nitrostyrene was briefly examined but was unsuccessful. Dimethyl benzylidenemalonate[172] **2-122** was then examined (Table 10). Gratifyingly, with this substrate, the optimal reaction conditions were quickly found; *fac*-Ir(ppy)$_3$ was the optimal catalyst for this transformation. The results were also reproducible. Noticeably, there was an apparent correlation between the reducing

ability of [Ir] and the yield of the reaction. *fac*-Ir(ppy)$_3$ (entry 1) being the most reducing catalyst was found to be the optimal catalyst.

Table 10. Optimization of reaction conditions for benzylidenemalonate

	$(n\text{-}Bu_4N)_2S_2O_8$ (1.0 equiv)		
	fac-Ir(ppy)$_3$ (0.5 mol%)		
	1,3-dioxolane, Ar		
	household LEDs (15W x 4)		

2-122 → **2-123**
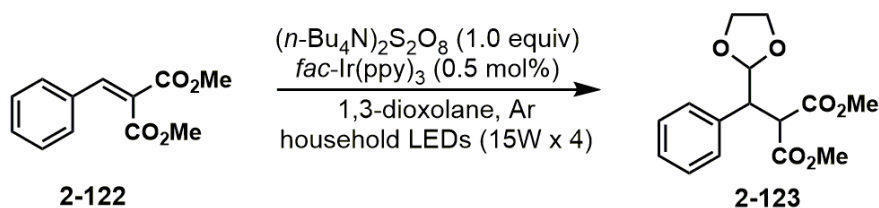
entry	changes from standard conditions	NMR yields
1	*fac*-Ir(ppy)$_3$	93%
2	Ir(dFppy)$_3$	89%
3	Ir(dtbbpy)(ppy)$_2$PF$_6$	87%
4	Ir[dF(CH$_3$)ppy]$_2$(dtbbpy)PF$_6$	85%
5	Ir[dF(CF$_3$)ppy]$_2$(dtbbpy)PF$_6$	77%
6	no [Ir]	76%
7	no [O]	NR
8	no *hv*	dec
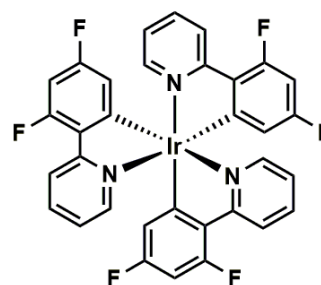
PF$_6^-$ for catalysts 3 to 5 are omitted for clarity sake

fac-**Ir(ppy)$_3$**
E$_{1/2}$(PC$^+$/PC*) = -1.73 V

Ir(dFppy)$_3$
E$_{1/2}$(PC$^+$/PC*) = -1.48 V
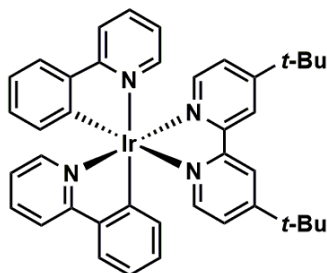
Ir(dtbbpy)(ppy)$_2$PF$_6$
E$_{1/2}$(PC$^+$/PC*) = -0.96 V
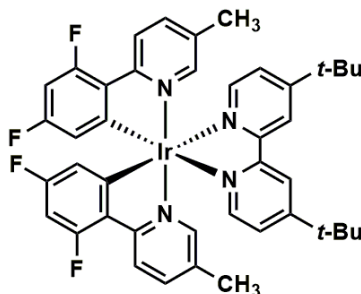
Ir[dF(CH$_3$)ppy]$_2$dtbbpyPF$_6$
E$_{1/2}$(PC$^+$/PC*) = -0.90 V
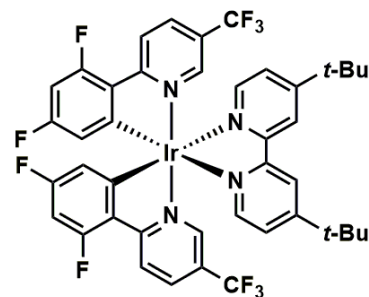
Ir[dF(CF$_3$)ppy]$_2$dtbbpyPF$_6$
E$_{1/2}$(PC$^+$/PC*) = -0.89 V

2.2.4 Preparation of Substrates Using Knoevenagel Condensation

With the optimal conditions, a series of alkylidenemalonates were synthesized using Knoevenagel condensation.[173] Commercially available aldehydes and malonates were refluxed with catalytic amounts of acetic acid and piperidine to afford the alkylidenemalonate products in moderate to good yields (Table 11).

Table 11. Synthesis of olefin substrates
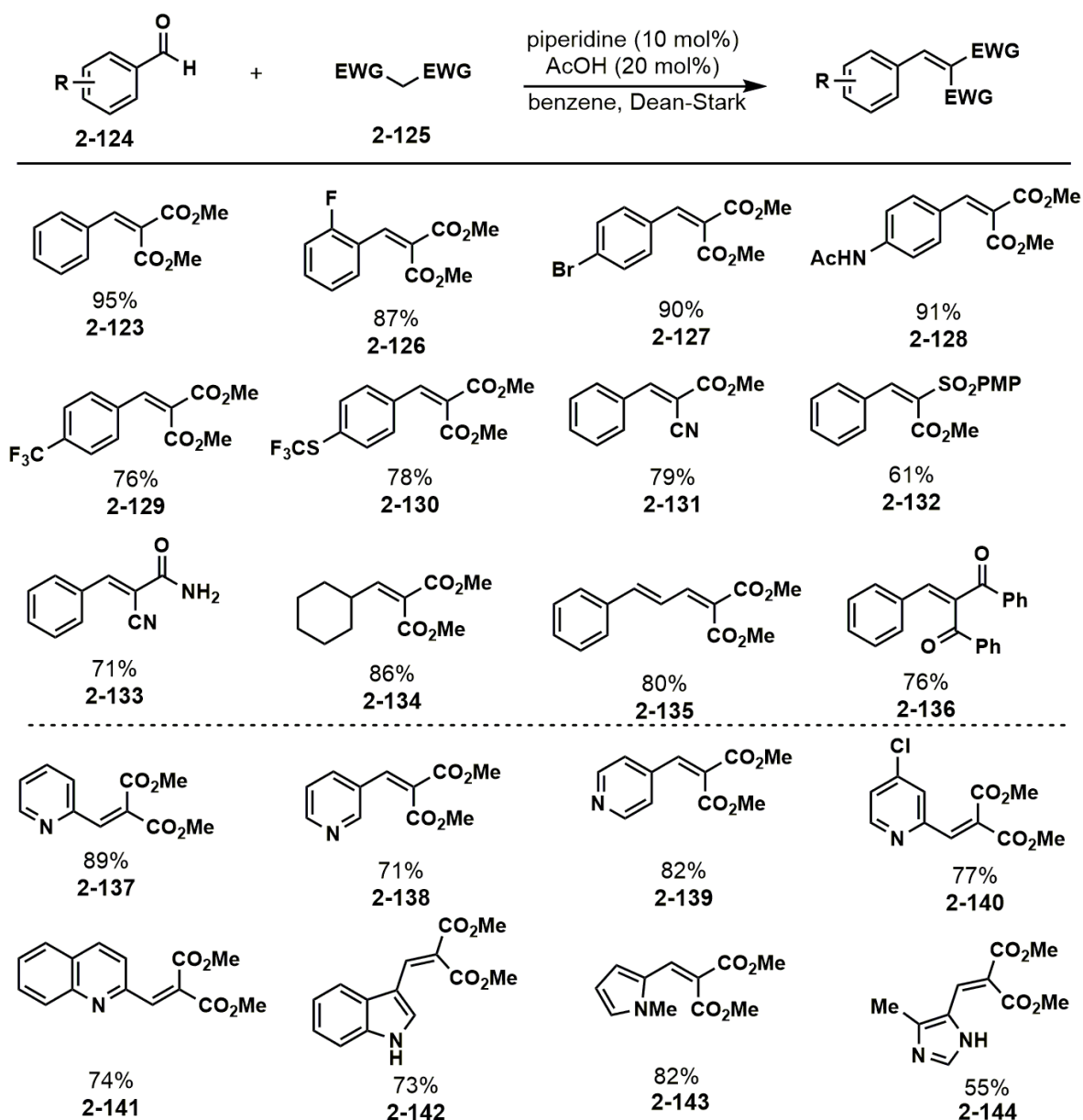
2.2.5 Aryl and Alkyl Substrate Scope

Differently substituted benzylidenemalonates can all be tolerated. Fluoro-, chloro-, and bromo- on the *o*-, *m*-, and *p*-positions all underwent the desired reaction smoothly (Table 12, **2-147** to **2-149**). Electron-donating substituents (methoxy and acetamide) also participated in the reaction

efficiently to give **2-151** and **2-152**. Under the current set of optimized conditions, previously examined substrates were reexamined. Expectedly, *trans*-chalcone and chromone gave 35% and 86% yields of **2-121** and **2-115**, respectively. Additionally, it was found that 3-chromone carboxylic acid **2-160** underwent concomitant decarboxylation to furnish **2-115** in 77% isolated yield (Table 12, bottom).

Table 12. Aryl and alkyl substrate scope

$(n\text{-Bu}_4N)_2S_2O_8$
Ir-**1**
1,3-dioxolane, Ar
household LEDs (15W x 4), 24 h

2-145

2-146

91% yield
2-122

85% yield
2-147

84% yield
2-148

92% yield
2-149

78% yield
2-150

35% yield
2-121

90% yield
2-151

76% yield[b]
2-152

86% yield[c]
2-115

78% yield
2-153

95% yield[e]
2-154

77% yield
2-155

76% yield
2-156

92% yield[d]
(dr = 1:1.2), **2-157**

95% yield[f]
2-158

83% yield[g]
2-159

decarboxylation[c]
2-160

2-115
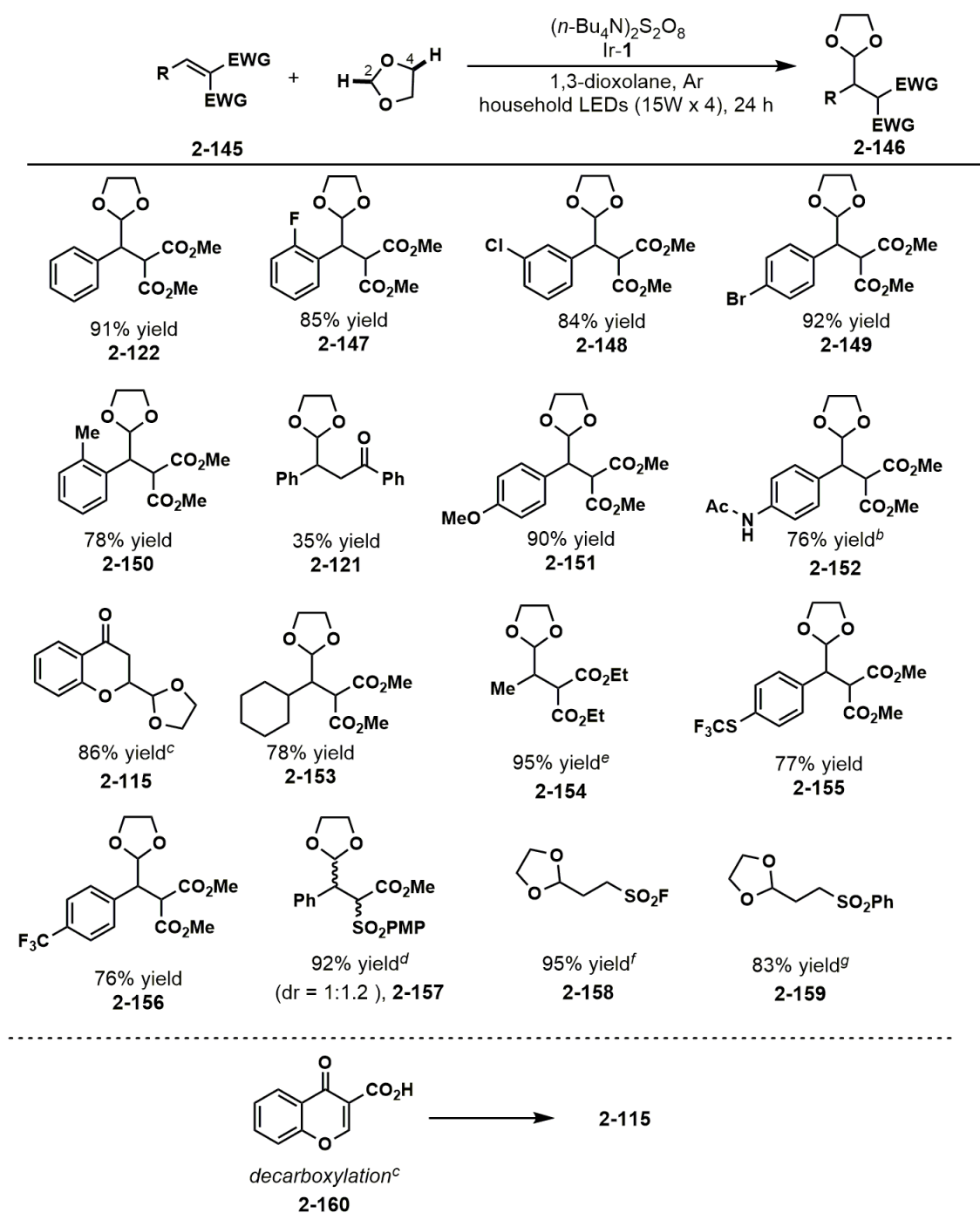
[a]General reaction conditions: alkene (1.0 equiv, 0.20 mmol), $(n\text{-Bu}_4N)_2S_2O_8$ (1.0 equiv, 0.20 mmol), 1,3-dioxolane (3.0 mL), *fac*-Ir(ppy)$_3$ (0.50 mol%), irradiated with household LEDs (15W x 4) for 24 h, external temp = 30 ºC. [b]0.50 equiv of (n-Bu$_4$N)$_2$S$_2$O$_8$ was used. [c]Chromone-3-carboxylic acid **2-160** afforded the decarboxylated product **2-115** in 77% yield. [d]0.10 mmol scale. dr was determined by ^{1}H NMR spectroscopy. [f]NMR yield using mesitylene as standard. PMP = *p*-methoxyphenyl. eInseparable mixture C-2/C-4 regioisomer (rr = 14 : 1).[g]Inseparable mixture of C-2/C-4 regioisomers (rr = 20 : 1).

Radical acceptors containing a single sulfone[174] or sulfonyl fluoride[149] are competent reacting partners. Thus formed **2-158** was anticipated to be useful for SuFEx chemistry.[175-176] During the examination of substrate scope, only **2-158** and **2-159** were formed as regioisomeric mixtures of C2–H (major, desired) and C4–H (minor, undesired) functionalizations. This is a known issue based on previous works by MacMillan and Doyle.[133,134b] However, it is intriguing to note that only sulfone and sulfonylfluoride have regioselectivity issues (*vide infra*).

2.2.6 *N*-Heterocyclic Substrate Scope

Because previous works[133-135] on *N*-heterocyclic substrates focused primarily on Minisci-type reactivity, it is interesting to test whether there could be orthogonal selectivity under our reaction conditions (Table 13). Pleasingly, when an alkylidenemalonate group was introduced on a pyridine ring, conjugate addition occurred preferentially. 2-, 3-, and 4-Pyridinyl substrates underwent smooth reaction with no observable Minisci reactivity (**2-161**, **2-162** and **2-163**). Chloropyridinyl substrate could also be functionalized to give **2-164**.

Table 13. *N*-Heteroaryl substrate scope

89% yield
2-161

71% yield
2-162

82% yield
2-163

77% yield
2-164

74% yield
2-165
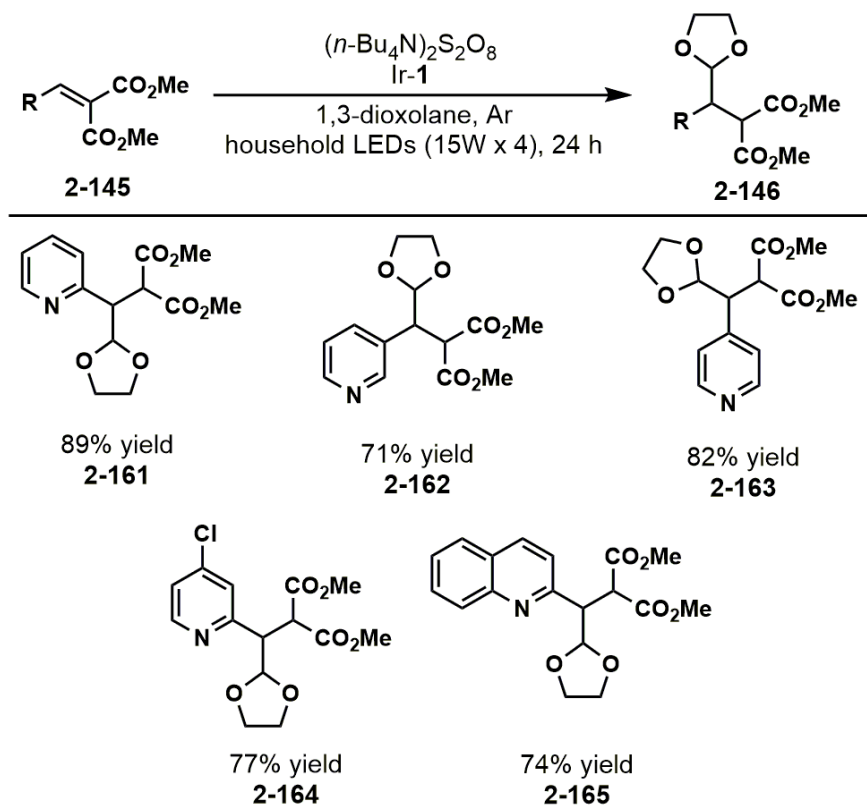
*a*General reaction conditions: alkene (1.0 equiv, 0.20 mmol), (n-Bu$_4$N)$_2$S$_2$O$_8$ (0.50 equiv, 0.10 mmol), *fac*-Ir(ppy)$_3$ (0.50 mol%), irradiated with household LEDs (15W x 4) for 24 h, external temp = 30 °C.

It was also observed that the pyridine containing products are highly water-soluble, and an aqueous workup ought to be avoided. To simplify the workup procedure, sub-stoichiometric (0.50 equiv) amount of (n-Bu$_4$N)$_2$S$_2$O$_8$ was used for the *N*-heterocyclic substrates. The crude materials without aqueous workup, after solvent removal, could be directly chromatographed to give products **2-161** to **2-165**.

In the literature,[137] vinylpyridine **2-166** has been a successful substrate toward hydroalkylation. However, under the current reaction conditions, no reaction could be observed (Scheme 50, top). It was wondered if the current reaction conditions would promote Minisci reaction in the absence of competing 1,4-addition pathways. When pyridine-2-carboxylate **2-167**

80

was subjected to the standard reaction conditions, no observable reaction was observed (Scheme 50, bottom). This suggested that an ester substituent alone was insufficient in activating a pyridine toward dioxolanyl addition.
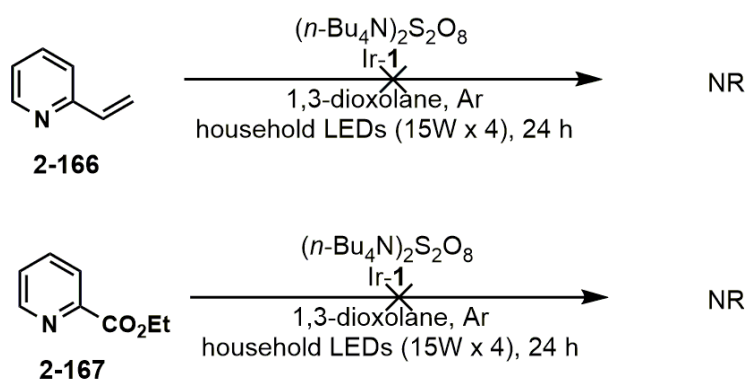
Scheme 50. Attempted dioxolane additions to pyridines

2.2.7 Limitations of Substrate Scope

The reaction is sensitive to the steric effects at the β-position of the olefin, which is unsurprising considering the usual steric preference of radical additions to less hindered positions of olefins (Figure 9).[178] The reaction with the tetrasubstituted olefin **2-167** did not afford any desired product; presumably due to the lack of a sterically accessible conjugate addition, the olefin starting material degraded under reaction conditions. The highly sterically encumbered enone **2-168** and chromone **2-117** both remained unreacted.

Alternate degradation pathways likely exist for highly conjugated substrates under the reaction conditions. α,β,γ,δ-Dienoate **2-135** was initially designed with the plan that thus formed α-centered radical undergoes an intramolecular cyclopropanation. However, the substrate degraded with no discernible product based on the ^{1}H NMR spectroscopic analysis of the reaction

mixture. The diaryl ketone **2-136** reacted to form the desired product in low yield (45%) determined by ^{1}H NMR analysis, along with another unidentifiable side-product. Unlike previous reports, malononitrile **2-59** was not a suitable substrate.[81] This stark difference in reactivity from literature precedents suggested a different mechanism might be operative. Benzoquinone **2-168** reacted partially to give a complex mixture. Although the electron-rich benzylidene substrates (**2-151** and **2-152**, see table 12) reacted efficiently, electron-rich *N*-heteroarylidene substrates were not suitable (**2-142** to **2-144**). β-Nitrostyrenes are likely also unstable under the reaction conditions, with 4-methoxy-β-nitrostyrene **2-170** affording low yield of 33% (NMR). Presumably due to the radical intermediacy of the reaction, phenol **2-171** failed to react. The reaction requires electron-deficient substrates due to the nucleophilic character of the dioxolan-2-yl radical, which was further corroborated by the lack of reactivity of the electron-rich squalene **2-172**.
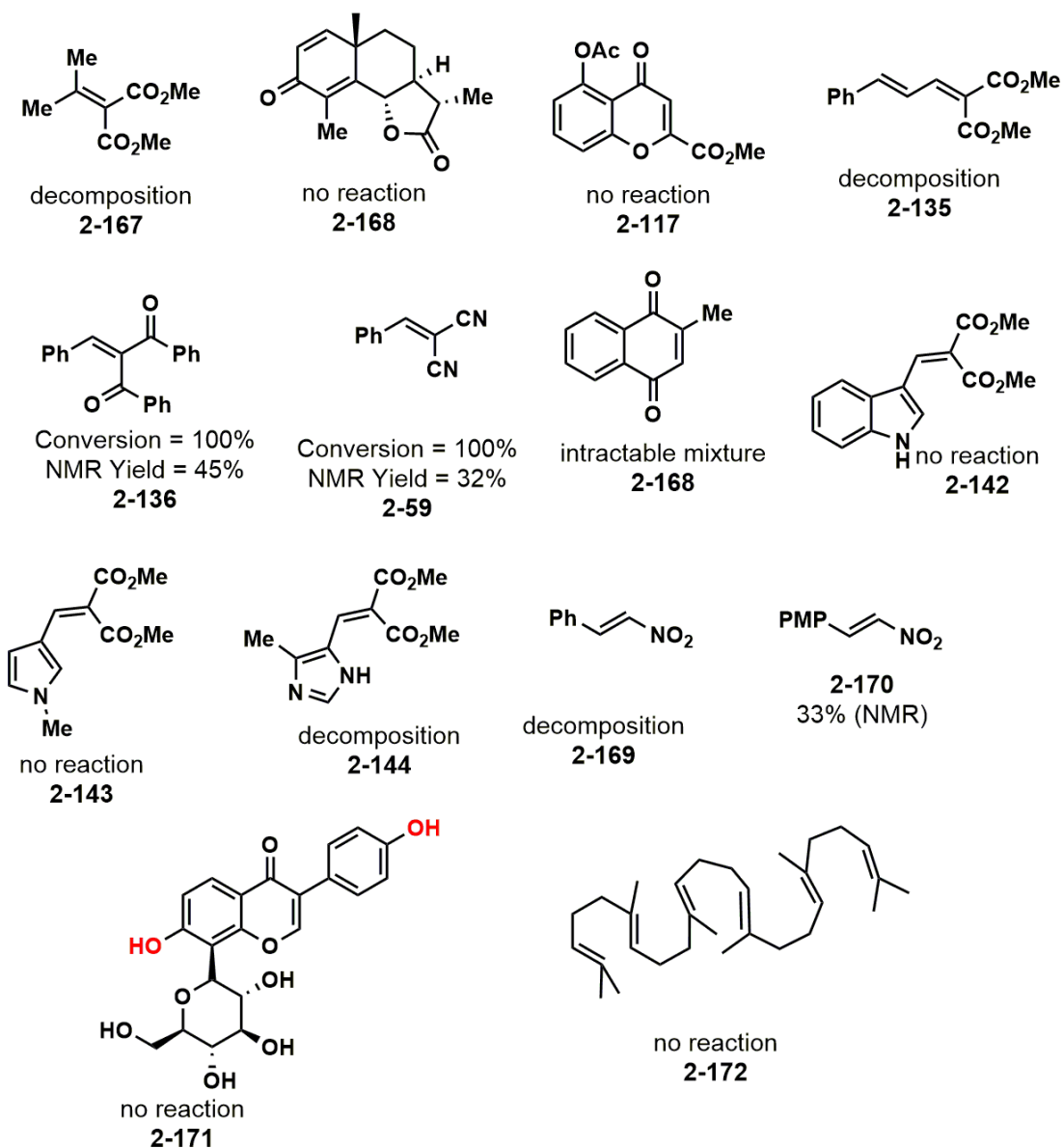
Figure 9. Attempted radical acceptors

Unlike previous works in the literature,[132, 133,137,138] this reaction has a more selective

substrate scope with regards to C–H donor (Table 14). Apart from 1,3-dioxolane, only the highly

structurally similar 1.3-benzodioxole[139] reacted to give **2-174** in 82% yield. Trioxane[135] showed

no apparent reactivity at room temperature but gave modest NMR yield of 38% when heated to 90

°C. It is surprising that the structurally similar diethyl acetal and trioxane are poor substrates. Phathalide and 4-chromanone are also unsuitable substrates for this reaction.

Table 14. Other C–H donors attempted

2-122

radical source (10 equiv)
(n-Bu$_4$N)$_2$S$_2$O$_8$ (1.0 equiv)
fac-Ir(ppy)$_3$ (0.50 mol%)

MeCN, Ar, rt
white LEDs (15W x 4)

+

R–H

2-173

82% (isolated)
2- 174

not detected
2-175

38% (NMR)
2-176

not detected
2-177

not detected
2-178
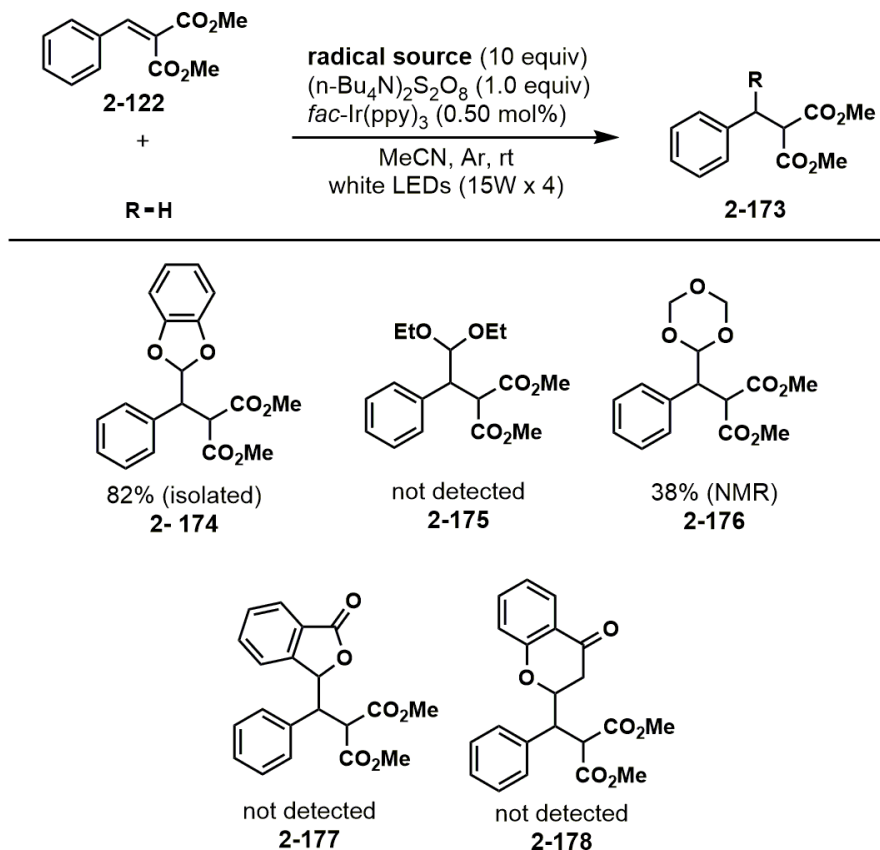
2.2.8 Mechanistic Investigations

An experiment to scavenge radical species with TEMPO confirmed the radical intermediacy of the mechanism (Scheme 51a). Most literature precedents for the light-mediated C–H functionalizations of ethers consists of a "closed" photoredox cycle. As mentioned previously, a closed photoredox cycle consists of an excited photocatalyst undergoing oxidative (or reductive)

quenching, and a terminal reductant (or oxidant) will be necessary to turn over the catalyst for closing the catalytic cycle.

In a radical chain process, issues such as the screening of a compatible terminal oxidant or reductant, its availability, and scalability can be avoided. Instead, a radical-chain approach would rely on the design of the substrate – their innate property that favors chain-propagating atom-abstraction processes. Because a sub-stoichiometric amount of (n-Bu$_4$N)$_2$S$_2$O$_8$ is enough for high yield and no reasonable turnover pathways could be perceived, it will be worthwhile to investigate the possibility of a radical chain mechanism.

a) Radical scavenging experiment

TEMPO (1.0 equiv)
(n-Bu$_4$N)$_2$S$_2$O$_8$ (0.50 equiv)
fac-Ir(ppy)$_3$ (0.5 mol%)
———————————————→
1,3-dioxolane, Ar
household LEDs

NR

2-122

----
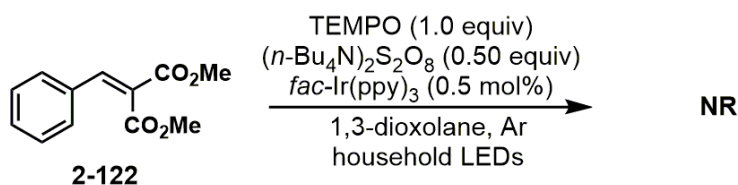
b) Catalytic [O] and low [Ir] loading experiments

2-122
(n-Bu$_4$N)$_2$S$_2$O$_8$ (n equiv)
fac-Ir(ppy)$_3$ (0.50 mol%)
———————————————→
1,3-dioxolane, Ar
household LEDs

2-123
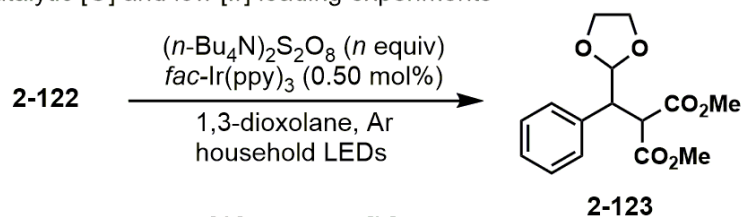
scale (mmol)	[O] (equiv)	[Ir] (mol%)	yields
0.20	0.25	0.50	97% (NMR)
5.0	1.0	0.050	89% (isolated)

----

c) Diethyl 2-bromo-2-methylmalonate as initiator

2-122
2-179 (0.25 equiv)
Ir[dF(CF$_3$)ppy]$_2$dtbbpyPF$_6$ (0.50 mol%)
———————————————→
1,3-dioxolane, Ar
household LEDs

2-123
93% yield
(isolated)

EtO$_2$C　CO$_2$Et
Me　Br
2-179

2-137
2-179 (0.10 equiv)
Ir[dF(CF$_3$)ppy]$_2$dtbbpyPF$_6$ (0.50 mol%)
———————————————→
1,3-dioxolane, Ar
household LEDs

2-161
85% yield
(isolated)
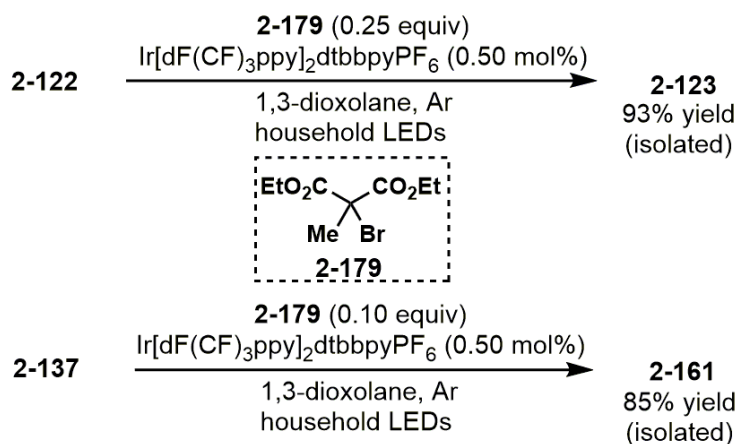
Scheme 51. Mechanistic experiments

The reaction was tested with 0.25 equiv of (n-Bu$_4$N)$_2$S$_2$O$_8$, but otherwise standard conditions, affording **2-123** in 97% yield (Scheme 51b). Additionally, it was hypothesized that if a radical chain was operative, the role of fac-Ir(ppy)$_3$ was solely to initiate the formation of sulfate radical anions, and the amount of the iridium reagent could be lowered below 0.50 mol%. The

reaction with a decreased loading of 0.050 mol% was examined, affording the desired product in 89% isolated yield (Scheme 51b). The lights-on/lights-off experiment (see the experimental section) also strongly suggest that a closed photoredox cycle is not operative. When diethyl 2-bromo-2-methylmalonate **2-179** was used in lieu of $(n\text{-Bu}_4\text{N})_2\text{S}_2\text{O}_8$ as the radical initiator, high isolated yields were also observed for the two substrates tested (Scheme 51c).

2.2.9 Proposed Mechanism

Firstly, it was reported[135] that under visible light conditions, $\text{SO}_4^{\cdot-}$ could be formed via photolysis of $\text{S}_2\text{O}_8^{2-}$ (Scheme 52). In line with this mechanism, control experiments had also shown that a moderate yield (76%) was obtained with visible light and $\text{S}_2\text{O}_8^{2-}$ (see Table 10, entry 6). Next, there appears to be correlation of the electrode potentials of Ir(III)* with the reaction yields (Table 10). This implies the role of [Ir] is to undergo oxidative quenching with $\text{S}_2\text{O}_8^{2-}$ to generate $\text{SO}_4^{\cdot-}$. Taken together, the formation of $\text{SO}_4^{\cdot-}$ occurs via two pathways: 1) [Ir] promotes single electron transfer (minor, path **A**), and 2) light promotes homolysis (major, path **B**). The oxygen-centered radical $\text{SO}_4^{\cdot-}$ then abstracts the hydrogen atom at the C-2 position from 1,3-dioxolane (step 2).[133,135] Subsequently, dioxolan-2-yl radical undergoes a 1,4-radical addition to **2-122** to form **2-180** (step 3). The regioselectivity of this step is presumably governed by the electronic bias of the nucleophilic radical[171] and the electrophilic olefin. The malonyl radical intermediate **2-180** abstracts the hydrogen atom from a second molecule of 1,3-dioxolane to generate another dioxolan-2-yl radical (step 4), propagating the radical chain.

Although the C–H abstraction by **2-180** (step 4) has been proposed in the literature,[137,172] to our knowledge, it has not been experimentally verified. If such abstraction is valid, then the

87

reaction can be initiated by a suitable source of the structurally and electronically related radical **2-181**. In the literature, 2-bromo-2-methyl malonate **2-179**, is a known source of the malonyl radical **2-181** via both C–Br bond homolysis and SET pathways.[179-181]
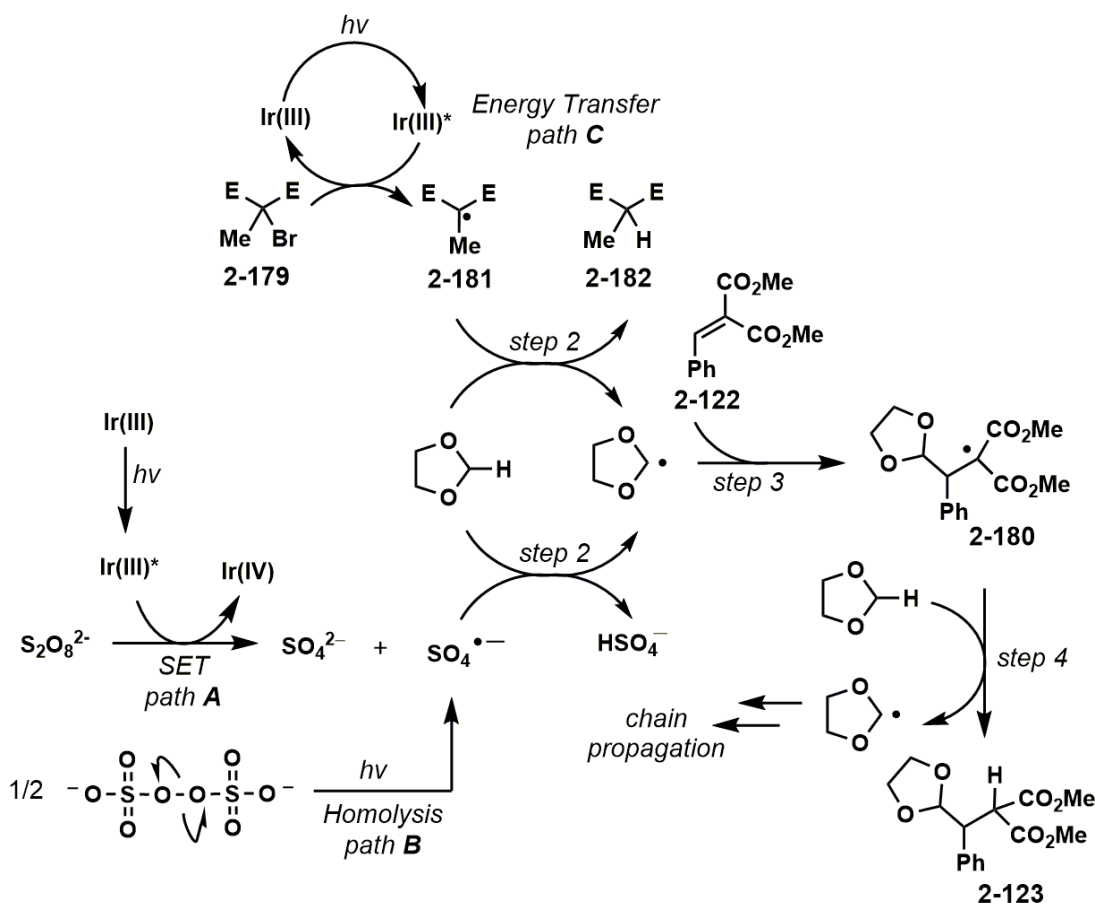
Scheme 52. Proposed mechanism with diverse initiation pathways

It is interesting from both a mechanistic and synthetic viewpoint to exploit the intermediacy of the radical **2-180**. We wondered whether a multicomponent reaction could be designed to trap the electrophilic radical (Scheme 53). Thus, a mixture of malonate **2-122** and excess styrene were reacted under standard reaction conditions. Unfortunately, the reaction appeared to be inhibited and no reaction was observed.
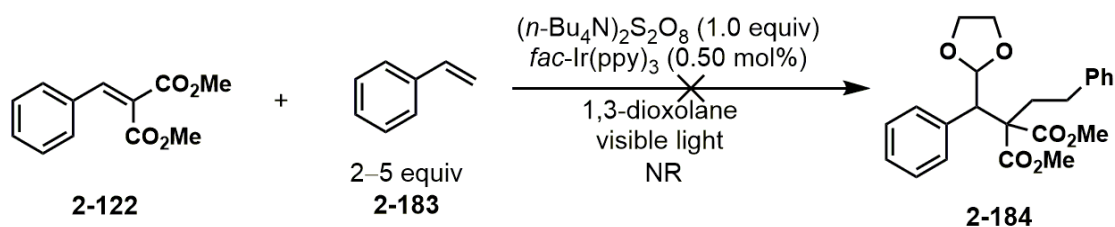
Scheme 53. Attempted trapping of malonyl radical

2.2.10 Investigation of α-Bromoesters and α-Bromomalonates as Radical Initiators

In the literature, there are examples of **2-179** forming malonyl radicals using Ru(II) and Ir(III).[179, 182-183] Both SET and energy transfer have been invoked as the pathway by which malonyl radicals are generated.[179, 182-184] Surprisingly, there was no observable reaction when **2-179** were used with *fac*-Ir(ppy)₃. Screenings with five commercially available [Ir] photocatalysts were performed (Table 15). The results show a direct correlation between the catalysts' emission energies and reaction efficiency. Ir[dF(CF₃)ppy]₂dtbbpyPF₆ having the highest emission energy of 60.5 kcal mol⁻¹ [185] gave the best yield. Because it is expected that malonyl radicals to be formed under both SET (with *fac*-Ir(ppy)₃) and energy transfer (with Ir[dF(CF)₃ppy]₂dtbbpyPF₆), it is intriguing that only the latter could promote a reaction.

Table 15. Optimization of conditions using bromomalonate as initiator
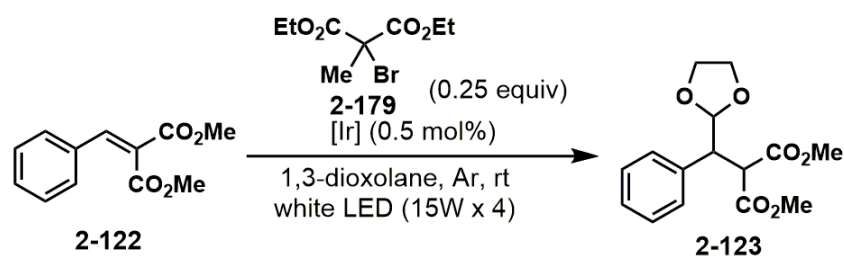
entry	photocatalyst	results
1	*fac*-Ir(ppy)$_3$	no reaction
2	Ir(dFppy)$_3$	no reaction
3	Ir(dtbbpy)(ppy)$_2$PF$_6$	no reaction
4	Ir[dF(CH$_3$)ppy]$_2$(dtbbpy)PF$_6$	partial conversion, nd
5	Ir[dF(CF$_3$)ppy]$_2$(dtbbpy)PF$_6$	86% (NMR yield)

nd = not determined

2.2.11 DFT Calculations of Dioxolane Addition

DFT calculations[186] were performed to study the proposed mechanism and to shed light on the factor(s) that limit(s) the reaction scope. Initially, we attempted to calculate the energetics using **2-122** and **2-154** as the substrates; however, conformational flexibilities in these acyclic molecules caused locating of transition states to be challenging. Specifically, attempts to locate transition states for the putative radical addition step were unsuccessful. It was considered whether the dioxolanyl radical addition might be concerted, but no transition states corresponding to a concerted addition step could be located. Eventually, chromone **2-114** was chosen as the substrate for DFT calculations due to its conformational rigidity. Gratifyingly, the transition states for radical addition and C–H abstraction could both be located. Since the dielectric constants of THF and 1,3-dioxolane are reasonably similar (7.50 and 7.13 D, respectively),[120] THF was chosen as a close approximate for solution-phase calculations.

First, dioxolanyl addition to **2-114** is exergonic by 6.9 kcal mol^{-1} (Scheme 54). The $\Delta G^{\ddagger}_{THF}$ of dioxolanyl addition was calculated to be 10.2 kcal mol^{-1}. The subsequent C–H abstraction step was found to be rate-limiting. Both *syn-* and *anti*-attacks with respect to the first dioxolane ring were considered in the calculations. The computed results showed that there is little facial preference for the C–H abstraction step ($\Delta G^{\ddagger}_{THF}$ = 21.2 vs 21.3 kcal mol^{-1}). Interestingly, the C–H abstraction is also endergonic by ca. 2.4 kcal mol^{-1}. Therefore, the C–H abstraction step might be reversible under the reaction conditions. This result might explain the underlying reason for needing large excess (>200 equiv) of dioxolane. In the presence of excess dioxolane, the equilibrium for C–H abstraction is driven toward **2-115**.
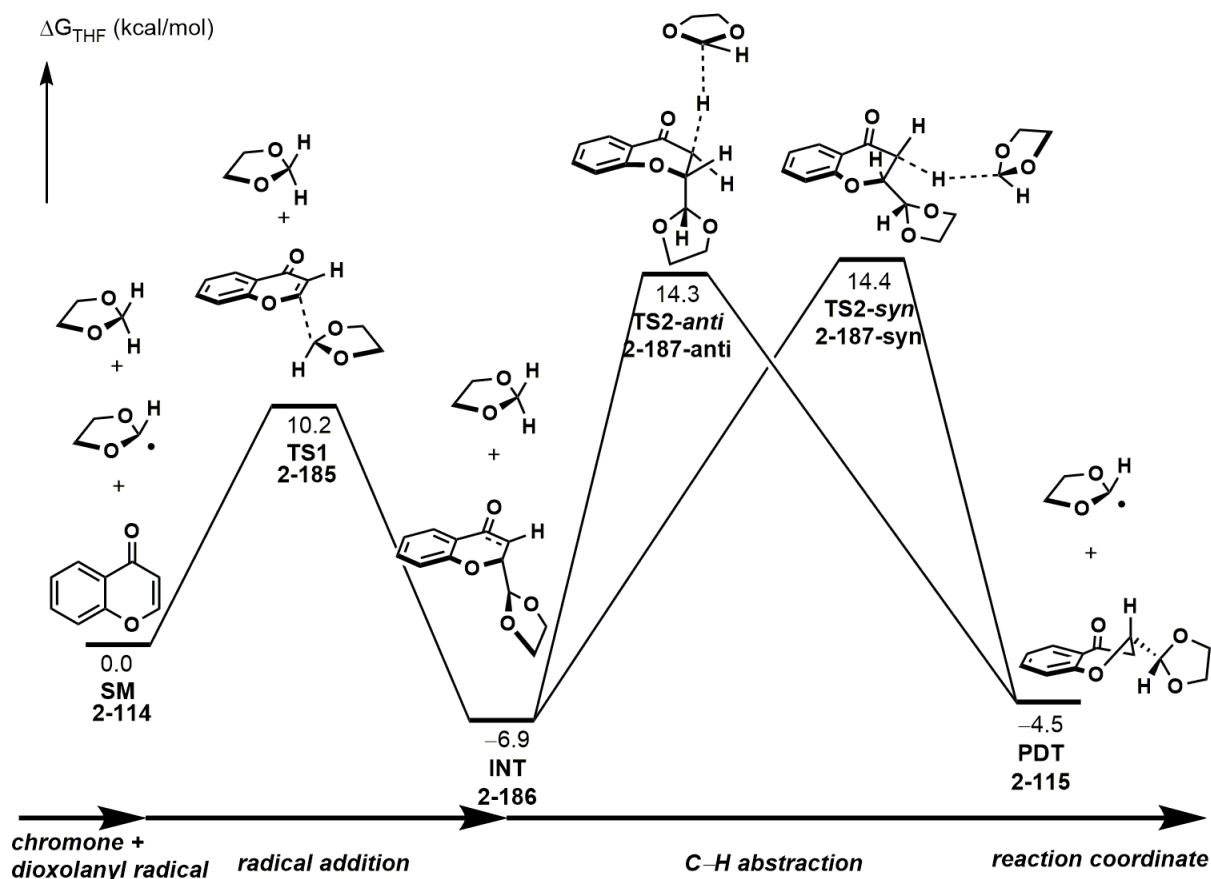
Scheme 54. DFT calculations for chromone **2-114**. M062X/6-311++G(d,p)/SMD(THF)//B3LYP/6-31G(d)

With the success in computing the mechanism for chromone **2-114**, we proceeded to use 2-methylchromone **2-188** as a substituted model substrate for computations (Scheme 55). Dioxolanyl addition to **2-188** had a slightly higher barrier of 12.2 kcal mol^{-1} and is also relatively less exergonic compared to that for **2-114**. The C–H abstraction step is still the rate-limiting step with a barrier of 21.6 kcal mol^{-1}. In this case, based on visual analysis of intermediate **2-190** (see the Experimental section for optimized structure), only the anti-attack was calculated, because syn-attack is deemed sterically inaccessible. The reaction is exergonic only by overall 1.7 kcal mol^{-1}. The data seem to suggest that the addition of steric bulk at the site of C–C bond formation might overall increase the reversibility of the reaction.
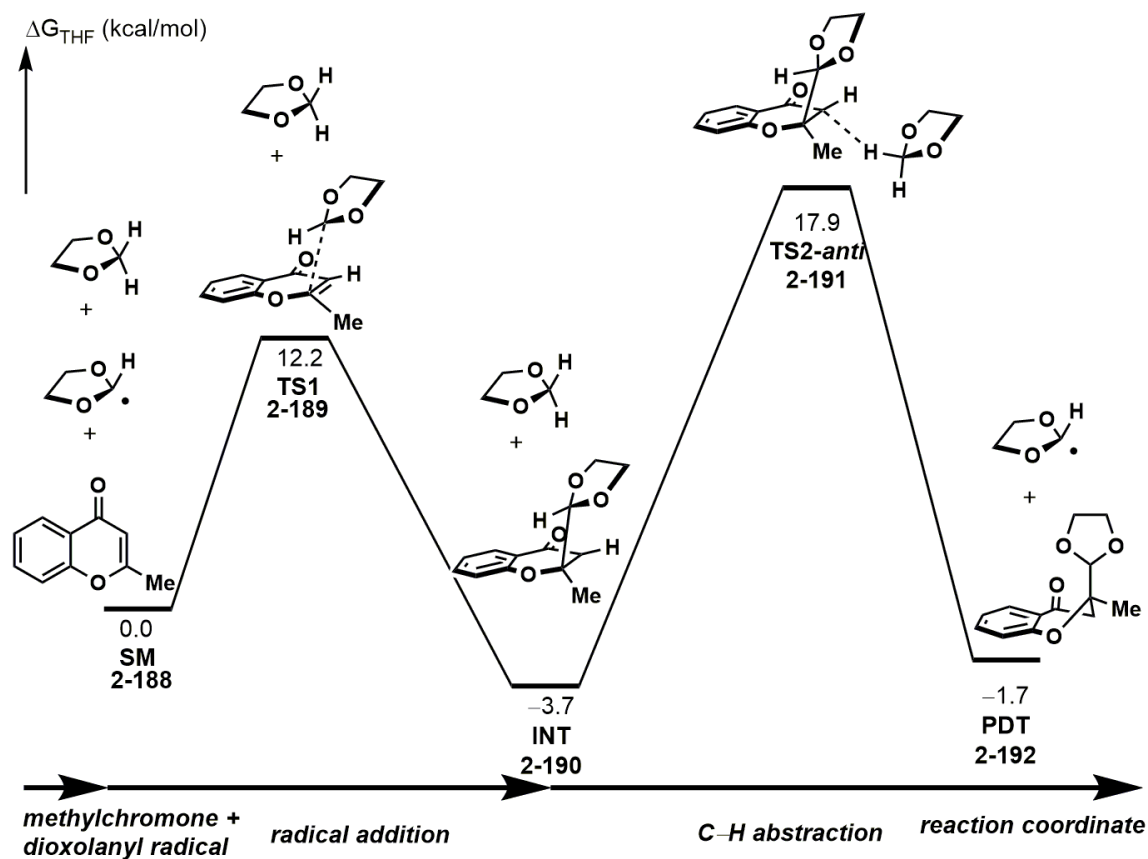
Scheme 55. DFT calculations for 2-methylchromone. M062X/6-311++G(d,p)/SMD(THF)//B3LYP/6-31G(d)

2.2.12 DFT Calculations of C–H Abstractions

It is uncertain whether the computational results of chromone could be applied for other substrates with different sterics and electronics (Table 16). Due to the challenges in locating the transition state for the addition step, efforts were focused on determining the energetics of the C–H abstraction step. The relationship of the ΔG and $\Delta G^{\ddagger}$ with respect to the sterics and electronics of the radicals were calculated.

Table 16. Calculation of ΔG and $\Delta G^{\ddagger}$ for C–H abstractions from dioxolane

	2-195	2-196	2-197
$\Delta G_{(THF)}$	1.6 kcal/mol	2.7 kcal/mol	4.9 kcal/mol
$\Delta G^{\ddagger}_{(THF)}$	22.7 kcal/mol	21.7 kcal/mol	23.9 kcal/mol

(SO$_3$ radical anion: $\Delta G_{(THF)}$ = -13.3 kcal/mol, $\Delta G^{\ddagger}_{(THF)}$ = 5.9 kcal/mol)
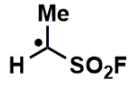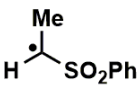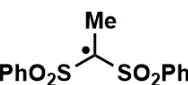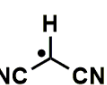
	2-198	2-199	2-200	2-201
$\Delta G_{(THF)}$	-5.9 kcal/mol	-7.3 kcal/mol	-3.4 kcal/mol	2.4 kcal/mol
$\Delta G^{\ddagger}_{(THF)}$	15.3 kcal/mol	18.5 kcal/mol	15.2 kcal/mol	16.9 kcal/mol

Level of theory: M062X/6-311++G(d,p)/SMD(THF)//B3LYP/6-31G(d)

Although a definitive trend could not be established, there appeared to be correlation with the reactivities of the substrates that possess these electron-withdrawing substituents. First, SO$_4^{\bullet-}$ undergoes the most exergonic C–H abstraction and has the lowest $\Delta G^{\ddagger}$ among all the radicals computed. Although C–H abstraction of dioxolane by SO$_4^{\bullet-}$ has been reported the literature,[69, 80]

there are no computational data to support its feasibility. Nevertheless, the formation of an O–H bond is likely the main driving force for a relatively more exergonic C–H abstraction.

Next, C(2)–H abstractions with sulfonyl **2-199**, bis-sulfonyl **2-200**, or sulfonylfluoride **2-198** radicals are exergonic. The $\Delta G^{\ddagger}$ values are also significantly lower than other substrates, with bis-sulfonyl radical **2-200** having the lowest $\Delta G^{\ddagger}$. The data imply that **2-198**, **2-299**, and **2-200** may even be reactive enough to also abstract the hydrogen from C4 of dioxolane. To correlate to the results in Table 12, these data helped explain why sulfonylfluoride **2-158** and sulfone **2-159** were formed as C-2/C-4 regioisomers. Although α,α-bisulfonylethylene was not examined as a substrate in Table 12, it is predicted that a regioisomeric mixture of C-2 and C-4 products should be formed.

Expectedly, radical **2-197** derived from arylketone is calculated to undergo endergonic C–H abstraction with 1,3-dioxolane. Furthermore, its $\Delta G^{\ddagger}$ was computed the highest among the radicals investigated. C–H abstraction by malonyl radical **2-196** as endergonic by 2.7 kcal mol^{-1}. Malononitrile radical **2-201** have comparable energetics compared to **2-196**. However, benzylidene malononitrile **2-59** (see Figure 9) is not a suitable substrate under standard reaction conditions. This is likely due to the instability of **2-59** under our reaction conditions. Lastly, the energetics for **2-196** caused us to reconsider the observations in Table 15 (entries 1 vs 5). As previously mentioned, depending on [Ir], malonyl radicals can be generated by either SET or energy transfer pathway. Additionally, under energy transfer pathway, bromine radicals are also generated (Scheme 56). The implication is that bromine radicals could be responsible for the result in Table 15, entry 5.
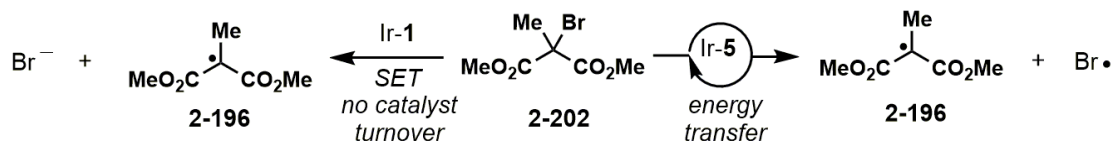
Scheme 56. α-Bromomalonate under SET and energy transfer pathways

Ethyl 2-bromo-2-phenylpropanoate **2-203** was then tested as the initiator. The desired reaction occurred in 93% yield (Scheme 57). When a stoichiometric reaction of α-bromomalonate **2-179** and dioxolane was performed under standard conditions, the reduced malonate **2-204** was observed in ca. 45% yield (Scheme 58). The formation of the reduced malonate was confirmed by comparing the ^{1}H NMR spectrum of the reaction mixture without purification to that of a commercial sample. Although designed as a mechanistic experiment, the stoichiometric experiment of Scheme 58 shows the potential method to reductively debrominate α-bromomalonate using 1,3-dioxolane as the hydrogen source.
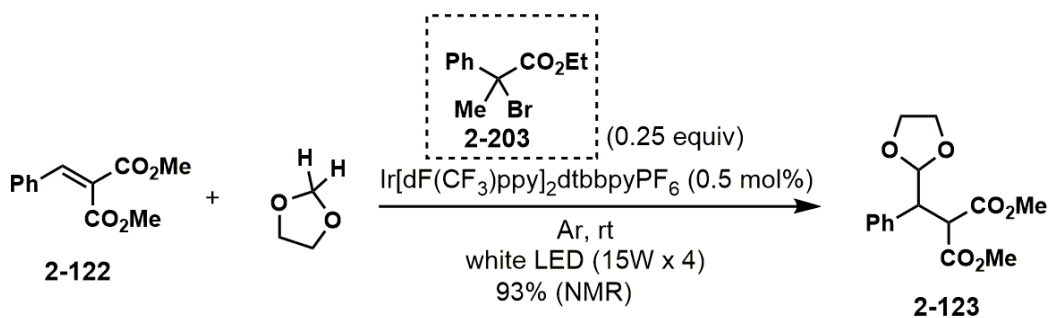
Scheme 57. Testing a different α-bromoester initiator
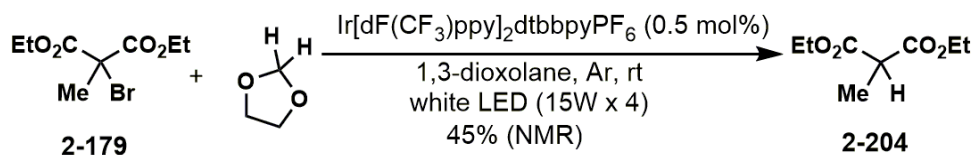
Scheme 58. Stoichiometric reaction of α-bromomalonate with dioxolane

Taking all computation and experimental results together, when the reaction between **2-122** and dioxolane was initiated by an α-bromomalonate, the initiation might include C–H abstraction from *both* malonyl and bromine radicals (Scheme 59). Under the energy transfer[188] pathway in which malonyl radicals could be continuously generated, C–H abstraction is possible despite the unfavorable energetics. In the case of a SET pathway, there is no catalyst turnover, and only a maximum of 0.5 mol% malonyl radicals could be formed, likely insufficient to generate a detectable amount of product. Lastly, it is noteworthy to mention that the reductive bromination of an α-bromomalonate was achieved with dioxolane as the hydrogen source. Previously, it has been shown that similar transformations were performed using silane[189] or Hunig's base[179, 190] as the hydrogen source.
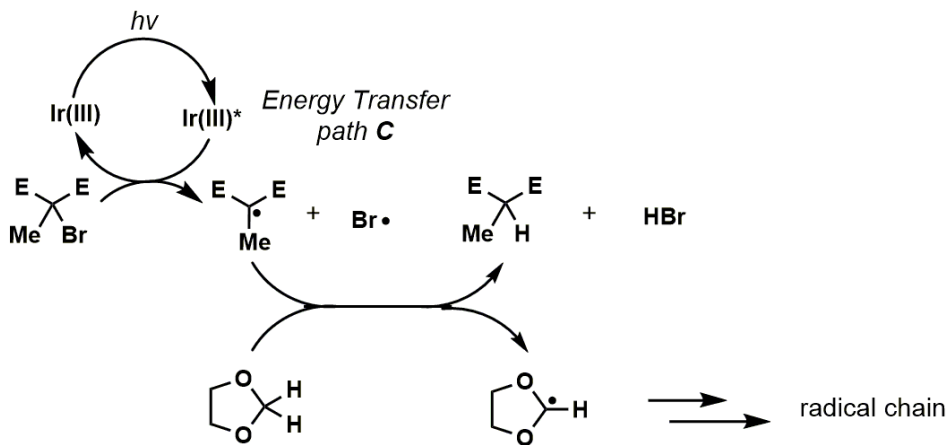
Scheme 59. Revised initiation step with α-bromomalonate

96

2.2.13 Attempted Synthetic Application

An obvious derivatization of the product would be the deprotection of the acetal in **2-122** to yield

the free aldehyde **2-205** (Scheme 60). Attempts to unmask the acetal under typical conditions (e.g.,

dilute HCl[138,146-148]) have thus far been unsuccessful. Furthermore, efforts to trap the free aldehyde

in an intramolecular aldol to give **2-206** failed as well.[191] It appears that the nucleophilic malonate

might be a cause for the difficulty in forming the free aldehydes.
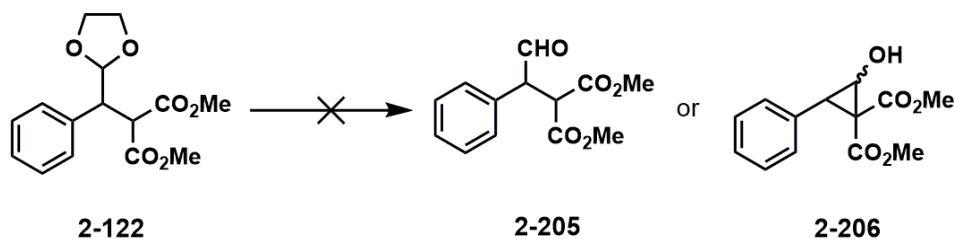
Scheme 60. Attempted deprotection of acetal

2.3 Conclusions

In conclusion, conjugate radical addition of 1,3-dioxolane to a variety of electronically

activated olefins was achieved. A radical-chain mechanism was proposed and supported by

mechanistic experiments. The same transformation could also be initiated by α-bromoesters or α-

bromomalonates. DFT calculations were performed to gain mechanistic insights. The C–H

abstraction step is likely the rate-limiting step. Further DFT calculations were performed for model

systems undergoing C–H abstractions with 1,3-dioxolane. The computed data provide a plausible

reason as to why substrates containing sulfonyl fluoride (**2-158**) or sulfone (**2-159**) are particularly

reactive and afforded regioisomers.

3.0 Experimental Section

3.1 General Considerations

Commercially available chemicals were purchased from Sigma-Aldrich, Alfa Aesar, Strem, Acros or Oakwood and used without further purification, unless otherwise indicated. MnO_2 was purchased from Alfa Aesar (catalog number: 14340). The nitro-Grela catalyst was purchased from Strem and used as received. Glasswares were either flamed-dried immediately prior use or oven-dried (140 °C, overnight). Moisture-sensitive reactions were performed under a nitrogen atmosphere with standard Schlenk techniques unless otherwise stated. K_2CO_3 was dried at 100 °C under high vacuum for 2 h immediately before use. Ethoxyacetylene was purchased from Alfa Aesar, distilled, and stored under argon at −20 °C. Cerium(III) chloride was dried according the procedure reported by Dimitrov et al.[192] Diisopropylamine and tetramethylpiperidine were distilled over CaH_2 and stored over KOH pellets.

Tetrahydrofuran (THF) was freshly distilled from sodium/benzophenone. *N,N*-Dimethylformamide (DMF) was distilled over silica gel and stored over 4Å molecular sieves, Dichloromethane (DCM) and 1,2-dichloroethane (DCE) were passed through a column of activated basic alumina (Al_2O_3) and stored over 3Å molecular sieves. Acetonitrile (MeCN) and methanol (MeOH) were stored over 3Å molecular sieves. 1,4-Dioxane was purchased from Acros Organics and used as received.

For photochemistry, solvents were degassed by sonication for 45 min or sparging with nitrogen gas for 30 min immediately before use. LEDs used are GE lighting Brightstik[TM] (15 W, 1600 lumen, daylight). Iridium photocatalysts were purchased from Strem or Sigma-Aldrich and

stored in dark amber bottles as secondary containers; the catalysts were used as received. Tetrabutylammonium persulfate (n-Bu$_4$N)$_2$S$_2$O$_8$ was prepared using a protocol reported by Yeung et al.[110] and stored in the dark at room temperature for up to two months.

Solvents used for NMR spectroscopy were purchased from Cambridge Isotope Laboratories. CDCl$_3$ was stored over anhydrous K$_2$CO$_3$. All 1D and 2D NMR spectra were recorded on Bruker AVANCE III 300, 400, and 500MHz spectrometers and calibrated using either tetramethylsilane or residual solvent peaks as internal reference. CDCl$_3$ with 1% w/w CD$_3$OD was used to characterize compounds with exchangeable protons. NMR yields were determined using mesitylene as external standard. Isolated yields refer to chromatographically purified materials, unless otherwise stated, and characterized by both NMR spectroscopy and high-resolution mass spectrometry (HRMS). The following abbreviations are used to indicate the multiplicities: s, singlet; d, doublet; t, triplet; q, quartet; m, multiplet; br, broad; app, apparent, or combinations thereof. HRMS data were obtained on a GCT, Micromass UK Ltd and Q-Tof Ultima API, Micromass UK Ltd. Reactions were monitored using thin-layer chromatography (TLC) or ^{1}H NMR spectroscopic analysis of crude material. All reactions were monitored by TLC carried out on 0.25-mm Merck silica gel plates (60F-254) using UV light (254 nm) for visualization or *p*-anisaldehyde in EtOH, 0.2% ninhydrin in EtOH, 2.4% phosphomolybdic acid/1.4% H$_3$PO$_4$/5% H$_2$SO$_4$ in water, or alkaline KMnO$_4$ solutions as a developing agents and heat for visualization as necessary. SiliaFlash P60 (230–400 mesh) was used for flash chromatography.

3.2 Experimental for Chapter 1

3.2.1 First Generation Route

(4*S*,5*S*)-2,2-dimethyl-4-((*R*)-oxiran-2-yl)-5-vinyl-1,3-dioxolane **(1-93)** Step 1) Concentrated H$_2$SO$_4$ (1.2 mL) was added portion-wise over 5 min to a stirring suspension of D-ribose (150 g, 1.00 mol) in acetone (2 L). The reaction was stirred at room temperature for 2 h. The crude solution was cooled in an icebath and neutralized with saturated K$_2$CO$_3$. The crude material was filtered through a pad of Celite®, and the filtrate was concentrated to give a pale-yellow syrup (606 g).

Step 2) A suspension of MePh$_3$P$^+$I$^-$ (294 g, 727 mmol) in THF (1.9 L) was mechanically stirred and cooled to 0 °C. *t*-BuOK (69.0 g, 621 mmol) was added portion-wise at 0 °C, and the resulting mixture was stirred at this temperature for 15 min. The reaction mixture was warmed to room temperature and stirred for an additional 2 h. The yellow suspension was recooled to 0 °C, and a portion of the product from step 1 (40.1 g, ca.207 mmol) in THF (100 mL) was added via an addition funnel over ca.30 min. The reaction temperature was gradually increased to room temperature overnight. The crude reaction mixture was quenched with water, and the layers partitioned. The aqueous layer was extracted with EtOAc, and the combined organic layer dried over Na$_2$SO$_4$. The crude material was azeotroped with PhH (3 × 100 mL) and dried under high vacuum overnight to give a brown syrup.

Step 3) Crude material from step 2 was dissolved in DCM (1 L), and n-Bu$_2$SnO (1.74 g, 7.00 mmol) was added in one-portion. p-TsCl (76.0 g, 0.40 mol) was added portion-wise to the stirring mixture. Et$_3$N (28.8 mL, 207 mmol) was added via an addition funnel over ca.15 min, and the resulting mixture was stirred at the same temperature overnight. The reaction was concentrated *in vacuo* to approximately half of its original volume to which MeOH (400 mL) was added. K$_2$CO$_3$ (77.1 g, 560 mmol) was added in one-portion, and the resulting suspension was stirred at room temperature for 40 h. Excess solid was filtered off, and the filtrate was concentrated *in vacuo*. The crude material was purified by flash column chromatography (SiO$_2$, 0→20% Et$_2$O in hexanes) afforded epoxide **7** as a yellow oil (18.0 g, 51% over 3 steps). The data for **7** were consistent with those of the literature.[56]
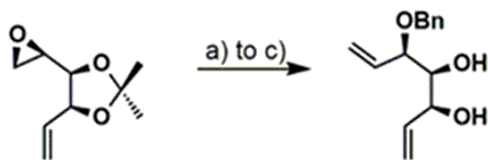
(3S,4S,5R)-5-(benzyloxy)hepta-1,6-diene-3,4-diol **(1-94)** Step a) A suspension of Me$_3$S$^+$I$^-$ (28.6 g, 140 mmol) in THF (150 mL) was cooled to −20 °C. n-BuLi (2.5 M in hexanes, 49 mL, 123 mmol) was added slowly along the walls of the round-bottom flask over 20 min, and the resulting mixture was stirred for an additional 20 min. Epoxide **7** (6.86 g, 40.3 mmol) in THF (10 mL) was added dropwise over 20 min. The reaction mixture was gradually warmed to −10 °C over 2.5 h. The reaction was quenched with brine (20 mL), and the solids were filtered off. The layers were partitioned, and the aqueous layer was extracted with Et$_2$O (80 mL × 2). The combined organic layers were dried over Na$_2$SO$_4$, filtered through a cotton plug, and concentrated *in vacuo* to afford the allylic alcohol as a yellow oil.

Step b) The crude allylic alcohol in DMF (120 mL) was cooled to -15 °C and NaH (3.00 g, 75.0 mmol) was added portion-wise at this temperature over 5 min. The reaction was stirred for another ca.45 min, and BnBr (3.8 mL, 32.0 mmol) was added dropwise over 5 min. The reaction was gradually warmed to 0 °C over 4 h and quenched with sat. NH_4Cl (50 mL). The aqueous layer was extracted with Et_2O (100 mL × 2). The combined organic layers were dried over Na_2SO_4 and filtered through a cotton plug. The solvent was removed *in vacuo* to afford the benzyl ether as a yellow oil. (*Note: We performed steps a and b in 40 mmol batches and combined three batches for step c*)

Step c) CSA (3.71 g, 16.0 mmol) was added to a solution of crude benzyl ether in MeOH (1 L). The reaction was stirred at room temperature for ca.3 d. The solvent was evaporated *in vacuo*, and the crude material purified by flash column chromatography (SiO_2, 10→40% EtOAc in hexanes) to give diol **1-94** as a yellow oil (17.0 g, 60% over 3 steps).

Data for **1-94**: R_f = 0.34 (50% EtOAc in hexanes); $[a]_D^{20} = -53.7$ (*c* 1.0, $CHCl_3$); IR (neat) 3400 (br, O-H), 3087, 2983, 2875, 1642, 1497, 1454, 1424, 1391, 1288, 1210, 1068, 1028 cm^{-1}; ^{1}H NMR (400 MHz, 1% CD_3OD in $CDCl_3$) δ 7.37–7.28 (m, 5H), 5.96 (ddd, *J* = 17.2, 10.4, 6.4 Hz, 1H), 5.89 (ddd, *J* = 17.2, 10.4, 8.0 Hz, 1H), 5.46–5.31 (*app* m, 3H), 5.25 (d, *J* = 10.4 Hz, 1H), 4.62 (d, *J* = 11.6 Hz, 1H), 4.35 (d, *J* = 11.6 Hz, 1H), 4.26 (*app* t, *J* = 6.0 Hz, 1H), 3.90 (*app* t, *J* = 7.2 Hz, 1H), 3.69 (*app* t, *J* = 6.0 Hz, 1H); ^{13}C NMR (100 MHz, 1% CD_3OD in $CDCl_3$) δ 137.7, 136.7, 135.2, 128.4, 127.9, 127.8, 120.4, 117.2, 81.9, 74.8, 73.6, 70.4; HRMS (ESI-TOF): *m/z* for [M + H]$^+$ $C_{14}H_{19}O_3$, calcd. 235.1329, found 235.1322.
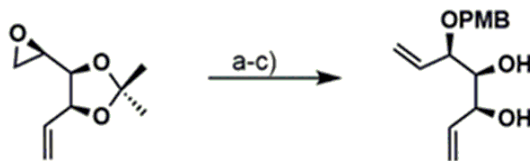
(3S,4S,5R)-5-((4-methoxybenzyl)oxy)hepta-1,6-diene-3,4-diol (1-95) Step a) Me$_3$S$^+$I$^-$ (7.10 g, 34.8 mmol) was suspended in THF and cooled to −20 °C. *n*-BuLi (2.5 M, 12.4 mL, 31.0 mmol) was added slowly along the walls of the round-bottom flask over 5 min, and the resulting mixture was stirred for an additional 1 h. Epoxide **7** (1.70 g, 10.0 mmol) was added dropwise over 10 min. The reaction mixture was gradually warmed to 0 °C over 1.5 h and stirred for another 1 h at the same temperature. The reaction was quenched with brine (20 mL), and the solids were filtered off using a frit funnel. The layers were partitioned, and the aqueous layer was extracted with Et$_2$O (20 mL × 2). The combined organic layers were dried over Na$_2$SO$_4$, filtered through a cotton plug, and concentrated *in vacuo* to afford the allylic alcohol as a yellow oil (1.85 g).

Step b) A solution of the crude allylic alcohol (1.85 g) in DMF (33 mL) and cooled to −20 °C. NaH (720 mg, 18.0 mmol) was added portion-wise over 5 min and the resulting mixture was stirred for an additional ca.30 min. PMBCl (1.4 mL, 10.0 mmol) was added dropwise and the reaction mixture was gradually warmed to room temperature overnight (ca.12H). The reaction mixture was cooled to 0 °C, quenched with sat. NH$_4$Cl (2 mL) and poured into water (330 mL). The aqueous layer was extracted with Et$_2$O (30 mL × 2). The combined organic layers were dried over Na$_2$SO$_4$, filtered through a cotton plug, and concentrated *in vacuo*. The crude PMB ether (3.25 g) was obtained as a yellow oil.

Step c) A solution of the PMB ether (3.25 g) in THF (100 mL) was cooled in a thawing ice-water bath (12 °C). 2 M HCl (120 mL) was added portion-wise, and the resulting reaction mixture was gradually warmed to room temperature over 6 h and stirred for an additional 3 h. THF

was removed *in vacuo*, and the crude material was dissolved in EtOAc, poured into water, and partitioned. The aqueous layer was extracted with EtOAc (30 mL × 2). The combined organic layers were dried over Na_2SO_4, filtered through a cotton plug, and concentrated *in vacuo*. The crude material was purified by flash column chromatography (SiO_2, 10→40% EtOAc in hexanes) to give diol **9** as a pale-yellow oil (1.65 g, 62% over 3 steps).

Data for **1-95**: R_f = 0.29 (50% EtOAc in hexanes); $[\alpha]_D^{23}$ = −40.5 (*c* 1.0, $CHCl_3$); IR (neat) 3433 (br, O-H), 2908, 1613, 1514, 1248, 1034 cm^{-1}; ^1H NMR (400 MHz, 1% CD_3OD in $CDCl_3$) δ 7.24 (d, *J* = 8.4 Hz, 2H), 6.88 (d, *J* = 8.4 Hz, 2H), 5.95 (ddd, *J* = 17.2, 10.4, 6.4 Hz, 1H), 5.88 (ddd, *J* = 17.6, 10.4, 8.0 Hz, 1H), 5.44 (d, *J* = 10.4 Hz, 1H), 5.39 (d, *J* = 17.2 Hz, 1H), 5.32 (d, *J* = 17.2 Hz, 1H), 5.24 (d, *J* = 10.8 Hz, 1H), 4.55 (d, *J* = 10.8 Hz, 1H), 4.28 (d, *J* = 11.2 Hz, 1H), 4.25 (*app* t, *J* = 5.6 Hz, 1H), 3.88 (*app* t, *J* = 6 Hz, 1H), 3.81 (s, 3H), 3.65 (*app* t, *J* = 6.0 Hz, 1H); ^{13}C NMR (100 MHz, 1% CD_3OD in $CDCl_3$) δ 159.3, 136.8, 135.3, 129.8, 129.6, 120.4, 117.2, 113.8, 81.7, 74.7, 73.7, 70.1, 55.3; HRMS (ESI-TOF): *m/z* for $[M + H]^+$ $C_{15}H_{21}O_4$, calcd 265.1434, found 265.1435.
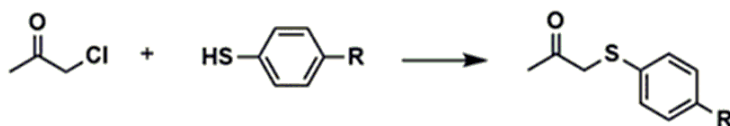
General procedure for the synthesis of α-(thiophenyl)acetones. Et_3N (1.6 equiv) was added to a solution of thiophenol (1.0 equiv) in acetone (0.5 M with respect to thiophenol), and the resulting mixture was stirred for 10 min. The round-bottom flask was placed in a water-bath, and chloroacetone (1.5 equiv) was added dropwise over 5 min. The reaction mixture was stirred at ambient temperature for 4 h and quenched with sat. NH_4Cl (ca.1.0 mL/mmol of Et_3N). Acetone was removed *in vacuo*, and the crude material was dissolved in EtOAc, poured into water and the

layers were partitioned. The aqueous layer was extracted with EtOAc (2×). The combined organic layers were dried over Na_2SO_4, filtered through a cotton plug, and concentrated *in vacuo*.

1-(phenylthio)propan-2-one

The crude material was recrystallized from Et_2O to yield an off-white crystalline solid (12.9 g, 78%). The spectroscopic data were consistent with those the literature.[193a,c]

1-((4-methoxyphenyl)thio)propan-2-one

The crude material was purified by flash column chromatography (SiO_2, 0→20% EtOAc in hexanes) to yield a pale-yellow oil (3.66 g, 93%) that solidified upon storage at −20 °C. The spectroscopic data were consistent with the literature.[193b, c]

1-((4-fluorophenyl)thio)propan-2-one

The crude material was purified by flash column chromatography (SiO_2, 5→15% EtOAc in hexanes) to yield a pale-yellow oil (3.43 g, 93%) that solidified at −20 °C. The spectroscopic data were consistent with literature.[193c]
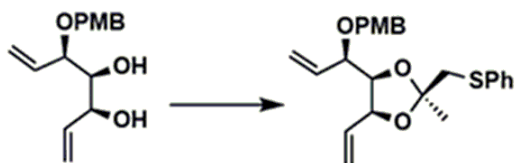
(2*S*,4*R*,5*S*)-4-((*R*)-1-((4-methoxybenzyl)oxy)allyl)-2-methyl-2-((phenylthio)methyl)-5-vinyl-1,3-dioxolane (1-102) Diol **1-95** (1.32 g, 5.00 mmol) was dissolved in MeCN (50 mL), and 2-(phenylthio)acetone (1.66 g, 10.0 mmol) was added in one-portion at room temperature. *p*-TsOH•H_2O (239 mg, 1.25 mmol) was then added in one portion. $HC(OEt)_3$ (4.7 mL, 28.9 mmol) was added dropwise over 5 min. The resulting reaction mixture was stirred at room temperature overnight and then quenched with Et_3N (3.0 mL). The crude mixture was concentrated *in vacuo*.

The crude material was dissolved in EtOAc, poured into sat. NaHCO$_3$, and the layers were partitioned. The aqueous layer was extracted with EtOAc (30 mL × 2). The combined organic layers were dried over solid NaHCO$_3$, filtered through a cotton plug, and concentrated *in vacuo*. The crude material was purified using flash column chromatography (SiO$_2$, 0→4% EtOAc in hexanes) to afford **1-102b** (660 mg, 32%) as a yellow oil.

Data for **1-102b**: R$_f$ = 0.21 (10% EtOAc in hexanes); $[\alpha]_D^{20}$ = −12.1 (*c* 1.0, CHCl$_3$); IR (neat) 3076, 2984, 2932, 2836, 1878, 1713 cm^{-1}; ^{1}H NMR (400 MHz, CDCl$_3$) δ 7.40 (dd, *J* = 8.8, 1.6 Hz, 2H), 7.28–7.14 (m, 5H), 6.86 (d, *J* = 8.4 Hz, 2H), 5.98 (ddd, *J* = 17.2, 10.8, 6.4 H, 1H), 5.81 (ddd, *J* = 17.6, 10.4, 7.6 Hz, 1H), 5.36 (m, 2H), 5.32 (dt, *J* = 7.6, 1.2 Hz, 1H), 5.21 (dt, *J* = 10.4, 1.2 Hz, 1H), 4.76 (*app* t, *J* = 6.4 Hz, 1H), 4.41 (d, *J* = 10.4 Hz, 1H), 4.15 (dd, *J* = 8.4, 6.8 Hz, 1H), 4.13 (d, *J* = 10.4 Hz, 1H), 3.79 (s, 3H), 3.25 (s, 3H), 1.45 (s, 3H); ^{13}C NMR (100 MHz, CDCl$_3$) δ 159.2, 137.4, 135.6, 133.3, 129.9, 129.7, 129.1, 128.7, 125.8, 119.2, 117.0, 113.7, 109.1, 79.6, 79.0, 78.4, 69.6, 55.2, 43.8, 23.4; HRMS (ESI-TOF): *m/z* for [M + H]$^+$ C$_{24}$H$_{29}$O$_4$S, calcd 413.1781, found 413.1781.

Note: Although we were able to obtain pure samples of the major diastereomer for characterization purposes, the isolated yields were significantly lower than the NMR yields. Performing column chromatography in Et$_3$N-deactivated SiO$_2$ causes poor resolution of the diastereomers. Hence, we eventually performed the five-step sequence without column purification as shown below.
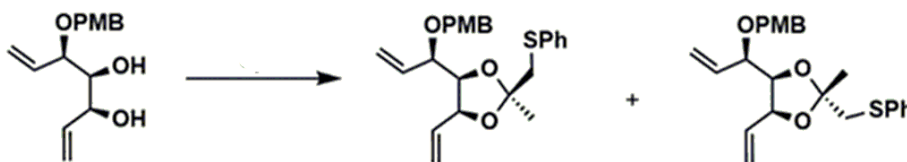
(2S,4R,5S)-4-((R)-1-((4-methoxybenzyl)oxy)allyl)-2-methyl-5-vinyl-1,3-dioxolane-2-carboxamide, 1-105a + 1-105b. Step d) Diol **1-94** (1.66 g, 6.28 mmol) and 2-(phenylthio)acetone (1.57 g, 9.42 mmol) were dissolved in MeCN/MeNO$_2$ (63 mL, 4:1), and the resulting solution was cooled to −15 °C. pTsOH•H$_2$O (112 mg, 0.62 mmol) was added, and the resulting solution was stirred for ca. 10 min at the same temperature. After this period, HC(OEt)$_3$ (1.66 mL, 10.0 mmol) was added at the same temperature. The reaction mixture was gradually warmed to 0 °C and left to stand at 8 °C for 24 h. The reaction was quenched with sat. NaHCO$_3$, and solvents were evaporated *in vacuo*. The crude material was dissolved in EtOAc (30 mL), poured into sat. NaHCO$_3$, and the layers were partitioned. The aqueous layer was extracted with EtOAc (30 mL × 1). The combined organic layers were dried over solid NaHCO$_3$, filtered through a cotton plug, and concentrated *in vacuo*. Crude **1-102** (2.96 g) was used directly in the next step.
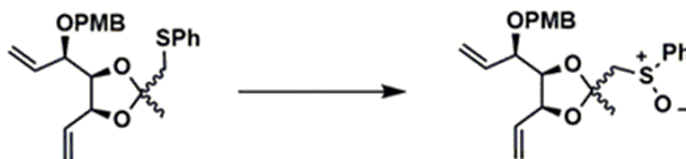
A solution of crude **1-102** (2.96 g) in DCM (84 mL) was cooled to −15 °C, and *m*CPBA (2.32 g, 9.42 mmol) was added portion-wise. The reaction mixture was gradually warmed to 5 °C over 2.5 h. The reaction was quenched with 10% (w/w) aqueous Na$_2$S$_2$O$_3$, and the resulting mixture was stirred at room temperature for 20 min. The crude mixture was poured into sat. NaHCO$_3$ (20 mL), and the layers were partitioned. The aqueous layer was extracted with EtOAc (20 mL × 3), and the combined organic layers were dried over solid NaHCO$_3$, filtered through a cotton plug, and concentrated *in vacuo*. The sulfoxide **1-103** was used without further purification for the next step.

The sulfoxide **1-103** (3.53 g) was dissolved in MeCN (62 mL), and the solution was cooled to −15 °C. 2,6-Lutidine (2.9 mL, 25.1 mmol) was added in one-portion at the same temperature. TFAA (4.4 mL, 31.4 mmol) was added portion-wise to the mixture, and the reaction mixture was gradually warmed to 0 °C over 1 h. Sat. $NaHCO_3$ (10 mL) and solid $NaHCO_3$ (ca.10 g) were added sequentially. The reaction mixture was warmed to room temperature over ca. 30 min and stirred for 1.5 h. MeCN was evaporated *in vacuo*, and the crude material was dissolved in DCM (50 mL) and washed with sat. $CuSO_4$ (50 mL × 3). The yellow-green solids were filtered off, and the filtrate concentrated *in vacuo* to afford the aldehyde **17** as a yellow oil (2.68 g).
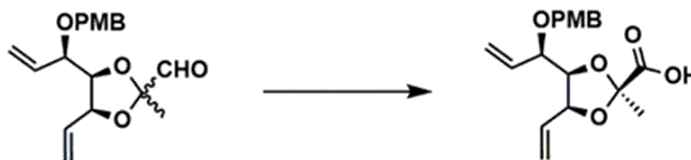
Crude aldehyde **1-104** (2.68 g) was dissolved in *t*-BuOH/H_2O (62 mL, 3:1) and cooled in a thawing ice-bath (ca. 9 °C). 2-Methyl-2-butene (13.0 mL, 124 mmol) and $NaH_2PO_4 \cdot H_2O$ (5.11 g, 37.0 mmol) were added sequentially. $NaClO_2$ (80% w/w, 1.40 g, 12.4 mmol) was added portion-wise. The reaction mixture was warmed to room temperature and stirred at the same temperature overnight. 10% (w/w) aqueous $Na_2S_2O_3$ was added to quench the reaction. The crude material was poured into water, and the layers were partitioned. The aqueous layer was extracted with EtOAc (40 mL × 1). The combined organic layers were dried over Na_2SO_4, filtered through a cotton plug, and concentrated to give a yellow oil (2.41 g).

109
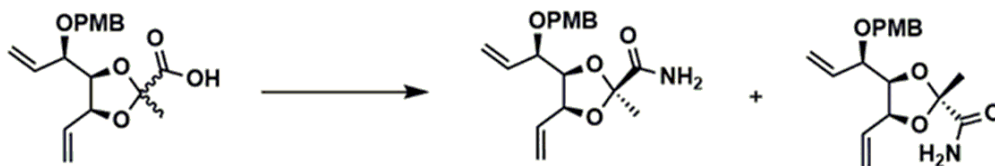
The crude acid **1-104** (2.41 g) obtained above was dissolved in DCM (62 mL), to which *i*-Pr$_2$NEt (2.1 mL, 12.4 mmol) was added in one-portion. HATU (3.53 g, 9.28 mmol) was then added in one-portion, and the resulting mixture was stirred for 5 min. Concentrated aqueous NH$_3$ (8.3 mL, 126 mmol) was added dropwise over 10 min, and the reaction was stirred at room temperature for 20 h. The crude reaction was poured into water, and the layers were partitioned. The aqueous layer was extracted multiple times with DCM. The combined organic layers were dried over Na$_2$SO$_4$, filtered through a cotton plug, and concentrated *in vacuo*. The crude material was purified by flash column chromatography (SiO$_2$, 10→50% EtOAc in hexanes) to give **1-105b** as a yellow oil (800 mg, 38% over 5 steps from diol **1-94**) and **1-105a** as an off-white solid (128 mg, 6% over 5 steps from diol **1-94**).

Data for **1-105a** (minor isomer): R$_f$ = 0.33 (70% EtOAc in hexanes); $[\alpha]_D^{24}$ = −8.9 (*c* 2.0, CHCl$_3$); m.p. = 84–86 °C; IR (thin film) 3477, 3394, 3055, 2989, 1697 (C=O), 1613, 1514, 1301, 1212, 1175, 1067, 1034 cm^{-1}; ^{1}H NMR (400 MHz, CDCl$_3$) δ 7.21 (d, *J* = 8.4 Hz, 2H), 6.87 (d, *J* = 8.8 Hz, 2H), 5.89 (ddd, *J* = 16.8, 10.4, 6.4 Hz, 1H), 5.84 (ddd, *J* = 17.2, 10.0, 7.2 Hz, 1H), 5.44 (d, *J* = 10.0 Hz, 1H), 5.40 (d, *J* = 17.2 Hz, 1H), 5.38 (d, *J* = 17.2 Hz, 1H), 5.27 (d, *J* = 10.8 Hz, 1H), 4.68 (*app* t, *J* = 6.4 Hz, 1H), 4.45 (d, *J* = 10.8 Hz, 1H), 4.17 (d, *J* = 10.8 Hz, 1H), 4.09 (dd, *J* = 8.0, 6.4 Hz, 1H), 3.80 (s, 3H), 3.76 (a*pp* t, *J* = 7.6 Hz, 1H), 1.63 (s, 3H); ^{13}C NMR (100 MHz, CDCl$_3$) δ 173.7, 159.3, 135.0, 132.3, 129.7 (2 C), 120.0, 118.0, 113.8, 105.7, 80.2, 79.5, 78.3, 69.7 55.3, 23.2; HRMS (ESI-TOF): *m/z* [M + H]$^+$ for C$_{18}$H$_{24}$O$_5$N, calcd 334.1649; found 334.1634.

Data for **1-105b** (major isomer): R_f = 0.37 (70% EtOAc in hexanes); $[\alpha]_D^{25}$ = −8.3 (*c* 0.70, CHCl$_3$); IR (neat) 3476, 2987, 2936, 1698 (C=O), 1613, 1514, 1374, 1302, 1201, 1175, 1069, 1033 cm^{-1}; ^{1}H NMR (400 MHz, 1% CD$_3$OD in CDCl$_3$) δ 7.18 (d, *J* = 8.4 Hz, 2H), 6.85 (dd, *J* = 6.8, 2.0 Hz, 2H), 5.92 (ddd, *J* = 17.2, 10.4, 6.8 Hz, 1H), 5.86 (ddd, *J* = 17.2, 10.4, 7.2 Hz, 1H), 5.40 (d, *J* = 10.0 Hz, 1H), 5.39 (d, *J* = 17.2 Hz, 1H), 5.35 (d, *J* = 16.4 Hz, 1H), 5.25 (d, *J* = 10.8 Hz, 1H), 4.76 (*app* t, *J* = 6.4 Hz, 1H), 4.43 (d, *J* = 10.4 Hz, 1H), 4.18 (dd, *J* = 8.4, 6.0 Hz, 1H), 4.13 (d, *J* = 10.4 Hz, 1H), 3.79 (*app* t, *J* = 7.2 Hz, 1H), 3.78 (s, 3H), 1.68 (br, 2H), 1.51 (s, 3H); ^{13}C NMR (100 MHz, 1% CD$_3$OD in CDCl$_3$) δ 172.9, 159.3, 135.2, 132.3, 129.7, 129.6, 120.2, 118.5, 113.8, 105.8, 80.2, 79.9, 78.6, 69.8, 55.2, 22.4; HRMS (ESI-TOF): *m/z* [M + H]$^+$ for C$_{18}$H$_{24}$O$_5$N, calcd 334.1649; found 334.1633.
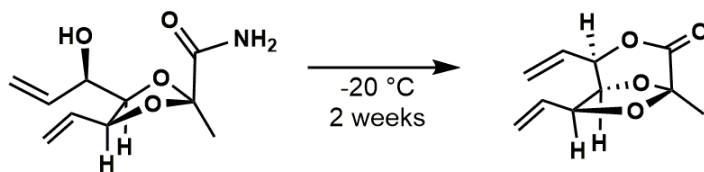
(2R,5S,7S)-5-methyl-2,7-divinyl-3,6,8-trioxabicyclo[3.2.1]octan-4-one, 1-109.
Hydroxyamide **1-108** (166 mg, 0.78 mmol) was transferred to a 1-dram vial, which was then sealed and stored at −20 °C for a period of ca. two weeks. The vial was removed from the freezer and allowed to warm to room temperature. The crude material was purified by flash column chromatography (0 → 25% Et$_2$O in hexanes) to give lactone **1-109** (43 mg, 28%) as a colorless liquid.

Date for **1-109**: ^{1}H NMR (400 MHz, CDCl$_3$) δ 5.95 (ddd, *J* = 17.2, 10.4, 7.2 Hz, 1H), 5.90 (ddd, *J* = 16.8, 10.4, 6.4 Hz, 1H), 5.43 (app dt, *J* = 17.2, 1.2 Hz, 1H), 5.41 (*app* dd, *J* = 17.4, 1.6 Hz, 1H), 5.32-5.27 (*app* m, 3H), 4.69 (*app* t, *J* = 6.0 Hz, 1H), 4.56 (dd, *J* = 5.2, 2.4 Hz, 1H), 1.71

(s, 3H); ^{13}C NMR (100 MHz, CDCl$_3$) δ 164.7, 132.4, 131.2, 119.4, 119.2, 103.0, 83.1, 79.6, 78.5, 18.4; IR (neat) 3087, 2991, 1755 (lactone), 1430, 1377, 1297, 1227, 1188, 1131, 996, 931 cm^{-1}; HRMS (ESI-TOF): *m/z* [M + H]$^+$ for C$_{10}$H$_{13}$O$_4$, calcd 197.0808; found 197.0809.

3.2.2 Second Generation Route

General Procedures for Optimization Studies

Method A

A 1-dram vial was charged sequentially with diol **1-94** (24 mg, 0.10 mmol), MeC(OMe)$_3$ (19 μL, 0.15 mmol) and DCM (0.8 mL). The mixture was stirred for 5 min. CSA (ca.1.2 mg, 5.0 μmol) was added, and the walls of the vial were rinsed with DCM (0.2 mL). The vial was flushed with Ar, and the reaction mixture was stirred at room temperature for 24 h, then cooled to −78 °C. TMSCN (50 μL, 0.40 mmol) and Lewis acid (*x* equiv) were added sequentially at the same temperature. The reaction mixture was stirred at the indicated temperature for ca. 8 h. Et$_3$N/MeOH/DCM (1:1:1, v/v/v, 0.1 mL) was added at −78 °C to quench the reaction. The crude was filtered through a plug of basic Al$_2$O$_3$ and concentrated.

Method B

A 1-dram vial was charged sequentially with diol **1-94** (24 mg, 0.10 mmol), MeC(OMe)$_3$ (19 μL, 0.15 mmol), and DCM (0.8 mL). The mixture was stirred for 5 min. CSA (ca.1.2 mg, 5.0 μmol) was added, and the walls of the vial were rinsed with DCM (0.2 mL). The vial was flushed with Ar, and the reaction mixture was stirred at room temperature for 24 h, then cooled to −78 °C. TMSCN (50 μL, 0.40 mmol) and Lewis acid (*x* equiv) were added sequentially at the same

temperature. The reaction mixture was stirred at the indicated temperature for ca. 8 h. Et$_3$N/MeOH/DCM (1:1:1, v/v/v, 0.1 mL) was added at −78 °C to quench the reaction. MgSO$_4$ was added and the quenched mixture was stirred overnight. The solids were filtered through a plug of Celite®, and the solvents were evaporated *in vacuo*. (*Note: We have typically used method B for any Al- and Ti-based Lewis acids.*)
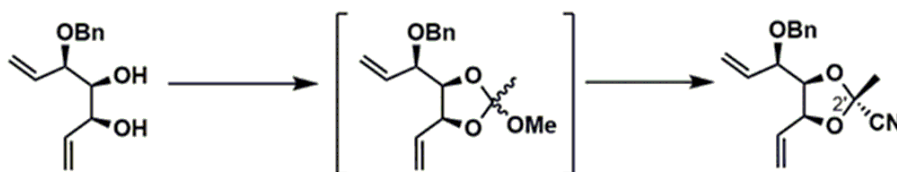
(2R,4R,5S)-4-((R)-1-(benzyloxy)allyl)-2-methyl-5-vinyl-1,3-dioxolane-2-carbonitrile (1-112) CSA (581mg, 2.5 mmol) was added to a solution of diol **1-94** (11.7 g, 49.9 mmol) and MeC(OMe)$_3$ (9.6 mL, 75.1 mmol) in DCM (450 mL). The reaction mixture was stirred at room temperature for 24 h and then cooled down to −78 °C. TMSCN (22.5 mL, 180 mmol) and BF$_3$•OEt$_2$ (9.4 mL, 74.8 mmol) were added sequentially at the same temperature. The reaction was gradually warmed up to −20 °C over 12 h. The reaction mixture was quenched with solid K$_2$CO$_3$ and stirred at 0 °C for 1 h. The crude mixture was filtered through a pad of basic Al$_2$O$_3$. The pad was washed with DCM and the solvents were concentrated *in vacuo* in a well-ventilated fume hood. The crude material was dried on the high-vacuum overnight to give a yellow oil (13.8 g). The diastereomeric mixture was spectroscopically pure and was used in the next step without further purification.

Note: *We could lower the amount of TMSCN to 3.2–3.6 equiv for scale-up reactions; we performed this reaction at maximum 50 mmol batches for safety concerns.*

Data for **1-112**: R$_f$ = 0.34 (10% EtOAc in hexanes); IR (neat) 3088, 3032, 2987, 2875, 2230 (C≡N), 1875, 1747, 1645, 1497, 1455, 1383, 1222, 1068 cm^{-1}; ^{1}H NMR (400 MHz, CDCl$_3$) δ 7.36-

7.25 (m, 5H), 5.86 (ddd, J = 17.2, 10.8, 6.4 Hz, 1H), 5.81 (ddd, J = 17.2, 10.4, 6.4 Hz, 1H), 5.45 – 5.36 (*app* m, 3H), 5.28 (d, J = 10.8 Hz, 1H), 4.89 (*app* t, J = 6.8 Hz, 1H), 4.54 (d, J = 11.2 Hz, 1H), 4.34 (*app* t, J = 7.6 Hz, 1H), 4.24 (d, J = 11.2 Hz, 1H), 3.78 (*app* t, J = 8.0 Hz, 1H), 1.80 (s, 3H); ^{13}C NMR (100 MHz, CDCl$_3$) δ 137.4, 134.5, 131.5, 128.4, 127.9, 127.8, 120.5, 118.9, 117.3, 99.0, 80.5, 79.9, 78.4, 70.1, 24.9; HRMS (EI): *m/z* for [M]$^-$ C$_{17}$H$_{19}$O$_3$N, calcd 285.1359, found 285.1346.
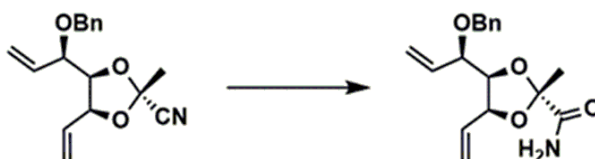
(2*R*,4*R*,5*S*)-4-((*R*)-1-(benzyloxy)allyl)-2-methyl-5-vinyl-1,3-dioxolane-2-carboxamide (1-113) Nitrile **1-112** (13.8 g, assumed 48.3 mmol) was dissolved in 1,4-dioxane (480 mL), to which acetaldoxime (29 mL, 483 mmol) was added. Pd(OAc)$_2$ (380 mg, 1.69 mmol) was added in one-portion at room temperature. The mixture was stirred at 100 °C for 1 h and cooled to room temperature. The crude mixture was concentrated *in vacuo*, and the resulting residue was purified by flash column chromatography (SiO$_2$, 10→50% EtOAc in hexanes). We combined two batches (50 mmol each) and subjected them to flash column chromatography to yield a semi-pure solid (24.3 g, mixed with acetamide). The solid was repurified using a second column to give pure **1-113** as a white solid (21.0 g, average 66% of two 50 mmol batches, from diol **1-94**).

Data for **1-113**: R$_f$ = 0.41 (80% EtOAc in hexanes); $[\alpha]_D^{22}$ = −4.0 (*c* 1.0, MeOH); m.p. = 100–102 °C; IR (thin film) 3420, 3188 (br, N-H), 3032, 2865, 1642 (C=O), 1205, 1125, 1063 cm^{-1}; ^{1}H NMR (400 MHz, CDCl$_3$) δ 7.36–7.29 (m, 5H), 5.89 (ddd, J = 16.8, 10.4, 6.4 Hz, 1H), 5.85 (ddd, J = 17.2, 10.4, 7.6 Hz, 1H), 5.42 (d, J = 10.8 Hz, 1H), 5.41 (*app* t, J = 16.8 Hz, 2H), 5.27 (d,

J = 10.4 Hz, 1H), 4.69 (*app* t, J = 6.4 Hz, 1H), 4.53 (d, J = 11.2 Hz, 1H), 4.24 (d, J = 11.2 Hz, 1H),

4.11 (*app* t, J = 8.0 Hz, 1H), 3.81 (*app* t, J = 7.6 Hz, 1H), 1.63 (s, 3H); ^{13}C NMR (100 MHz,

CDCl$_3$) δ 173.8, 137.6, 134.9, 132.3, 128.3, 128.0, 127.7, 120.0, 118.0, 105.7, 80.1, 79.5, 78.6,

70.0, 23.2; HRMS (ESI-TOF): *m/z* for [M + H]$^+$ C$_{17}$H$_{22}$NO$_4$, calcd 304.1543, found 304.1554.
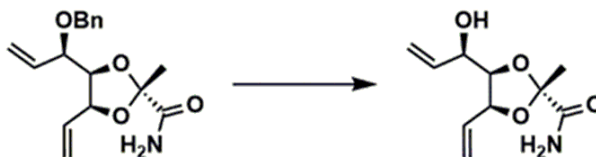
(2*R*,4*R*,5*S*)-4-((*R*)-1-hydroxyallyl)-2-methyl-5-vinyl-1,3-dioxolane-2-carboxamide (1-114) Amide **1-113** (909 mg, 3.00 mmol) was dissolved in EtSH (10 mL), to which BF$_3$•OEt$_2$ (1.90

mL, 15.0 mmol) was added dropwise at room temperature. The mixture was stirred in a sealed

tube for 1 d. After EtSH was evaporated in the well-ventilated fume hood, the dark-yellow oil was

dissolved in DCM (20 mL) and cooled to 0 °C. The crude reaction mixture was quenched with pH

7 buffer (1.2 M, 2 mL) and stirred at the same temperature for 30 min. Na$_2$SO$_4$ was added to the

crude mixture. The crude mixture was filtered through a short column of SiO$_2$ (4 mL), and the

column was flushed with EtOAc. The solvents were evaporated *in vacuo*, and the crude material

was purified by flash column chromatography (SiO$_2$, 33 mL, 10→80% EtOAc in hexanes) to give

allylic alcohol **1-114** as a yellow oil (410 mg, 64%).

Data for **1-114**: R$_f$ = 0.24 (100% EtOAc); $[\alpha]_D^{20}$ = +18.5 (*c* 1.0, MeOH); IR (neat) = 3438

(br, O-H), 2921, 2581, 1681 (C=O), 1376, 1209, 1169, 1016 cm^{-1}; ^{1}H NMR (400 MHz, CDCl$_3$) δ

6.56 (br, s, 1H), 6.07–5.98 (m, 3H), 5.48 (d, J = 17.2 Hz, 1H), 5.38 (d, J = 17.2 Hz, 1H), 5.36 (d,

J = 10.4 Hz, 1H), 5.28 (d, J = 10.4 Hz, 1H), 4.69 (*app* t, J = 6.4 Hz, 1H), 4.23 (*app* t, J = 6.4 Hz,

1H), 4.06 (*app* t, J = 6.4 Hz, 1H), 1.66 (s, 3H); ^{13}C NMR (100 MHz, CDCl$_3$) δ 173.91, 136.74,

132.4, 119.3, 117.2, 105.8, 81.2, 79.5, 70.7, 23.2; HRMS (ESI-TOF): *m/z* for [M + H]$^+$ C$_{10}$H$_{16}$O$_4$N, calcd 214.1074, found 214.1075.

*Note: Due to the water solubility of **1-114**, extractions were avoided. We also observed decrease in yields to varying extents when the reaction was quenched with either sat. NaHCO$_3$ or sat. K$_2$CO$_3$, with yields ranging from 42–60%.*

*Note: We have occasionally obtained **25** as a white to off-white solid. In most cases – we obtained a yellow oil. Spectroscopic data reported herein correspond to **25** that was isolated as a yellow oil. All batches underwent efficient subsequent RCM at low catalyst loadings.*
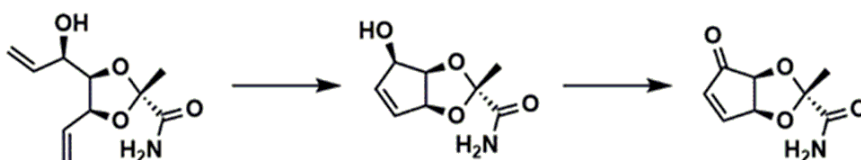
(2*R*,3a*S*,6a*S*)-2-methyl-4-oxo-3a,6a-dihydro-4H-cyclopenta[d][1,3]dioxole-2-carboxamide, 1-89. Allylic alcohol **1-114** (256 mg, 1.20 mmol) was dissolved in 1,2-DCE (Ar-sparged), to which the nitro-Grela catalyst (3.7 mg, 5.5 µmol) was added. The reaction mixture was stirred at 60 °C for 1 h and cooled to room temperature. MnO$_2$ (574 mg, 6.60 mmol) was added at room temperature, and the reaction mixture was stirred at 60 °C. Additional MnO$_2$ were added periodically (53 mg × 2, 0.60 mmol × 2) until the complete consumption of intermediate cyclopentenol (ca.28 h). The crude material was filtered through a pad of SiO$_2$ (4 mL)/Celite® (0.2 g)/charcoal (0.5 g), and the pad was washed with EtOAc. The solvents were concentrated *in vacuo* to give spectroscopically pure cyclopentenone **1-89** as a white solid (185 mg, 84%).

Note: We could lower the catalyst loading down to 0.36 mol% with the yield over two steps = 77%.

116

*Note: We have occasionally obtained light-brown solids after the first filtration. We dissolved the semi-pure solids in EtOAc and stirred with additional charcoal ca.1 g/mmol of **1-99** overnight. Subsequent filtration through a plug of SiO₂ typically affords a white solid.*

Data for **1-89**: R_f = 0.18 (100% EtOAc); $[\alpha]_D^{21}$ = +15.8 (*c* 0.5, acetone); m.p. = 163–166 ˚C; IR (neat) 3433 (N-H), 3327 (N-H), 3081, 3062, 1705 (C=O), 1613 (C=O), 1359, 1214, 1160, 1044 cm^{-1}; ^{1}H NMR (400 MHz, acetone-d_6) δ 7.74 (dd, *J* = 6.0, 2.4 Hz, 1H), 6.22 (d, *J* = 6.0 Hz, 1H), 5.41 (dd, *J* = 5.2, 2.0 Hz, 1H), 4.52 (d, *J* = 5.6 Hz, 1H), 1.46 (s, 3H); ^{13}C NMR (100 MHz, acetone-d_6) δ 201.9, 172.0, 159.9, 134.6, 112.1, 80.4, 77.6, 23.4; HRMS (ESI-TOF): *m/z* [M + H]$^+$ $C_8H_{10}O_4N$, calcd 184.0604, found 184.0598.
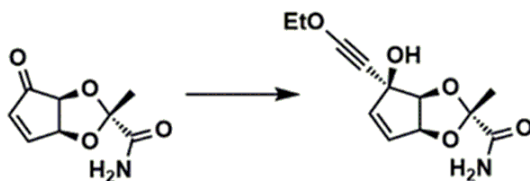
(2*R*,3a*S*,4*S*,6a*S*)-4-(ethoxyethynyl)-4-hydroxy-2-methyl-3a,6a-dihydro-4H-cyclopenta[d][1,3]dioxole-2-carboxamide, 1-90. A suspension of anhydrous CeCl₃ (660 mg, 2.43 mmol) in THF (10 mL) was stirred vigorously at room temperature until the solid fully dissolved (ca. 15 min). The resulting solution was cooled to −78 °C, and *n*-BuLi (0.96 mL, 2.40 mmol) was added dropwise. The yellow solution was stirred at the same temperature for 15 min, and ethoxyacetylene (0.5 mL, 2.43 mmol) was added. The mixture was stirred at the same temperature for 1 h, and enone **1-89** (130 mg, 0.71 mmol) in THF (15 mL) was added slowly over 15 min at −78 ˚C. The reaction mixture was gradually warmed to −50 ˚C and quenched with brine. The crude was poured into brine, and the layers were separated. The aqueous layer was extracted multiple times with EtOAc. The combined organic layers were dried over Na₂SO₄, filtered through

a cotton plug, and the solvents were concentrated *in vacuo*, and the crude material purified by flash column chromatography to give alcohol **1-90** as a pale-yellow oil (106 mg, 59%).

Note: Performing this reaction with non-distilled ethoxyacetylene gave significantly lower yield of ca. 24%.

Data for **1-90**: R_f = 0.21 (100% EtOAc); $[\alpha]_D^{21}$ = +138.9 (*c* 1.0, CHCl$_3$); IR (neat) 3332 (br, O-H), 2989 (N-H), 2937 (N-H), 2264 (C≡C), 1686 (C=O), 1590 cm^{-1}; ^{1}H NMR (500 MHz, CDCl$_3$) δ 6.46 (br, 1H), 5.92 (d, *J* = 5.5 Hz, 1H), 5.90 (br, 1H), 5.82 (dd, *J* = 5.5, 1.5 Hz, 1H), 5.22 (d, *J* = 4.5 Hz, 1H), 4.68 (d, *J* = 5.5 Hz, 1H), 4.11 (q, *J* = 7.0 Hz, 2H), 3.17 (br, 1H), 1.61 (s, 3H), 1.36 (t, *J* = 7.0 Hz, 3H); ^{13}C NMR (125 MHz, CDCl$_3$) δ 172.7, 139.2, 129.1, 109.2, 94.7, 84.8, 84.6, 75.2, 75.0, 38.5, 23.6, 14.3; HRMS (ESI-TOF): *m/z* for [M + H]$^+$ C$_{12}$H$_{16}$O$_5$N, calcd 254.1023, found 254.1028.

Method A: Meyer-Schuster Rearrangement
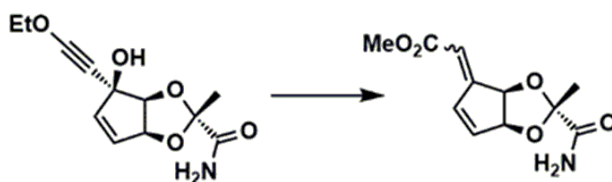
Methyl 2-((2*R*,3a*R*,6a*S*)-2-carbamoyl-2-methyl-3a,6a-dihydro-4H-cyclopenta[d][1,3]dioxol-4-ylidene)acetate, 1-81a + 1-81b. Propargylic alcohol **2** (66.5 mg, 0.26 mmol) was dissolved in DCM/MeOH (26 mL, 25:1 v/v). Ph$_3$PAuCl (5.0 mg, 0.010 mmol) and AgOTf (3.3 mg, 0.013 mmol) were added sequentially to the solution. The reaction mixture was stirred at room temperature for ca. 80 min, and the solvents were evaporated *in vacuo*. The crude

material was purified by flash column chromatography (10→80% EtOAc in hexanes) to give **1-81a** as a white solid (22.3 mg, 36%) and **1-81b** as a pale-yellow oil (15.1 mg, 24%).

Note: We could also use crude 2 directly for Meyer-Schuster rearrangement with no effect on the overall yield, ca.36% of 1a + 1b over 2 steps from enone 3.

Data for **1-81a**: R_f = 0.33 (100% EtOAc); $[\alpha]_D^{20}$ = +87.4 (*c* 0.5, CHCl$_3$); m.p. = 166–168 ˚C ; IR (thin film) = 3464 (N-H), 3193 (N-H), 2954, 1715 (C=O), 1673 (C=O), 1649, 1432, 1400, 1377, 1234, 1147 cm^{-1}; ^{1}H NMR (500 MHz, CDCl$_3$) δ 7.39 (d, *J* = 6.0 Hz, 1H), 6.48 (d, *J* = 6.0 Hz, 1H), 6.45 (br, 1H), 6.02 (s, 1H), 5.86 (br, 1H), 5.20 (dd, *J* = 5.5, 2.0 Hz, 1H), 5.02 (d, *J* = 5.5 Hz, 1H), 3.76, (s, 3H), 1.57 (s, 3H); ^{13}C NMR (125 MHz, CDCl$_3$) δ 173.1, 166.4, 156.0, 141.5, 133.6, 115.2, 109.0, 82.5, 80.3, 51.5, 23.4; HRMS (ESI-TOF): *m/z* [M + H]$^+$ C$_{11}$H$_{14}$O$_5$N, calcd 240.0867, found 240.0868.

Data for **1-81b**: R_f = 0.23 (100% EtOAc); $[\alpha]_D^{19}$ = +86.0 (*c* 0.5, CHCl$_3$); IR (neat) = 3454 (N-H), 3412, 3341 (N-H), 3210 (N-H), 2954, 1753 (C=O), 1724 (C=O), 1686, 1439, 1377, 1166, 1146 cm^{-1}; ^{1}H NMR (400 MHz, CDCl$_3$) δ 6.72 (br, 1H), 6.50 (d, *J* = 4.8 Hz, 1H), 6.36 (d, *J* = 5.6 Hz, 1H), 6.02 (s, 1H), 5.69 (d, *J* = 5.6 Hz, 1H), 5.5 (br, 1H), 5.23 (d, *J* = 4.4 Hz, 1H), 3.78 (s, 3H), 1.60 (s, 3H); ^{13}C NMR (100 MHz, CDCl$_3$) δ 173.1, 166.3, 156.6, 142.3, 134.9, 115.6, 108.6, 83,6, 77.2, 51.6, 23.1; HRMS (ESI-TOF): *m/z* [M + H]$^+$ C$_{11}$H$_{14}$O$_5$N, calcd 240.0867, found 240.0869.

Method B: Ce-Mediated Peterson Olefination of 1-89
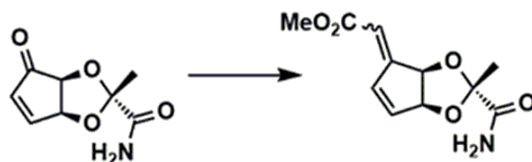
Methyl 2-((2R,3aR,6aS)-2-carbamoyl-2-methyl-3a,6a-dihydro-4H-cyclopenta[d][1,3]dioxol-4-ylidene)acetate, 1-81a + 1-81b. A solution of diisopropylamine (467 μL, 3.33 mmol) in THF (6 mL) was cooled to −78 °C. *n*-BuLi (2.5 M, 1.3 mL, 3.25 mmol) was added dropwise, and the resulting mixture was stirred for 40 min at the same temperature. Methyl trimethylsilylacetate (546 μL, 3.33 mmol) in THF (1 mL) was added dropwise over ca. 5 min, and the resulting mixture stirred for ca. 45 min at −78 °C. The cerium enolate was then transferred to a mixture of enone **1-89** (174 mg, 0.95 mmol) and CeCl₃ (660 mg, 2.67 mmol) in THF (20 mL) at −78 °C (Enone **1-89** and CeCl₃ were premixed and stirred at room temperature for ca. 1.5 h before cooling). The reaction was stirred at −78 °C for 4.5 h and quenched with sat. NH₄Cl. The layers were partitioned, and the aqueous layer was extracted with EtOAc (10 mL × 2). The combined organic layers were dried over Na₂SO₄, filtered through a cotton plug, and the solvents were concentrated *in vacuo*. The crude material was purified by flash column chromatography twice (SiO₂, 10→80% EtOAc in hexanes) to give **1-81a** as a white solid (66.3 mg, 29%) and **1-81b** as a pale-yellow oil (24.7 mg, 11%). The spectroscopic data matched those obtained via method **A**.

*Note: We typically obtained fractions of pure **1-81a** and fractions of **1-81a** + **1-81b** after the first column. The mixed fractions were concentrated and subjected to a second column. The pure fractions from the two columns were then combined and concentrated to afford the pure products.*

Conditions for Debenzylation of 1-113

entry	reagents (equiv)/conditions	results[a]
	oxidative conditions	
1	DDQ (2.0), MeNO$_2$/pH 7 buffer, 60 °C	N.R.
2	DDQ (4.0), MeNO$_2$/pH 7 buffer, 60 °C	N.R.
3	DDQ (5.0), MeNO$_2$/pH 7 buffer, 60 °C	trace conversion
4	DDQ (5.0), DCE/pH 7 buffer, 60 °C	48–78%[b]
5	DDQ (5.0), DCE/pH 7 buffer, 60 °C	13–39%[c]
6	DDQ (0.30), MnO$_2$ (5.0), MeNO$_2$, 50 °C	N.R.
7	DDQ (0.30), FeCl$_3$ (3.0), DCE/pH 7 buffer, 80 °C	full conversion[d] difficult work-up
8	DDQ (2.0), DCE/pH 7 buffer, 90 °C	trace
9	IBX (3.0), DMSO, 80 °C	N.R.
	reductive conditions	
10	Na (5.0)/NH$_3$, -78 to -60 °C	N.R.
11	Na/naphthalene (2.0), THF, -78 °C to rt	N.R.
12	Na/anthracene, THF, -78 °C to rt	N.R.
13	Li (5.0)/NH$_3$, -78 °C	trace

14	Pd(OAc)$_2$ (0.05)/Et$_3$N(0.15)/Et$_3$SiH(1.5), rt	trace hydrogenation of alkenes

Lewis acidic conditions

15	BBr$_3$ (2.0), DCM, -78 °C	trace
16	Sc(OTf)$_3$ (0.10), Me$_2$S (2.0), MeCN, 60 °C	N.R.
17	BF$_3$•OEt$_2$ (2.0), PhSH (1.1), DCM, 50 °C	N.R.
18	BF$_3$•OEt$_2$ (14), HSCH$_2$CO$_2$H, DCM, rt	N.R.
19	BF$_3$•OEt$_2$ (12), EtSH, rt	52%[e]
20	BF$_3$•OEt$_2$ (8.0), EtSH, rt	52%[f]
21	BF$_3$•OEt$_2$ (4.0), EtSH, rt	60%[g]
22	BF$_3$•OEt$_2$ (5.0), EtSH, rt	64%[g]

[a] N.R. = no reaction, yields are isolated yields after flash column chromatography

[b] 0.05–0.18 mmol scale

[c] 3.5–22 mmol scale

[d] We observed full conversion based on TLC analysis but were unable to remove [Fe] resulting in difficult ^{1}H NMR analysis and subsequent RCM failed to work in the presence of [Fe].

[e] 0.20 mmol scale

[f] 2.0 mmol scale

[g] 3.0 mmol scale

3.3 Computation Details for Chapter 1

3.3.1 Calculation of Transition States for Cyanation

3.3.1.1 General Considerations

All calculations were performed using supercomputing clusters provided by the University of Pittsburgh Center for Research Computing (PittCRC). Density functional theory (DFT) calculations were carried out using Gaussian 09, Revision D.01.[4] All structures were subjected to initial Stochastic Conformational Sampling using Chem3D of ChemOffice 2016 package, employing force field method (MMFF94). Duplicate conformers were removed and conformers within 5 kcal mol^{-1} energy differences were optimized at B3LYP/6-31G(d) in the gas phase at 298 K. Transition state geometries scans were computed using HF/3-21G, varying the oxocarbenium-nucleophile C-C bond distance. The scanned geometry was subjected to optimization using the Berny algorithm at B3LYP/6-31G(d) level. Vibrational frequencies were computed at the same level and each transition state was verified by having one imaginary frequency along the appropriate reaction coordinate (C-C bond formation). Each transition state was further verified by computing an IRC calculation at the B3LYP/6-31G(d) level. The IRC calculations were calculated for both directions, maximum points of 10 and recalculating force constants for every nth point, using the additional keywords "irc=(maxpoints=10,recalc=2,calcfc)". Single-point energies were computed using M06-2x/6-311++G(d,p) using "integral=ultrafine" as additional keywords and implicit solvent model (smd,solvent=dichloromethane). Energies are calculated by the formula: G(M06-2x) = E(M06-2x) + G(B3LYP) − E(B3LYP) and 1 Hartree = 627.509 kcal/mol conversion.

3.3.1.2 Optimized Transition States

TS1
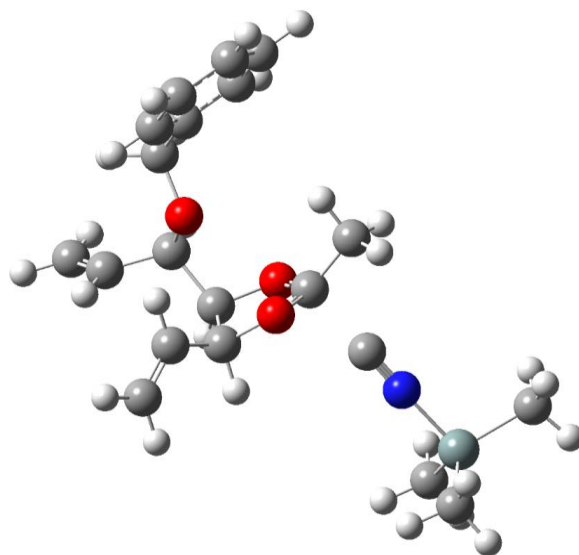
$$G_{rel} = 0$$

1 1

C	0.11999400	1.65511000	-0.56323800
H	-0.47207600	2.47910400	-0.96629600
C	-0.18272000	1.43644300	0.94525500
H	-1.18216700	1.83004600	1.17030600
O	-0.39572800	0.41747600	-1.15730900
O	-0.28162000	-0.02910800	1.01606600
C	-0.62718200	-0.47731900	-0.18632200
C	0.79775000	1.90108600	1.97297900

H	1.79302200	1.47457100	1.89771900
C	0.47225300	2.77717800	2.92371900
H	-0.52652900	3.20108900	3.00406500
H	1.19839100	3.10859700	3.65967900
C	1.57685800	1.79853800	-1.02776300
H	1.55179600	1.66232400	-2.12203700
C	2.15792600	3.16164000	-0.73134700
H	2.30781600	3.40877800	0.31708800
C	2.48532400	4.03716400	-1.68249800
H	2.35721800	3.81343700	-2.73995000
H	2.89755800	5.01286200	-1.44222100
O	2.28840800	0.72584000	-0.42677400
C	3.57753600	0.46053300	-1.01762300
H	4.24366000	1.31418400	-0.84001900
H	3.45540800	0.34788400	-2.10479200
C	4.12656000	-0.80075700	-0.40750900
C	3.95193300	-2.03467100	-1.04716200
C	4.79564300	-0.76239500	0.82218600

125

C	4.43469700	-3.20980400	-0.46865200
H	3.45280000	-2.07228700	-2.01348100
C	5.27694800	-1.93477700	1.40437500
H	4.94738600	0.19212900	1.32111600
C	5.09627600	-3.16080400	0.75972400
H	4.30513500	-4.15930700	-0.98064300
H	5.80067500	-1.89179900	2.35515600
H	5.47906400	-4.07298700	1.20857200
C	-0.28038500	-1.90619900	-0.48610800
H	-0.70340500	-2.20874500	-1.44597000
H	0.81312900	-1.95614000	-0.53538400
H	-0.63764300	-2.56200100	0.31029100
C	-2.52315700	-0.54480700	-0.12353200
N	-3.68570400	-0.57748400	-0.08774600
Si	-5.53105700	-0.67074700	-0.04148100
C	-5.93696100	-0.58239600	1.78117000
H	-7.02323800	-0.64594000	1.91977100
H	-5.48470200	-1.40897300	2.33948800

H	-5.60262200	0.35982400	2.22835600
C	-6.07685000	0.81806200	-1.03226100
H	-5.70755800	0.77789900	-2.06257600
H	-7.17240000	0.85041500	-1.07562000
H	-5.73800100	1.75611700	-0.57966300
C	-5.90877500	-2.31660500	-0.84382300
H	-5.46848900	-3.15125100	-0.28794300
H	-6.99414500	-2.47330900	-0.86904400
H	-5.54582400	-2.35864800	-1.87630300

TS2 (Disfavored)
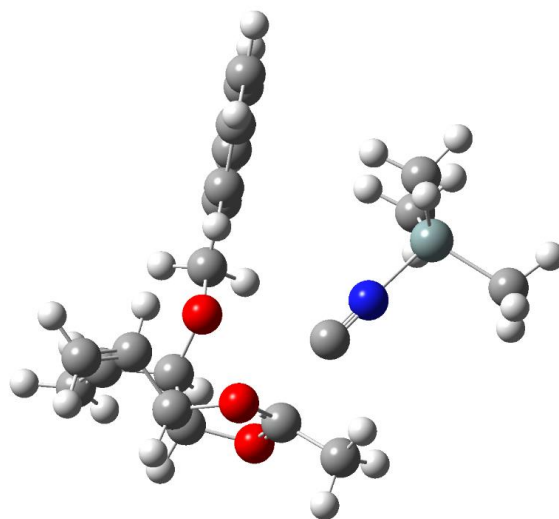
$G_{rel} = 3.9$ kcal/mol

1 1

C	-2.99303100	-0.75615100	-0.61432800
H	-3.95804700	-0.91104900	-1.09935900
C	-3.13556100	-0.89357100	0.92838200
H	-4.07285300	-1.40799100	1.15833000
O	-2.20106300	-1.94551400	-0.95665600
O	-2.08536200	-1.89900400	1.24753000
C	-1.61956300	-2.42010400	0.13158700
C	-2.99650700	0.30819200	1.80347800
H	-2.10979500	0.91594400	1.66477300

C	-3.92701100	0.62500900	2.70582800
H	-4.82366700	0.02566700	2.84854900
H	-3.82653000	1.50256300	3.33732200
C	-2.36068400	0.49725300	-1.23134500
H	-2.13360300	0.23049100	-2.27639300
C	-3.33244200	1.65746500	-1.22499200
H	-3.56456400	2.08249300	-0.25062100
C	-3.89529200	2.14828300	-2.32973300
H	-3.67381500	1.74718600	-3.31704600
H	-4.60227400	2.97179100	-2.29074100
O	-1.15242900	0.77919600	-0.53154300
C	-0.32196400	1.73528200	-1.19724100
H	-0.94039700	2.57333100	-1.54695600
H	0.12092200	1.26645600	-2.09059300
C	0.76187900	2.25591900	-0.27869300
C	0.83758100	1.91587100	1.07470500
C	1.70870500	3.14572600	-0.80847900
C	1.83811400	2.46069200	1.88687300

H	0.11819900	1.22306100	1.49652900
C	2.70706900	3.68697100	0.00002700
H	1.65729500	3.42699800	-1.85865200
C	2.77445800	3.34637700	1.35399200
H	1.87581300	2.19782600	2.94080700
H	3.42783600	4.37978500	-0.42485600
H	3.54600200	3.77465000	1.98718300
C	-1.24962100	-3.87345400	0.13566400
H	-2.18385700	-4.44502700	0.19397600
H	-0.72465800	-4.13888500	-0.78288100
H	-0.63681800	-4.10542400	1.00761700
Si	3.30277000	-1.52194200	-0.26222400
C	3.60709300	-0.29526900	-1.64007800
H	4.68535400	-0.20253500	-1.81915600
H	3.14478600	-0.61975000	-2.57884800
H	3.22433200	0.69854600	-1.38569500
C	3.80527900	-3.27386600	-0.69795100
H	4.89384800	-3.32522000	-0.82259000

H	3.53061600	-3.98637300	0.08736600
H	3.35129700	-3.60451800	-1.63847300
C	3.89035700	-0.96197800	1.42156500
H	3.49545800	0.02823000	1.67109800
H	3.59379400	-1.66446100	2.20797900
H	4.98538500	-0.89886100	1.42996200
C	0.32180900	-1.73371700	-0.00098800
N	1.47828400	-1.62210400	-0.10882600

3.3.2 Computation of NMR Data

3.3.2.1 General Considerations

All calculations were performed using supercomputing clusters provided by PittCRC. DFT calculations were carried out using Gaussian 09, Revision D.01.[4] All structures were subjected to initial Stochastic Conformational Sampling using Chem3D of ChemOffice 2018 package, employing force field method (MMFF94). Duplicate conformers were removed and conformers within 5 kcal/mol energy differences were optimized using either B3LYP/6-31G(d) or B3LYP/6-31+G(d,p). The optimized conformers were subsequently subjected to single-point NMR calculations using either GIAO/mPW1PW91/6-311+G(2d,p)/SMD(chloroform), GIAO/PBE0/6-311+G(2d,p)/SMD(chloroform), GIAO/B3LYP/6-311+G(2d,p)/SMD(chloroform), or

GIAO/B3LYP/6-31+G(d,p)/SMD(chloroform) method. Calculated isotropic values were scaled according to scaling-factors of the respective methods (eq 1); the scaling-factors were documented by Tantillo et al., and others.[5]

$$\delta = \frac{intercept - \sigma}{-slope} \quad (1)$$

$$\frac{P_i}{P_j} = e^{\Delta G / RT} \quad (2)$$

The performances of different methods were initially tested using the original reported structure (**1a**), and the scaled ^{13}C NMR were compared with our experimental spectra. GIAO/mPW1PW91/6-311+G(2d,p)/SMD(chloroform)//B3LYP/6-31+G(d,p) gave the lowest mean absolute deviation (MAD) and thus was chosen as the method for subsequent calculations.

The relative abundance (mole fractions/percentages) of the conformers were calculated according to eq 2 (ΔG in J mol^{-1}, R is gas constant in J K^{-1} mol^{-1}, T = 298 K), and subsequently used to calculated the weighted-averaged of the chemical shifts.

3.3.2.2 Optimized Structures of Originally Reported Structures
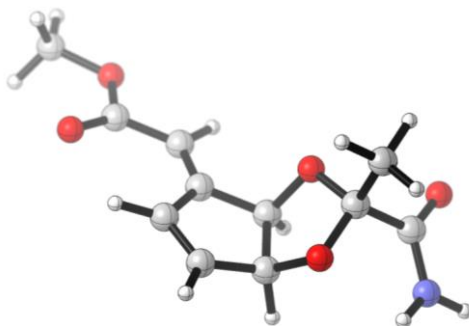
Original Conformer 1, optimized at B3LYP/6-31+G(d,p)

0 1

O	-2.32639200	1.19456900	0.22395100
C	-2.36162400	-0.18874000	0.60744500
O	-1.03490300	-0.65840300	0.48980000
C	-3.30903300	-0.99144800	-0.34347000
C	-2.82036200	-0.32580000	2.04731000
O	-3.28952700	-2.21347700	-0.37495200
N	-4.15721900	-0.22587100	-1.08319200
C	3.42432700	-0.16153600	-0.04507000
O	4.20845700	-1.26032600	-0.17688200
O	3.86340600	0.92909300	0.28331400
C	5.60679800	-1.07028700	0.10286800
H	1.90976100	2.31610000	0.40539400
H	-0.45585100	3.40234800	0.07917100
H	-1.56455900	1.64313900	-1.65334000
H	-0.53497000	-0.57169500	-1.53080100
H	1.82304300	-1.52313600	-0.63192800
H	-2.12916700	0.22139600	2.69220700
H	-3.82762900	0.08339400	2.16444200

H	-2.83024200	-1.38202500	2.32457800
H	-4.85649100	-0.68475900	-1.64886600
H	-4.15700900	0.77790000	-0.98256300
H	6.06820900	-2.04503300	-0.05275700
H	5.74729200	-0.73634900	1.13391200
H	6.03418500	-0.32720500	-0.57503300
C	1.01816900	1.81299700	0.05526300
C	-0.19763800	2.36796500	-0.12032700
C	-1.19831000	1.37657600	-0.65381300
C	-0.43587800	0.02554200	-0.61688700
C	1.00405100	0.39343000	-0.29673100
C	2.02044000	-0.49280300	-0.35390800
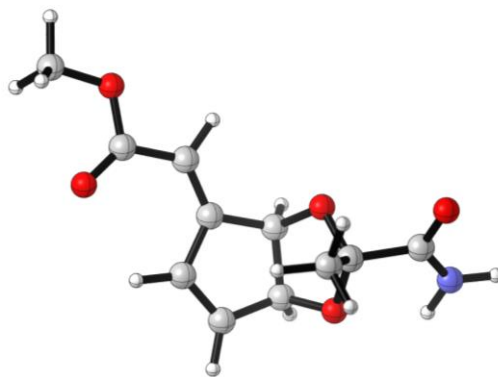
Original Conformer 2, optimized at B3LYP/6-31+G(d,p)

134

0 1

O	-2.36770700	1.13635200	0.06641700
C	-2.17059900	-0.24976800	0.36603600
O	-1.15618300	-0.70970700	-0.53510500
C	-3.45809600	-1.04597000	0.00911900
C	-1.78237200	-0.47748300	1.82062400
O	-3.58500300	-2.21135900	0.35857000
N	-4.37573000	-0.36453000	-0.72210500
C	3.33134500	-0.18768500	-0.03931400
O	4.11895500	-1.21788600	-0.43557000
O	3.72606400	0.70173100	0.69808900
C	5.46536400	-1.21092200	0.07173500
H	1.81519700	2.10917600	0.96040500
H	-0.51992300	3.29813800	0.83401900
H	-1.55227900	2.27938200	-1.41510700
H	-0.34446700	0.27917900	-2.12681000
H	1.82010300	-1.18831400	-1.25320600
H	-0.84707200	0.03786300	2.04730300

H	-2.56821300	-0.09470600	2.47889200
H	-1.66789400	-1.54852000	1.99617200
H	-4.25635800	0.62229800	-0.89164100
H	-5.23909400	-0.82803700	-0.96322200
H	5.93670400	-2.09977900	-0.34657000
H	5.98947500	-0.30742100	-0.24973500
H	5.46166900	-1.25309900	1.16373300
C	0.95782300	1.77550000	0.39048200
C	-0.24246400	2.38499300	0.31842300
C	-1.19945200	1.65238800	-0.58935100
C	-0.40966400	0.39698900	-1.04100000
C	0.97636900	0.55511300	-0.41403500
C	1.98395600	-0.31773800	-0.62583700
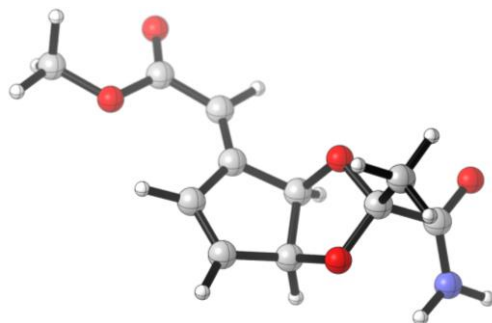
Original Conformer 3, optimized at B3LYP/6-31+G(d,p)

136

0 1

O	-2.16690600	1.30871900	0.14782900
C	-2.34602400	-0.03410100	0.62630900
O	-1.07935000	-0.65146100	0.53057300
C	-3.38835400	-0.79106300	-0.26061800
C	-2.79563000	-0.02282100	2.07528100
O	-3.51340400	-2.00518800	-0.19397800
N	-4.14254200	0.00789500	-1.06437100
C	3.39864000	-0.87443300	-0.14031100
O	3.89063800	0.35279700	0.16683000
O	4.10391600	-1.86611800	-0.21158300
C	5.31017600	0.40795700	0.40746400
H	2.16404300	1.95756500	0.25059100
H	-0.06074900	3.27472000	-0.12417000
H	-1.37670800	1.55649100	-1.75461200
H	-0.61023300	-0.75441400	-1.49717600
H	1.59150800	-1.91125400	-0.61575800
H	-2.03805900	0.48389000	2.67728800

H	-3.74854000	0.50492000	2.17092400
H	-2.92071200	-1.05033100	2.42318100
H	-4.89543900	-0.40891800	-1.59260600
H	-4.02952300	1.00992600	-1.03679000
H	5.52482700	1.45205000	0.63472500
H	5.57892500	-0.23396500	1.24961000
H	5.86011900	0.08444000	-0.47936300
C	1.22396200	1.53007800	-0.06961900
C	0.07697500	2.20868300	-0.26918300
C	-1.03436200	1.30894600	-0.74189800
C	-0.42800800	-0.11412700	-0.62634200
C	1.05250800	0.10325800	-0.34618000
C	1.94331500	-0.91077300	-0.38367400

3.3.2.3 Optimized Structures of Candidate Structures 1–5
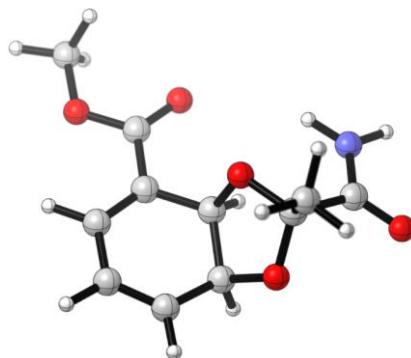
Candidate 1_conformer 1, optimized at B3LYP/6-31+G(d,p)

0 1

C	1.85374500	1.77540600	0.07013100
C	0.91326600	2.89073600	0.03219800
C	-0.35321400	2.72441000	-0.39026000
C	-0.84877000	1.40001100	-0.90502600
C	0.03243800	0.19674200	-0.51526300
C	1.46825000	0.50640100	-0.19014000
O	-2.12932500	1.08861800	-0.32976500
C	-2.01170000	-0.07756600	0.48996200
O	-0.62059800	-0.28940400	0.67968300
C	-2.67339400	-1.28698800	-0.24531800

C	-2.68997300	0.15589300	1.82831600
O	-3.82584700	-1.22536900	-0.65154400
N	-1.88793900	-2.39195100	-0.34696400
C	2.37494300	-0.66072400	-0.11858900
O	2.01949600	-1.80612900	-0.35142900
O	3.64210300	-0.33887000	0.22456000
C	4.56851100	-1.43861000	0.30736100
H	2.88763500	1.97536700	0.33280000
H	1.26256000	3.86553200	0.36000100
H	-1.06061900	3.54891400	-0.40809400
H	-0.97522400	1.45862300	-1.99509800
H	-0.01909100	-0.57564600	-1.29071700
H	-3.75093100	0.35278800	1.66215700
H	-2.58708900	-0.72796200	2.46449600
H	-2.22456500	1.01343000	2.31994700
H	-0.94559800	-2.40198900	0.01773000
H	-2.27310400	-3.21860800	-0.77987600
H	5.52075500	-0.99218600	0.59217000

H	4.23851600	-2.15830100	1.06017400

H	4.65107800	-1.94133600	-0.65919900
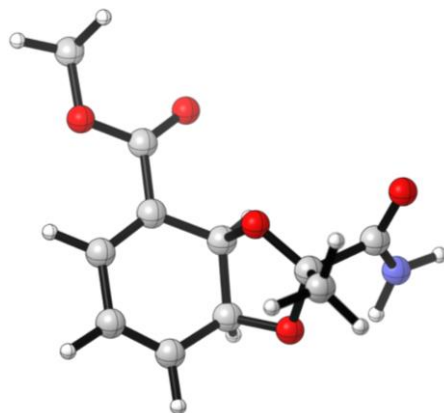
Candidate 1_conformer 2, optimized at B3LYP/6-31+G(d,p)

0 1

C	1.86508700	1.70417900	0.15574400

C	0.91881400	2.81621800	0.14425000

C	-0.32652600	2.66706500	-0.34061500

C	-0.78846500	1.36163200	-0.93156300

C	0.05677100	0.14570800	-0.51425800

C	1.49383700	0.44764500	-0.17344900

O	-2.10759300	1.02039100	-0.45957400

C	-2.00263600	-0.05362700	0.50016600

O	-0.61866600	-0.28128500	0.68805200
C	-2.67657900	-1.34001100	-0.07331300
C	-2.63573100	0.33432100	1.82387000
O	-2.77076200	-2.34905400	0.61064400
N	-3.11806500	-1.24909600	-1.35770900
C	2.43416400	-0.69865400	-0.19494300
O	2.15587500	-1.79442900	-0.64917300
O	3.64757700	-0.40059600	0.32574200
C	4.61103100	-1.47107100	0.31172600
H	2.89422500	1.89975700	0.43874000
H	1.25049700	3.77620200	0.52938700
H	-1.03478100	3.49099400	-0.35851000
H	-0.85029300	1.45619600	-2.02453600
H	0.00166900	-0.64862300	-1.26640800
H	-3.69305700	0.57342800	1.67813700
H	-2.55552200	-0.50130600	2.52148500
H	-2.11852400	1.20896700	2.22509800
H	-3.15523900	-0.34873800	-1.81088900

H	-3.62423000	-2.03357300	-1.74289700
H	5.50730500	-1.05836800	0.77408600
H	4.23873600	-2.32445600	0.88309300
H	4.81561100	-1.78746300	-0.71402600
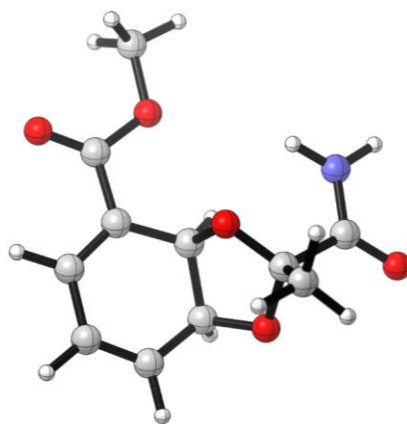
Candidate 1_conformer 3, optimized at B3LYP/6-31+G(d,p)

0 1

C	1.83776000	2.00929400	0.13847800
C	0.82630500	3.05257800	0.02270800
C	-0.39913900	2.78236300	-0.46174700
C	-0.76459700	1.41230400	-0.96507700
C	0.17038800	0.28304000	-0.48652700
C	1.56316500	0.70784900	-0.10136800

O	-2.05538200	1.02128400	-0.46891600
C	-1.90974200	-0.07005200	0.44292300
O	-0.51632500	-0.20479100	0.69094200
C	-2.49570100	-1.35572800	-0.22138600
C	-2.64029800	0.22703500	1.74142200
O	-3.64084600	-1.38270500	-0.64898300
N	-1.64889300	-2.42077200	-0.24531100
C	2.63627100	-0.29997700	0.07713100
O	3.77876700	-0.05499300	0.42077200
O	2.20613900	-1.55825600	-0.19933100
C	3.19484400	-2.59670400	-0.05851300
H	2.84462500	2.27816400	0.44493400
H	1.08697000	4.05770300	0.34092300
H	-1.16398700	3.54974500	-0.54313600
H	-0.82441100	1.43389300	-2.06207100
H	0.20102500	-0.51375800	-1.23764100
H	-2.51722100	-0.60139800	2.44527800
H	-2.23056600	1.13939800	2.18113900

H	-3.70344100	0.35998100	1.53151800
H	-0.73390400	-2.36059400	0.17733900
H	-1.99158400	-3.30105100	-0.60141300
H	4.03888700	-2.41161500	-0.72685400
H	3.55595000	-2.63986000	0.97165600
H	2.68554300	-3.52153200	-0.32863100

Candidate 2_conformer 1, optimized at B3LYP/6-31+G(d,p)

0 1

C	1.87108000	0.05857500	-0.31412900
C	1.59792700	1.50209900	-0.21172800
C	0.35047500	1.98948600	-0.29471400
C	-0.83588700	1.09623500	-0.51291700
C	-0.50413900	-0.35871800	-0.92928600
C	0.88711800	-0.81465100	-0.60460900

O	-1.53571000	0.91509700	0.73343800
C	-2.27532000	-0.27442700	0.59915200
O	-1.46494900	-1.15580100	-0.20237500
C	-3.63518900	0.00362000	-0.12304400
C	-2.51997800	-0.88290900	1.96797700
O	-4.38609000	0.88851400	0.26187100
N	-3.91128500	-0.82672400	-1.16562600
C	3.24199400	-0.48855700	-0.07346100
O	3.54007300	-1.66683000	-0.12895900
O	4.13474300	0.48519700	0.21474800
C	5.48496500	0.04537800	0.45920200
H	2.43725400	2.16402700	-0.03359100
H	0.15364500	3.04912200	-0.16464600
H	-1.52474400	1.54377100	-1.24298700
H	-0.68096000	-0.50201200	-2.00553300
H	1.09307300	-1.88006600	-0.64446400
H	-3.03783400	-1.84085500	1.86852900
H	-1.55927000	-1.04122000	2.46308300

H	-3.13677900	-0.20401200	2.56048800
H	-3.27773100	-1.57667900	-1.39797600
H	-4.81627100	-0.76274300	-1.60898100
H	6.05064800	0.95256500	0.66890700
H	5.51278600	-0.63549800	1.31300700
H	5.88236100	-0.46553400	-0.42088800

Candidate 2_conformer 2, optimized at B3LYP/6-31+G(d,p)

0 1

C	1.88608900	-0.01216700	-0.24176300
C	1.60001200	1.42143700	-0.06602300
C	0.36984100	1.91886100	-0.26216600
C	-0.77053100	1.06603100	-0.73945300
C	-0.52846600	-0.46300600	-0.63704100
C	0.90049200	-0.89537500	-0.49272200

147

O	-1.93540200	1.28601700	0.09220200
C	-2.36463000	0.02286400	0.62395700
O	-1.24173800	-0.82708900	0.55821600
C	-3.53500000	-0.55709300	-0.23732800
C	-2.80024500	0.17842600	2.06952100
O	-3.92084000	-1.70747900	-0.08762800
N	-4.08572000	0.31974900	-1.12134000
C	3.27911100	-0.54317500	-0.10490200
O	3.59742000	-1.70643400	-0.26045300
O	4.16399300	0.42789400	0.21509400
C	5.53187200	0.00188000	0.37069600
H	2.41418800	2.06516800	0.24517200
H	0.15759400	2.97293700	-0.10622800
H	-1.03322500	1.34438200	-1.76986200
H	-0.98670200	-0.97347200	-1.49612100
H	1.12196000	-1.95534400	-0.56219600
H	-3.62974200	0.88759700	2.13915300
H	-3.12547800	-0.78967300	2.45586000

H   -1.95662500   0.54970500   2.65566500

H   -3.77032200   1.27768500   -1.14770800

H   -4.90875900   0.03670800   -1.63343800

H   6.08846900   0.90406200   0.62218900

H   5.60933800   -0.73787500   1.17076100

H   5.90060000   -0.43550600   -0.55998500
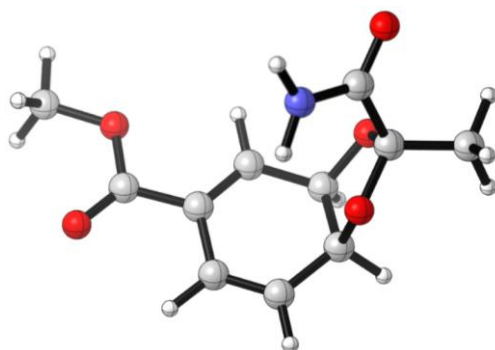
Candidate 3_conformer 1, optimized at B3LYP/6-31+G(d,p)

0 1

C   -1.04163800   1.77774400   -0.18424400

C   -0.58242100   0.79003100   -1.26705600

O   -1.85810100   0.93765800   0.66858900

C   -2.43349800   -0.09392000   -0.13280900

O   -1.66941500   -0.13937900   -1.35089800

C   -2.27341600   -1.46187300   0.59233600

C	-3.89031000	0.18131200	-0.46754500
O	-2.87771300	-2.44921900	0.19414400
N	-1.41238300	-1.46466600	1.64002600
C	0.73146900	0.11333200	-0.98125400
C	1.61962900	0.64448200	-0.11707200
C	1.29198300	1.85572500	0.65254900
C	0.06183000	2.39266500	0.63076700
C	2.96192800	0.03901500	0.12679000
O	3.77252100	0.49333000	0.91495500
O	3.18978600	-1.06405700	-0.61537100
C	4.46716100	-1.70124500	-0.41919300
H	-1.67957400	2.55210100	-0.62883400
H	-0.51263300	1.27954500	-2.24852400
H	-4.48320700	0.22713200	0.45037300
H	-4.27724300	-0.62166100	-1.09719100
H	-3.97027200	1.13491400	-0.99646500
H	-1.27945300	-2.32280500	2.15412200
H	-1.01539900	-0.59817400	1.97113200

H   0.95127400   -0.79278000   -1.53583200

H   2.08161100   2.27939800   1.26404800

H   -0.18169800   3.25934500   1.23754800

H   4.57625600   -2.02246300   0.61929200

H   4.46648700   -2.55915900   -1.09060600

H   5.27760200   -1.01301100   -0.67020200
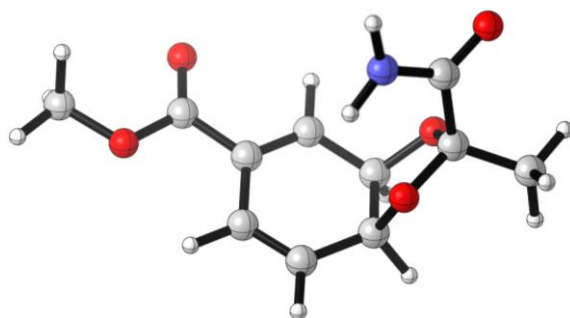
Candidate 3_conformer 2, optimized at B3LYP/6-31+G(d,p)

0 1

C   0.91391200   -1.74994400   0.06202500

C   0.65162200   -0.90657500   -1.19555700

O   1.73362700   -0.86153400   0.85844700

C   2.49977900   -0.05011300   -0.03079800

O   1.82351100   -0.08828500   -1.30032900

C   2.49110900   1.42117300   0.47412100

C	3.92092000	-0.56282200	-0.20181300
O	3.25867100	2.24497800	-0.00553000
N	1.57174800	1.69966500	1.43112100
C	-0.61132100	-0.09241500	-1.14900900
C	-1.62251100	-0.40413200	-0.31363900
C	-1.48235300	-1.50062800	0.66012100
C	-0.31140200	-2.13242700	0.84344000
C	-2.87634300	0.40634600	-0.39106500
O	-3.06816300	1.31792100	-1.17267500
O	-3.79498700	0.00911000	0.51996500
C	-5.03937600	0.73619900	0.51211900
H	1.50549700	-2.63733600	-0.19712400
H	0.62343500	-1.53528200	-2.09685700
H	4.45478200	0.07560600	-0.90766400
H	3.89884600	-1.58872200	-0.57958600
H	4.44470800	-0.54298200	0.75813700
H	1.52011500	2.64033000	1.79268800
H	1.02646900	0.95721400	1.84226300

H   -0.70777800   0.73202500   -1.84926800

H   -2.35186700   -1.76991200   1.24864100

H   -0.20778000   -2.90992000   1.59412000

H   -5.52808500   0.64043400   -0.46017200

H   -5.64434500   0.28197700   1.29615800

H   -4.86173300   1.79341300   0.72212900
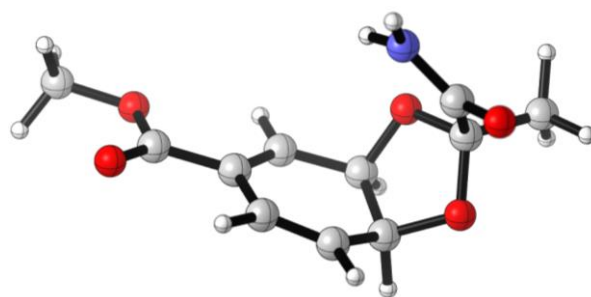
Candidate 3_conformer 3, optimized at B3LYP/6-31+G(d,p)

0 1

C   1.00651900   -0.67293700   1.51065600

C   0.41653000   -1.45091300   0.31960900

O   2.38288500   -0.52929600   1.13222000

C   2.45027300   -0.42593400   -0.28056600

O   1.25612200   -1.04694100   -0.79179200

C   2.50058300   1.07153700   -0.71826600

C	3.69351000	-1.15217800	-0.76932500
O	3.37395000	1.81340600	-0.28847700
N	1.56486900	1.44119000	-1.62932100
C	-1.01785600	-1.14215000	-0.01565600
C	-1.62573900	-0.03997900	0.46930500
C	-0.91407600	0.90284900	1.34643500
C	0.32119300	0.63759000	1.79712800
C	-3.03494100	0.31066000	0.11197500
O	-3.59533400	1.32137500	0.49472100
O	-3.62625500	-0.60643600	-0.68264100
C	-4.98584300	-0.32037900	-1.06612600
H	1.01558200	-1.28231100	2.42283800
H	0.54917900	-2.52917100	0.46895300
H	3.65130500	-2.19517900	-0.44573100
H	3.74658000	-1.11352900	-1.86094700
H	4.58046400	-0.67056200	-0.35249600
H	1.53708400	2.40450500	-1.92948600
H	0.82348600	0.80336500	-1.87649700

H	-1.53418100	-1.80795600	-0.69801700

H	-1.42671700	1.82374700	1.60218200

H	0.85831800	1.33938700	2.42888600

H	-5.03418200	0.61784600	-1.62376600

H	-5.62246000	-0.24616600	-0.18150400

H	-5.29039900	-1.15815900	-1.69242500
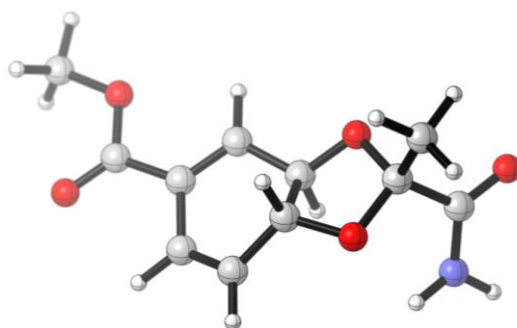
Candidate 4_conformer 1, optimized at B3LYP/6-31+G(d,p)

0 1

C	-0.60881200	0.91942200	0.70704400

C	-0.36475800	-0.22401400	-0.22817000

O	-2.00842200	1.02010200	0.63253500

C	-2.49351800	-0.30405100	0.47774900

O	-1.37562100	-1.10964800	0.15655600

C	-3.48593500	-0.35890200	-0.69961400
C	-3.13127200	-0.81548300	1.75035300
O	-4.16536800	-1.32994900	-0.86613200
N	-3.49153200	0.71227600	-1.51731400
C	1.06508400	-0.65210500	-0.14263400
C	1.94604600	0.34841700	-0.09348800
C	1.49304900	1.76710900	-0.04642300
C	0.24997400	2.07952900	0.30341900
C	3.41677900	0.11298500	-0.11773900
O	4.21923800	0.99236400	-0.14095900
O	3.74087300	-1.16858500	-0.11362600
C	5.12385700	-1.48093000	-0.13911500
H	-0.33553100	0.61890300	1.71853500
H	-0.54702700	0.11079400	-1.25023900
H	-2.40797500	-0.77204600	2.55519100
H	-3.45592800	-1.83596500	1.60939700
H	-3.98729300	-0.20410100	2.01028700
H	-4.17672500	0.73372900	-2.23911100

H	-3.06159600	1.56119300	-1.23468900
H	1.35342500	-1.68299900	-0.20205900
H	2.22167000	2.52048900	-0.27481400
H	-0.09403200	3.09353600	0.38890000
H	5.58328900	-1.08731900	-1.03390300
H	5.61934500	-1.07042900	0.72838500
H	5.18054600	-2.55785800	-0.12996100
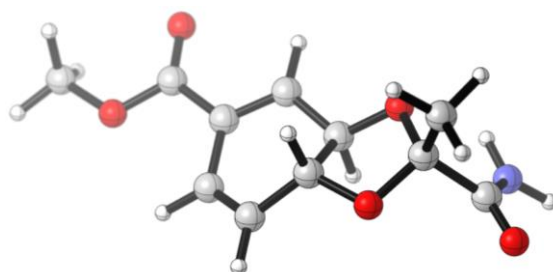
Candidate 4_conformer 2, optimized at B3LYP/6-31+G(d,p)

0 1

C	-0.55792800	1.01185000	0.36042600
C	-0.41634300	-0.39884600	-0.14797300
O	-1.95081700	1.23873800	0.18135800
C	-2.58284200	-0.01965000	0.49732800
O	-1.54594300	-1.03710000	0.44576200
C	-3.66392800	-0.25727400	-0.59093600

C	-3.20410100	-0.00677000	1.88390800
O	-4.60783300	0.51029000	-0.71039500
N	-3.47192500	-1.36130100	-1.35953000
C	0.95716600	-0.91160900	0.13570300
C	1.95936200	-0.02865100	-0.10075600
C	1.66137300	1.36314400	-0.51497700
C	0.43065300	1.89128200	-0.34523400
C	3.36583800	-0.51070600	0.04317800
O	3.68242900	-1.64195300	0.36097300
O	4.26614700	0.46264000	-0.21999400
C	5.65172700	0.08448400	-0.10053700
H	-0.32359800	1.02753400	1.44259500
H	-0.54740400	-0.38117200	-1.24820500
H	-4.01329900	0.72573500	1.90543500
H	-2.44645900	0.25405900	2.62699200
H	-3.60816900	-0.99468600	2.12504600
H	-4.17521200	-1.59946000	-2.04342000
H	-2.73483200	-2.01258100	-1.13537600

H	1.16015200	-1.94214900	0.40760900
H	2.47035600	1.95362400	-0.92839700
H	0.19305300	2.92025100	-0.59421100
H	5.88676000	-0.72111900	-0.79996300
H	5.86643200	-0.24896700	0.91729600
H	6.21796800	0.98359100	-0.34110100
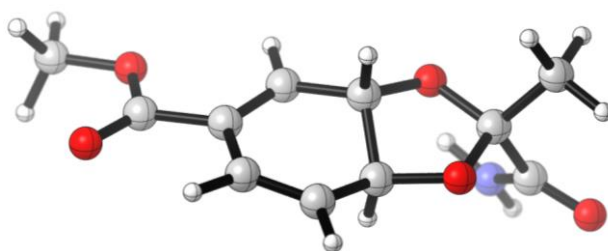
Candidate 5_conformer 1, optimized at B3LYP/6-31+G(d,p)

0 1

C	-0.71858100	0.96428600	-0.41188500
C	-0.31346700	0.10317600	0.75708800
O	-2.08410100	1.22255500	-0.10008900
C	-2.58556800	-0.00580700	0.46263000
O	-1.42381100	-0.78548500	0.86706500
C	-3.36692300	-0.78284300	-0.63622200

C	-3.47984500	0.31854400	1.64294200
O	-4.45963200	-0.38368400	-1.01439900
N	-2.74086700	-1.87935900	-1.13852500
C	1.05891000	-0.44965900	0.54277900
C	1.95563900	0.43259100	0.03386400
C	1.54099000	1.79921500	-0.35684800
C	0.24052600	2.10928400	-0.54065300
C	3.40204900	0.10019200	-0.11612900
O	4.24091600	0.89155000	-0.50672400
O	3.69045300	-1.17437300	0.22694900
C	5.07403500	-1.55797100	0.10395900
H	-0.66728900	0.36392900	-1.34086800
H	-0.27579600	0.74176600	1.66084800
H	-3.86162600	-0.60418400	2.08876900
H	-2.90839000	0.87283900	2.39135900
H	-4.32357200	0.92080700	1.30126700
H	-3.23566700	-2.44458700	-1.81326100
H	-1.90340300	-2.22663700	-0.69619200

H   1.34436700   -1.43952000   0.88021300

H   2.32904500   2.52383300   -0.52879300

H   -0.08827900   3.08591900   -0.88038100

H   5.11145300   -2.60270900   0.41081900

H   5.40927200   -1.44553000   -0.92966900

H   5.69876000   -0.94096800   0.75400100
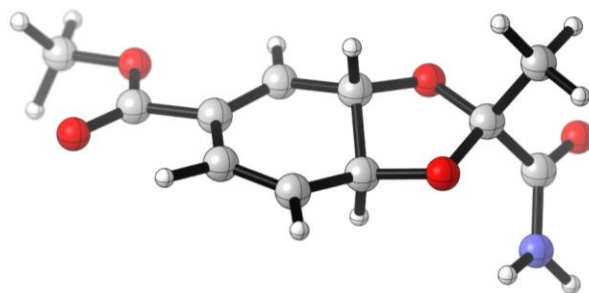
Candidate 5_conformer 2, optimized at B3LYP/6-31+G(d,p)

0 1

C   0.67513800   1.01457000   0.25521300

C   0.29446500   -0.07816400   -0.70893000

O   2.05158400   1.21080100   -0.08009100

C   2.55376000   -0.09849600   -0.45409900

O   1.40403000   -0.95936900   -0.61370800

C   3.41873700   -0.72096200   0.67497600

C	3.35020400	0.01892700	-1.74256300
O	3.90773000	-1.83381600	0.54513900
N	3.58227100	0.06461400	1.77161200
C	-1.07671800	-0.58505100	-0.39641000
C	-1.98725200	0.37581000	-0.09902200
C	-1.58671500	1.79850500	-0.00596000
C	-0.29128100	2.15381100	0.12270900
C	-3.43232900	0.07033600	0.10619700
O	-4.27825100	0.91892600	0.32523100
O	-3.71042700	-1.24808100	0.02280900
C	-5.09085600	-1.61269100	0.21588000
H	0.61277300	0.61701400	1.28635900
H	0.25841700	0.35834800	-1.72724500
H	4.16931400	0.73313600	-1.61435400
H	3.76424400	-0.95849200	-1.99760000
H	2.70066300	0.36971900	-2.54840200
H	4.18369900	-0.26317500	2.51315100
H	3.24192300	1.01427400	1.77059700

H	-1.34238600	-1.62971800	-0.50895400
H	-2.38161800	2.53607500	-0.00506700
H	0.02405600	3.18507900	0.24412400
H	-5.71912500	-1.13782200	-0.54129300
H	-5.11843100	-2.69721900	0.11593900
H	-5.42965300	-1.30677800	1.20847800
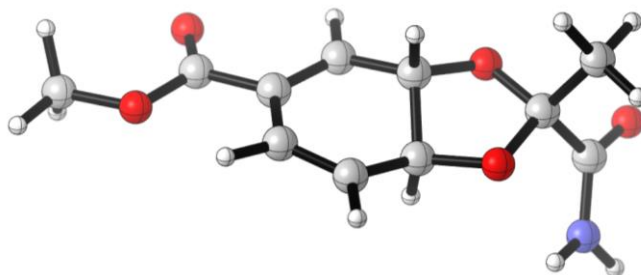
Candidate 5_conformer 3, optimized at B3LYP/6-31+G(d,p)

0 1

C	0.61268400	0.93221700	0.16195100
C	0.37120300	-0.27505000	-0.70617500
O	1.96726600	1.24650900	-0.17055200
C	2.61334100	-0.02764400	-0.42930200
O	1.56627000	-1.01857000	-0.51980500

C	3.52483700	-0.45546200	0.75200100
C	3.41060100	0.06737200	-1.71932000
O	4.13425600	-1.51450300	0.71729100
N	3.58726800	0.42995900	1.78125600
C	-0.94439000	-0.89420400	-0.36546500
C	-1.95969300	-0.01717600	-0.16558400
C	-1.71434400	1.44423800	-0.19855200
C	-0.46544100	1.94453700	-0.08627000
C	-3.33044400	-0.56701500	0.05532600
O	-3.60755000	-1.75112100	0.08342100
O	-4.24910900	0.41139400	0.22515500
C	-5.60262200	-0.03238900	0.44413100
H	0.56825400	0.62138400	1.22339600
H	0.31003000	0.06423100	-1.75987700
H	4.14426500	0.87630000	-1.64904900
H	2.73855800	0.27411700	-2.55596000
H	3.93330400	-0.87626800	-1.88681800
H	4.21035300	0.22966400	2.54985300

164

H	3.14776800	1.33449200	1.70203200
H	-1.11012400	-1.96624900	-0.38148100
H	-2.57236900	2.10041000	-0.28480700
H	-0.26213200	3.01025300	-0.06081600
H	-5.95386400	-0.61480300	-0.41079200
H	-6.18981600	0.87802400	0.55983800
H	-5.65855300	-0.64749100	1.34516800

3.3.2.4 Comparison of NMR Methods on Reported Structure

GIAO/B3LYP/6-31+G(d,p)/SMD(chloroform)//B3LYP/6-31G(d)

	conformer1 (56.3%)	conformer 2 (26.4%)	conformer3 (17.4%)	weighted- average	expt	absolute deviation
OCH$_3$	51.25	51.4	51.26	51.3	51.5	0.2
C1	167.765	167.88	167	167.8	166.4	1.4
C2	112.15	112.06	114.62	112.7	115.2	2.5
C3	162.14	165.83	158.95	162.7	156.0	6.7
C4	132.81	134.28	132.53	133.3	133.6	0.3
C5	146.31	148.31	146.4	147.0	141.5	5.5
C6	86.15	86.08	85.92	86.2	82.5	3.7
C7	82.98	82.81	84.2	83.2	80.3	2.9
C3'	22.55	22.42	22.86	22.6	23.4	0.8
C2'	114.49	115.69	114.62	114.9	109.0	5.9
C1'	171.33	168.91	171.29	170.9	173.1	2.2

MAD = 2.9

GIAO/B3LYP/6-311+G(2d,p)/SMD(chloroform)//B3LYP/6-31+G(d,p)

	conformer1 (57.5%)	conformer2 (22.9%)	conformer3 (19.6%)	weighted-average	expt	absolute deviation
OCH$_3$	50.70	50.57	50.54	50.6	51.5	0.9
C1	167.08	167.07	166.52	167.0	166.4	0.6
C2	112.03	112.27	114.70	112.6	115.2	2.6
C3	159.70	163.36	157.26	160.1	156.0	4.1
C4	132.33	134.24	132.57	132.8	133.6	0.8
C5	146.65	147.50	146.14	146.7	141.5	5.2
C6	83.66	84.62	83.78	83.9	82.5	1.4
C7	80.91	81.59	81.56	81.2	80.3	0.9
C3'	22.26	22.18	22.16	22.2	23.4	1.2
C2'	111.07	112.68	111.04	111.4	109.0	2.4
C1'	170.68	168.06	170.64	170.1	173.1	3.0

MAD =

2.1

GIAO/PBE0/6-311+G(2d,p)/SMD(chloroform)//B3LYP/6-31+G(d,p)

	conformer1 (57.5%)	conformer2 (22.9%)	conformer3 (19.6%)	weighted-average	expt	absolute deviation
OCH$_3$	50.66	50.56	50.56	50.6	51.5	0.9
C1	166.49	166.48	165.86	166.4	166.4	0.0
C2	112.51	112.70	115.10	113.1	115.2	2.1
C3	158.88	162.52	156.33	159.2	156.0	3.2
C4	132.90	134.76	133.09	133.4	133.6	0.2
C5	147.16	148.02	146.69	147.3	141.5	5.8
C6	82.80	83.78	82.88	83.0	82.5	0.5
C7	79.98	80.71	80.58	82.6	80.3	2.3
C3'	22.12	22.29	22.05	22.1	23.4	1.3
C2'	109.51	111.06	109.46	109.9	109.0	0.9
C1'	170.14	167.50	170.08	169.5	173.1	3.6

MAD =

1.9

GIAO/mPW1PW91/6-311+G(2d,p)/SMD(chloroform)//B3LYP/6-31+G(d,p)

	conformer1 (57.5%)	conformer2 (22.9%)	conformer3 (19.6%)	weighted-average	natural	absolute deviation
OCH$_3$	50.78	50.68	50.68	50.7	51.5	0.8
C1	166.60	166.60	165.98	166.5	166.4	0.1
C2	112.45	112.67	115.01	113.0	115.2	2.2
C3	158.84	162.53	156.30	159.2	156.0	3.2
C4	132.87	134.69	133.05	133.3	133.6	0.3
C5	147.01	147.84	146.56	147.1	141.5	5.6
C6	82.79	83.75	82.87	83.0	82.5	0.5
C7	79.94	80.67	80.55	80.2	80.3	0.1
C3'	22.09	22.26	22.02	22.1	23.4	1.3
C2'	109.55	111.06	109.49	109.9	109.0	0.9
C1'	170.22	167.56	170.16	169.6	173.1	3.5

MAD =

1.7

3.3.2.5 Calculation of NMR for Candidate Structures

Candidate Structure 1 ^{13}C NMR

	conformer1 (53.4%)	conformer2 (5.3%)	conformer3 (41.3%)	weighted- average	natural	absolute deviation
OCH$_3$	51.16	51.12	51.35	51.2	52.2	1.0
C1	166.30	165.36	165.86	166.1	164.5	1.6
C2	123.35	124.44	122.98	123.3	130.0	6.7
C3	137.85	137.50	139.92	138.7	136.2	2.5
C4	120.26	121.34	120.55	120.4	124.4	4.0
C5	139.69	139.31	139.92	139.8	129.1	10.7
C6	73.65	74.93	74.22	74.0	79.2	5.2
C7	68.26	67.59	68.59	68.4	80.9	12.5
C3'	21.60	21.13	21.75	21.6	22.1	0.5
C2'	101.88	103.24	102.25	102.1	109.8	7.7
C1'	169.20	169.91	169.40	169.3	172.1	2.8

MAD = 5.0

RMSD = 6.2

Candidate Structure 1 ¹H NMR

	conformer1 (53.4%)	conformer2 (5.3%)	conformer3 (41.3%)	weighted-average	natural	absolute deviation
OCH$_3$	3.61	3.58	3.63	3.62	3.79	0.17
C1	-	-	-	-	-	-
C2	-	-	-	-	-	-
C3	7.17	7.15	7.35	7.24	7.43	0.19
C4	6.08	6.10	6.11	6.09	6.43	0.34
C5	6.22	6.18	6.24	6.21	6.56	0.35
C6	4.80	4.94	4.81	4.80	4.42	0.38
C7	4.81	4.79	4.73	4.76	4.46	0.30
C3'	1.42	1.44	1.41	1.41	1.66	0.25
C2'	-	-	-	-	-	-
C1'	-	-	-	-	-	-

MAD = 0.28

RMSD = 0.29

Candidate Structure 2 ^{13}C NMR

	conformer1 (57.6%)	conformer2 (42.4%)	weighted-average	natural	absolute deviation
OCH3	51.55	51.59	51.6	52.2	0.4
C1	164.19	164.33	164.2	164.5	0.3
C2	124.78	129.35	126.7	130.0	3.3
C3	139.65	134.82	137.6	136.2	1.4
C4	125.18	119.49	122.8	124.4	1.6
C5	123.79	128.18	125.7	129.1	3.4
C6	68.07	72.13	69.8	79.2	9.4
C7	73.05	68.58	71.2	80.9	9.7
C3'	21.13	21.19	21.2	22.1	0.9
C2'	101.88	101.71	101.8	109.8	8.0
C1'	170.14	170.08	170.1	172.1	2.0

MAD =

3.7

RMSD =

5.1

Candidate Structure 2 ^{1}H NMR

	conformer1 (57.6%)	conformer2 (42.4%)	weighted-average	natural	absolute deviation
OCH3	3.61	3.62	3.61	3.79	0.18
C1	-	-	-	-	
C2	-	-	-	-	-
C3	6.97	7.16	7.05	7.43	0.38
C4	6.63	6.38	6.52	6.43	0.09
C5	6.05	5.87	6.97	6.56	0.41
C6	4.26	4.74	4.46	4.42	0.04
C7	4.85	4.47	4.69	4.46	0.23
C3'	1.46	1.45	1.46	1.66	0.20
C2'	-	-	-	-	-
C1'	-	-	-	-	-

MAD =

0.22

RMSD =

0.25

Candidate Structure 3 ^{13}C NMR

	conformer1 (64.5%)	conformer2 (15.2%)	conformer3 (20.3%)	weighted-average	natural	absolute deviation
OCH$_3$	51.3	51.5	51.4	51.4	52.2	0.8
C1	164.4	163.8	165.1	164.5	164.5	0.0
C2	125.0	125.2	129.5	125.9	130.0	4.1
C3	141.7	143.8	133.5	140.4	136.2	4.2
C4	127.1	126.8	122.4	126.1	124.4	1.7
C5	123.7	123.7	131.2	125.2	129.1	3.9
C6	68.8	68.8	74.8	70.0	79.2	9.2
C7	74.7	74.8	69.2	73.6	80.9	7.3
C3'	19.9	19.5	22.3	20.3	22.1	1.8
C2'	103.9	103.6	105.9	104.3	109.8	5.5
C1'	167.8	167.3	169.9	168.2	172.1	3.9

MAD =

3.9

RMSD =

4.7

Candidate Structure 3 ^{1}H NMR

	conformer1 (64.5%)	conformer2 (15.2%)	conformer3 (20.3%)	weighted-average	natural	absolute deviation
OCH$_3$	3.59	3.58	3.62	3.59	3.79	0.20
C1	-	-	-	-	-	-
C2	-	-	-	-	-	-
C3	6.84	7.00	7.05	6.91	7.43	0.52
C4	6.84	6.71	6.51	6.75	6.43	0.32
C5	6.14	6.12	5.91	6.09	6.56	0.47
C6	4.42	4.43	4.91	4.52	4.42	0.10
C7	4.96	4.98	4.49	4.87	4.46	0.41
C3'	1.47	1.44	1.49	1.47	1.66	0.19
C2'	-	-	-		-	-
C1'	-	-	-		-	-

MAD = 0.32

RMSD = 0.35

Candidate Structure 4 ^{13}C NMR

	conformer1 (89.3%)	conformer2 (10.7%)	weighted-average	natural	absolute deviation
OCH$_3$	51.37	51.50	51.4	52.2	0.8
C1	164.19	163.77	164.1	164.5	0.4
C2	129.00	129.31	129	130.0	1.0
C3	141.64	142.76	141.8	136.2	5.6
C4	131.89	123.73	131	124.4	6.6
C5	131.08	132.11	131.2	129.1	2.1
C6	78.65	77.73	78.6	79.2	0.6
C7	80.22	81.57	80.4	80.9	0.5
C3'	20.67	21.10	20.7	22.1	1.4
C2'	110.69	111.61	110.8	109.8	1.0
C1'	176.88	167.96	175.9	172.1	3.8

MAD =

2.2

RMSD =

3.0

Candidate Structure 4 ^{1}H NMR

	conformer1 (89.3%)	conformer2 (10.7%)	weighted-average	natural	absolute deviation
OCH$_3$	3.58	3.59	3.58	3.79	0.21
C1	-	-	-	-	-
C2	-	-	-	-	-
C3	7.41	7.61	7.43	7.43	0.00
C4	6.54	6.34	6.52	6.43	0.09
C5	6.50	6.50	6.50	6.56	0.06
C6	4.53	4.49	4.53	4.42	0.11
C7	4.65	4.58	4.64	4.46	0.18
C3'	1.53	1.51	1.53	1.66	0.13
C2'	-	-	-	-	-
C1'	-	-	-	-	-

MAD =

0.11

RMSD =

0.13

Candidate Structure 5 ^{13}C NMR

	conformer1 (72.2%)	conformer2 (20.3%)	conformer3 (7.5%)	weighted-average	natural	absolute deviation
OCH$_3$	51.30	51.29	51.39	51.3	52.2	0.90
C1	163.75	163.93	163.58	163.8	164.5	0.70
C2	129.14	128.80	128.65	129	130.0	1.00
C3	140.70	141.90	144.10	141.2	136.2	5.00
C4	124.28	124.83	124.29	124.40	124.4	0.00
C5	131.79	131.04	130.97	131.60	129.1	2.50
C6	78.67	79.72	79.40	78.90	79.2	0.30
C7	80.31	79.55	80.07	80.10	80.9	0.80
C3'	21.07	21.18	21.24	21.10	22.1	1.00
C2'	110.72	111.43	111.39	110.90	109.8	1.10
C1'	168.46	167.77	168.03	168.30	172.1	3.80

MAD =

1.6

RMSD =

2.2

Candidate Structure 5 ^{1}H NMR

	conformer1 (72.2%)	conformer2 (20.3%)	conformer3 (7.5%)	weighted-average	natural	absolute deviation
OCH$_3$	3.57	3.57	3.59	3.57	3.79	0.22
C1	-	-	-	-	-	-
C2	-	-	-		-	-
C3	7.45	7.44	7.63	7.46	7.43	0.03
C4	6.47	6.46	6.38	6.46	6.43	0.03
C5	6.52	6.49	6.47	6.51	6.56	0.05
C6	4.57	4.51	4.47	4.55	4.42	0.13
C7	4.58	4.62	4.58	4.59	4.46	0.13
C3'	1.56	1.51	1.51	1.55	1.66	0.11
C2'	-	-	-	-	-	MAD = 0.10
C1'	-	-	-	-	-	RMSD = 0.12

3.4 Experimental Section for Chapter 2

3.4.1 General Procedures for Visible-Light Mediated Dioxolane Addition

Method A

Alkene (0.20 mmol, 1.0 equiv), $(n\text{-}Bu_4N)_2S_2O_8$ (0.20 mmol, 1.0 equiv), and *fac*-Ir(ppy)$_3$ (1.0 µmol, 0.50 mol%) were mixed in a 2-dram vial. Degassed 1,3-dioxolane (3.0 mL) was added using a syringe, and the vial was flushed with argon for 1 min and sealed. The vial was stirred under household LED irradiation (15 W × 4) for 24 h. The vial was placed ca. 5 cm from each LED and ca. 15 cm from the fan. The reaction vial was shielded with an aluminum-foil wall to maximize absorption. Upon completion of reaction as indicated by TLC analysis, the solvent was removed *in vacuo*. The crude material was dissolved in EtOAc (2 mL), the resulting mixture was poured into DI water (5 mL), and the layers were partitioned. The aqueous layer was extracted with EtOAc (2 mL × 2). The combined organic layers were filtered through a plug of Na_2SO_4 and concentrated *in vacuo*. The crude material was purified by flash column chromatography (3 mL of SiO_2).

(a) Start of the reaction

(b) During the reaction.

Figure 10. Typical experimental set up for visible light mediated reactions

Method B

Alkene (0.20 mmol, 1.0 equiv), (n-Bu$_4$N)$_2$S$_2$O$_8$ (0.10 mmol, 0.50 equiv), fac-Ir(ppy)$_3$ (1.0 μmol, 0.50 mol%) were mixed in a 2-dram vial. Degassed 1,3-dioxolane (3.0 mL) was added using a syringe, and the vial was flushed with argon for 1 min and sealed. The vial was stirred under household LED irradiation (15W × 4) for 24 h. The vial was placed ca. 5 cm from each LED and ca. 15 cm from the fan. The reaction vial was shielded with an aluminum-foil wall to maximize absorption. Upon completion of reaction as indicated by TLC analysis, the solvent was removed *in vacuo*. The crude material was directly purified using flash column chromatography (3 mL of SiO$_2$).

Method C

2-122 (0.10 mmol, 1.0 equiv), (n-Bu$_4$N)$_2$S$_2$O$_8$ (0.10 mmol, 1.0 equiv), and *fac*-Ir(ppy)$_3$ (0.0010 mmol, 0.50 mol%) were mixed in a 2-dram vial. Degassed 1,3-dioxolane (1.0 mL) was added using a syringe, the vial was flushed with argon for 1 min and sealed. The vial was stirred under household LED irradiation (15W × 4) for 24 h. The vials are placed ca. 5 cm from each LED and ca. 15 cm from the fan. The reaction vial was shielded with an aluminum-foil wall to maximize absorption. Upon completion of reaction as indicated by TLC analysis, the solvent was removed *in vacuo*. Mesitylene was added as external standard (for accuracy, the mass of mesitylene was recorded instead of volume). The NMR yield was determined by comparing the peaks at δ 6.79 (aromatic C-H of mesitylene) and δ5.14 (C2-H from dioxolanyl of product).

Method D

Alkene (0.10 mmol, 1.0 equiv), (n-Bu$_4$N)$_2$S$_2$O$_8$ (0.10 mmol, 1.0 equiv), *fac*-Ir(ppy)$_3$ (0.0010 mmol, 0.50 mol%), and C–H donors (10 equiv) were mixed in a 2-dram vial. Degassed MeCN (3.0 mL) was added using a syringe, and the vial was flushed with argon for 1 min and sealed. The vial was stirred under household LED irradiation (15W × 4) for 24 h. The vials are placed ca. 5 cm from each LED and ca. 15 cm from the fan. The reaction vial was shielded with an aluminum-foil wall to maximize absorption. Upon completion of reaction as indicated by TLC analysis, the solvent was removed *in vacuo*. The crude material was dissolved in EtOAc (2 mL) poured into DI water (5 mL), and the layers were partitioned. The aqueous layer was extrated with EtOAc (2 mL × 2). The combined organic layers were filtered through a plug of Na$_2$SO$_4$ and concentrated *in vacuo*. The crude material was purified by flash column chromatography (3 mL of SiO$_2$).
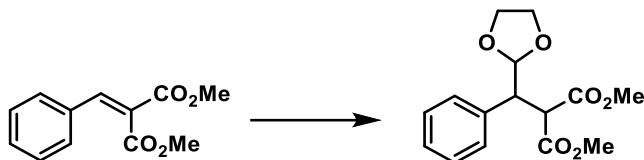
Dimethyl 2-((1,3-dioxolan-2-yl)(phenyl)methyl)malonate (2-122) was obtained as a colorless oil (54 mg, 91%) using method A in the general procedure. $R_f = 0.20$ (20% EtOAc in hexanes); IR (neat) 2955, 2894, 1737, 1455, 1498, 1455, 1436 cm^{-1}; ^{1}H NMR (CDCl$_3$, 500 MHz) δ 7.31-7.27 (m, 4H), 7.25-7.22 (m, 1H), 5.14 (d, $J = 4.0$ Hz, 1H), 4.08 (d, $J = 11.0$ Hz, 1H), 3.84-3.79 (*m*, 4H), 3.84-3.79 (*m*, 1H), 3.77 (s, 3H), 3.42 (s, 3H); ^{13}C {^{1}H} NMR (125 MHz, CDCl$_3$) δ 168.5, 167.9, 136.6, 129.2, 128.2, 127.4, 104.5, 65.1 65.0, 52.8, 52.6, 52.3, 49.0; HRMS (ESI-TOF): *m/z* for [M+H]$^+$ C$_{15}$H$_{19}$O$_6$, calcd 295.1176, found 295.1162.
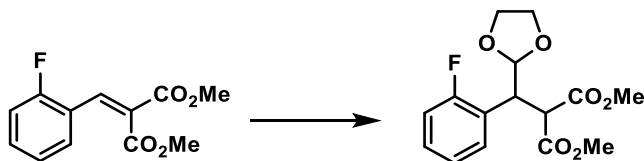
Dimethyl 2-((1,3-dioxolan-2-yl)(2-fluorophenyl)methyl)malonate (2-147) was obtained as a colorless oil (53 mg, 85%) using method A in the general procedure. $R_f = 0.18$ (20% EtOAc in hexanes); IR (neat) 2956, 2895, 1737, 1587, 1494, 1435 cm^{-1}; ^{1}H NMR (CDCl$_3$, 500 MHz) δ 7.31 (*app* dt, $J = 7.5, 1.5$ Hz, 1H), 7.23 (*app* dq, $J = 4.0, 2.0$ Hz, 1H), 7.08 (*app* dt, $J = 8.0, 1.5$ Hz, 1H), 7.03 (ddd, $J = 10.0, 8.0, 1.0$ Hz, 1H), 5.20, (d, $J = 4.0$ Hz, 1H), 4.20 (d, $J = 11.5, 4.5$ Hz, 1H), 4.12 (*app* d, $J = 11.0$ Hz, 1H), 3.86 (dd, $J = 6.0, 2.0$ Hz, 1H), 3.85-3.81 (m, 3H), 3.78 (s, 3H), 3.47 (s, 3H); ^{13}C {^{1}H} NMR (125 MHz, CDCl$_3$) δ 168.3, 167.7, 161.0 ($J_{CF} = 245$ Hz), 130.0 ($J_{CF} = 3.8$ Hz), 129.0 ($J_{CF} = 8.8$ Hz), 123.9 ($J_{CF} = 13.8$ Hz), 123.8 ($J_{CF} = 3.8$ Hz), 115.4 ($J_{CF} = 22.5$ Hz), 103.9, 65.10, 65.0, 52.7, 52.4, 52.2, 41.9; HRMS (ESI-TOF) *m/z* for [M+H]$^+$ C$_{15}$H$_{18}$O$_6$F, calcd 313.1082, found 313.1068.
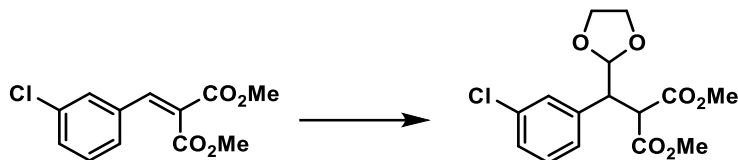
Dimethyl 2-((3-chlorophenyl)(1,3-dioxolan-2-yl)methyl)malonate (2-148) was obtained as a pale-yellow oil (55 mg, 84%) using method A in the general procedure. $R_f = 0.39$ (40% EtOAc in hexanes); IR (neat) 2955, 2894, 1738, 1598, 1573, 1435 cm^{-1}; ^{1}H NMR (500 MHz, CDCl$_3$) δ 7.32 (d, J = 1.0 Hz, 1H), 7.23-7.18 (m, 3H), 5.12 (d, J = 3.5 Hz, 1H), 4.05, (d, J = 11.5 Hz, 1H), 3.81-3.79 (m, 5H), 3.77 (s, 3H), 3.48 (s, 3H); ^{13}C {^{1}H} NMR (125 MHz, CDCl$_3$) δ 168.24, 167.7, 138.7, 134.0, 129.5, 129.4, 127.7, 127.6, 104.2, 65.24, 65.15, 52.7, 52.6, 52.5, 48.6; HRMS (ESI-TOF) m/z for [M+H]$^+$ C$_{15}$H$_{18}$O$_6$Cl, calcd 329.0786, found 329.0771.

Dimethyl 2-((4-bromophenyl)(1,3-dioxolan-2-yl)methyl)malonate (2-149) was obtained as a pale-yellow oil (69 mg, 92%) using method A in the general procedure. $R_f = 0.13$ (20% EtOAc in hexanes); IR (neat) 2959, 2892, 1748, 1492 cm^{-1}; ^{1}H NMR (500 MHz, CDCl$_3$) δ 7.42 (dd, J = 7.0, 2.0 Hz, 2H), 7.19 (dd, J = 6.5, 2.0 Hz, 2H), 5.10, (d, J = 3.5 Hz, 1H), 4.03, (d, J = 11.0 Hz, 1H), 3.81-3.78 (m, 5H), 3.7 (s, 3H), 3.47 (s, 3H); ^{13}C {^{1}H} NMR (125 MHz, CDCl$_3$) δ 168.3, 167.7, 135.6, 131.3, 131.1, 121.6, 104.2, 65.22, 65.15, 52.7, 52.6, 52.5, 48.4; HRMS (ESI-TOF) m/z for [M+H]$^+$ C$_{15}$H$_{18}$O$_6$Br, calcd 373.02813, found 373.0266 and 376.0273.
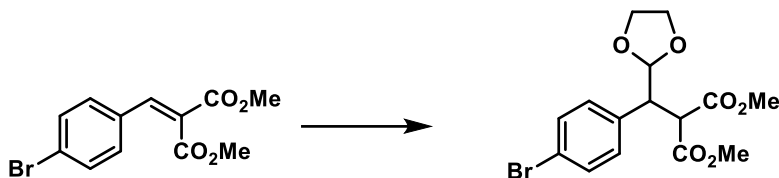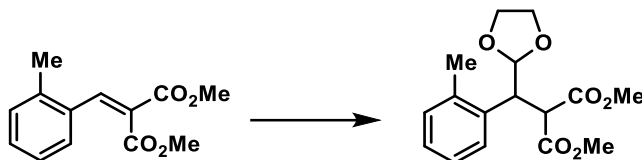
Dimethyl 2-((1,3-dioxolan-2-yl)(o-tolyl)methyl)malonate (2-150) was obtained as a colorless oil (48 mg, 78%) using method A in the general procedure. R_f = 0.38 (30% EtOAc in hexanes); IR (neat) 2955, 2892, 1739, 1495, 1435 cm^{-1}; ^{1}H NMR (500 MHz, CDCl$_3$) δ 7.24 (dd, J = 8.5, 2.0 Hz, 1H), 7.16-7.11 (m, 1H), 5.09 (d, J = 3.5 Hz, 1H), 4.18 (dd, J = 11.5, 4.0 Hz, 1H), 4.10 (d, J = 11.5 Hz), 3.83-3.78 (m, 4H), 3.78 (s, 3H), 3.41 (s, 3H), 2.45 (s, 3H); ^{13}C {^{1}H} NMR (125 MHz, CDCl$_3$) δ 168.71, 167.94, 137.7, 135.3, 130.3, 127.4, 127.1, 125.7, 104.8, 65.2, 65.1, 53.0, 52.7, 52.3, 43.6, 20.1; HRMS (ESI-TOF) m/z for [M+H]$^+$ C$_{16}$H$_{21}$O$_6$, calcd 309.1333, found 309.1318.
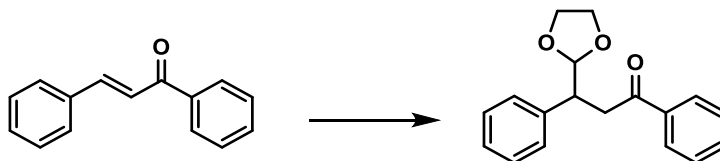
3-(1,3-dioxolan-2-yl)-1,3-diphenylpropan-1-one (2-121) was obtained as a white solid (20 mg, 35%) using method A of the general procedure. X-ray crystals were obtained by slow evaporation in EtOAc/hexanes. R_f = 0.33 (20% EtOAc in hexanes); m.p. = 88–90 °C; IR (thin film) 3065, 2882, 1733, 1675, 1596, 1580, 1498, 1450 cm^{-1}; ^{1}H NMR (300 MHz, CDCl$_3$) δ 7.94 (dd, J = 8.1, 1.2 Hz, 2H), 7.51 (*app* dt, J = 8.1, 1.2 Hz, 1H), 7.43-7.41 (m, 2H), 7.38-7.35 (m, 2H), 7.32-7.28 (m, 3H), 7.26-721 (m, 1H), 5.10 (d, J = 3.6 Hz, 1H), 3.90-3.82 (m, 4H), 3.81-3.76 (m, 1H), 3.58 (dd, J = 16.8, 5.4 Hz, 1H), 3.37 (dd, J = 16.8, 8.1 Hz, 1H); ^{13}C {^{1}H} NMR (75 MHz, CDCl$_3$) δ 198.3, 139.8, 137.2, 132.9, 128.8, 128.5, 128.3, 128.1, 126.9, 106.0, 65.2, 65.0, 44.7, 38.8, 29.7; HRMS (ESI-TOF) m/z for [M+H]$^+$ C$_{18}$H$_{19}$O$_3$ calcd 283.1329, found 283.1319.
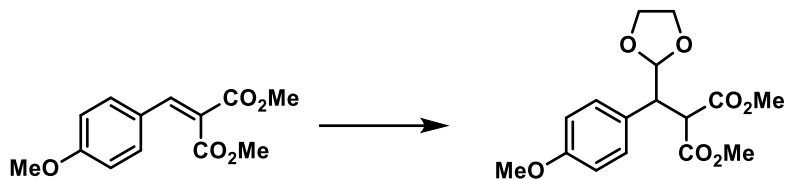
Dimethyl 2-((1,3-dioxolan-2-yl)(4-methoxyphenyl)methyl)malonate (2-151) was

obtained as a pale-yellow oil (59 mg, 90%) using method A in the general procedure. R_f = 0.30

(40% EtOAc in hexanes); IR (neat) 2955, 2896, 1738, 1613, 1515, 1435 cm^{-1}; ^{1}H NMR (400 MHz,

CDCl$_3$) δ 7.23 (d, J = 8.8 Hz, 2H), 6.82 (d, J = 8.8 Hz, 2H), 5.11 (d, J = 3.6 Hz, 1H), 4.03 (d, J =

10.8 Hz, 1H), 3.83-3.76 (m, 5H), 3.77 (s, 3H), 3.76 (s, 3H), 3.45 (s, 3H); ^{13}C {^{1}H} NMR (100

MHz, CDCl$_3$) δ 168.6, 167.9, 158.8, 130.2, 128.5, 113.6, 104.7, 65.13, 65.05, 55.1, 52.9, 52.6,

52.3, 48.2; HRMS (ESI-TOF) m/z for [M+H]$^+$ C$_{16}$H$_{21}$O$_7$, calcd 325.1282, found 325.1267.
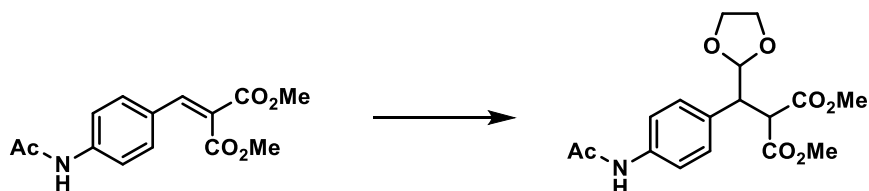
Dimethyl 2-((4-acetamidophenyl)(1,3-dioxolan-2-yl)methyl)malonate (2-152) was

ontained as a yellow oil (53 mg, 76%) using method B in the general procedure. R_f = 0.13 (60%

EtOAc in hexanes); IR (neat) 3319 (br); 3123, 2955, 2926, 2854, 1737, 1671, 1602, 1632, 1436

cm^{-1}; ^{1}H NMR (500 MHz, CDCl$_3$) δ 7.80 (br s, 1H), 7.43 (d, J = 8.5 Hz, 2H), 7.23 (d, J = 8.5 Hz,

2H), 5.10 (d, J = 3.5 Hz, 1H), 4.05 (d, J = 11.0 Hz, 1H), 3.86-3.79 (m, 5H), 3.77 (s, 3H), 3.45 (s,

3H), 2.14 (s, 3H); ^{13}C {^{1}H} NMR (125 MHz, CDCl$_3$) δ 168.5, 168.47, 168.0, 137.4, 132.1, 130.5,

129.7, 119.4, 104.5, 65.1, 65.0, 52.8, 52.6, 52.4, 48.4, 24.4; HRMS (ESI-TOF) m/z for [M+H]$^+$

C$_{17}$H$_{22}$O$_7$N, calcd 352.1391, found 352.1374.
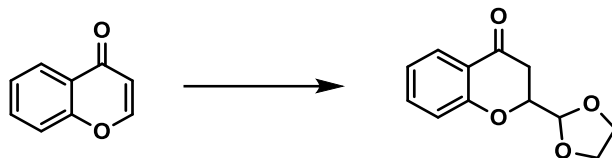
2-(1,3-dioxolan-2-yl)chroman-4-one (2-115) was obtained as a colorless oil (38 mg, 86%) using method A of the general procedure. R_f = 0.22 (30% EtOAc in hexanes); IR (neat) 2892, 1683, 1609, 1579, 1474, 1465 cm^{-1}; ^{1}H NMR (500 MHz, CDCl$_3$) δ 7.87 (dd, J = 8.0, 1.5 Hz, 1H), 7.48 (ddd, J = 9.0, 7.5, 1.5 Hz, 1H), 7.03 (*app* d, J = 8.0 Hz, 1H), 7.01 (d, J = 7.0 Hz), 5.20 (d, J = 3.5 Hz, 1H), 4.53 (*app* dt, J = 12.0, 4.0 Hz, 1H), 4.07-4.01 (m, 2H), 4.01-3.96 (m, 2H), 2.89 (dd, J = 17.0, 12.0 Hz, 1H), 2.77 (dd, J = 17.0, 3.5 Hz, 1H); ^{13}C {^{1}H} NMR (125 MHz, CDCl$_3$) δ 191.3, 160.7, 136.0, 126.7, 121.5, 121.1, 117.9, 103.0, 65.7, 65.4, 37.1; HRMS (ESI-TOF) *m/z* for [M+H]$^+$ C$_{12}$H$_{13}$O$_4$ calcd 221.0808, found 221.0808.
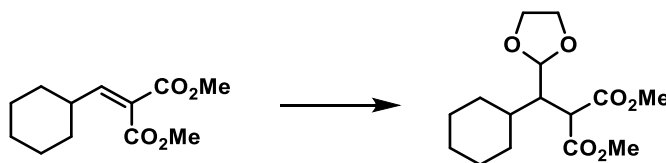
Dimethyl 2-(cyclohexyl(1,3-dioxolan-2-yl)methyl)malonate (2-153) was obtained as a color oil (47 mg, 78%) using method A of the general procedure. R_f = 0.26 (20% EtOAc in hexanes); IR (neat) 2928; 2854, 1737, 1450, 1435 cm^{-1}; ^{1}H NMR (500 MHz, CDCl$_3$) δ 5.14 (d, J = 4.5 Hz, 1H), 3.91-3.87 (m, 2H), 3.85-3.81 (m, 2H), 2.50 (ddd, J = 9.0, 7.0, 4.5 Hz, 1H), 1.74-1.72 (m, 4H), 1.65-1.60 (m, 2H), 1.26-1.21 (m, 5H); ^{13}C {^{1}H} NMR (125 MHz, CDCl$_3$) δ 169.6, 169.5, 103.3, 64.9, 64.5, 52.3, 49.7, 47.6, 37.9, 31.6, 29.9, 26.9, 26.7, 26.4; HRMS (ESI-TOF) *m/z* for [M+H]$^+$ C$_{15}$H$_{25}$O$_6$, calcd 301.1646, found 301.1634.

187
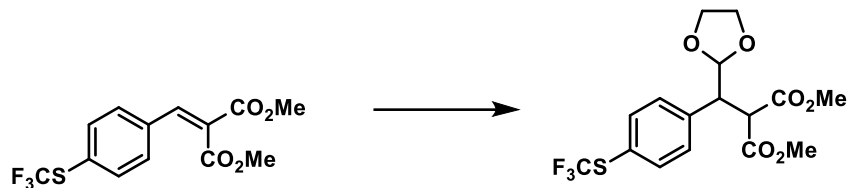
Dimethyl 2-((1,3-dioxolan-2-yl)(4-((trifluoromethyl)thio)phenyl)methyl)malonate (2-155) was obtained as a pale-yellow oil (61 mg, 77%) using method A of the general procedure. R_f = 0.41(40% EtOAc in hexanes); IR (neat) 1736, 1436, 1304, 1255 cm^{-1}; ^{1}H NMR (500 MHz, CDCl$_3$) δ 7.58 (d, J = 8.0 Hz, 2H), 7.38 (d, J = 8.5 Hz, 2H), 5.14 (d, J = 3.5 Hz, 1H), 4.06 (d, J = 11.0 Hz, 1H), 3.88 (dd, J = 11.0, 3.5 Hz, 1H), 3.82 (dd, J = 1.5, 1.5 Hz, 1H), 3.81 (dd, J = 4.5, 3.0 Hz, 1H), 3.79 (dd, J = 2.0, 2.0 Hz, 1H), 3.77 (s 3H), 3.42 (s, 3H); ^{13}C {^{1}H} NMR (125 MHz, CDCl$_3$) δ 168.2, 167.7, 139.9, 136.0, 130.6, 104.1, 65.2, 65.1, 52.8, 52.6, 52.4, 48.7; HRMS (ESI-TOF) m/z for [M+H]$^+$ C$_{16}$H$_{16}$O$_6$F$_3$S, calcd 393.0614, found 393.0615.
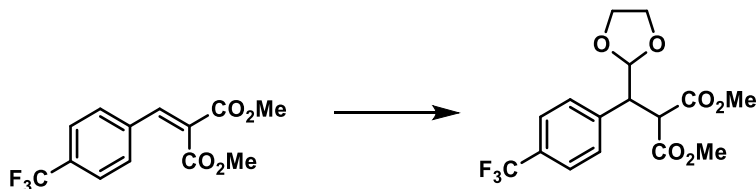
Dimethyl 2-((1,3-dioxolan-2-yl)(4-(trifluoromethyl)phenyl)methyl)malonate (2-156) was obtained as a colorless oil (55 mg, 76%) using method A of the general procedure. R_f = 0.15 (20% EtOAc in hexanes); IR (neat) 2958, 2896, 1740, 1621, 1436, 1423 cm^{-1}; ^{1}H NMR (500 MHz, CDCl$_3$) δ 7.55 (d, J = 8.0 Hz, 2H), 7.44 (d, J = 8.5 Hz, 2H), 5.13 (d, J = 4.0 Hz, 1H), 4.10 (d, J = 11.0 Hz, 1H), 3.91 (dd, J = 11.0, 3.5 Hz, 1H), 3.82-3.79 (m, 4H), 3.78 (s, 3H), 3.46 (s, 3H); ^{13}C {^{1}H} NMR (125 MHz, CDCl$_3$) δ 168.1, 167.6, 140.8, 129.8, 125.1, 125.0, 104.1, 65.2, 65.1, 52.8, 52.5, 52.4, 48.7; ^{19}F NMR (471 MHz, CDCl$_3$) δ –63.6; HRMS (ESI-TOF) m/z for [M+H]$^+$ C$_{16}$H$_{17}$O$_6$F$_3$, calcd 362.0972, found 362.0931.
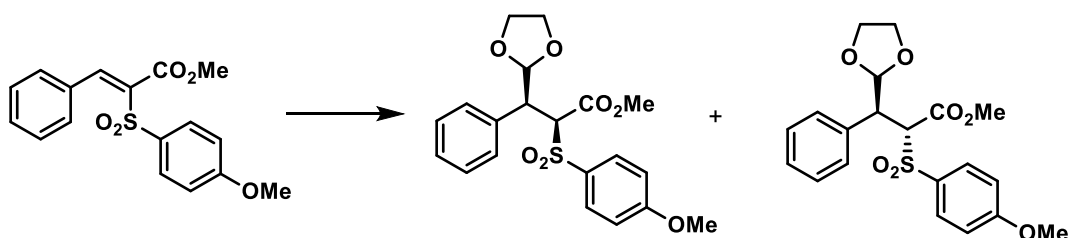
Methyl 3-(1,3-dioxolan-2-yl)-2-((4-methoxyphenyl)sulfonyl)-3-phenylpropanoate (2-157) was obtained as a pale-yelow solid, mixture of both diastereomers (75 mg, 92%, dr = 1:1.2) using method A from the general procedure. $R_f = 0.30$ (40% EtOAc in hexanes), 0.21 (40% EtOAc in hexanes); IR (neat) 2955, 2892, 1746, 1591, 1497, 1455 cm^{-1}; ^{1}H NMR (500 MHz, CDCl$_3$) δ 7.85 (d, J = 9.0 Hz, 2H), 7.28 (dd, J = 9.0, 2.0 Hz, 2H), 7.25-7.13 (m, 9H), 7.00 (d, J = 9.0 Hz, 2H), 6.71 (d, J = 9.0 Hz, 2H), 5.73 (d, J = 2.5 Hz, 1H), 4.95 (d, J = 2.5 Hz, 1H), 4.80 (d, J = 10.5 Hz, 1H), 4.69 (d, J = 11.5 Hz, 1H), 3.90 (*app* d, J = 2.5 Hz, 1H), 3.88 (s, 3H), 3.85 (*app* d, J = 3.0 Hz, 1H), 3.82 (s, 3H), 3.81 (*app* s, 4H), 3.22-3.10 (m, 1H), 3.17 (s, 3H); ^{13}C {^{1}H} NMR (125 MHz, CDCl$_3$) δ 166.1, 165.4, 164.2, 163.4, 134.8, 133.8, 131.5, 130.7, 130.4, 130.1, 129.4, 127.9, 127.8, 127.7, 127.6, 114.2, 113.8, 104.6, 102.6, 72.3, 71.4, 65.4, 65.3, 65.1, 65.0, 55.7, 55.6, 52.9, 52.3, 48.6, 47.7; HRMS (ESI-TOF) *m/z* for [M+H]$^+$ C$_{20}$H$_{21}$O$_7$S, calcd 405.1003, found 405.0998.

(14 : 1)
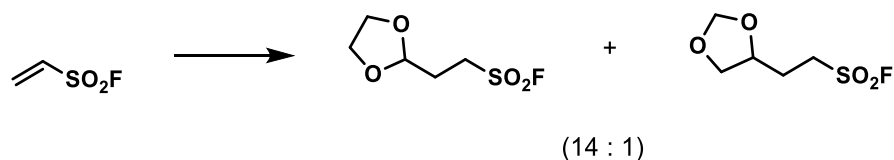
2-(1,3-dioxolan-2-yl)ethane-1-sulfonyl fluoride (2-158) was obtained as a colorless oil, as an inseparable mixture of regioisomers (70 mg, 95%, r.r = 14 : 1) using method B from the general procedure. R_f = 0.35 (30% EtOAc in hexanes); IR (neat) 2959, 2897, 1738, 1404, 1365, 1256, 1198 cm^{-1}; ^{1}H NMR (400 MHz, CDCl$_3$) δ 5.06 (dd, J = 3.6, 3.6 Hz, 1H), 3.99 (ddd, J = 11.2, 9.2, 6.4 Hz, 2H), 3.92 (ddd, J = 11.2, 9.2, 6.8 Hz, 2H), 3.53 (d, J = 8.0, 4.8 Hz, 1H), 3.51 (dd, J =

8.4, 4.8 Hz, 1H), 2.34 (dd, *J* = 8.0, 3.2 Hz, 1H), 2.31 (dd, *J* = 4.4, 3.2 Hz, 1H); ^{13}C {^{1}H} NMR

(100 MHz CDCl$_3$) δ 100.7, 95.2, 72.6, 69.1, 65.3, 47.5, 47.3, 45.2, 45.0, 27.3; ^{19}F NMR (376 MHz,

CDCl$_3$) δ −151.9; HRMS (ESI-TOF) *m/z* for [M+H]$^+$ C$_5$H$_{10}$FO$_4$S calcd 185.0284, found 185.0271.

(20 : 1)
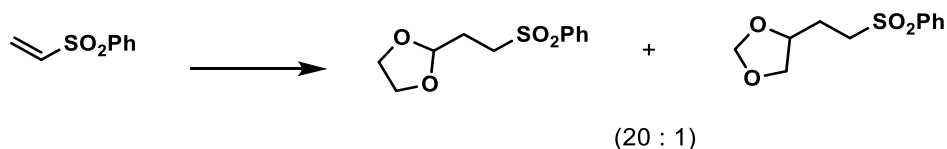
2-(2-(phenylsulfonyl)ethyl)-1,3-dioxolane (2-159) was obtained as a pale-yellow oil, as

an inseparable mixture of regioisomers (40 mg, 83%, r.r = 20 : 1) using method A from the general

proceure. ^{1}H NMR (500 MHz, CDCl$_3$) δ 7.91 (*app* d, *J* = 7.5 Hz, 2H), 7.67 (dd, *J* = 7.0, 1.0 Hz,

1H), 7.58 (m, 2H), 4.96 (*app* t, *J* = 4.0 Hz, 1H), 4.80 (s, 2H, C4-isomer), 3.91 (ddd, *J* = 11.0, 9.0,

6.5 Hz, 2H), 3.83 (ddd, *J* = 11.0, 9.0, 7.0 Hz, 2H), 3.95 (ddd, *J* = 11.0, 9.0, 6.5 Hz, 2H), 3.84 (ddd,

J = 11.0, 9.0, 7.0 Hz, 2H), 3.23 (m, 2H); ^{13}C {^{1}H} NMR (125 MHz, CDCl$_3$) δ 138.9, 133.8, 133.7,

129.3, 129.2, 128.0, 127.9, 101.7, 95.0, 73.6, 69.1, 651, 52.7, 50.6, 27.0, 26.4. The NMR

spectroscopic data are consistent with those of the literature.[194]
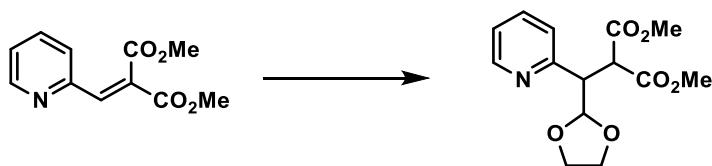
Dimethyl 2-((1,3-dioxolan-2-yl)(pyridin-2-yl)methyl)malonate (2-161) was obtained as

yellow oil (53 mg, 89%) using method B of the general procedure. R$_f$ = 0.31 (60% EtOAc in

hexanes); IR (neat) 2955, 2894, 1736, 1633, 1593, 1473 cm^{-1}; ^{1}H NMR (500 MHz, CDCl$_3$) δ 8.52

(ddd, *J* = 5.0, 1.5, 1.0 Hz, 1H), 7.62 (*app* dt, *J* = 7.5, 1.5 Hz, 1H), 7.31 (*app* d, *J* = 7.5 Hz, 1H),

7.14 (ddd, *J* = 7.5, 5.0, 1.0 Hz, 1H), 5.28, (d, *J* = 5.0 Hz, 1H), 3.93, (dd, *J* = 10.5, 5.0 Hz, 1H),

3.89-3.79 (m, 4H), 3.78 (s, 3H), 3.53 (s, 3H); ^{13}C {^{1}H} NMR (125 MHz, CDCl$_3$) δ 169.0, 168.4, 157.3, 149.0, 136.1, 124.9, 122.0, 104.9, 65.1, 65.0, 52.6, 52.4, 51.8, 50.6; HRMS (ESI-TOF) *m/z* for [M+H]$^+$ C$_{14}$H$_{18}$O$_6$N, calcd 296.1129, found 296.1118.
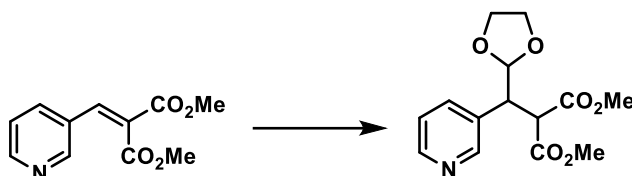
Dimethyl 2-((1,3-dioxolan-2-yl)(pyridin-3-yl)methyl)malonate (2-162) was obtained as a yellow oil (42 mg, 71%) using method B of the general procedure. R$_f$ = 0.30 (100% EtOAc); IR (neat) 2956, 2895, 2362, 2341, 1735, 1700, 1653, 1577 cm^{-1}; ^{1}H NMR (500 MHz, CDCl$_3$) δ 8.56 (*app* d, *J* = 2.0 Hz, 1H), 8.50 (dd, *J* = 4.5, 1.5 Hz, 1H), 7.66 (*app* dt, *J* = 8.0, 2.0 Hz, 1H), 5.14 (d, *J* = 3.0 Hz, 1H), 4.08 (d, *J* = 11.0 Hz, 1H), 3.86 (dd, *J* = 11.0, 3.5 Hz, 1H), 3.82-3.76 (m, 3H), 3.76 (s, 3H), 3.74 (dd, *J* = 3.5, 1.5 Hz, 1H), 3.46 (s, 3H); ^{13}C {^{1}H} NMR (125 MHz, CDCl$_3$) δ 168.1, 167.6, 150.9, 148.8, 136.9, 132.1, 123.0, 103.8, 65.3, 65.2, 52.8, 52.5, 52.4, 46.6; HRMS (ESI-TOF) *m/z* for [M+H]$^+$ C$_{14}$H$_{18}$O$_6$N, calcd 296.1129, found 296.1122.
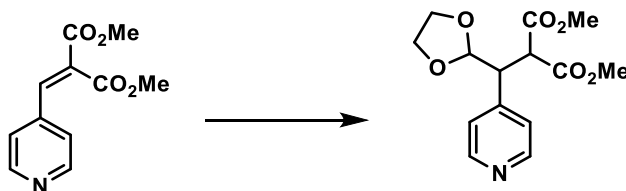
Dimethyl 2-((1,3-dioxolan-2-yl)(pyridin-4-yl)methyl)malonate (2-163) was obtained as a pale-ywllow oil (48 mg, 82%) using method B of the general procedure. R$_f$ = 0.16 (80% EtOAc in hexanes); IR (neat) 2956, 2895, 1738, 1601, 1560, 1436 cm^{-1}; ^{1}H NMR (500 MHz, CDCl$_3$) δ 8.53 (*app* d, *J* = 6.0 Hz, 1H), 7.24 (dd, *J* = 4.5, 1.5 Hz, 2H), 5.12 (d, *J* = 3.0 Hz, 1H), 4.09 (d, *J* =

11.0 Hz, 1H), 3.84 (*app* d, *J* = 3.5 Hz, 1H), 3.82-3.79 (m, 3H), 3.78 (s, 3H), 3.48 (s, 3H); ^{13}C {^{1}H}

NMR (125 MHz, CDCl$_3$) δ 167.96, 167.5, 149.6, 145.7, 124.6, 103.7, 65.3, 65.2, 52.8, 52.6, 52.2,

48.3; HRMS (ESI-TOF) *m/z* for [M+H]$^+$ C$_{14}$H$_{18}$O$_6$N, calcd 296.1129, found 296.1115.

Dimethyl 2-((4-chloropyridin-2-yl)(1,3-dioxolan-2-yl)methyl)malonate (2-164) was

obtained as a yellow oil (51 mg, 77%) using method B of the general procedure. R$_f$ = 0.45 (40%

EtOAc in hexanes); IR (neat) 2595, 2895, 1738, 1576, 1557, 1468 cm^{-1}; ^{1}H NMR (500 MHz,

CDCl$_3$) δ 8.40 (*app* d, *J* = 5.5 Hz, 1H), 7.35 (*app* d, *J* = 2.0 Hz, 1H), 7.16 (dd, *J* = 5.5, 2.0 Hz, 1H),

5.24 (d, *J* = 5.0 Hz, 1H), 3.90-3.80 (m, 5H), 3.78 (s, 3H), 3.56 (s, 3H); ^{13}C {^{1}H} NMR (125 MHz,

CDCl$_3$) δ 168.8, 168.2, 159.0, 149.7, 144.1, 125.3, 122.6, 104.5, 65.2, 65.1, 52.7, 52.5, 51.7, 50.4;

HRMS (ESI-TOF) *m/z* for [M+H]$^+$ C$_{14}$H$_{17}$O$_6$NCl, calcd 330.0739, found 330.0726.
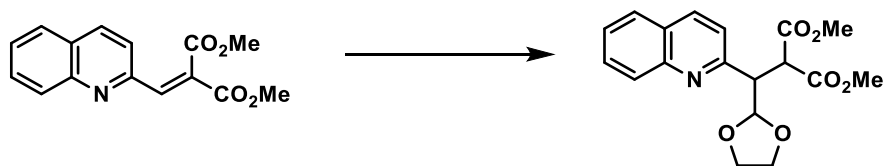
Dimethyl 2-((1,3-dioxolan-2-yl)(quinolin-2-yl)methyl)malonate (2-165) was obtained

as a yellow oil (51 mg, 74%) using method B of the general procedure. R$_f$ = 0.13 (30% EtOAc in

hexanes); IR (neat) 2954, 2894, 1756, 1737, 1600, 1505, 1434 cm^{-1}; ^{1}H NMR (500 MHz, CDCl$_3$)

δ 8.08 (*app* d, *J* = 8.5 Hz, 1H), 8.00 (*app* d, *J* = 8.5 Hz, 1H), 7.77 (*app* d, *J* = 8.0 Hz, 1H), 7.65

(*app* dt, *J* 8.5, 1.5 Hz, 1H), 7.48 (*app* dt, *J* = 8.0, 1.0 Hz, 1H), 7.44 (d, *J* = 8.5 Hz, 1H), 5.38 (d, *J*

= 5.5 Hz, 1H), 4.11 (dd, J = 10.5, 5.5 Hz, 1H), 3.92-3.88 (m, 2H), 3.86-3.83 (m, 2H), 3.81 (app s, 4H), 3.53, (s, 3H) ^{13}C {^{1}H} NMR (125 MHz, CDCl$_3$) δ 169.2, 168.7, 157.9, 147.6, 135.9, 129.3, 129.2, 127.5, 127.2, 126.2, 122.8, 105.1, 65.1, 65.0, 52.6, 52.4, 52.1, 51.2; HRMS (ESI-TOF) m/z for [M+H]$^+$ C$_{18}$H$_{20}$O$_6$N calcd 346.1285, found 346.1269.
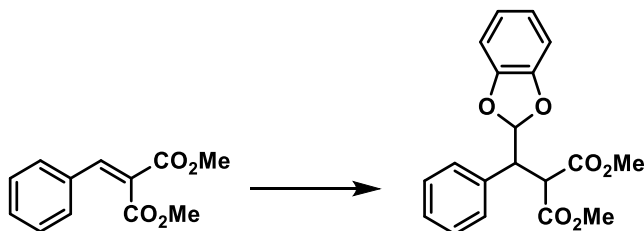
Dimethyl 2-(benzo[d][1,3]dioxol-2-yl(phenyl)methyl)malonate (2-174) was obtained as a white solid (56 mg, 82%) using method D of the general procedure. Addition note: the bulk of benzo-1,3-dioxole could be removed by drying the crude material on the high vacuum overnight prior flash column chromatography. X-ray quality crystals were obtained by slow evaporation in ethyl acetate/hexanes. ^{1}H NMR (400 MHz, CDCl$_3$) δ 7.34-7.32 (m, 2H), 7.30-7.27 (m, 2H), 7.26-7.23 (m, 2H), 6.76-6.70 (m, 3H), 6.70-6.67 (m, 1H), 4.17 (d, J = 10.4 Hz, 1H), 4.08 (dd, J = 10.4, 4.0 Hz, 1H), 3.71 (s, 3H), 3.46 (s, 3H); ^{13}C {^{1}H} NMR (100 MHz, CDCl$_3$) δ 168.2, 167.4, 147.2, 147.1, 134.7, 129.4, 128.4, 127.9, 121.6, 121.5, 110.8, 108.5, 108.4, 52.8, 52.5, 49.3; HRMS (ESI-TOF) m/z for [M+H]$^+$ C$_{19}$H$_{19}$O$_6$, calcd 343.1186, found 343.1159.

Lights On/Lights Off Experiment

Alkene **2-122** (0.30 mmol, 1.0 equiv), (n-Bu$_4$N)$_2$S$_2$O$_8$ (0.075 mmol, 0.25 equiv), *fac*-Ir(ppy)$_3$ (0.0015 mmol, 0.50 mol%) and mesitylene (0.30 mmol, 1.0 equiv) were mixed in a teflon-coated 2-dram vial. Degassed 1,3-dioxolane (4.5 mL) was added, and the vial was flushed with argon (1 min) and sealed. The vial was irradiated with household LEDs (15W x 4) and cooled with a fan. During the lights-off period, the vial was wrapped with aluminum foil and stirred in the dark. Aliquots (100 µL) were removed periodically (1 h, 2 h, 3 h, 5 h, 6 h) using syringes, transferred to NMR tubes, diluted with CDCl$_3$ (ca. 0.6 mL) and analyzed by ^{1}H NMR.
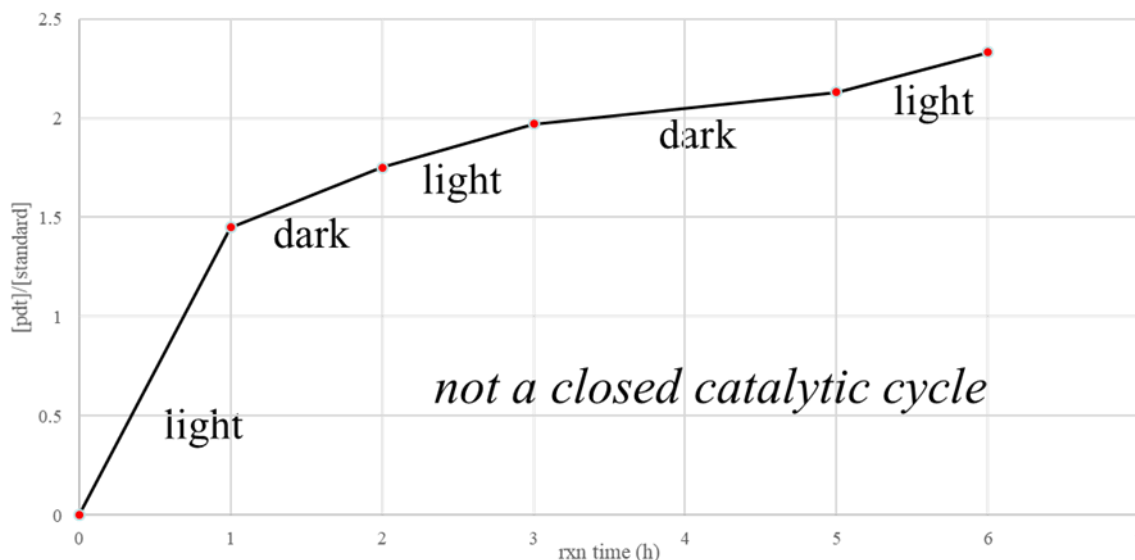
Figure 11. Lights on/lights off experiment

3.5 Computation Details for Chapter 2

3.5.1 Optimized Structures

Optimized Structure for Chromone 2-114
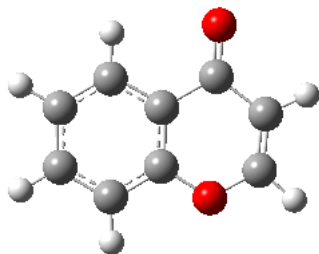
0 1

H	3.40680400	0.07909900	-0.00000200
H	2.59526500	-2.29298800	-0.00000100
H	-0.82401800	2.48715100	0.00000000
H	-1.86034600	-2.37842500	0.00000000
H	-3.72020200	-0.71260200	-0.00000100
H	-3.21266900	1.72318000	-0.00000100
O	1.71256400	2.13896500	-0.00000100
C	1.38728600	0.95386500	0.00000200
C	2.34745600	-0.15065000	-0.00000100
C	1.93470400	-1.43304300	0.00000000
O	0.63938700	-1.82622000	0.00000000
C	-1.08333300	1.43314200	0.00000000
C	-0.02753900	0.50666900	0.00000100

C	-0.33974300	-0.86069900	0.00000000
C	-1.66318100	-1.31133900	0.00000000
C	-2.68793000	-0.37400600	0.00000000
C	-2.40112700	1.00149800	0.00000000

Optimized Structure for 1,3-Dioxolane
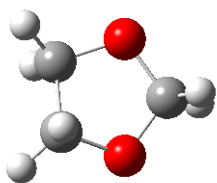
0 1

C	0.89796800	0.78666800	0.19940900
O	-0.42519900	1.10598200	-0.22289400
C	-1.20152900	-0.04165000	0.04943100
C	0.99261800	-0.69498700	-0.15872900
H	1.59461700	1.43027600	-0.34309200
H	1.01893800	0.94556100	1.28235500
H	-1.71390500	0.03825100	1.02180700
H	-1.94004800	-0.14752000	-0.75545300
H	1.69211500	-1.26016700	0.46446900
H	1.25683400	-0.83336200	-1.21730400
O	-0.33016200	-1.16513500	0.09871300

Optimized Structure for 1,3-Dioxolanyl Radical
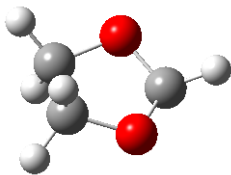
0 2

C	-0.92233400	-0.74273300	0.15174500
O	0.43386800	-1.13732000	-0.10411800
C	1.20549700	0.00873700	-0.14278100
C	-0.90555600	0.75860300	-0.14823400
H	-1.58927900	-1.31561900	-0.49758400
H	-1.16799500	-0.95056300	1.20158100
H	2.14477700	-0.04220600	0.41179000
H	-1.57107100	1.35098300	0.48277800
H	-1.11753100	0.96417300	-1.20607200
O	0.44556500	1.11801900	0.15950800

Optimized Structure for Transition State 2-185
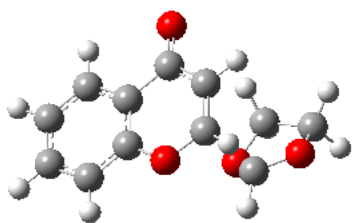
0 2

H	-2.42970900	-2.67203800	0.10300400

H	-4.34495300	-1.65298500	-1.13143800
H	-4.42068700	0.80726000	-1.50291300
O	3.30609000	-0.75502800	0.21178500
C	3.67778600	0.33358600	-0.65859300
C	2.37692600	0.65813500	-1.40470200
O	1.63241100	-0.57201500	-1.29141100
C	2.06557500	-1.19155200	-0.16055900
O	-0.34081300	2.68070700	0.55155700
C	-0.38571800	1.45933600	0.75076100
C	0.60444200	0.72702000	1.50461700
C	0.62056700	-0.64991900	1.51813700
O	-0.43828400	-1.40582900	1.08665900
C	-2.56197400	1.16738300	-0.48129400
C	-1.48274100	0.60783000	0.21824200
C	-1.45915500	-0.78174200	0.41259800
C	-2.48405200	-1.60165900	-0.06830000
C	-3.54479600	-1.02162500	-0.75476000
C	-3.58723700	0.36521200	-0.96458200
H	-2.55984800	2.24370900	-0.62281700
H	1.25008600	-1.22316800	2.18963800
H	1.42218400	1.27105200	1.96475000
H	1.91717300	-2.27225400	-0.15534800
H	2.51724200	0.86362500	-2.46756900

H	1.81444100	1.47240500	-0.93882100
H	4.04712800	1.16197100	-0.05000600
H	4.47398000	-0.01428000	-1.32659100

Optimized Structure for Intermediate 2-186
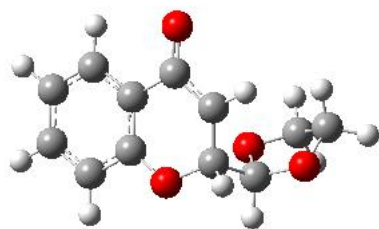
0 2

H	2.21070200	-2.68431200	-0.52900500
H	4.28259000	-2.02270200	0.68589900
H	4.60721800	0.33765500	1.41490500
O	-3.21149200	-0.31309500	-0.56521700
C	-3.58494800	0.36244100	0.64184000
C	-2.78013400	-0.38303800	1.70325900
O	-1.58626700	-0.71890700	0.99575600
C	-1.95389800	-0.92954900	-0.34753100
O	0.63557400	2.84272600	-0.12181100
C	0.51681000	1.63747800	-0.39637200
C	-0.65483200	1.12250100	-1.05129300
C	-0.87343900	-0.32597900	-1.29156600
O	0.29562300	-1.14614900	-1.18235800

C	2.72344900	0.99192000	0.60519800
C	1.55391600	0.62995800	-0.07887500
C	1.38100700	-0.70700400	-0.47965200
C	2.36834100	-1.66039600	-0.20584200
C	3.52022300	-1.27800600	0.47281000
C	3.70442800	0.05015200	0.88437200
H	2.82985200	2.03118700	0.90042200
H	-1.25149500	-0.48592000	-2.31094500
H	-1.45291500	1.81259900	-1.30429300
H	-2.04341600	-2.00369900	-0.57069200
H	-3.30062200	-1.29037000	2.04251900
H	-2.50327500	0.22463300	2.56763300
H	-3.30324400	1.42288300	0.59366200
H	-4.66844900	0.27857800	0.76082500

Optimized Structure for syn-Transition State 2-187-syn
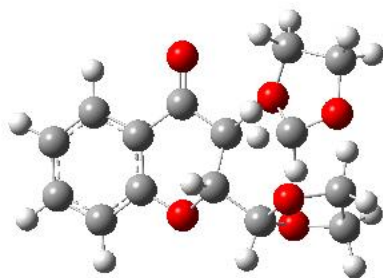
0 2

H	-3.28958400	-2.28235600	-1.57896800
H	-5.43498200	-1.02358100	-1.40714100

H	-5.56669100	1.03982400	-0.01847200
O	2.06685400	-2.34497800	1.22219500
C	3.31705000	-1.82870100	0.75021400
C	3.17491400	-1.91491700	-0.76725800
O	1.77622000	-1.69199300	-0.95242500
C	1.13162300	-2.29201200	0.14986200
O	-1.03888600	1.84729600	1.73655300
C	-1.05615400	0.77140400	1.12660500
C	0.15226000	-0.03911300	0.91028700
C	-0.10006800	-1.49350600	0.58835600
O	-1.08316400	-1.65670400	-0.44456300
C	-3.49840000	0.94420000	0.56979000
C	-2.28429400	0.24661200	0.47808300
C	-2.22987400	-0.92764100	-0.29835200
C	-3.36320100	-1.37784200	-0.98356600
C	-4.55469300	-0.66660900	-0.87886300
C	-4.63093700	0.49402400	-0.09587100
H	-3.51091200	1.84996400	1.16822500
H	-0.47642200	-2.00446700	1.49261400
H	0.75504100	0.56036600	-0.17498800
H	0.92770300	0.11688900	1.66106600
H	0.82204600	-3.31890200	-0.10223400
H	3.46279300	-2.90537100	-1.14933300

H	3.71679400	-1.13640200	-1.30769200
H	3.44791600	-0.78901100	1.07424700
H	4.12486000	-2.44565800	1.15479000
C	1.43437400	1.30692900	-1.07110800
O	0.79184700	2.51404600	-1.20142200
H	1.43696700	0.72546300	-1.99463900
O	2.70436600	1.50290800	-0.53367100
C	1.30551600	3.33477600	-0.13552100
C	2.75782300	2.85188700	-0.02789100
H	1.20487900	4.37837500	-0.43854000
H	0.72992500	3.14478100	0.77745700
H	3.13294500	2.83678200	0.99908400
H	3.44321000	3.43175100	-0.65740500

Optimized Structure of anti-Transition State 2-187-anti
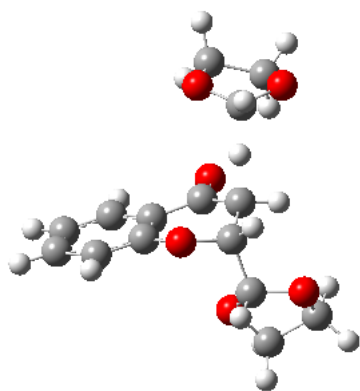
0 2

H	1.85448700	2.94641300	-2.15221200

H	1.61909800	4.92514300	-0.65546200
H	0.49750300	4.69321200	1.55744300
O	2.16804100	-2.69703300	-0.56658000
C	2.68647900	-3.00334700	0.73269100
C	3.39921300	-1.71157700	1.13846800
O	2.62003100	-0.71709000	0.47833700
C	2.23407900	-1.28573800	-0.74978700
O	-0.99607200	0.01505100	1.89216400
C	-0.35738000	0.17026400	0.84198000
C	-0.21929500	-0.90218400	-0.15348400
C	0.85750600	-0.75581800	-1.20167100
O	1.01058100	0.59075600	-1.67859900
C	0.09603100	2.59520400	1.28788100
C	0.21842800	1.47577500	0.45155700
C	0.86716800	1.61885800	-0.78876500
C	1.36377700	2.86403000	-1.18759700
C	1.22652500	3.96104100	-0.34256200
C	0.59653700	3.83213500	0.90297100
H	-0.40829000	2.45600200	2.23916400
H	0.60301100	-1.33686500	-2.09574500
H	-0.28274000	-1.90779300	0.26387200
H	2.97797000	-1.06057300	-1.53244400
H	4.43902700	-1.69405600	0.77882600

H	3.38071400	-1.50379700	2.21041700
H	1.86400300	-3.24384800	1.41855200
H	3.35529400	-3.86622700	0.65478400
H	-1.44059100	-0.88142100	-0.79935300
C	-2.73705900	-0.90459300	-1.18483600
O	-3.35230600	-1.94683500	-0.52984400
H	-2.75215300	-1.03060500	-2.27163800
O	-3.26739900	0.30116300	-0.77028900
C	-3.73282700	-1.41637000	0.75564300
C	-3.99749400	0.06617600	0.45230700
H	-4.61100700	-1.96842500	1.09532300
H	-2.90579400	-1.52810700	1.46408900
H	-3.60975400	0.72470400	1.23199700
H	-5.05390800	0.28501700	0.26209600

Optimized Structure of Product 2-115
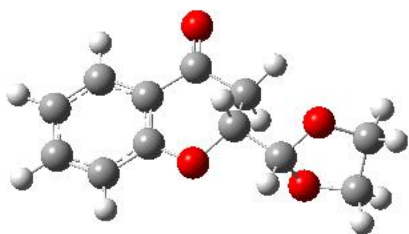
0 1

H	-2.07469600	-2.84981400	0.08486000
H	-4.51194000	-2.34569200	-0.02512900
H	-5.30282000	0.01458300	-0.10445900

O	3.04763600	0.15227100	1.10348100
C	4.18076300	0.36103400	0.25308500
C	3.94787500	-0.62141300	-0.90083800
O	2.52664400	-0.72607000	-0.93550500
C	2.12345400	-0.68241700	0.41237000
O	-1.26105500	2.83603100	-0.14087600
C	-0.94510300	1.65675100	-0.10621900
C	0.50352400	1.20090700	-0.21256900
C	0.71874200	-0.09948000	0.55240100
O	-0.18501600	-1.12803000	0.11396900
C	-3.31166600	0.82854300	-0.06410100
C	-1.93376800	0.55684400	-0.01632700
C	-1.50166600	-0.78270300	0.04848100
C	-2.43437700	-1.82701800	0.03697000
C	-3.79165500	-1.53174600	-0.02124200
C	-4.23960400	-0.20224800	-0.06437400
H	-3.61573500	1.86966100	-0.11428100
H	0.54639500	0.06741600	1.62620200
H	0.74104200	1.03881900	-1.27213200
H	1.16265600	1.98651700	0.16539400
H	2.14494300	-1.69429200	0.85109100
H	4.40318100	-1.60132400	-0.69360100
H	4.28923300	-0.26225600	-1.87411500

H	4.19406600	1.40230700	-0.09231100
H	5.09887900	0.15813200	0.81411100

Optimized Structure of Methylchromone 2-188
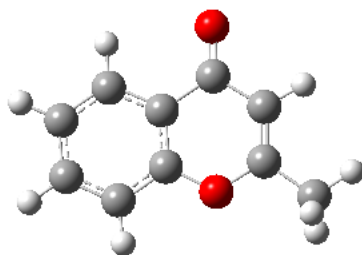
0 1

C	-2.96996800	0.10282900	-0.00002900
C	-2.68695700	-1.27319500	-0.00002900
C	-1.37391800	-1.72673500	0.00000100
C	-0.33772300	-0.78811800	0.00003300
C	-0.59513900	0.58896500	0.00004400
C	-1.93097200	1.02164300	0.00000600
O	0.94339200	-1.28537800	0.00003100
C	1.99960800	-0.42381000	0.00000400
C	1.84633300	0.91994300	0.00000900
C	0.53077700	1.55397100	0.00011900
O	0.36273500	2.77245500	-0.00007500
C	3.29931000	-1.16379900	-0.00004500
H	-4.00128600	0.44325900	-0.00005200
H	-3.49981900	-1.99408400	-0.00005700

H	-1.13197100	-2.78463500	-0.00000800
H	-2.10983700	2.09233100	0.00001800
H	2.72011000	1.56164800	-0.00004800
H	4.13960500	-0.46655300	-0.00013300
H	3.37309600	-1.80933300	0.88309900
H	3.37297800	-1.80941600	-0.88313800

Optimized Structure of Transition State 2-189
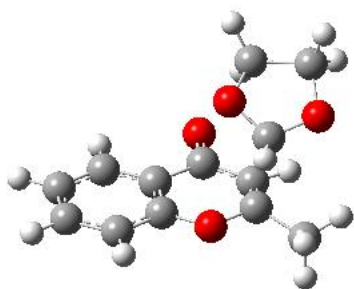
0 2

C	-3.72368800	-0.77341700	-0.56194600
C	-3.63793400	0.50805800	-1.12666700
C	-2.52339700	1.30846800	-0.90071800
C	-1.48817700	0.81894600	-0.09889700
C	-1.55501300	-0.45733500	0.47787700
C	-2.68685700	-1.24728000	0.23155300
O	-0.41598300	1.65310200	0.09634500
C	0.67258500	1.20827200	0.82388900
C	0.60402400	0.02190200	1.54117600
C	-0.44119500	-0.94624300	1.33130300

207

O	-0.42906800	-2.09106400	1.80923600
C	1.54956800	2.36484800	1.22483100
C	1.90729500	0.57601700	-0.92821200
O	1.33126900	-0.51935700	-1.49018600
C	2.03764300	-1.67465200	-0.99172600
C	3.42131500	-1.10369000	-0.65418200
O	3.17745700	0.30943600	-0.49721300
H	-4.59861900	-1.39035300	-0.74582900
H	-4.44633700	0.88322000	-1.74846900
H	-2.43593300	2.30165500	-1.32976000
H	-2.71549500	-2.23294000	0.68571900
H	1.42990700	-0.24547400	2.19219700
H	1.69962000	3.05544400	0.38924900
H	2.52273700	2.00269600	1.56385300
H	1.07785800	2.92586800	2.04119100
H	1.78714400	1.49057500	-1.51163100
H	1.51825000	-2.07402700	-0.11627700
H	2.05186000	-2.42111100	-1.78817000
H	4.14672200	-1.23962100	-1.46426000
H	3.83586400	-1.49621200	0.27705100

208

Optimized Structure of Intermediate 2-190
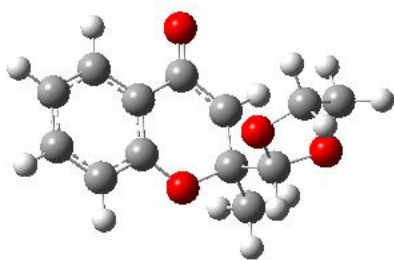
0 2

C	-3.80185800	-0.46509300	-0.69253500
C	-3.58998800	0.88798600	-0.99583100
C	-2.40226700	1.51981500	-0.64430200
C	-1.40556500	0.79539400	0.02041400
C	-1.60618200	-0.56001300	0.33528100
C	-2.81131900	-1.17705000	-0.02981300
O	-0.28488500	1.48982300	0.36986600
C	0.90217500	0.80897800	0.83123000
C	0.64755300	-0.57061700	1.33213200
C	-0.55632600	-1.30832100	1.05952900
O	-0.68839800	-2.49144200	1.41521600
C	1.50734400	1.70746200	1.91803800
C	1.86715000	0.78103800	-0.40226700
O	1.29963900	0.00399700	-1.43212500
C	2.34645600	-0.78762000	-1.99366800
C	3.26572200	-1.00641300	-0.79587200
O	3.12765300	0.22256500	-0.07322700

209

H	-4.73283100	-0.94883000	-0.97271100
H	-4.35922700	1.45445300	-1.51419100
H	-2.22353600	2.56524400	-0.87423300
H	-2.93713700	-2.22388400	0.22897000
H	1.44577600	-1.07818200	1.86432000
H	1.65309200	2.71842600	1.52367300
H	2.47339700	1.31000900	2.23993900
H	0.83375700	1.76359400	2.77743900
H	2.02262600	1.82011700	-0.73119700
H	1.90407500	-1.70286300	-2.39362500
H	2.85649300	-0.24208900	-2.80066700
H	4.31992200	-1.13280700	-1.05574600
H	2.93415400	-1.85601800	-0.18382500

Optimized Structure of Transition State 2-191
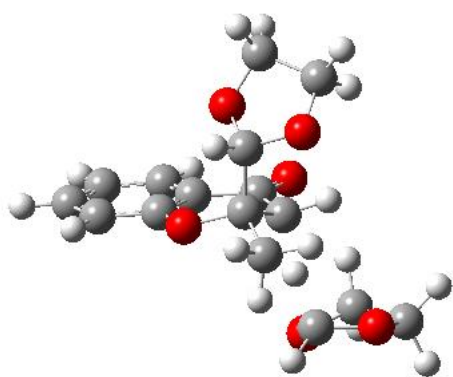
0 2

C	1.85067800	3.64745600	-0.71033300

C	2.44245000	3.48960600	0.55051500
C	2.20921100	2.34634600	1.30877000
C	1.37278000	1.34302500	0.80729000
C	0.76094100	1.49321900	-0.44987300
C	1.01563000	2.65094200	-1.19892700
O	1.17186400	0.25971100	1.61456900
C	0.56335700	-0.93986000	1.07693800
C	-0.46016800	-0.63171400	0.00130000
C	-0.15998200	0.45061400	-0.95063100
O	-0.71440600	0.52798400	-2.05443600
C	-0.04393000	-1.65642200	2.28522000
C	1.72225700	-1.81855200	0.52408000
O	2.32766300	-1.20990300	-0.59195500
C	2.72421300	-2.26525000	-1.46423600
C	1.60537400	-3.28549000	-1.26293500
O	1.24063900	-3.09373200	0.10812300
H	2.04093700	4.54211400	-1.29598000
H	3.09638000	4.26359900	0.94420000
H	2.66704300	2.20665700	2.28295500
H	0.53052900	2.73720600	-2.16637700
H	-0.86295200	-1.52788500	-0.47262300
H	0.73488000	-1.89221900	3.01816600
H	-0.52406600	-2.58679700	1.97193700

H	-0.78231600	-1.01321600	2.77059500
H	2.46016900	-1.96864500	1.32960200
H	2.79068900	-1.86254300	-2.47717200
H	3.70148500	-2.67217600	-1.16436000
H	1.92382900	-4.32338800	-1.39861300
H	0.74961900	-3.07798800	-1.91854500
H	-1.62390600	-0.19782100	0.61281900
C	-2.88154300	0.15163200	0.99109500
O	-3.23058800	1.27956800	0.28680000
H	-2.84740400	0.33645800	2.06969100
O	-3.70901400	-0.90644700	0.64328600
C	-3.80032100	0.80136500	-0.94860100
C	-4.47300600	-0.50414000	-0.50996900
H	-4.49527900	1.56158100	-1.30952500
H	-2.99949000	0.63446300	-1.67686900
H	-4.42066900	-1.29286600	-1.26515500
H	-5.51640200	-0.36063200	-0.20406600

Optimized Structure of 2-192
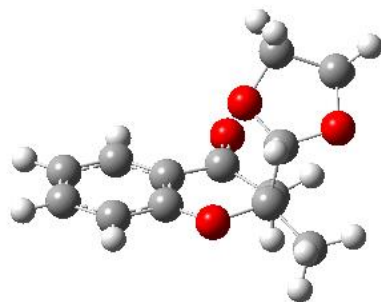
0 1

C	-3.73476000	-0.79882300	-0.39535600
C	-3.66990500	0.45341200	-1.02349300
C	-2.53406700	1.24886100	-0.91612300
C	-1.44119900	0.79779400	-0.16593900
C	-1.49842600	-0.44953300	0.48194600
C	-2.64958600	-1.24073400	0.34867100
O	-0.36563700	1.63515100	-0.10176000
C	0.89038600	1.17186400	0.45800300
C	0.66604800	0.18529400	1.60951100
C	-0.35943200	-0.89921700	1.30710300
O	-0.27319600	-2.01934100	1.78728800
C	1.60468600	2.43809500	0.92681100
C	1.69910700	0.53410600	-0.69490200
O	1.08135900	-0.65085900	-1.14244400
C	2.13292700	-1.52313700	-1.55249300
C	3.23237400	-1.19793200	-0.54251700
O	3.01241300	0.18969900	-0.25975900
H	-4.62512000	-1.41325500	-0.48965900
H	-4.51355100	0.81040200	-1.60862600
H	-2.46722100	2.21404800	-1.40795200
H	-2.65888700	-2.20179400	0.85406800
H	1.61218900	-0.27535800	1.90318200

H	0.29096400	0.74252800	2.48008600
H	1.73166600	3.13636200	0.09272000
H	2.59037400	2.18961300	1.32838100
H	1.01229500	2.93403400	1.70127500
H	1.78017300	1.26154200	-1.51931600
H	1.76228000	-2.54874600	-1.50050300
H	2.44603800	-1.29424100	-2.58177400
H	4.24472200	-1.31951400	-0.93913700
H	3.12566000	-1.79311400	0.37332400

3.5.2 Optimized Structures for C–H Abstraction Calculations

Optimized Structure of Sulfate Radical Anion
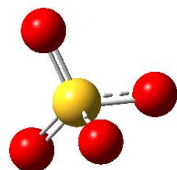
-1 2

S	-0.08137500	0.00008200	0.00033500
O	-0.88160100	1.24352000	0.00227900
O	-0.88882100	-1.23877200	-0.00336600
O	0.96599700	-0.00555200	1.13139200
O	0.96717300	0.00063900	-1.13097500

Optimized Structure of Transition State
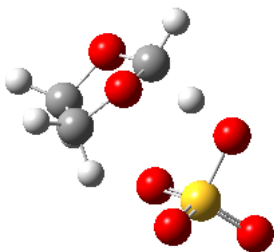
-1 2

C	1.96999100	-0.92523400	-0.77573400
O	2.05127300	0.47279700	-1.12536500
C	1.63496300	1.16248300	0.00005800
C	1.97017600	-0.92536300	0.77559700
H	1.03667600	-1.33425300	-1.17090800
H	2.84313100	-1.41947800	-1.21527100
H	2.01175500	2.19201600	0.00017800
H	0.35325800	1.25378600	-0.00009600
H	2.84360800	-1.41936800	1.21483600
H	1.03711300	-1.33478100	1.17093000
O	2.05103500	0.47262900	1.12545800
O	-0.92427700	1.37485700	-0.00039500
S	-1.62347700	-0.11249500	0.00002400
O	-1.16094900	-0.79554200	-1.23907700
O	-3.05672400	0.26913400	0.00022300
O	-1.16044500	-0.79504000	1.23920900

Optimized Structure of Hydogensulfate Anion
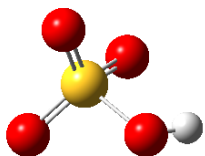
-1 1

S	0.14612200	0.00103500	0.05554500
O	0.81732400	1.23890300	-0.39160800
O	0.81874100	-1.25137300	-0.34659200
O	-1.32571200	-0.01594700	-0.81799300
O	-0.35646700	0.02629200	1.45646000
H	-1.96903100	0.00043100	-0.09086100

Optimized Structure of Radical 2-195
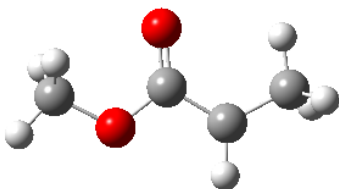
0 2

C	2.53308200	0.00701400	-0.00001500
C	1.21122200	-0.66847000	-0.00000300
C	-0.02472900	0.08925300	0.00001400
O	-1.11498800	-0.72840900	0.00003200
O	-0.10530500	1.31119000	0.00001200
C	-2.37788700	-0.05263900	-0.00003100

H	3.12746300	-0.28388700	-0.87899900
H	2.40969000	1.09247100	-0.00002500
H	3.12745400	-0.28385600	0.87899100
H	1.14336400	-1.75219800	0.00000600
H	-3.13290800	-0.83991200	-0.00069600
H	-2.48172500	0.57659400	0.88894700
H	-2.48112400	0.57758600	-0.88836400

Optimized Structure of Transition State
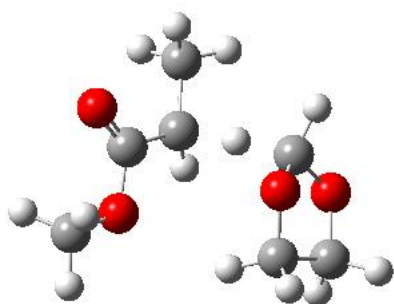
0 2

C	-1.31350900	2.60715700	-0.21142600
C	-0.89268600	1.19484700	-0.55211500
C	-1.75750300	0.11602900	-0.04210600
O	-1.49429600	-1.07629900	-0.66457400
O	-2.58001300	0.21721200	0.85131800
C	-2.26333600	-2.18661900	-0.18423500
H	-0.50445000	3.31801000	-0.41401700
H	-2.18409400	2.91939800	-0.80414000

H	-1.59601900	2.68094400	0.84272400
H	0.30772500	1.00078700	0.09262300
H	-0.56385000	1.03428600	-1.58067600
H	-1.95211600	-3.04346800	-0.78420900
H	-2.06458700	-2.36870800	0.87595900
H	-3.33346300	-2.00106700	-0.31225700
C	1.53192000	0.78615900	0.64133100
O	1.53388900	-0.47770600	1.20012200
H	1.67933000	1.56306900	1.39828200
O	2.46457300	0.84697400	-0.38955600
C	1.91175900	-1.35825900	0.13108600
C	2.89356400	-0.49593000	-0.67083400
H	2.35761200	-2.25235300	0.57092800
H	1.02503500	-1.62649700	-0.45525800
H	2.84528000	-0.67110400	-1.74923400
H	3.92911900	-0.61504200	-0.32940400

Optimized Structure of Ester Product
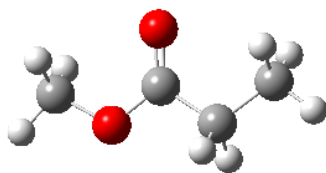
0 1

C	2.48294100	0.11132500	-0.00011800

C	1.21669200	-0.74260300	0.00002400
C	-0.05217600	0.08842600	-0.00001600
O	-1.14862700	-0.70621300	0.00005600
O	-0.10586900	1.29903800	-0.00003000
C	-2.40796600	-0.01569600	0.00007600
H	3.37344700	-0.52559800	-0.00006600
H	2.51994800	0.75790600	-0.88184900
H	2.51999700	0.75812400	0.88145100
H	1.18084100	-1.40678700	0.87326200
H	1.18077200	-1.40698900	-0.87305500
H	-3.17026700	-0.79550200	0.00006200
H	-2.50285100	0.61374500	0.88921600
H	-2.50285700	0.61378900	-0.88903000

Optimized Structure of 2-190
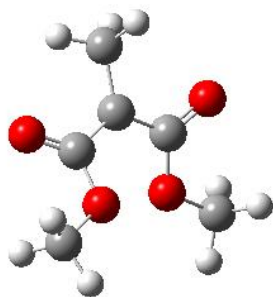
0 2

C	1.30647900	0.29083800	0.08352800
C	-0.00067900	0.96865500	-0.01914100
C	-1.31410100	0.29723300	-0.09894500

O	-1.30901600	-0.97935100	0.33433800
O	-2.32068400	0.86576400	-0.49328700
C	-2.57778900	-1.64831600	0.26954100
O	1.30961000	-0.99029000	-0.33647500
O	2.30556300	0.86979400	0.48093800
C	2.58056700	-1.65295600	-0.25370500
C	0.01152300	2.45993900	0.00964300
H	-3.32071700	-1.12627600	0.87892900
H	-2.39638500	-2.65064100	0.65815800
H	-2.93601600	-1.69416600	-0.76249100
H	2.40829800	-2.65861300	-0.63789600
H	3.32780300	-1.13109800	-0.85804500
H	2.92785400	-1.69067500	0.78242300
H	-0.93312700	2.85392000	-0.36820700
H	0.85362700	2.85928900	-0.56401600
H	0.14887700	2.81856600	1.04151200

Optimized Structure of Transition State
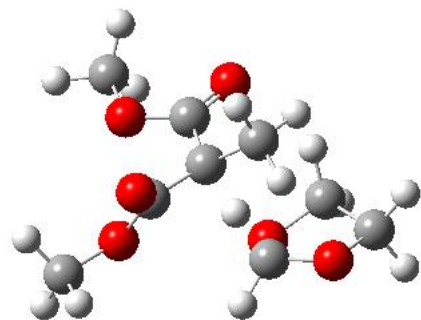
0 2

C	-1.73655000	-0.92185200	0.40924300
C	-0.52314500	-0.14875900	0.83591200
C	-0.47569600	1.30690200	0.50990400
O	-1.48971400	1.72010800	-0.28164500
O	0.40477100	2.05834700	0.90090800
C	-1.44416000	3.10139100	-0.66816800
O	-1.83121400	-1.01598900	-0.93896300
O	-2.51773100	-1.45963100	1.16874900
C	-2.98920900	-1.71204400	-1.42271800
C	-0.04570500	-0.48221800	2.24052900
H	0.46268600	-0.62459500	0.02477100
H	-1.47731100	3.75002500	0.21130500
H	-2.32390000	3.25739500	-1.29343000
H	-0.53091400	3.31283700	-1.23114900
H	-2.90834600	-1.69472200	-2.51027600
H	-3.00465100	-2.74137800	-1.05385200
H	-3.90357200	-1.20721900	-1.09909000
H	0.80885400	0.14576200	2.50101600
H	0.24827700	-1.53390000	2.31160600
H	-0.84430300	-0.31138100	2.97139100
C	1.51843500	-1.05686800	-0.74270600
O	2.01774200	0.02466000	-1.43159100

H	1.08614600	-1.80964800	-1.40857700
O	2.48005100	-1.56374000	0.11657100
C	3.01495900	0.60496200	-0.56838700
C	3.57006700	-0.62319300	0.16211500
H	3.74532400	1.11510800	-1.19897100
H	2.53562700	1.31472900	0.11366700
H	3.82877600	-0.42681400	1.20574200
H	4.43209300	-1.06616400	-0.35072100

Optimized Structure of Malonate Product

0 1

C	1.12125000	0.21625700	0.18170200
C	-0.04162900	0.91217700	-0.52050900
C	-1.35647400	0.23189300	-0.13017500
O	-1.25253500	-1.10929000	-0.23858900
O	-2.36679800	0.80656800	0.20284900
C	-2.43847700	-1.85068000	0.09810200
O	1.91625900	-0.43101700	-0.69317900
O	1.31799000	0.25604900	1.37633600

C	3.03425200	-1.12245600	-0.10901000
C	-0.07251500	2.40503300	-0.17392200
H	0.07983100	0.76556200	-1.59988300
H	-2.72987000	-1.65414200	1.13291600
H	-2.17373200	-2.89979200	-0.03478500
H	-3.26292500	-1.57419200	-0.56428800
H	3.56663200	-1.57518100	-0.94576700
H	3.68029300	-0.42232600	0.42695400
H	2.68584400	-1.88975200	0.58715300
H	-0.95085100	2.87728600	-0.61971400
H	0.82762500	2.90253500	-0.54868300
H	-0.12062100	2.53816900	0.90964000

Optimized Structure of 2-197
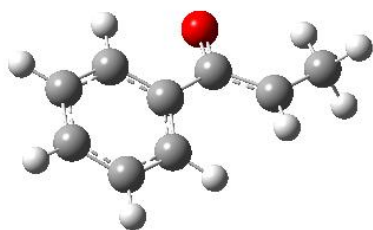
0 2

C	-2.47996600	1.01679100	0.11442500
C	-1.09972400	1.19297800	0.08255000
C	-0.23861200	0.08916100	-0.01991300
C	-0.79550500	-1.19627800	-0.10539100
C	-2.17894600	-1.37262500	-0.08072200

C	-3.02436700	-0.26799700	0.03396400
H	-3.13383700	1.88059000	0.20025400
H	-0.65852700	2.18272300	0.13491700
H	-0.15844900	-2.06879300	-0.21291700
H	-2.59594300	-2.37344300	-0.15415900
H	-4.10199600	-0.40702900	0.05673900
C	1.23963400	0.36034000	-0.05104900
O	1.65180600	1.52553600	-0.20668800
C	2.18069200	-0.71981100	0.12758000
H	1.82133900	-1.72218700	0.34121000
C	3.64814700	-0.49424000	0.07821300
H	4.11877400	-0.75837200	1.03709500
H	4.11911800	-1.13862100	-0.67860600
H	3.86695100	0.55092400	-0.14897700

Optimized Structure of Transition State
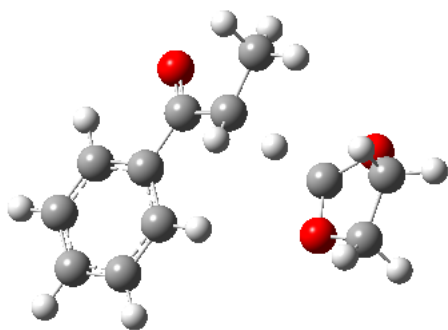
0 2

C	-4.13514100	-0.40073900	-0.31202500

C	-3.17591500	0.60746700	-0.32647700
C	-1.85210900	0.34124800	0.05776800
C	-1.50519200	-0.96375500	0.44132100
C	-2.46536900	-1.97642300	0.44471800
C	-3.78207200	-1.69695900	0.07518200
H	-5.15844500	-0.17987600	-0.60451200
H	-3.42478800	1.61809200	-0.63356200
H	-0.48139200	-1.20562000	0.70944700
H	-2.18296000	-2.98542000	0.73366200
H	-4.52945500	-2.48622900	0.08399100
C	-0.86757400	1.47655500	0.01744100
O	-1.16082200	2.52671500	-0.55964300
C	0.46010000	1.30579400	0.65517000
H	0.44462400	0.66996500	1.54486300
H	1.17203500	0.50054500	-0.16519500
C	1.29554200	2.56113800	0.79298600
H	0.88044500	3.22776000	1.56046200
H	2.32708300	2.32455800	1.07682900
H	1.30676100	3.12032000	-0.14607000
C	2.01864300	-0.32454800	-0.88821000
O	3.30631600	0.17725900	-0.85129600
H	1.61333100	-0.32275000	-1.90561700
O	1.98289600	-1.57687300	-0.27887800

225

C	3.94270300	-0.45318300	0.26713600
C	3.27984700	-1.83226800	0.28483100
H	5.01774500	-0.47273000	0.07931600
H	3.73898100	0.11174100	1.18661000
H	3.15696900	-2.24941000	1.28757000
H	3.81116300	-2.55370100	-0.34830900

Optimized Structure of Ketone Product
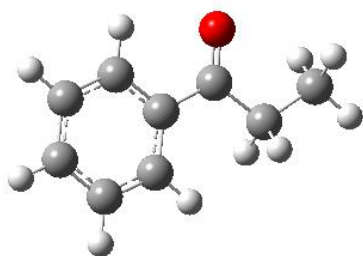
0 1

C	2.52429500	1.02473700	0.00010200
C	1.14546400	1.21137100	0.00007100
C	0.27582900	0.10914300	-0.00003600
C	0.81743400	-1.18548100	-0.00011100
C	2.19958000	-1.37261000	-0.00008200
C	3.05454000	-0.26892400	0.00002300
H	3.18814600	1.88509500	0.00018500
H	0.71111600	2.20581200	0.00012600
H	0.16548800	-2.05341700	-0.00019400
H	2.60878200	-2.37922600	-0.00014300

H	4.13138900	-0.41613100	0.00004300
C	-1.20200300	0.37664400	-0.00001300
O	-1.62330600	1.52393600	-0.00019100
C	-2.16655000	-0.80646000	0.00019400
H	-1.94417600	-1.43509800	-0.87399100
H	-1.94430100	-1.43464800	0.87473600
C	-3.63371900	-0.38080500	0.00000400
H	-3.86592100	0.22473300	-0.88083700
H	-4.28726700	-1.25946300	0.00018700
H	-3.86602300	0.22517600	0.88051200

Optimized Structure of 2-198
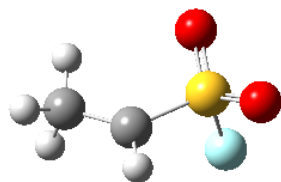
0 2

C	1.07643300	-0.76002400	-0.05379300
S	-0.48470100	0.01805600	-0.14606200
O	-0.34788000	1.36121600	-0.68066000
O	-1.47188300	-0.92898700	-0.63025300
F	-0.80098700	0.20953500	1.44049400
H	1.02590000	-1.83349500	0.09669300
C	2.33716200	0.01836300	0.00098100

H	3.14690800	-0.53470500	-0.48793900
H	2.22132900	0.99476000	-0.47707400
H	2.64651000	0.19086500	1.04505200

Optimized Structure of Transition State
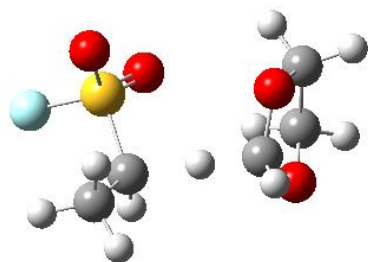
0 2

C	-0.92830500	1.04728400	0.50875100
S	-1.44643200	-0.53158200	-0.05343900
O	-1.80782100	-0.49938800	-1.46038100
O	-0.56626200	-1.56116900	0.48769600
F	-2.85756100	-0.71433100	0.75910900
H	-0.77750400	1.01425100	1.58829400
H	0.50010200	1.10612000	0.04984400
C	-1.66216800	2.23969500	-0.04889900
H	-1.15476600	3.15969200	0.26086900
H	-1.69485200	2.20626000	-1.14147100
H	-2.69600300	2.28873200	0.31945700
C	1.73281900	1.10994600	-0.26824500
O	2.48525800	0.83640000	0.85585200

H	1.94426900	2.11231200	-0.65812500
O	1.92064100	0.12202700	-1.21802000
C	2.59650200	-0.59866700	0.90811200
C	2.54659200	-1.00579300	-0.57221900
H	3.53750300	-0.84013100	1.40574800
H	1.75409100	-1.01708800	1.46811600
H	1.93972700	-1.89665500	-0.74392900
H	3.54122800	-1.13695400	-1.01193400

Optimized Structure of Sulfonylfluoride Product
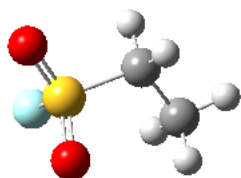
0 1

C	1.06201700	0.86488700	0.04646500
S	-0.53172200	0.01980700	0.12613700
O	-0.51577100	-1.01820500	1.14061300
O	-1.61222100	0.98215100	0.01908400
F	-0.44989600	-0.74259700	-1.30910700
H	1.00736000	1.50780000	-0.83623900
H	1.06783700	1.50381300	0.93557700
C	2.24757500	-0.09466500	0.01476700
H	3.17572100	0.48514800	0.00170100

H	2.25181200	-0.73991000	0.89681200
H	2.22027400	-0.72328100	-0.87905700

Optimized Structure of 2-199
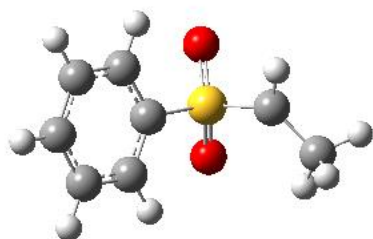
0 2

C	1.91198200	-0.15313300	1.10021500
S	1.15939700	0.43436400	-0.38639500
O	1.33859000	1.89645800	-0.42479100
O	1.61724800	-0.42499000	-1.49216000
C	-0.59419700	0.11803500	-0.13769600
C	-1.38961400	1.10343400	0.45262800
C	-2.74536900	0.84565500	0.65549900
C	-3.29098700	-0.38100000	0.26864300
C	-2.48644300	-1.35452900	-0.32980900
C	-1.12948000	-1.10974800	-0.53686900
H	-0.95107500	2.05841300	0.72297200
H	-3.37693400	1.60514300	1.10758400
H	-4.34808800	-0.57621700	0.42684000
H	-2.91757000	-2.30148800	-0.64202800

H	-0.49184900	-1.84378900	-1.01851500
C	2.86497700	-1.29100100	1.11725100
H	3.86163500	-0.96118900	1.44678400
H	2.54074800	-2.06681200	1.82668500
H	2.95901300	-1.73512800	0.12318700
H	1.68184100	0.43324300	1.98524600

Optimized Structure of Transition State
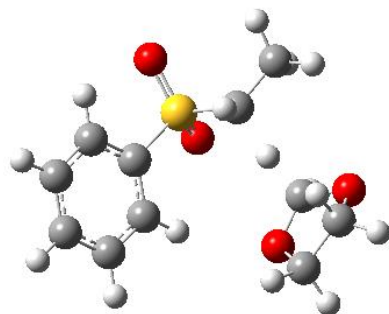
0 2

C	-0.53512300	1.42875600	-0.72587300
S	0.87888900	1.50182800	0.37137700
O	1.78679100	2.57676100	-0.08047900
O	0.36362500	1.51298800	1.75522400
C	1.72977200	-0.06487700	0.09465800
C	2.84385800	-0.08369400	-0.74646200
C	3.51260000	-1.29000900	-0.95808500
C	3.06687700	-2.45607000	-0.33149900
C	1.95447500	-2.42126800	0.51319500

231

C	1.27862200	-1.22080900	0.73574000
H	-1.48122400	0.57051500	-0.05020300
H	3.18172400	0.83911500	-1.20622600
H	4.38472400	-1.31717200	-1.60540200
H	3.59190000	-3.39322300	-0.49638200
H	1.61709900	-3.32784600	1.00798400
H	0.41847300	-1.18116600	1.39441000
C	-1.25237900	2.75285300	-0.86956600
H	-0.64006400	3.48948100	-1.40391200
H	-2.18494500	2.60669700	-1.42564100
H	-1.50208100	3.17113900	0.11126000
H	-0.26751800	0.93074900	-1.66064400
C	-2.45359800	-0.03035600	0.57302600
O	-3.58747700	-0.00834200	-0.22808800
H	-2.60037100	0.53980900	1.49527700
O	-2.09034800	-1.35615100	0.81797700
C	-3.50682400	-1.19277600	-1.02690200
C	-2.84079200	-2.19373100	-0.07447800
H	-4.51799900	-1.46829500	-1.33225000
H	-2.89174100	-1.00880100	-1.91886500
H	-2.16147700	-2.88670000	-0.57924700
H	-3.57438600	-2.76369600	0.50821000

Optimized Structure of Sulfone Product
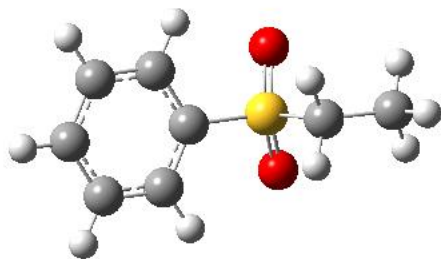
0 1

C	1.83746800	-0.00093000	1.19768800
S	1.09503200	0.00041700	-0.47043100
O	1.43729800	1.28313400	-1.11015700
O	1.43732600	-1.28120200	-1.11232700
C	-0.67748100	0.00011400	-0.14489300
C	-1.34833100	1.21869100	-0.02403500
C	-2.71855900	1.21199200	0.23846000
C	-3.39984700	-0.00035500	0.37254600
C	-2.71829700	-1.21247900	0.23760800
C	-1.34809000	-1.21871200	-0.02490700
H	1.45485600	-0.89222000	1.70439700
H	-0.80440400	2.14847500	-0.15587800
H	-3.25506300	2.15213500	0.32979000
H	-4.46744600	-0.00055600	0.57469200
H	-3.25463000	-2.15278600	0.32827100
H	-0.80402300	-2.14831000	-0.15747600
C	3.36188200	-0.00093600	1.10170100

H	3.71716000	0.88766100	0.57256600
H	3.79169300	-0.00178700	2.10866300
H	3.71701800	-0.88861400	0.57098000
H	1.45485500	0.88956700	1.70575900

Optimized Structure of 2-200
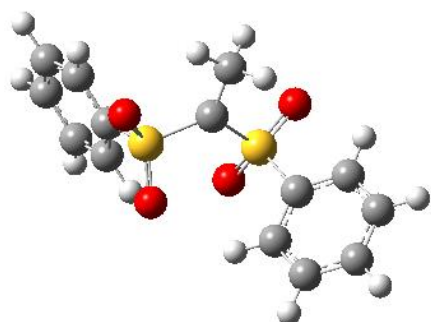
0 2

C	0.03397500	-0.39175400	0.97621000
C	0.24445500	-0.91340900	2.35392100
S	0.93661000	1.08448000	0.47786400
O	0.25592500	1.68443600	-0.67660200
O	1.14580400	1.85152200	1.71615700
C	2.53227000	0.45436200	-0.05241700
C	2.65682000	-0.12477500	-1.31962800
C	3.90788300	-0.59350100	-1.71739500
C	5.00775200	-0.47943800	-0.86235400
C	4.86675000	0.10531900	0.39845000
C	3.62150400	0.57642100	0.81442300

S	-1.03296600	-1.27308000	-0.18207500
O	-1.34864400	-2.55115600	0.47609500
O	-0.38441000	-1.24415900	-1.50093600
C	-2.54786600	-0.31706000	-0.26090500
C	-2.66155400	0.72702500	-1.18351600
C	-3.85871700	1.43904000	-1.24009300
C	-4.91653400	1.10763900	-0.38943900
C	-4.78915200	0.05690700	0.52283100
C	-3.59933000	-0.66576200	0.59267700
H	-0.00073700	-0.14241000	3.09510800
H	1.30005700	-1.17969800	2.51078100
H	-0.36354600	-1.80468400	2.51965800
H	1.79073300	-0.21395800	-1.96544000
H	4.02354900	-1.04723600	-2.69729100
H	5.97937500	-0.84675200	-1.18113700
H	5.72572500	0.19914800	1.05659900
H	3.48895500	1.04983400	1.78132200
H	-1.82723100	0.97414400	-1.82795600
H	-3.96458100	2.25337400	-1.95071100
H	-5.84576500	1.66850200	-0.43993000
H	-5.61738100	-0.20430100	1.17511300
H	-3.48639600	-1.49959200	1.27695800

235

Optimized Structure of Transition State
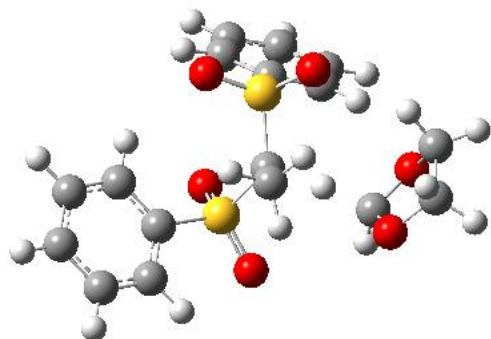
0 2

C	0.10504700	0.65089800	0.30625100
C	0.71855300	1.74953700	1.15567000
S	1.15796700	0.11016900	-1.06998900
O	0.74413600	-1.24140700	-1.47629200
O	1.11348000	1.22744800	-2.03356100
C	2.84902500	0.01880500	-0.44953200
C	3.22589400	-1.03853400	0.38336200
C	4.54705500	-1.10561700	0.82426900
C	5.47181300	-0.13504600	0.42916200
C	5.08078300	0.91228200	-0.40742600
C	3.76029600	0.99755000	-0.85057700
S	-0.66537100	-0.61830900	1.36312900
O	-1.65231900	0.14142100	2.16036000
O	0.40538600	-1.36668500	2.05342300
C	-1.57489600	-1.78600100	0.34129900
C	-1.11903800	-3.10286800	0.28138400

C	-1.85799400	-4.03944100	-0.43945600
C	-3.03021700	-3.65452300	-1.09314700
C	-3.47446500	-2.33248700	-1.02118000
C	-2.75232300	-1.38689500	-0.29344300
H	-0.96260800	1.36085200	-0.38148700
H	1.03563700	2.57384800	0.51072700
H	1.57990500	1.38904800	1.72941800
H	-0.02721200	2.12631700	1.86012800
H	2.49847100	-1.78087300	0.69065600
H	4.85428200	-1.91900000	1.47525500
H	6.50034800	-0.19658800	0.77425200
H	5.80237100	1.66274800	-0.71764800
H	3.43344500	1.79557300	-1.50831700
H	-0.20508000	-3.37849200	0.79385800
H	-1.51444300	-5.06840300	-0.49384800
H	-3.60005900	-4.38677300	-1.65869400
H	-4.38821500	-2.03474100	-1.52754700
H	-3.09859900	-0.36138300	-0.23133100
C	-1.77585400	2.22297500	-0.94214600
O	-3.08881900	1.92889100	-0.62761800
H	-1.56972600	2.12079900	-2.01143400
O	-1.44576300	3.47371300	-0.44045900
C	-3.36657900	2.64224900	0.59483300

C	-2.50782400	3.90011400	0.43384000
H	-4.43984100	2.83651200	0.62972500
H	-3.05987200	2.03065900	1.44948800
H	-2.07675300	4.25463600	1.37354400
H	-3.04803900	4.72048000	-0.05277300

## Optimized Structure of Bissulfone Product
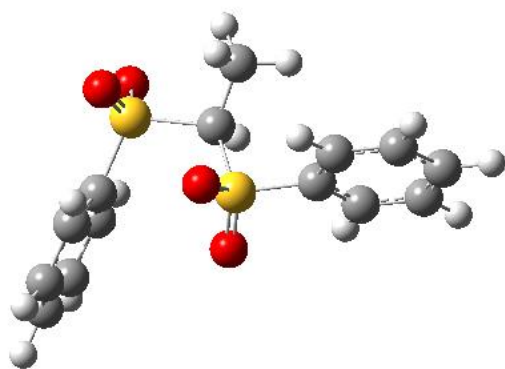
0 1

C	0.20483000	1.07809700	-0.52405000
C	1.04631100	2.31973200	-0.24177100
S	0.77523300	-0.42112800	0.40211900
O	0.59388300	-0.17221900	1.84069300
O	0.16307400	-1.58242700	-0.26195100
C	2.54569100	-0.48523900	0.07339600
C	3.43432200	0.02811100	1.02042600
C	4.80444400	-0.04866900	0.76863600
C	5.26812700	-0.63079700	-0.41363800
C	4.36726500	-1.14951900	-1.34750000

C	2.99509500	-1.08319400	-1.10653800
S	-1.57825400	1.55337600	-0.18350700
O	-1.96536100	2.27186000	-1.41009200
O	-1.61007400	2.21869800	1.12456500
C	-2.55896200	0.05763800	-0.08194700
C	-2.76380000	-0.53363100	1.16623000
C	-3.55545400	-1.67876900	1.23854200
C	-4.12822100	-2.21062500	0.08100400
C	-3.92015200	-1.59987500	-1.15810500
C	-3.13094500	-0.45444900	-1.24790000
H	0.21922000	0.78723100	-1.57739300
H	2.07969200	2.16178800	-0.56084300
H	1.02316600	2.56447600	0.82272000
H	0.63941200	3.16561200	-0.80369200
H	3.05144400	0.45986700	1.93908100
H	5.50871200	0.34089000	1.49797400
H	6.33612000	-0.68812000	-0.60459500
H	4.73279400	-1.61462000	-2.25841600
H	2.28236300	-1.50785400	-1.80605200
H	-2.30855500	-0.10432100	2.05148300
H	-3.72514400	-2.15432700	2.19998800
H	-4.74406300	-3.10353400	0.14515200
H	-4.37638700	-2.01168400	-2.05363900

H   -2.97394000   0.04845700 -2.19601300

Optimized Structure of 2-201
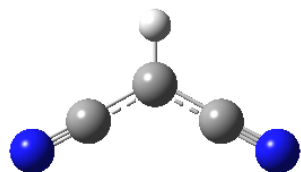
0 2

|			
C	0.00000000	0.73194700	0.00005500
C	-1.22334500	0.05524400	-0.00016600
N	-2.25978200	-0.49094700	0.00009700
C	1.22334700	0.05524900	-0.00016600
N	2.25978000	-0.49095000	0.00009700
H	-0.00000200	1.81863600	0.00029500

Optimized Structure of Transition State
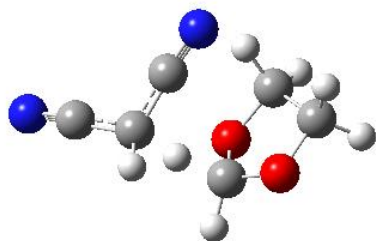
0 2

C	1.57602100	0.23896600	-0.70148200
C	1.18795800	1.47371200	-0.07171200
N	0.77371900	2.43386100	0.44126300
C	2.57446100	-0.54099400	-0.02113300

N	3.34677100	-1.22328800	0.52025400
H	0.40955600	-0.50213300	-0.70411200
H	1.76455200	0.34575600	-1.77267200
C	-0.85800600	-1.03540800	-0.68152900
O	-1.17501400	-1.35533300	0.61099200
H	-0.80792600	-1.91244000	-1.33498200
O	-1.67296100	-0.03301500	-1.15459400
C	-1.77872500	-0.17658200	1.18360000
C	-2.40025800	0.52114200	-0.03502700
H	-2.50573400	-0.50630200	1.92730800
H	-1.00850400	0.43740500	1.66093100
H	-2.26025700	1.60378200	-0.02403400
H	-3.46001400	0.28169000	-0.17054900

Optimized Structure of Malononitrile Product
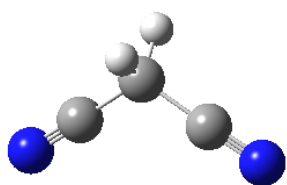
0 1

C	0.00000000	0.84007200	0.00000000
C	1.22419700	0.02665000	-0.00000600
N	2.20161600	-0.59610100	0.00000200
C	-1.22417500	0.02661400	0.00000300

```
N        -2.20163200   -0.59608000   -0.00000100

H         0.00000000    1.49262100    0.88242700

H        -0.00001300    1.49263600   -0.88241500
```

Appendix A (^{1}H, ^{13}C, and ^{19}F NMR Spectra for New Compounds)

¹H NMR Spectrum of S-1 (400 MHz, CDCl₃, 298 K)
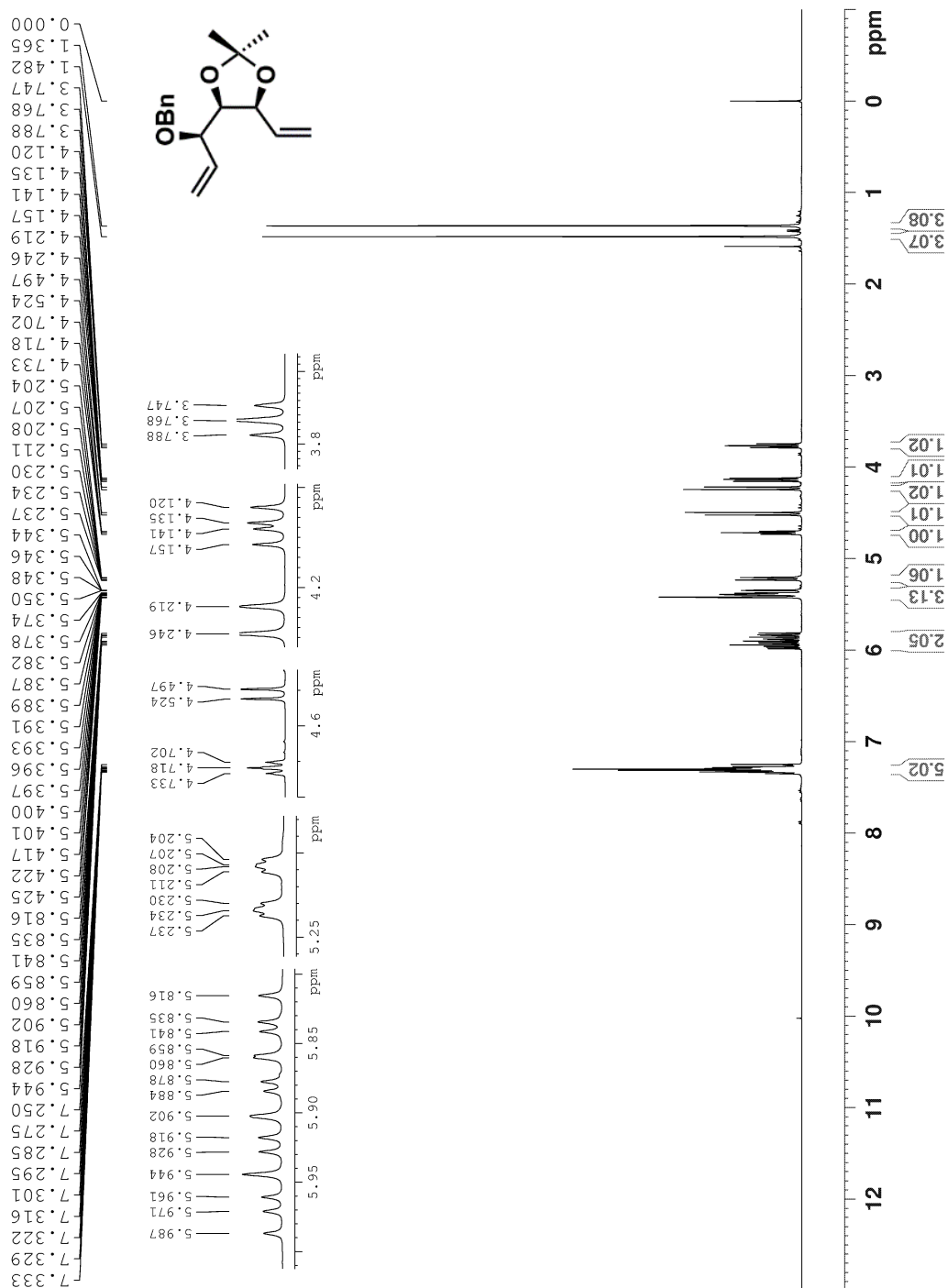
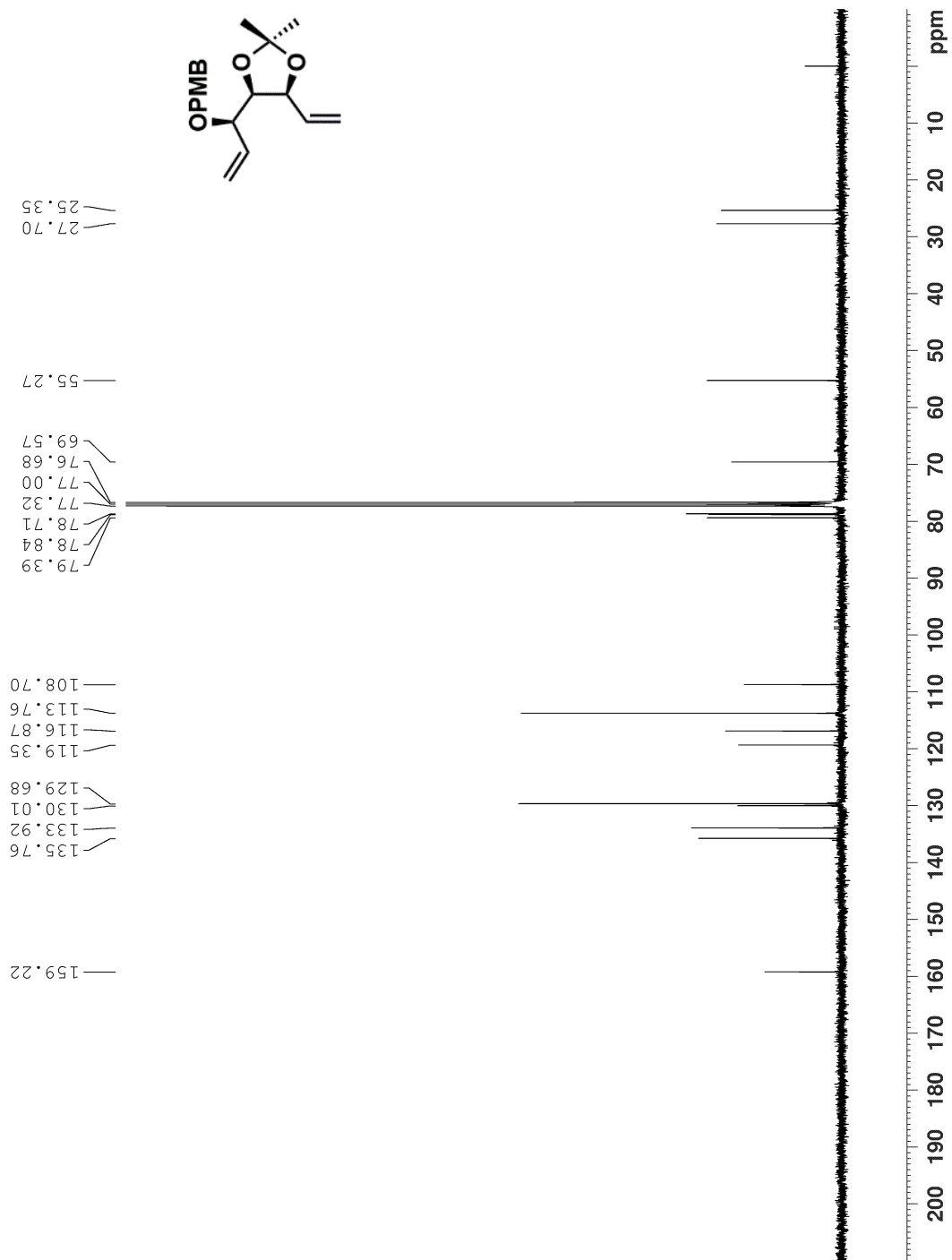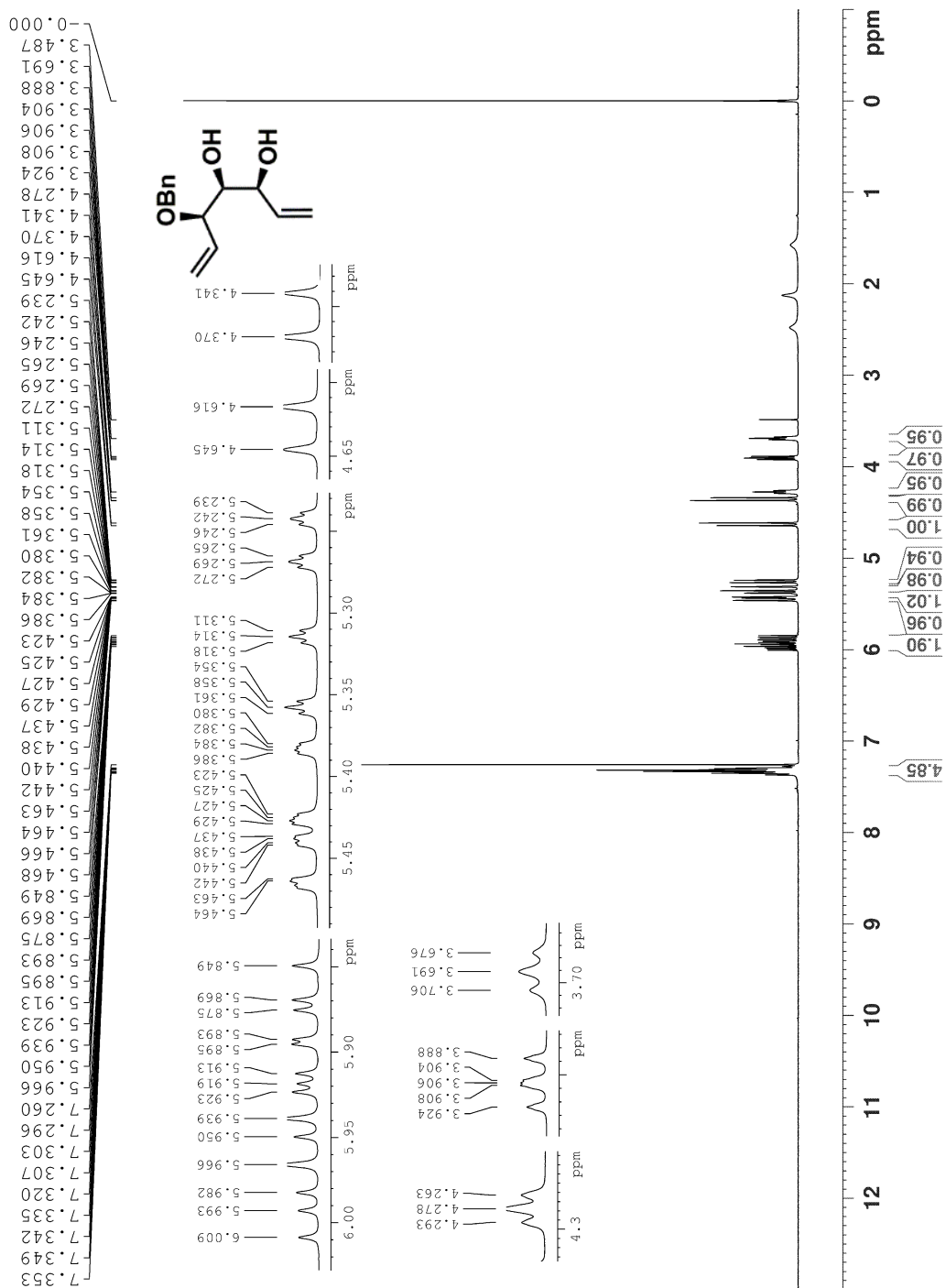**^{13}C NMR Spectrum of S-1 (100 MHz, CDCl$_3$, 300 K)**

25.34
27.68

69.90
76.68
77.00
77.32
78.70
79.11
79.38

108.71

116.88
119.40
127.63
127.97
128.31
133.85
135.64
137.89
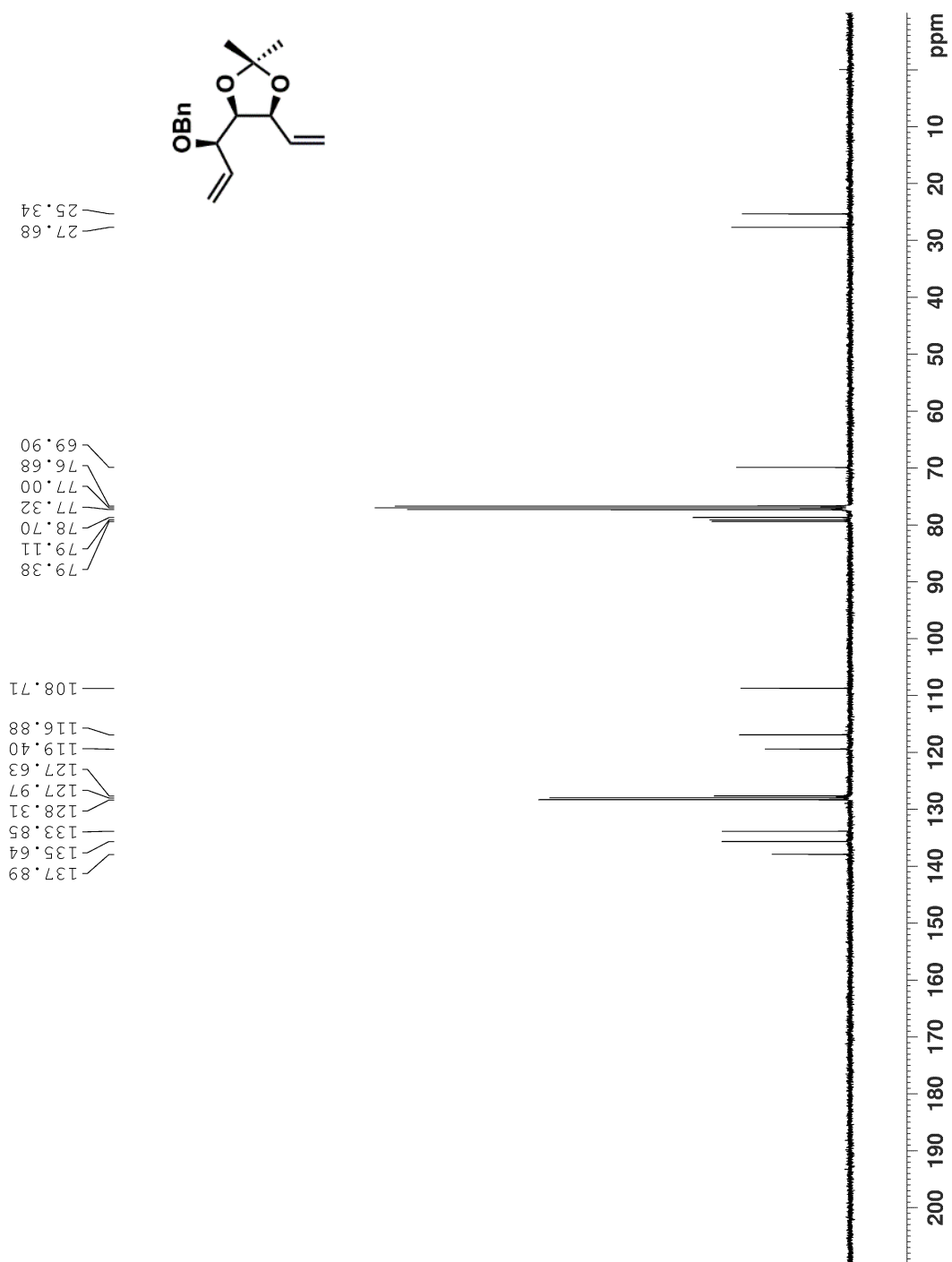
^{1}H NMR Spectrum of S-2 (400 MHz, CDCl$_3$, 300 K)
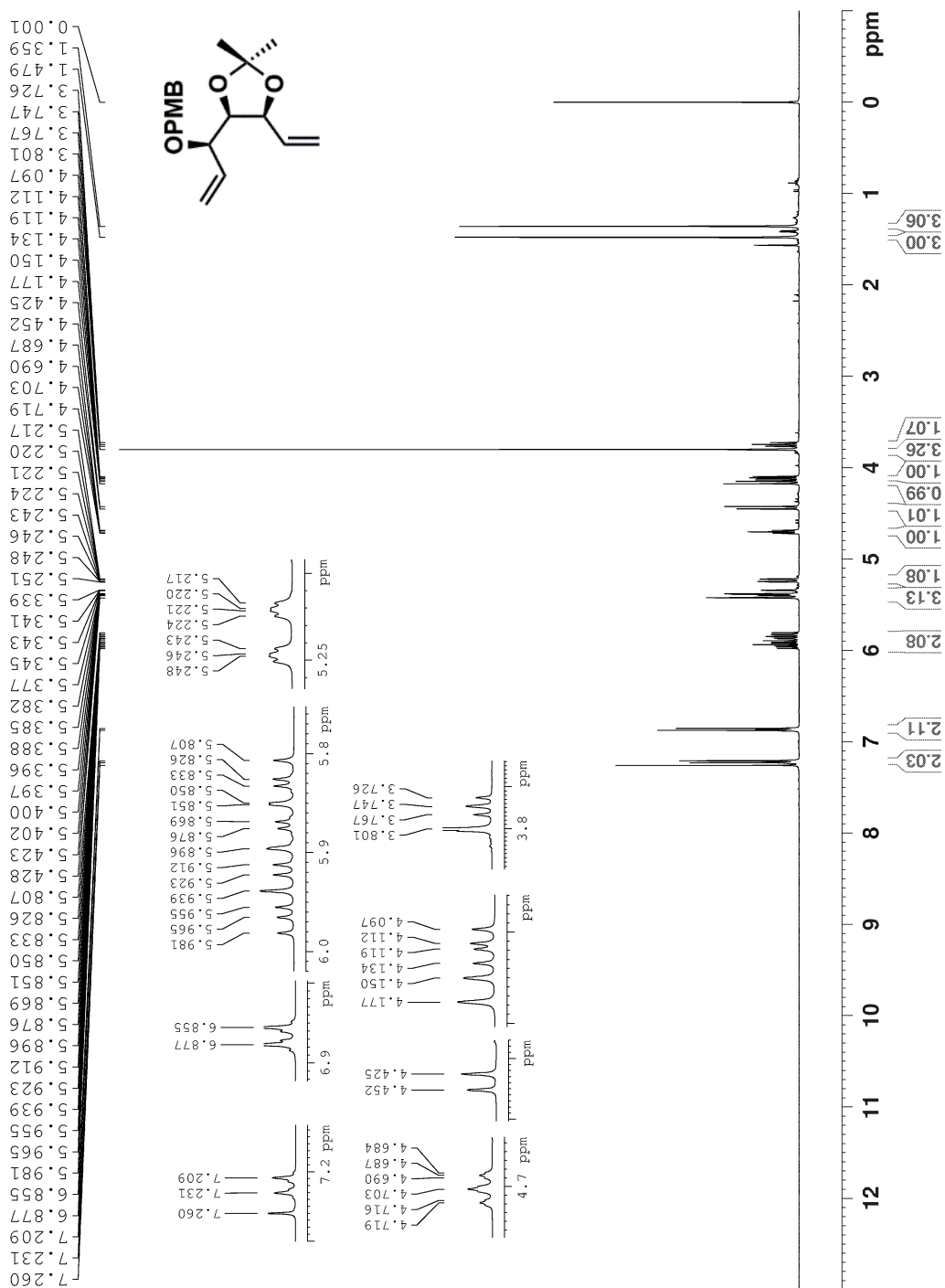
¹³C NMR Spectrum of S-2 (100 MHz, CDCl₃, 300 K)

25.35
27.70

55.27

69.57
76.68
77.00
77.32
78.71
78.84
79.39

108.70
113.76
116.87
119.35

129.68
130.01
133.92
135.76

159.22

200 190 180 170 160 150 140 130 120 110 100 90 80 70 60 50 40 30 20 10 ppm

¹H NMR Spectrum of 1-94 (400 MHz, 1% CD₃OD in CDCl₃, 298 K)

^{13}C NMR Spectrum of 1-94 (100 MHz, 1% CD$_3$OD in CDCl$_3$, 300 K)

70.37
73.55
74.76
76.68
77.00
77.31
81.90

117.15
120.39
127.76
127.89
128.40
135.15
136.71
137.69
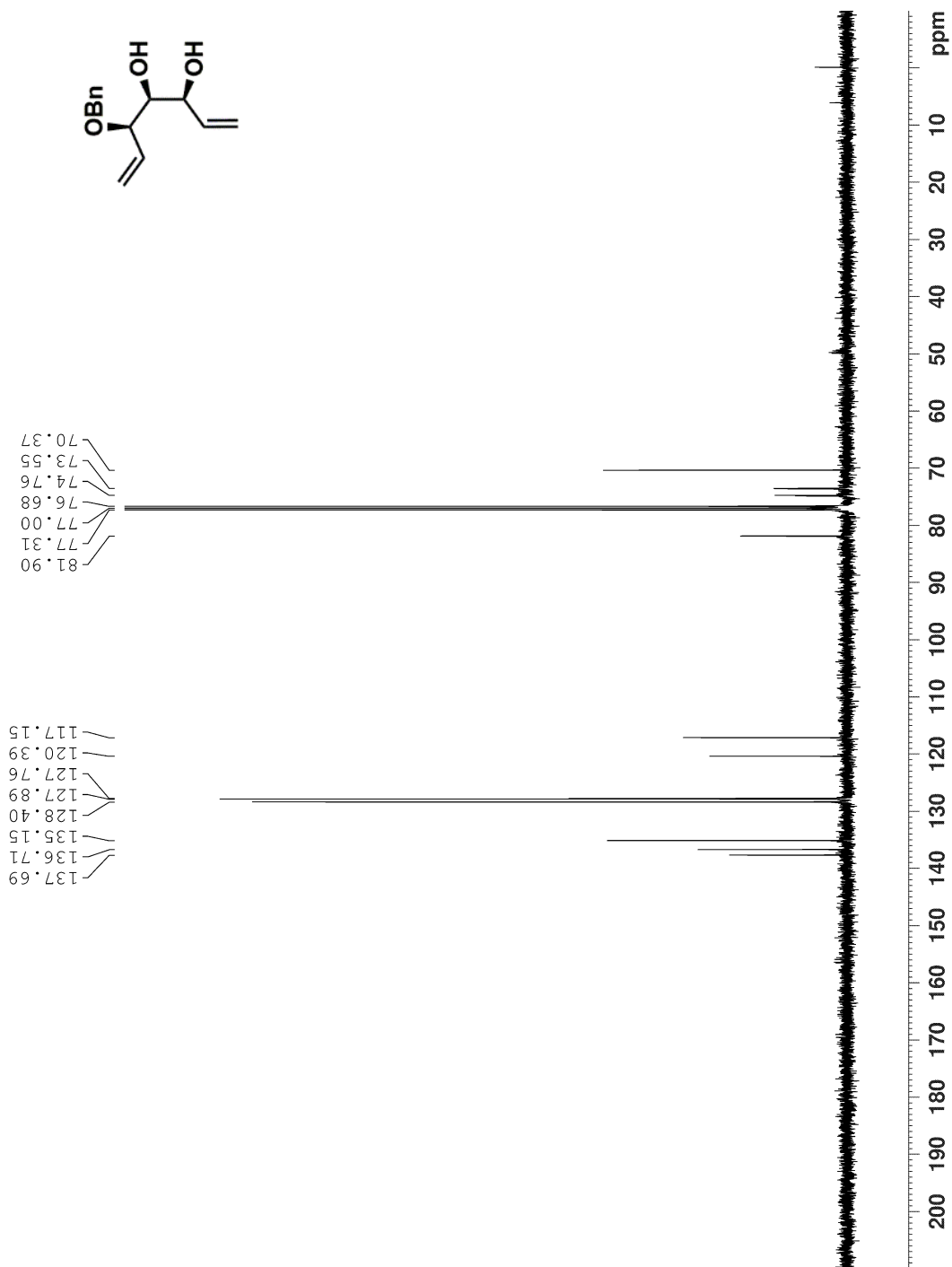
^{1}H NMR Spectrum of 1-95 (400 MHz, 1% CD$_3$OD in CDCl$_3$, 300 K)
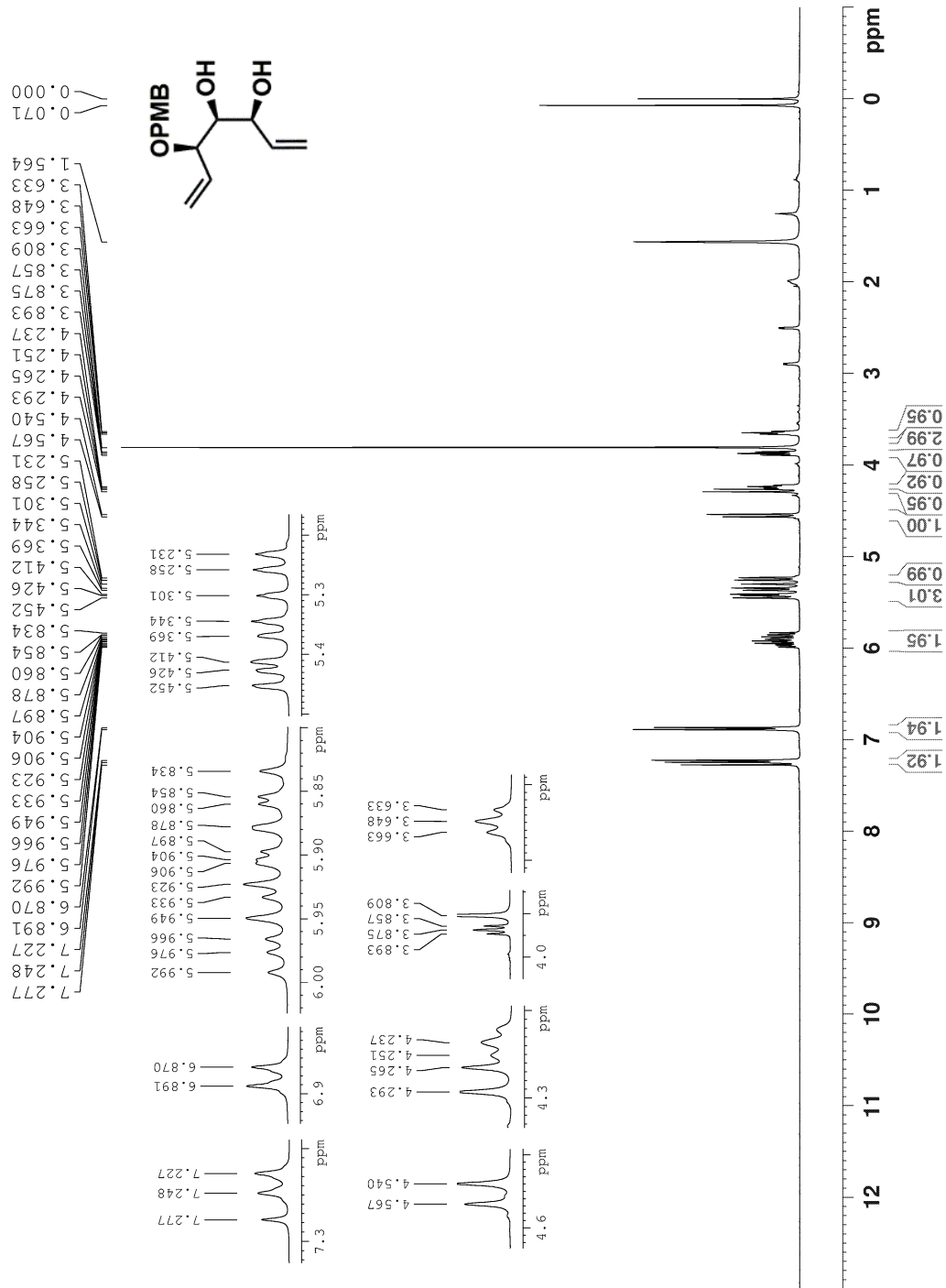
¹³C NMR Spectrum of 1-95 (100 MHz, 1% CD₃OD in CDCl₃, 300 K)

-0.07
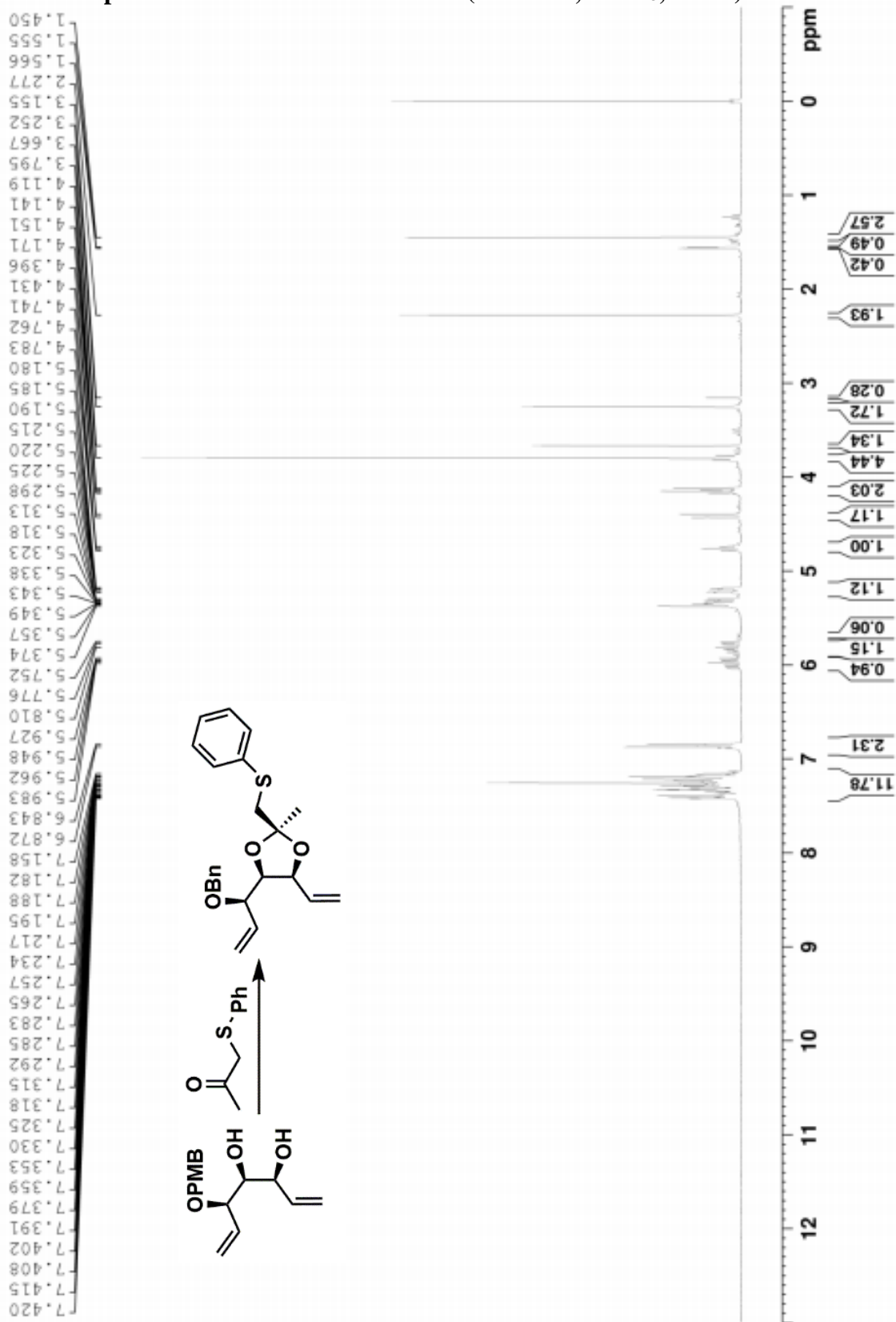0.96

55.25

70.05
73.70
74.68
76.69
77.00
77.32
81.74

113.84
117.18
120.37

129.58
129.75
135.29
136.79

159.27

200 190 180 170 160 150 140 130 120 110 100 90 80 70 60 50 40 30 20 10 ppm
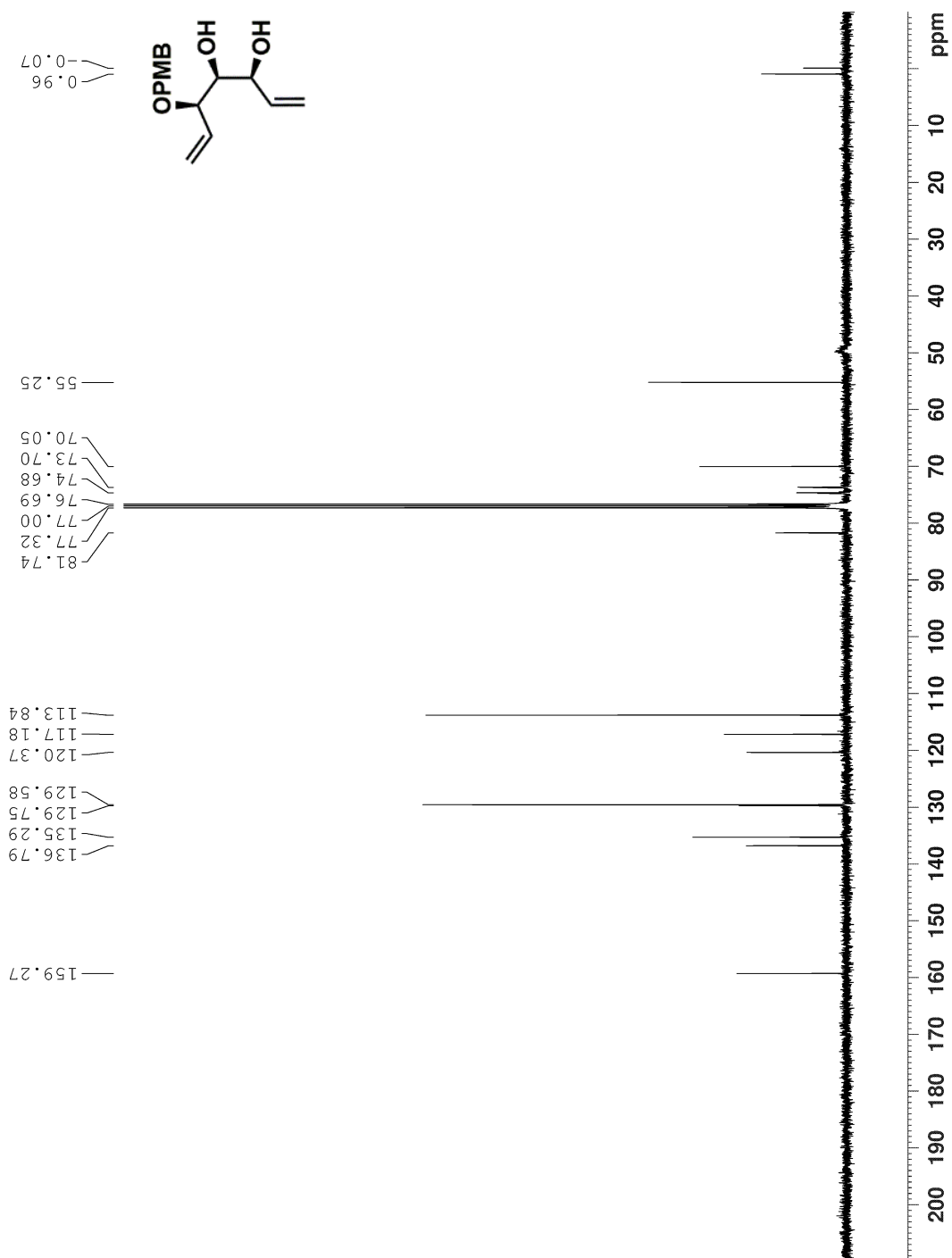
^{1}H NMR Spectrum of Crude 1-99a/1-99b (400 MHz, CDCl$_3$, 298 K)
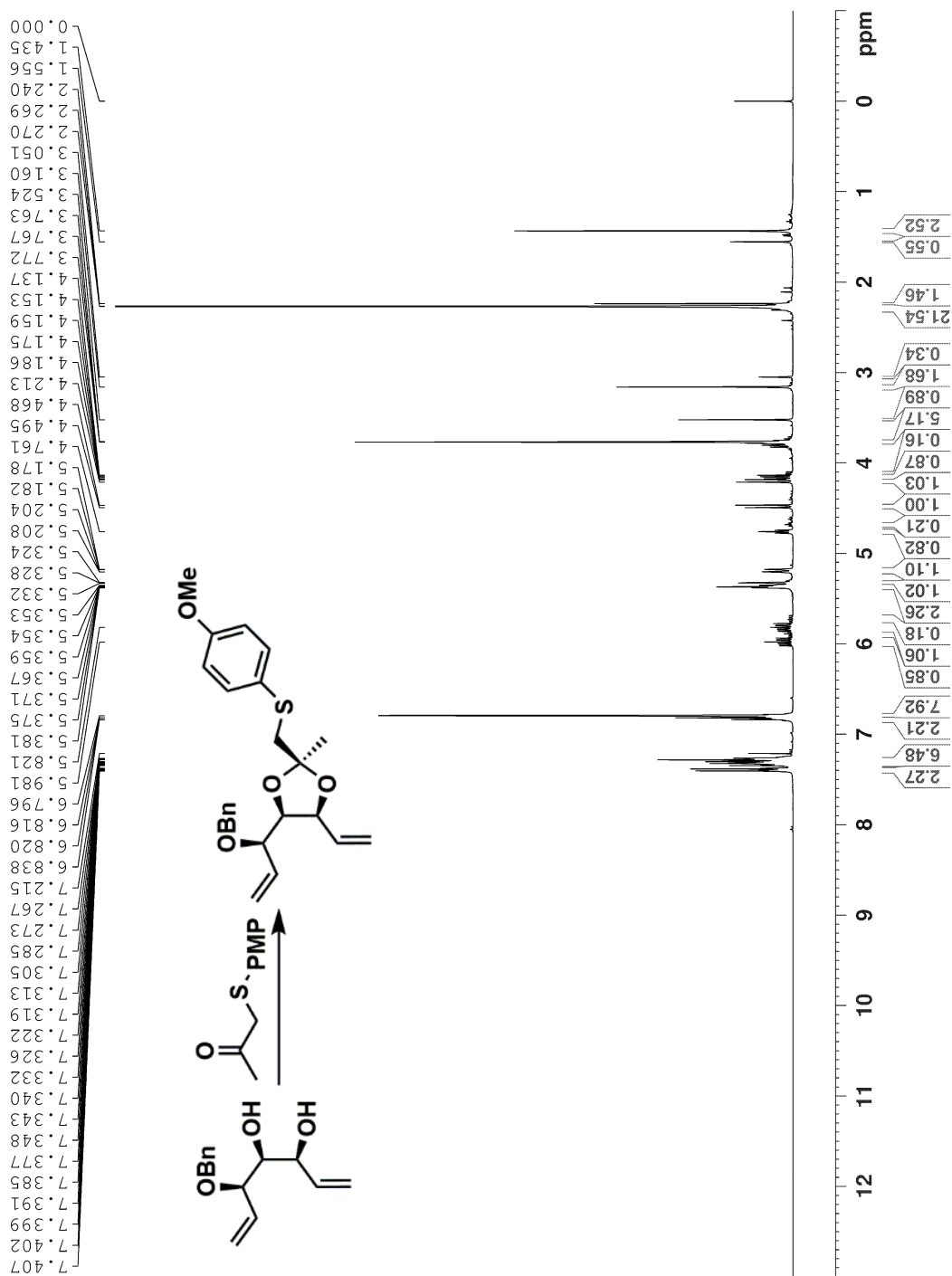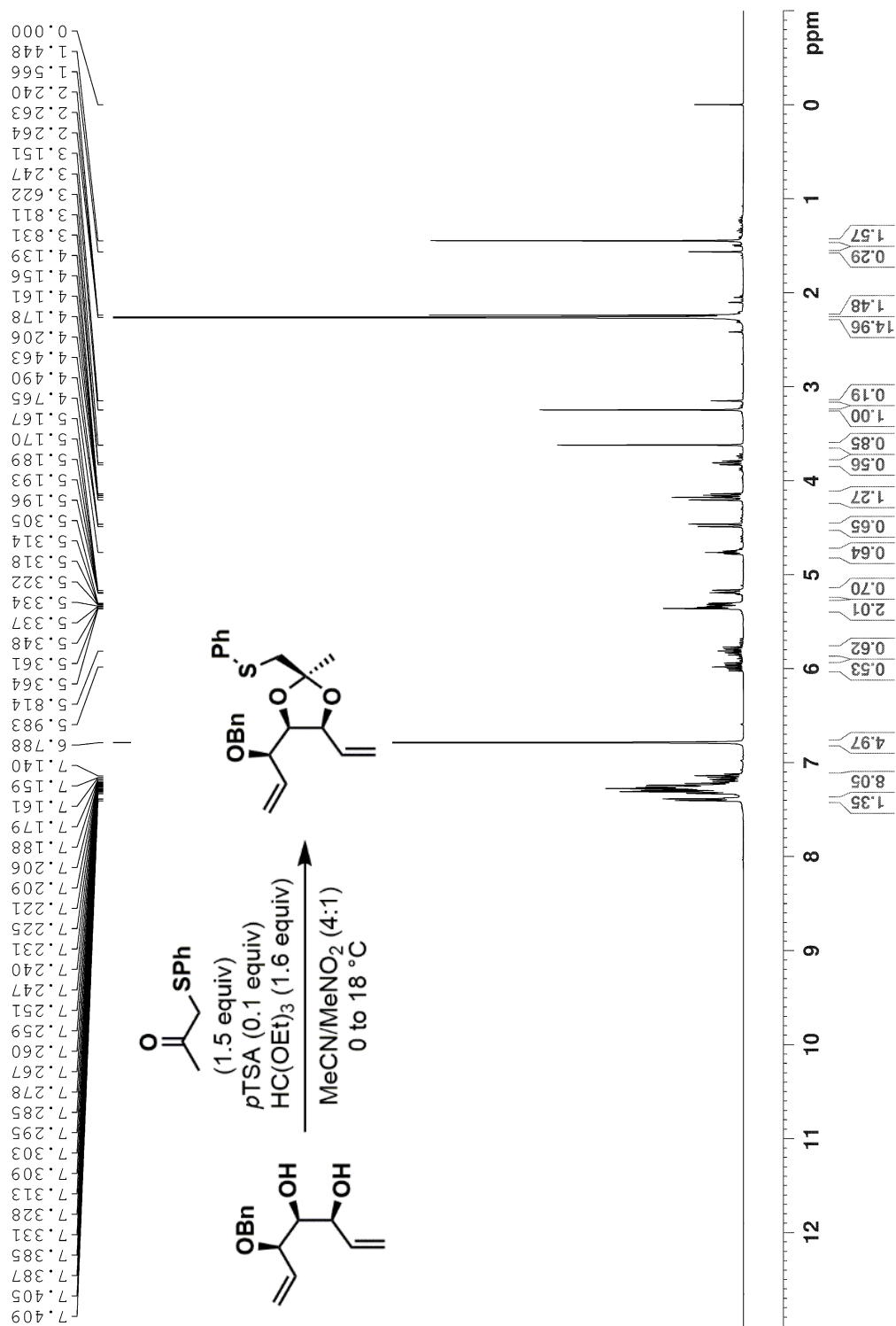
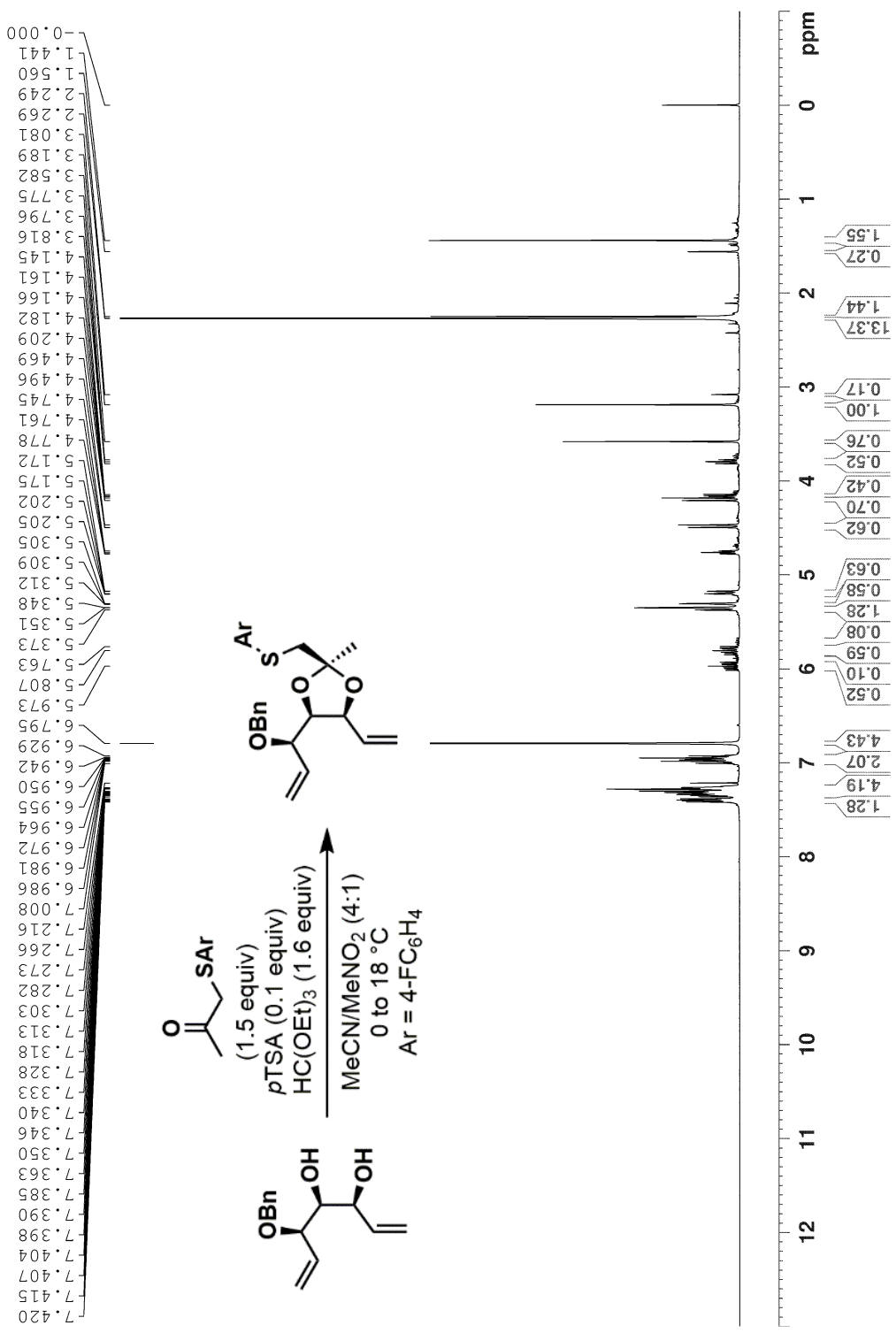**^{1}H NMR Spectrum of Crude 1-100a/1-100b (400 MHz, CDCl$_3$, 298 K)**
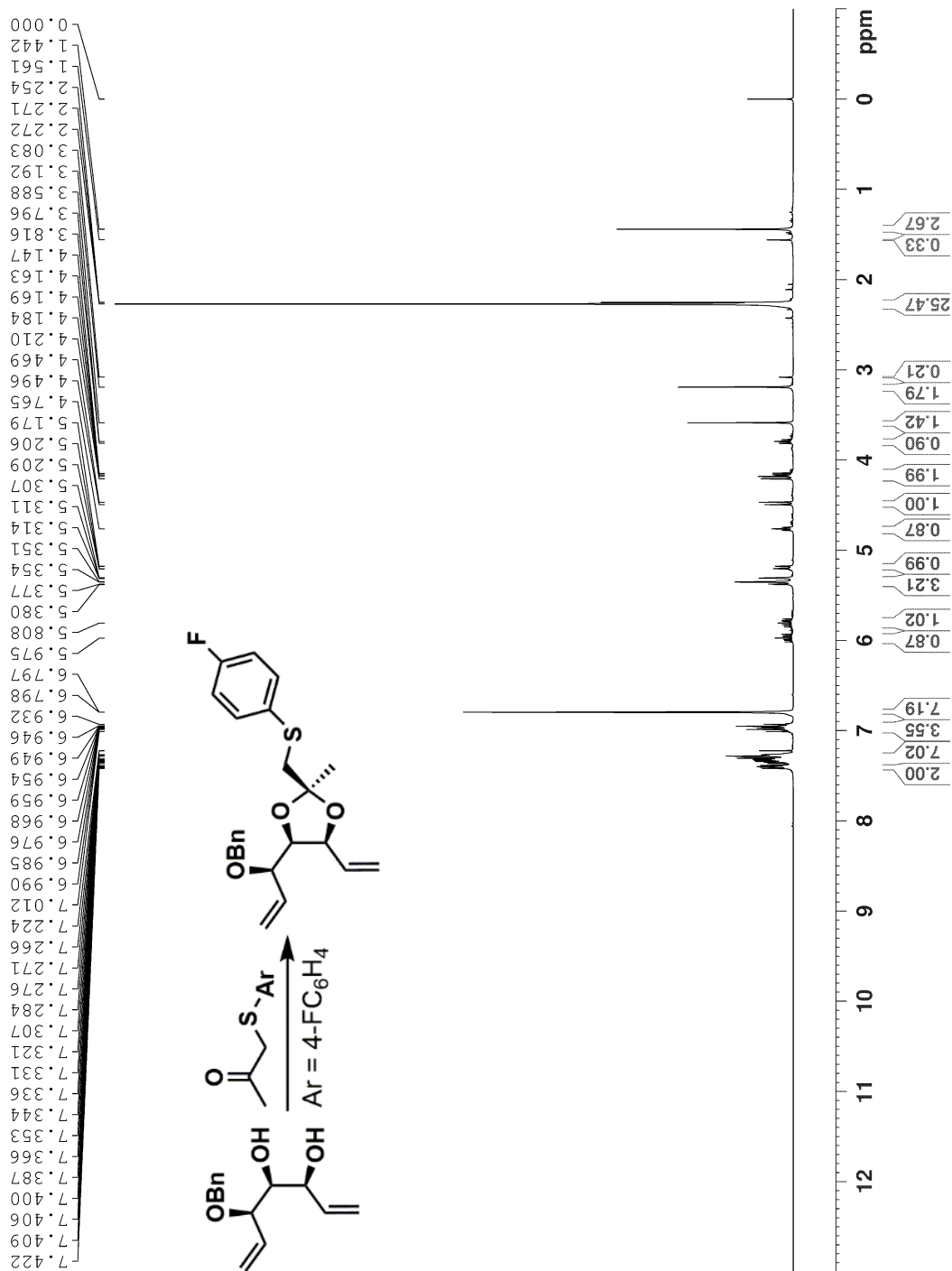
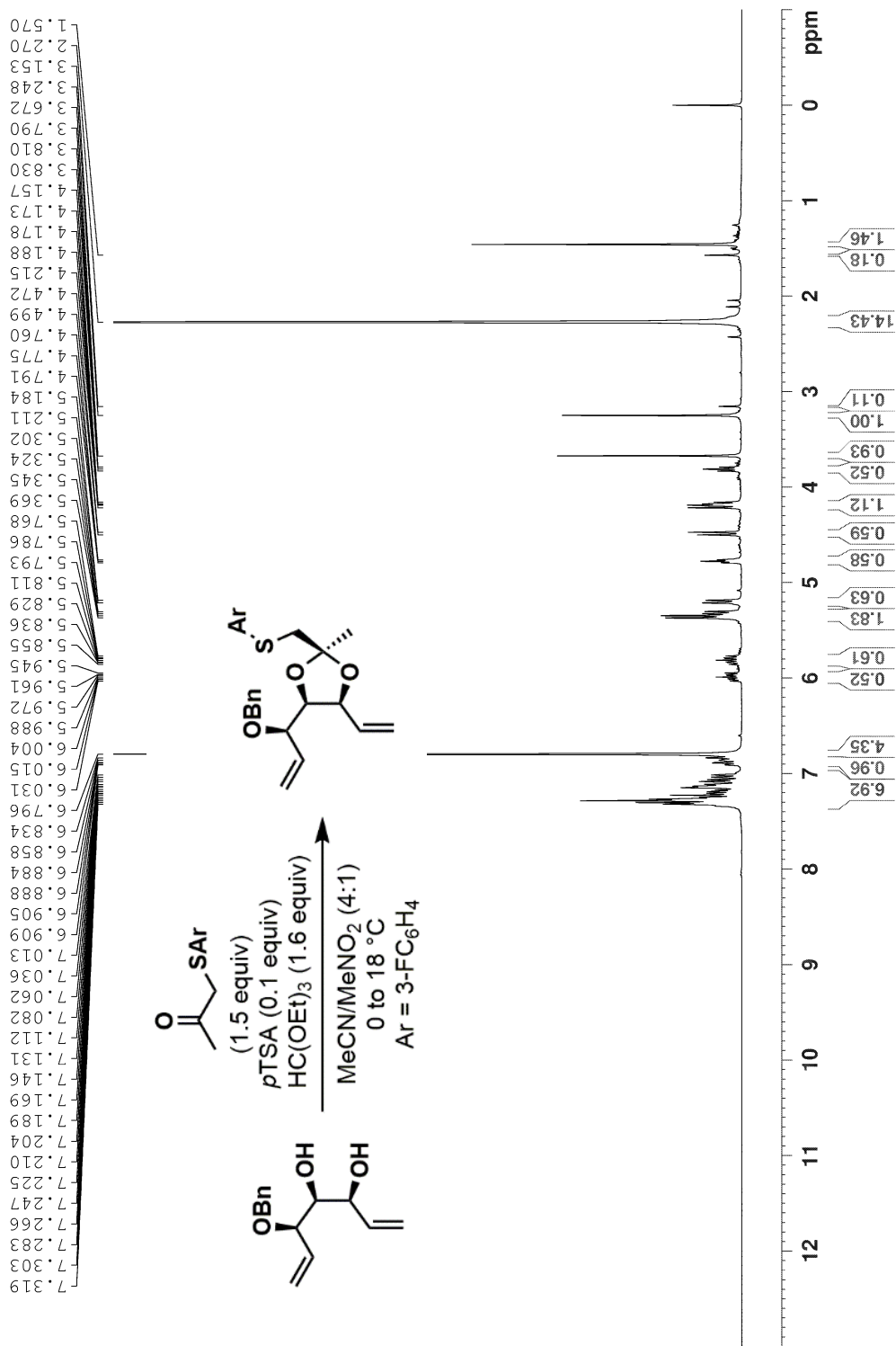**1H NMR Spectrum of Crude 1-101a/1-101b (300 MHz, CDCl₃, 298 K)**

^{1}H NMR Spectrum of Crude 1-94 + (Phenylthio)acetone + Mesitylene (400 MHz, CDCl$_3$, 298 K)

¹H NMR Spectrum of Crude 1-94 + ((3-Fluorophenyl)thio)acetone + Mesitylene (400 MHz, CDCl₃, 298 K)

^{1}H NMR Spectrum of Crude 1-94 + ((3,4-Dimethoxyphenyl)thio)acetone + Mesitylene (400 MHz, CDCl$_3$, 298 K)

^{1}H NMR Spectrum of Crude 1-95 + (Phenylthio)acetone + Mesitylene (400 MHz, CDCl$_3$, 298 K)
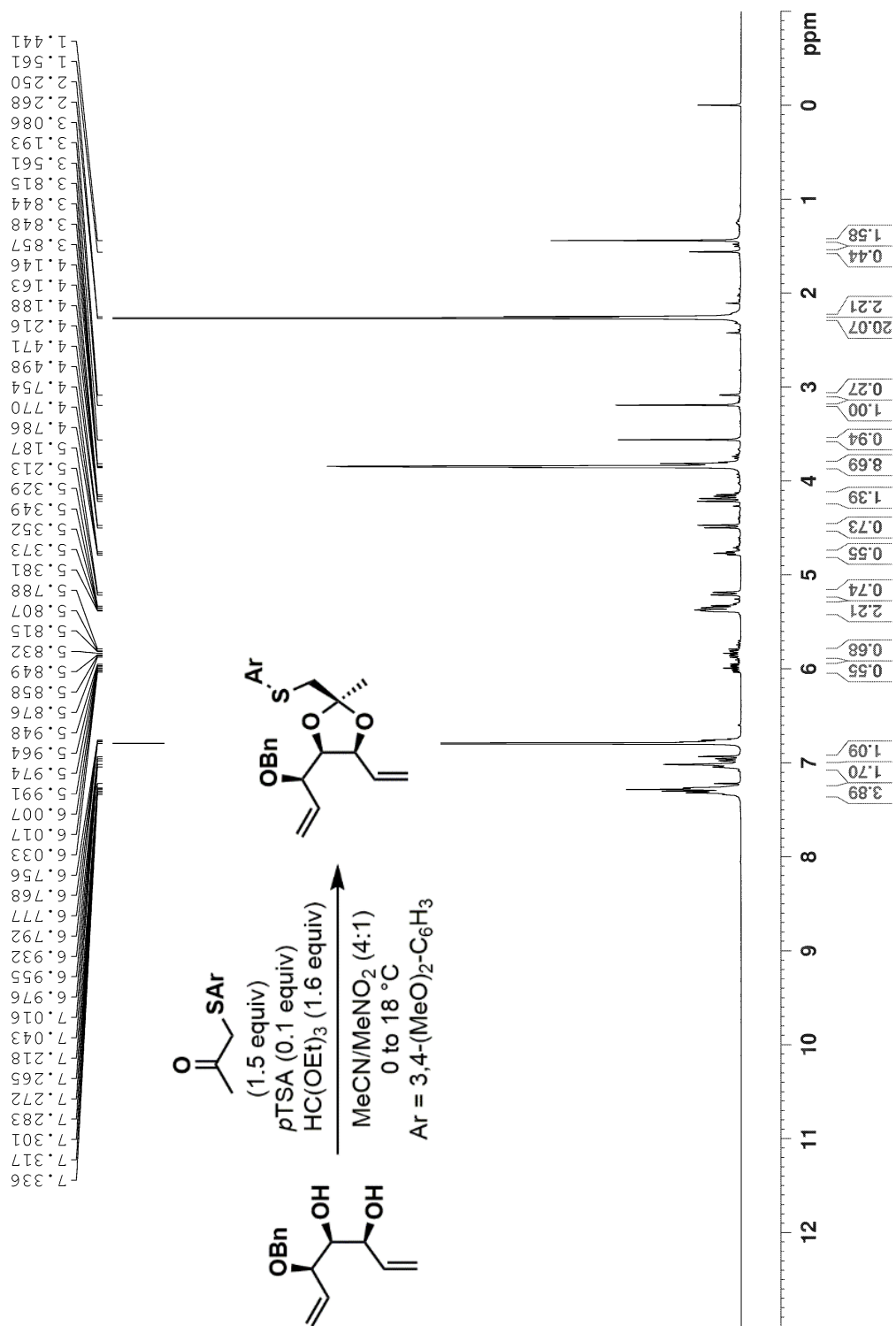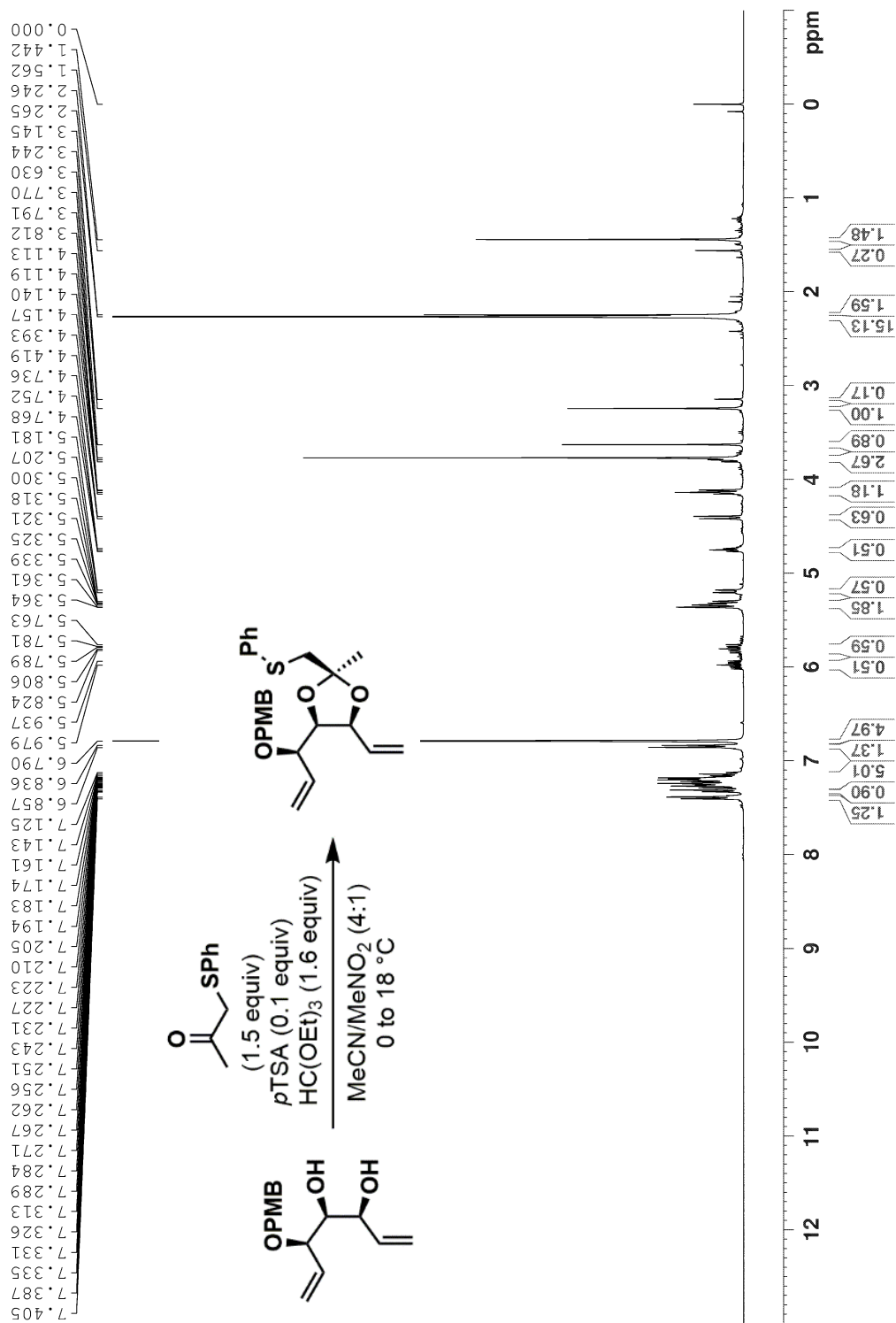
^{1}H NMR Spectrum of Crude 1-95 + ((4-Fluorophenyl)thio)acetone + Mesitylene (400 MHz, CDCl$_3$, 298 K)

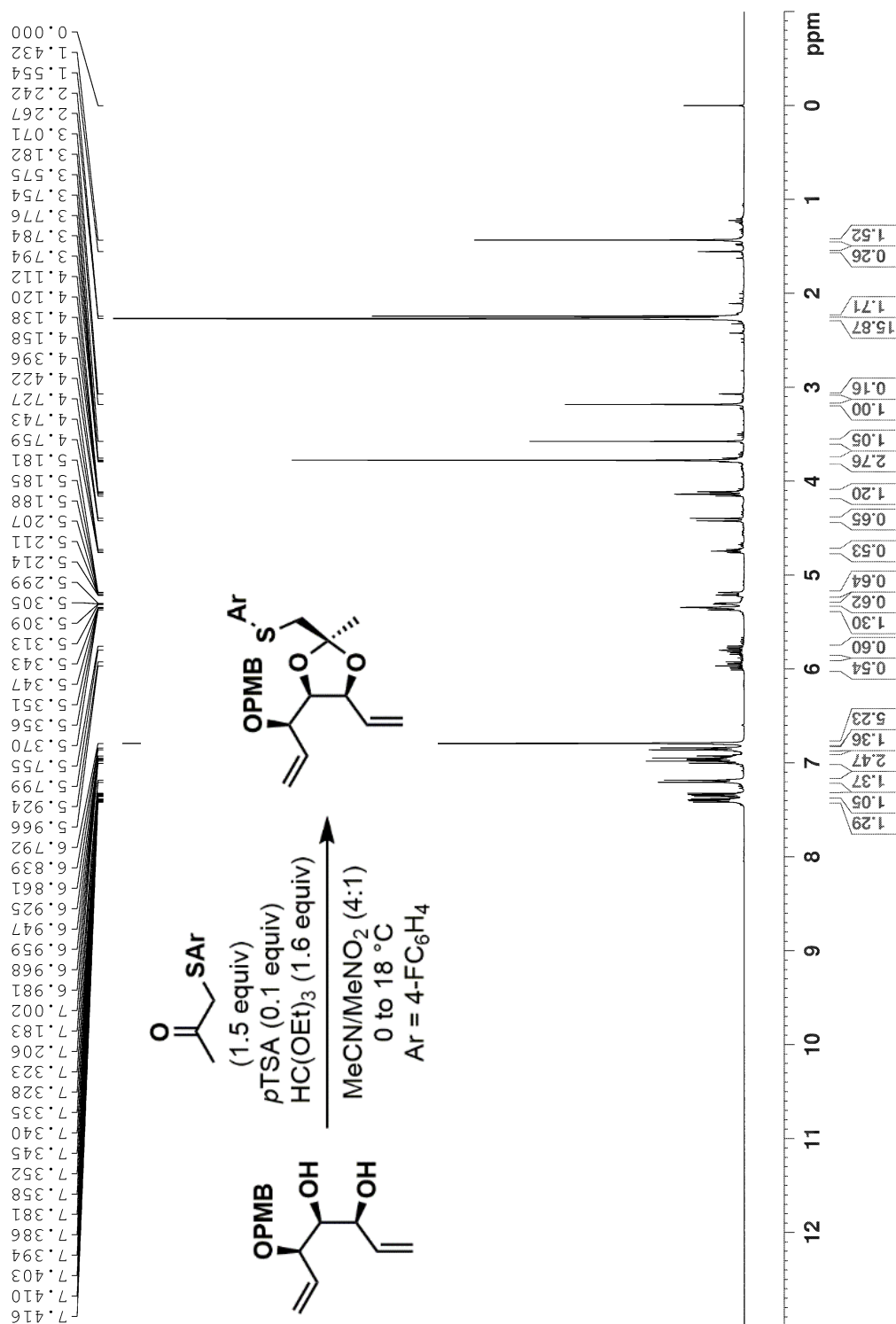**¹H NMR Spectrum of Crude 1-95 + ((3-Fluorophenyl)thio)acetone + Mesitylene (400 MHz, CDCl₃, 298 K)**

^{1}H NMR Spectrum of Crude 1-95 + ((3,4-Dimethoxyphenyl)thio)acetone + Mesitylene (400 MHz, CDCl$_3$, 298 K)
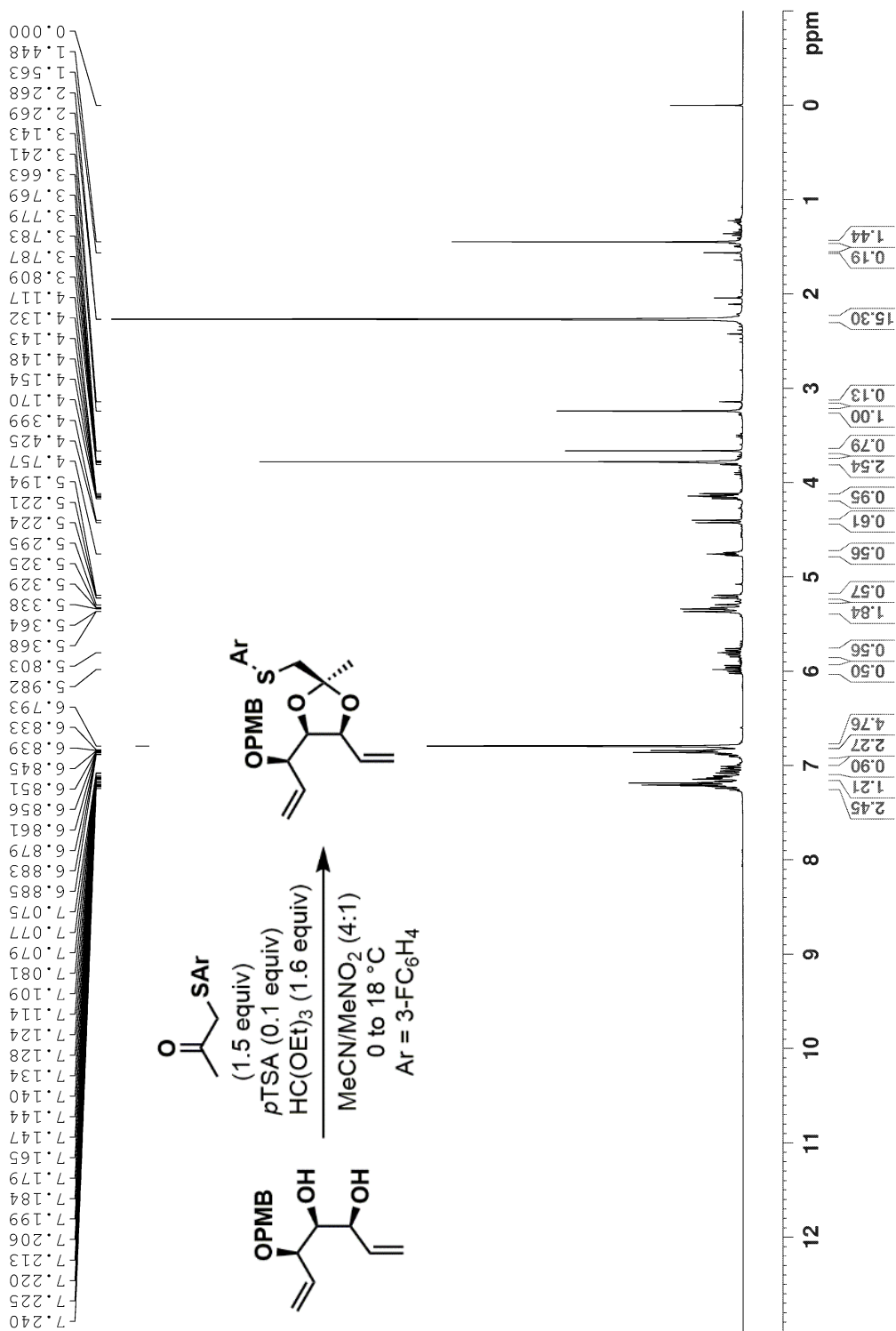
¹H NMR Spectrum of 1-101b (400 MHz, CDCl₃, 298 K)
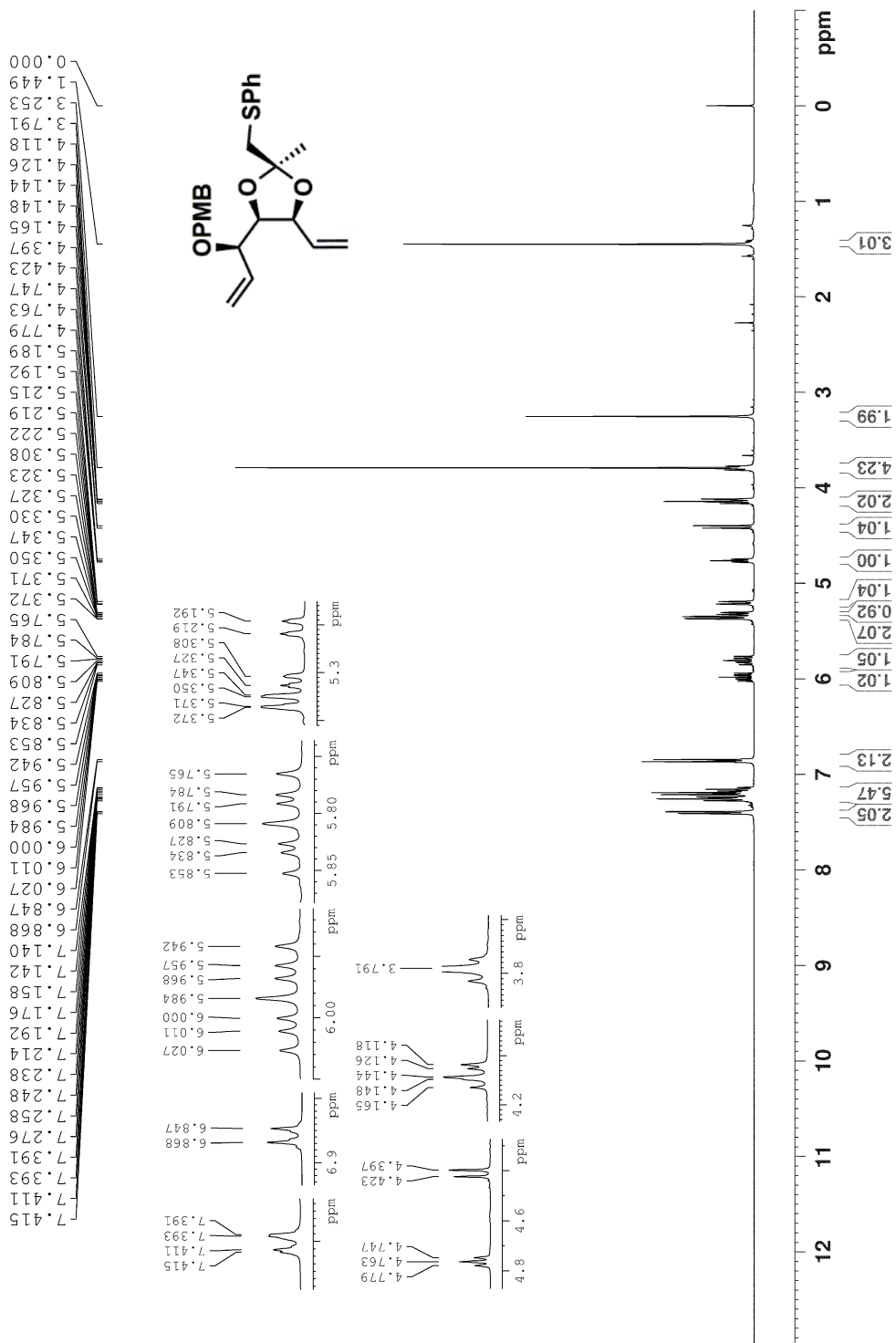
¹³C NMR Spectrum of 1-101b (100 MHz, CDCl₃, 298 K)

23.42

43.77

55.24

69.59
76.68
77.00
77.32
78.43
78.99
79.64

109.11
113.73
116.96
119.23
125.78
128.72
129.06
129.68
129.92
133.31
135.59
137.44

159.20

ppm
10
20
30
40
50
60
70
80
90
100
110
120
130
140
150
160
170
180
190
200

¹H NMR Spectrum of 1-105a (400 MHz, CDCl₃, 298 K)

^{13}C NMR Spectrum of 1-105a (100 MHz, CDCl$_3$, 298 K)

23.22

55.25

69.67
76.69
77.00
77.32
78.30
79.49
80.16

105.68

113.76
118.03
119.96

129.67
132.33
135.02

159.25

173.74

ppm
10
20
30
40
50
60
70
80
90
100
110
120
130
140
150
160
170
180
190
200
210

266
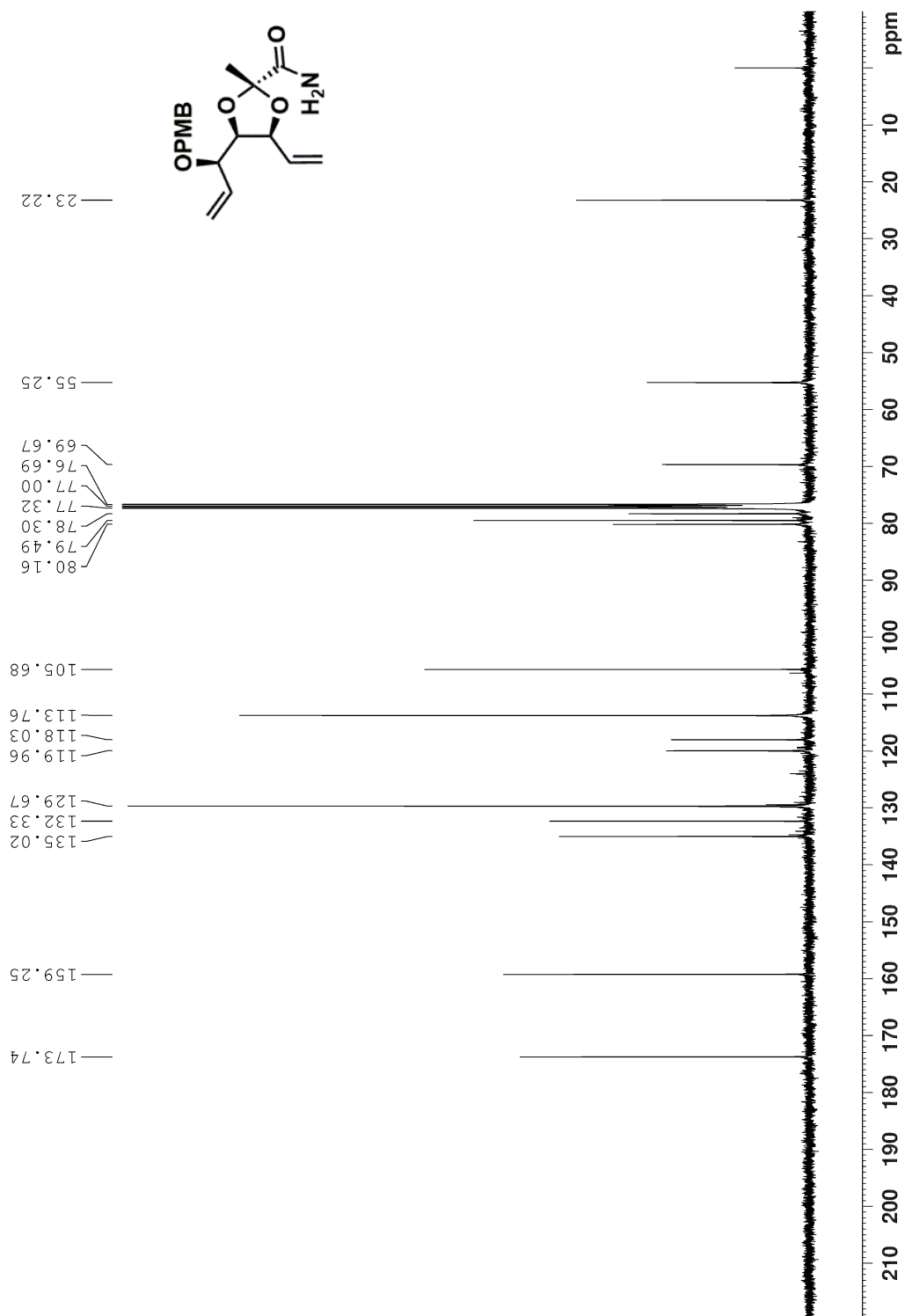
^{1}H NMR Spectrum of 1-106b (400 MHz, 1% CD$_3$OD in CDCl$_3$, 298 K)
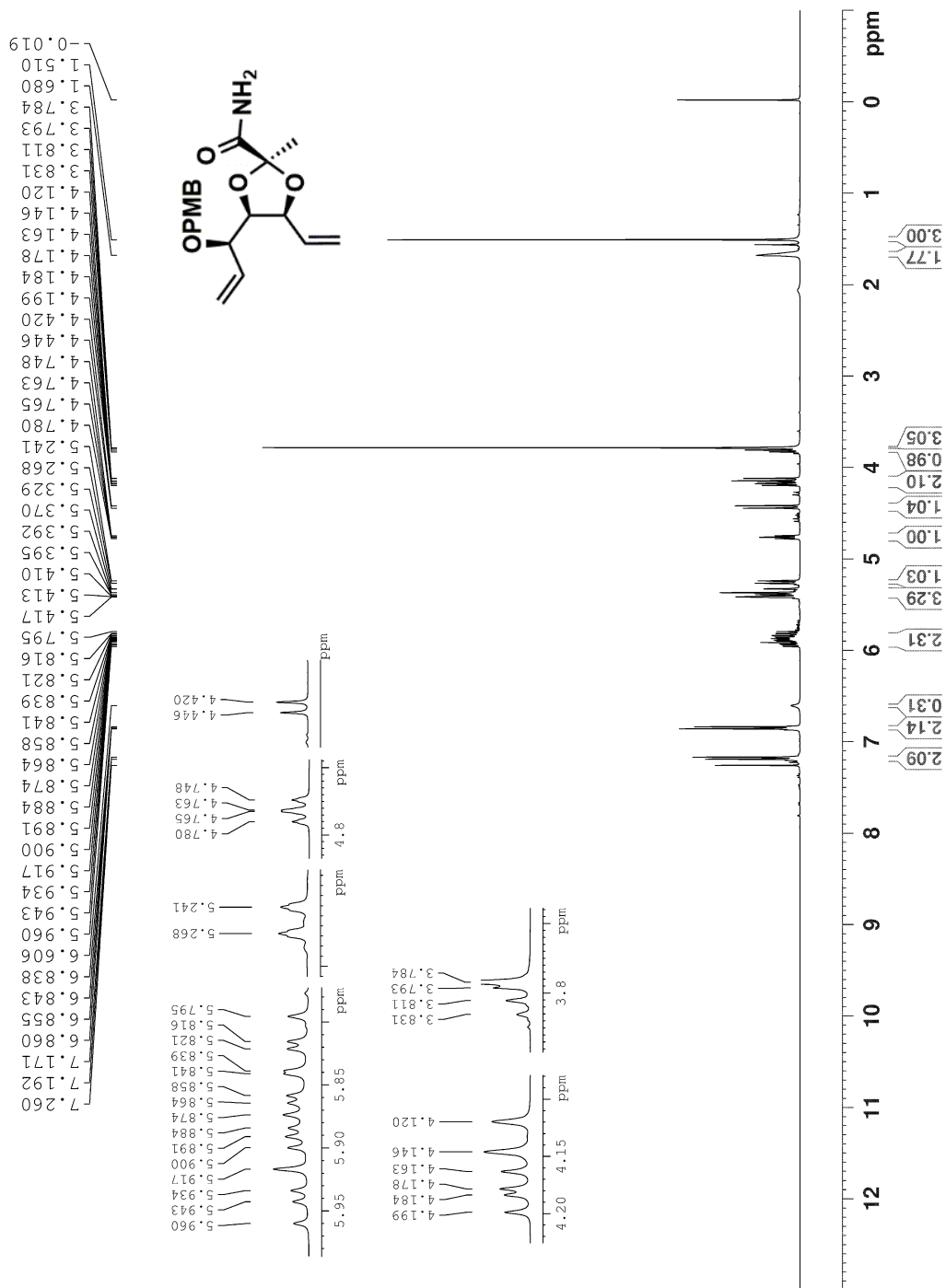
¹³C NMR Spectrum of 1-106b (100 MHz, 1% CD₃OD in CDCl₃, 298 K)

23.14

55.23

69.66
76.68
77.00
77.32
78.30
79.48
80.14

105.61

113.74
118.06
119.96

129.65
129.68
132.30
134.94

159.24

173.89

ppm

10
20
30
40
50
60
70
80
90
100
110
120
130
140
150
160
170
180
190
200

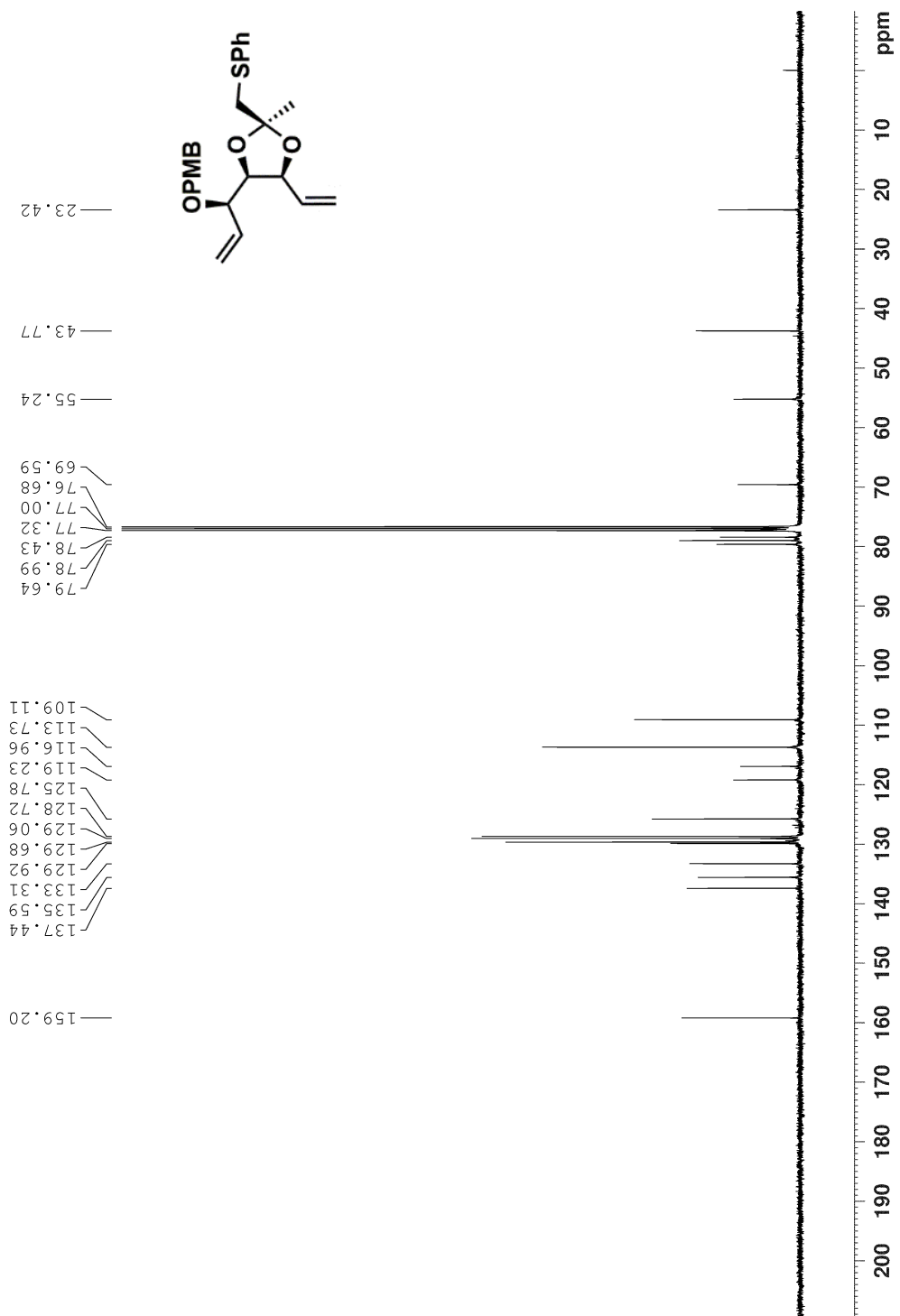# ¹H NMR Spectrum of 1-109 (400 MHz, CDCl₃, 298 K)
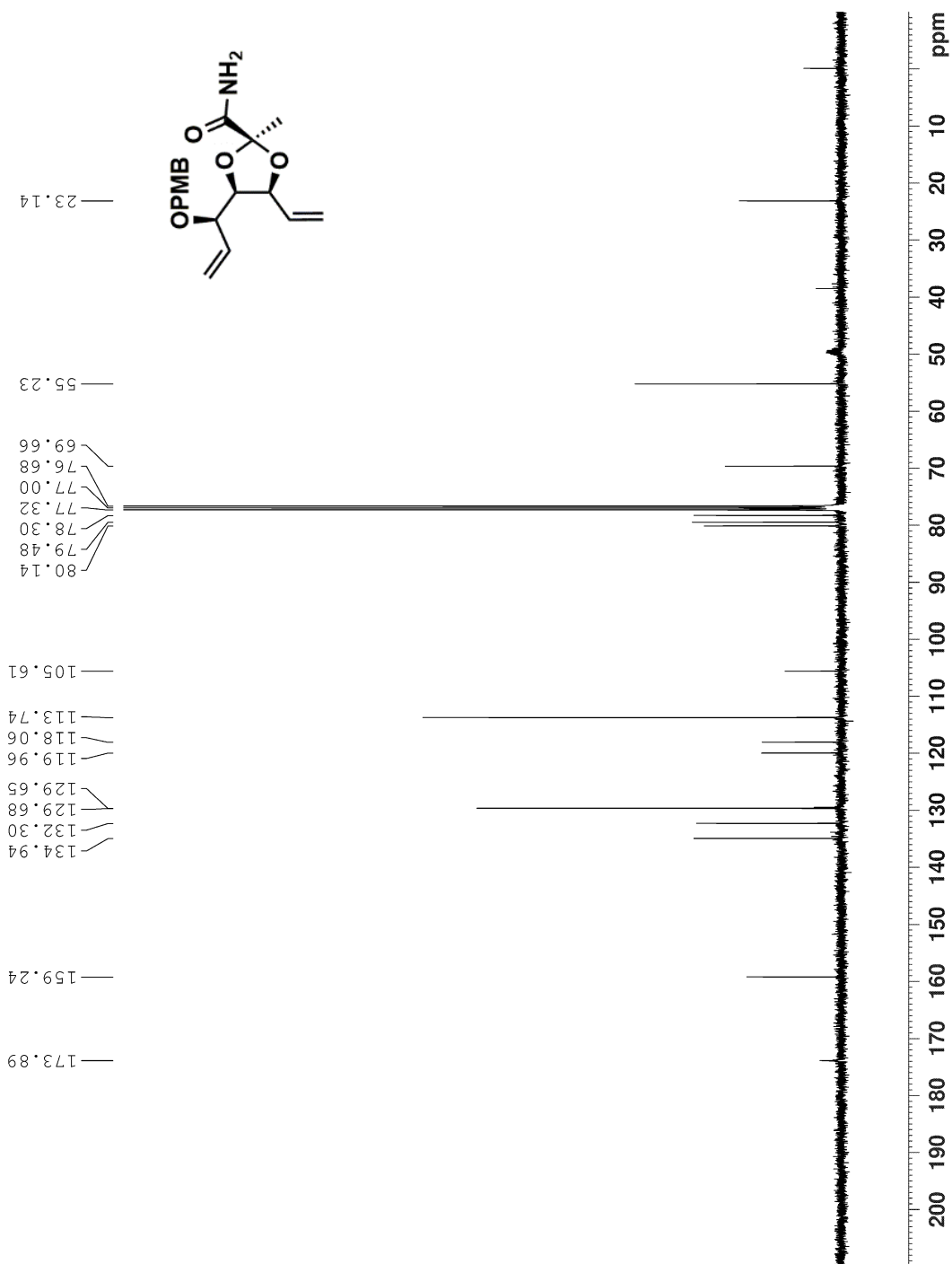
¹³C NMR Spectrum of 1-109 (100 MHz, CDCl₃, 298 K)

18.41 ——

76.69
77.00
77.32
78.49
79.64
83.09

102.95 ——

119.20
119.41

131.20
132.39

164.71 ——
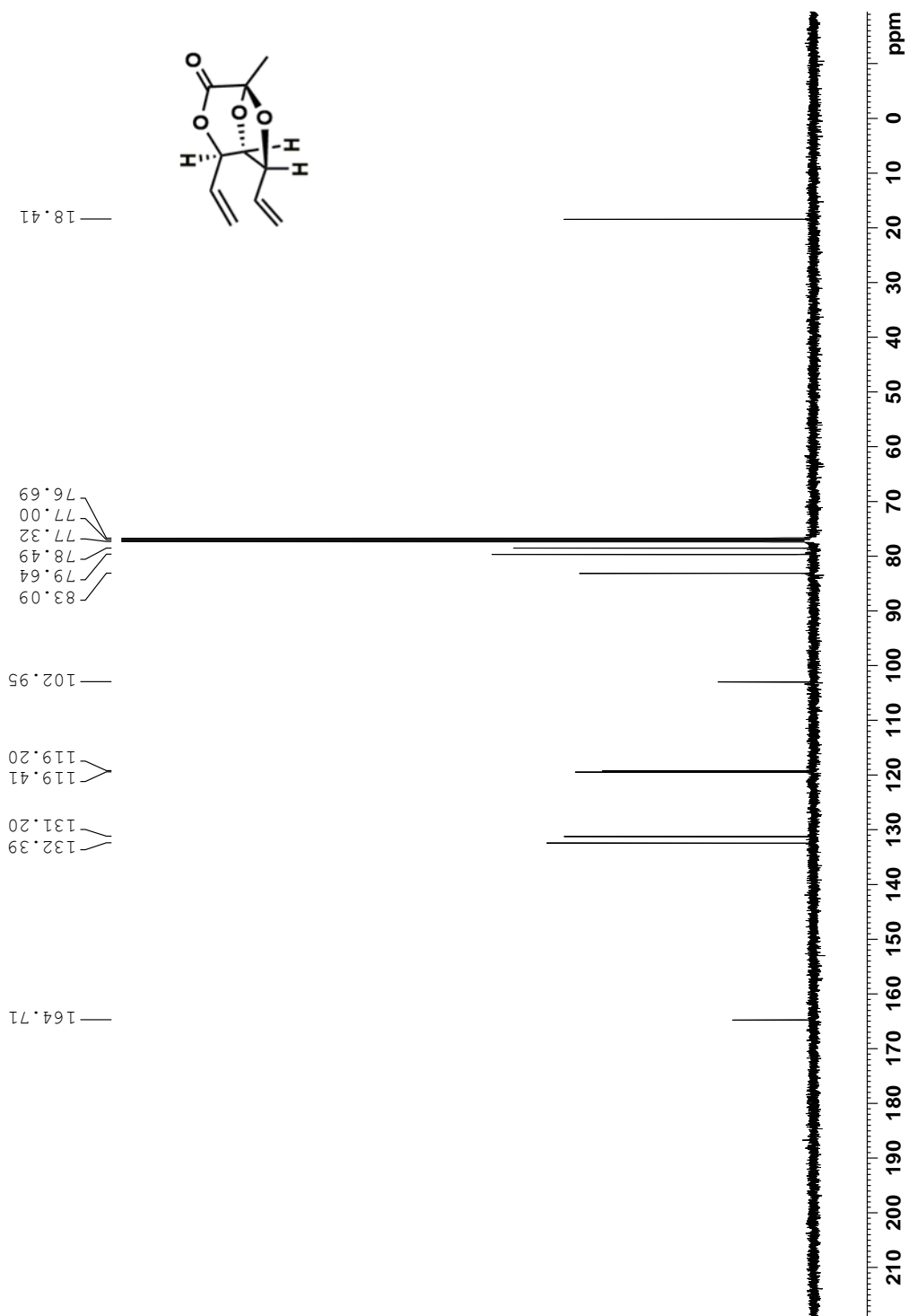
DEPT-135 of 1-109
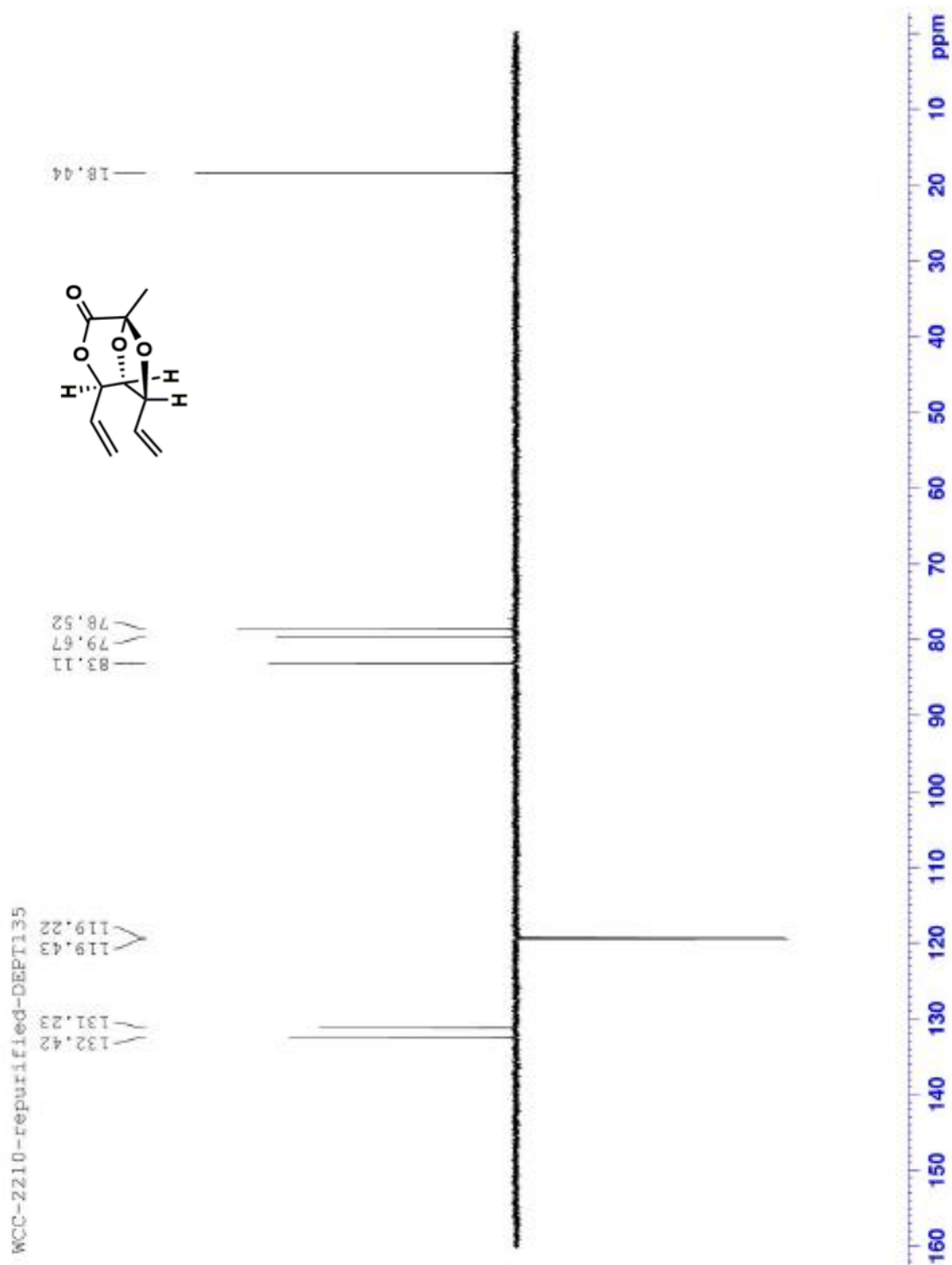
COSY of 1-109
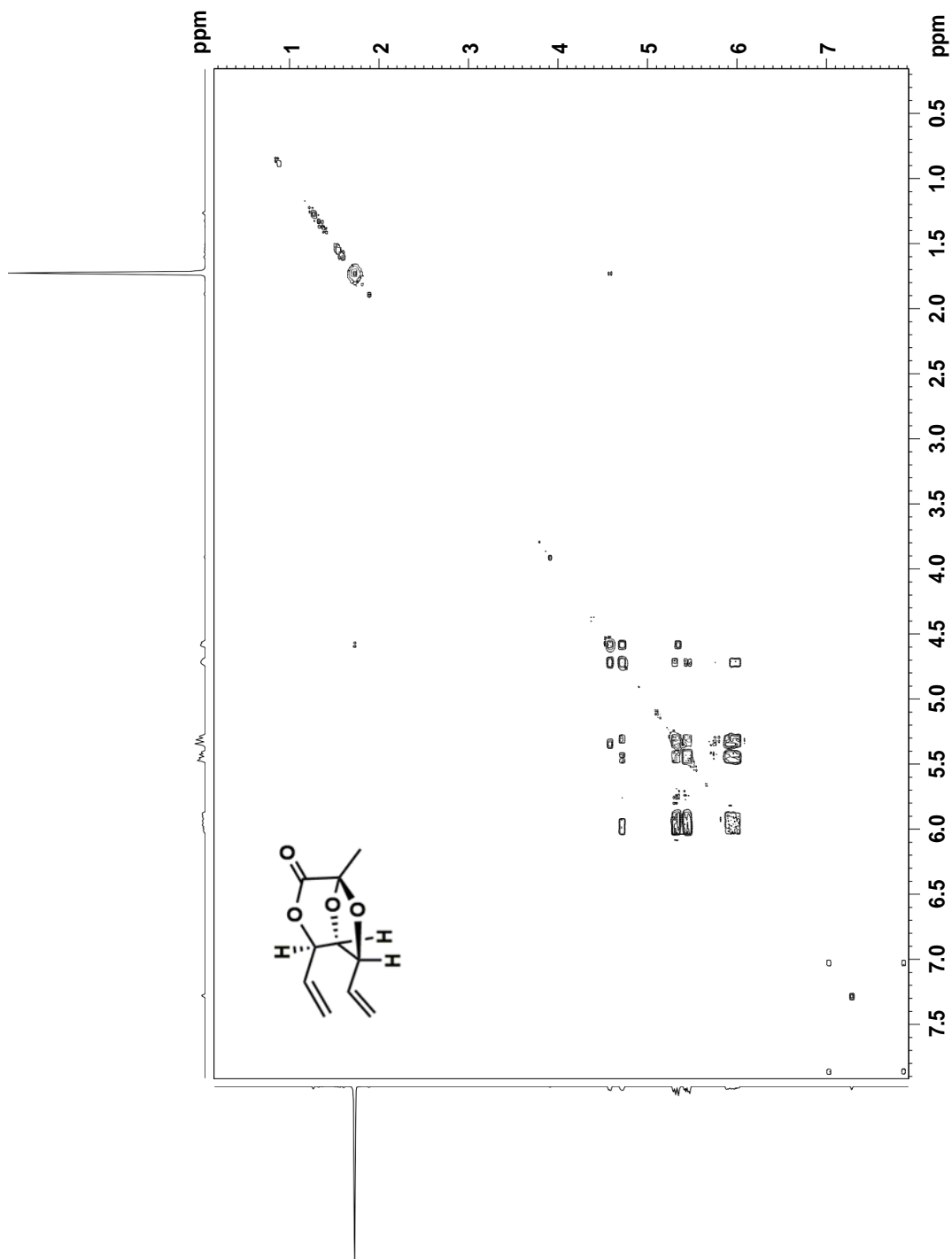
HSQC of 1-109
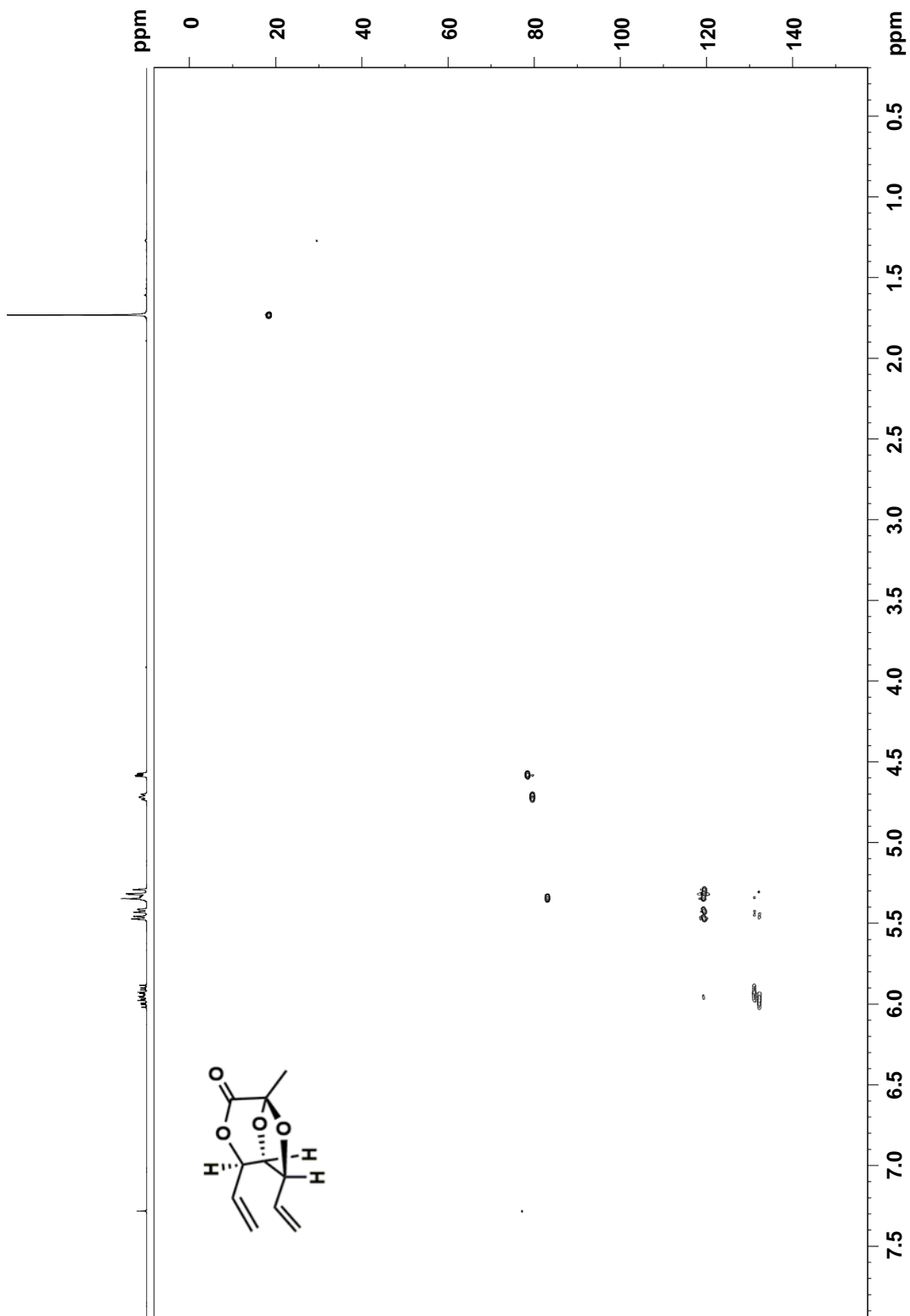
HSQC of 1-109 (Zoomed)
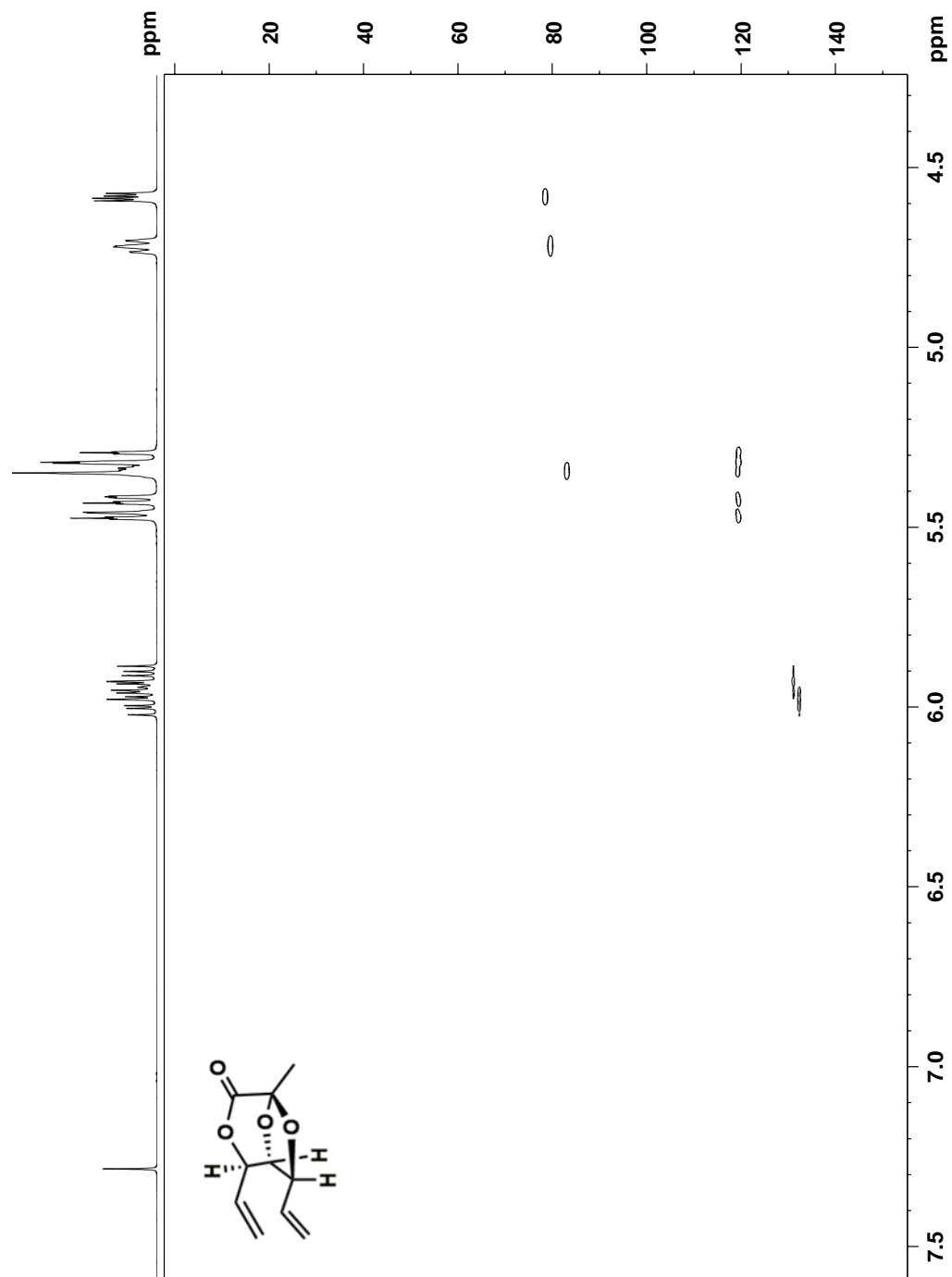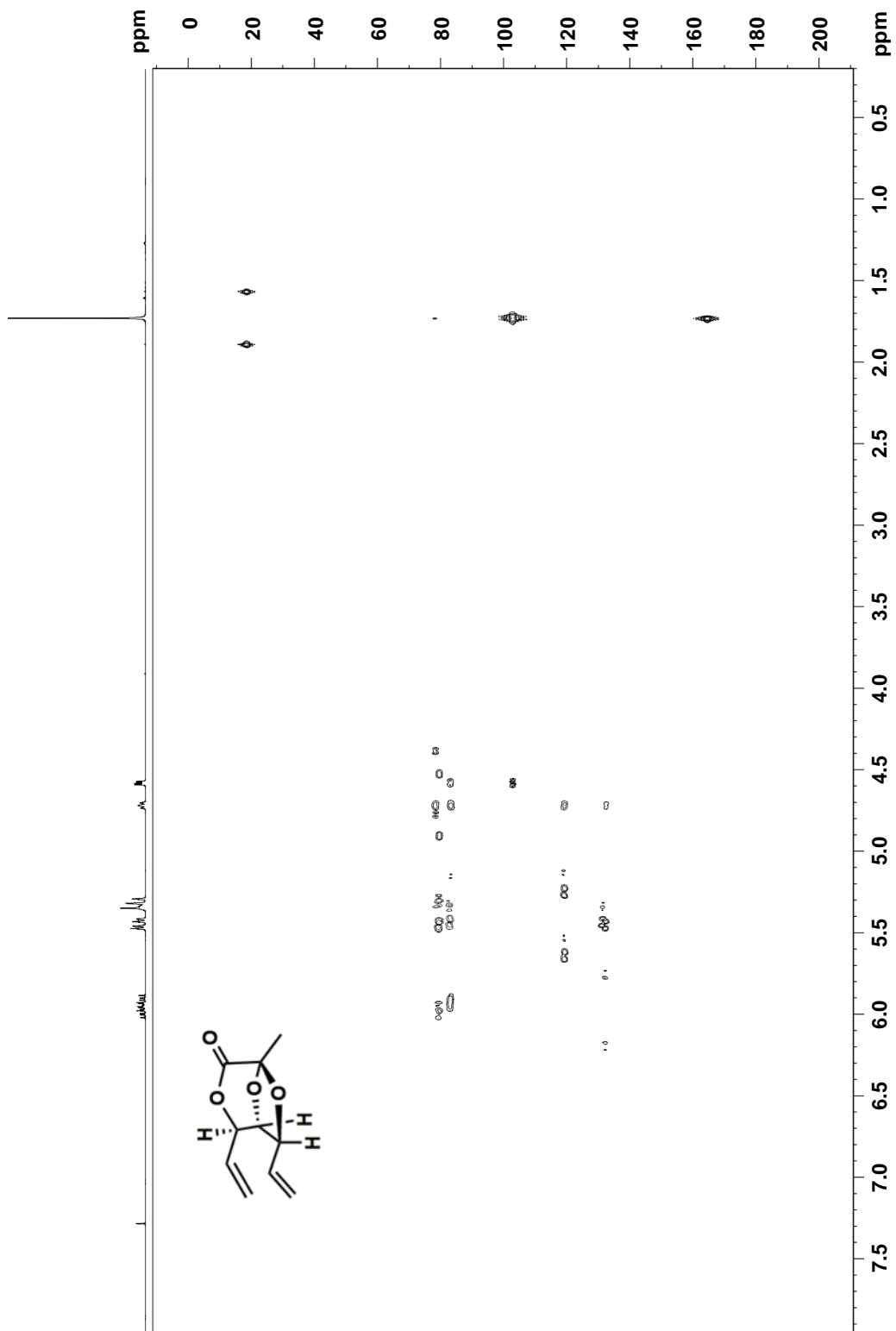
^{13}C NMR Spectrum of 1-112 (100 MHz, CDCl$_3$, 298 K)
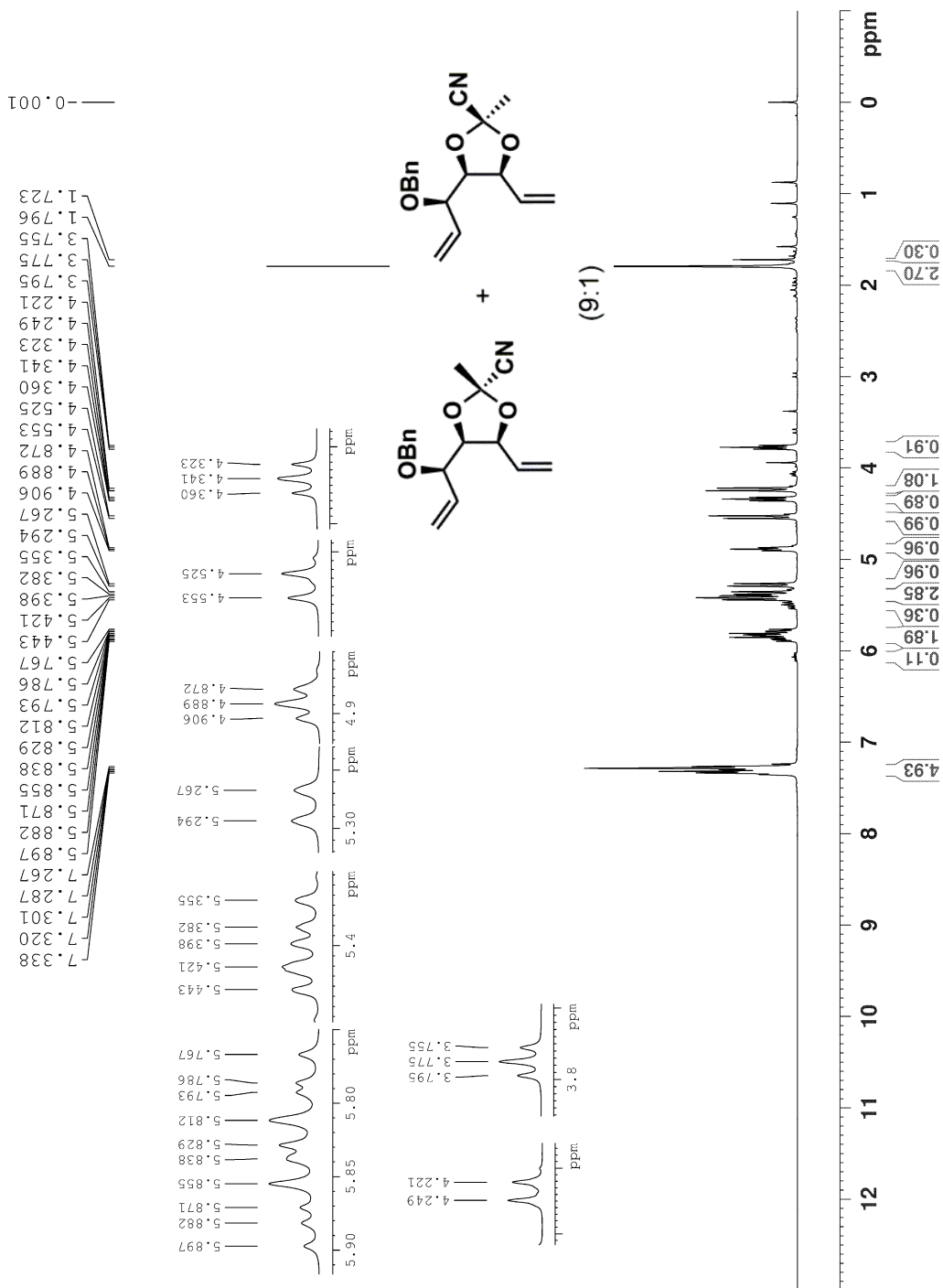
24.91

70.05
76.68
77.00
77.32
78.41
79.90
80.48

99.00

117.32
118.89
120.50
127.79
127.91
128.37
131.45
134.49
137.44

200 190 180 170 160 150 140 130 120 110 100 90 80 70 60 50 40 30 20 10 ppm

¹H NMR Spectrum of 1-113 (400 MHz, CDCl₃, 298 K)
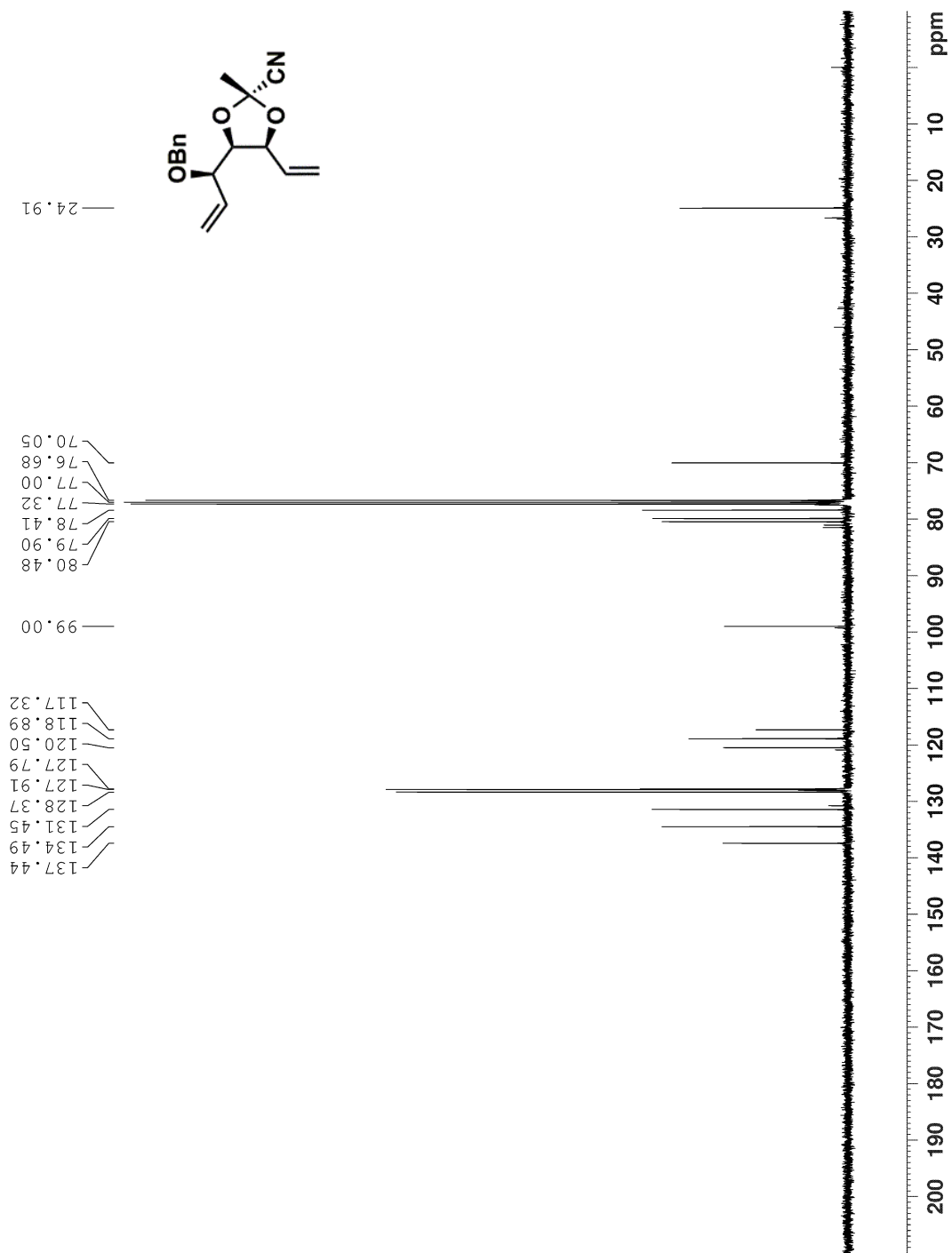
^{13}C NMR Spectrum of 1-113 (100 MHz, CDCl₃, 298 K)

23.20

70.00
76.68
77.00
77.32
78.60
79.48
80.13

105.69

118.04
120.04
127.73
127.95
128.34
132.28
134.88
137.62

173.77
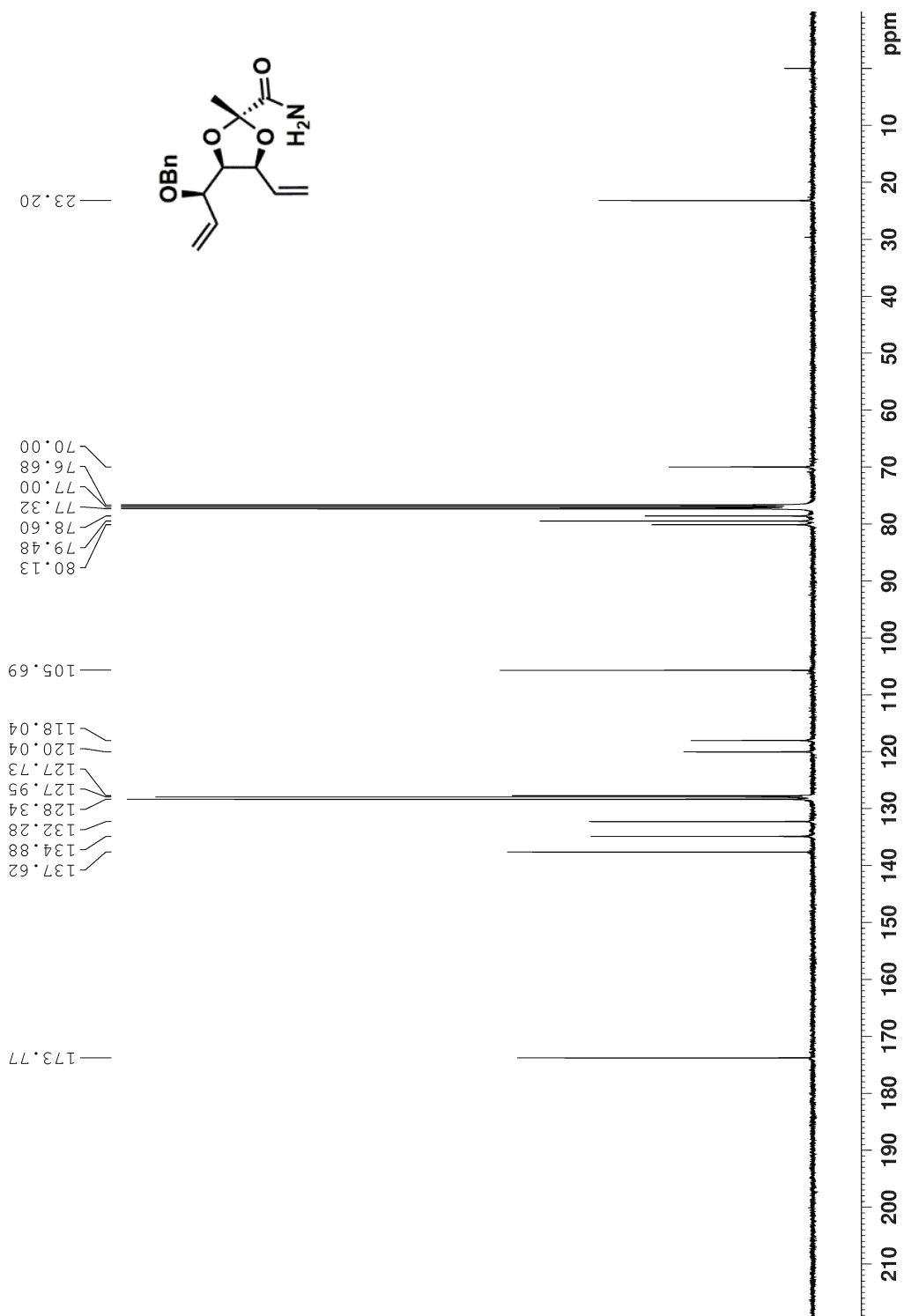
¹H NMR Spectrum of 1-114 (400 MHz, CDCl₃, 298 K)

13C NMR Spectrum of 1-114 (100 MHz, CDCl₃, 298 K)

¹³C NMR Spectrum of 1-114 (100 MHz, CDCl₃, 298 K)

23.15

70.74
76.68
77.00
77.31
79.47
81.22

105.83

117.23
119.30

132.39
136.74

173.91

ppm
200 190 180 170 160 150 140 130 120 110 100 90 80 70 60 50 40 30 20 10
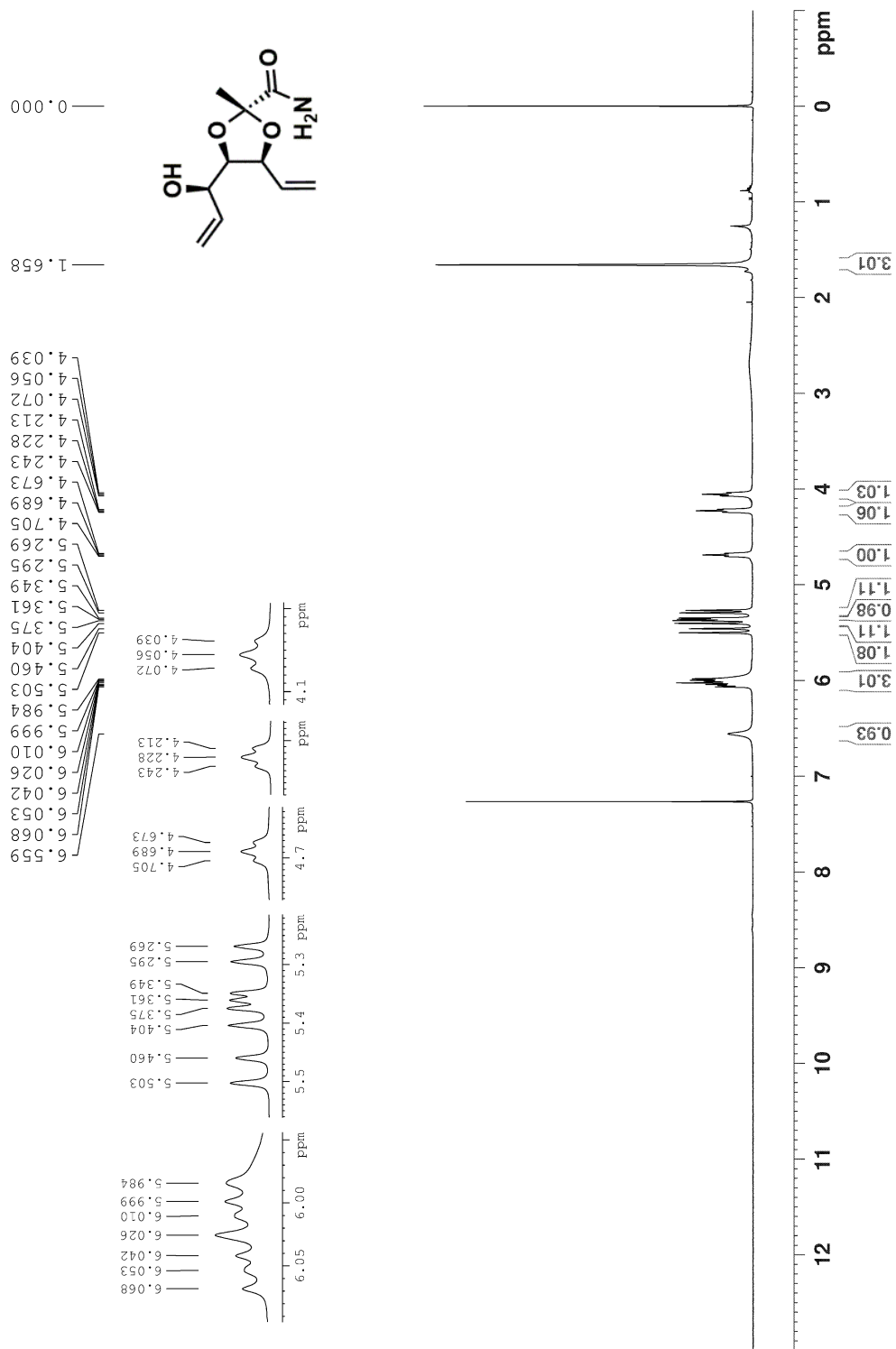
1H NMR Spectrum of 1-89 (400 MHz, Acetone-d₆, 298 K)
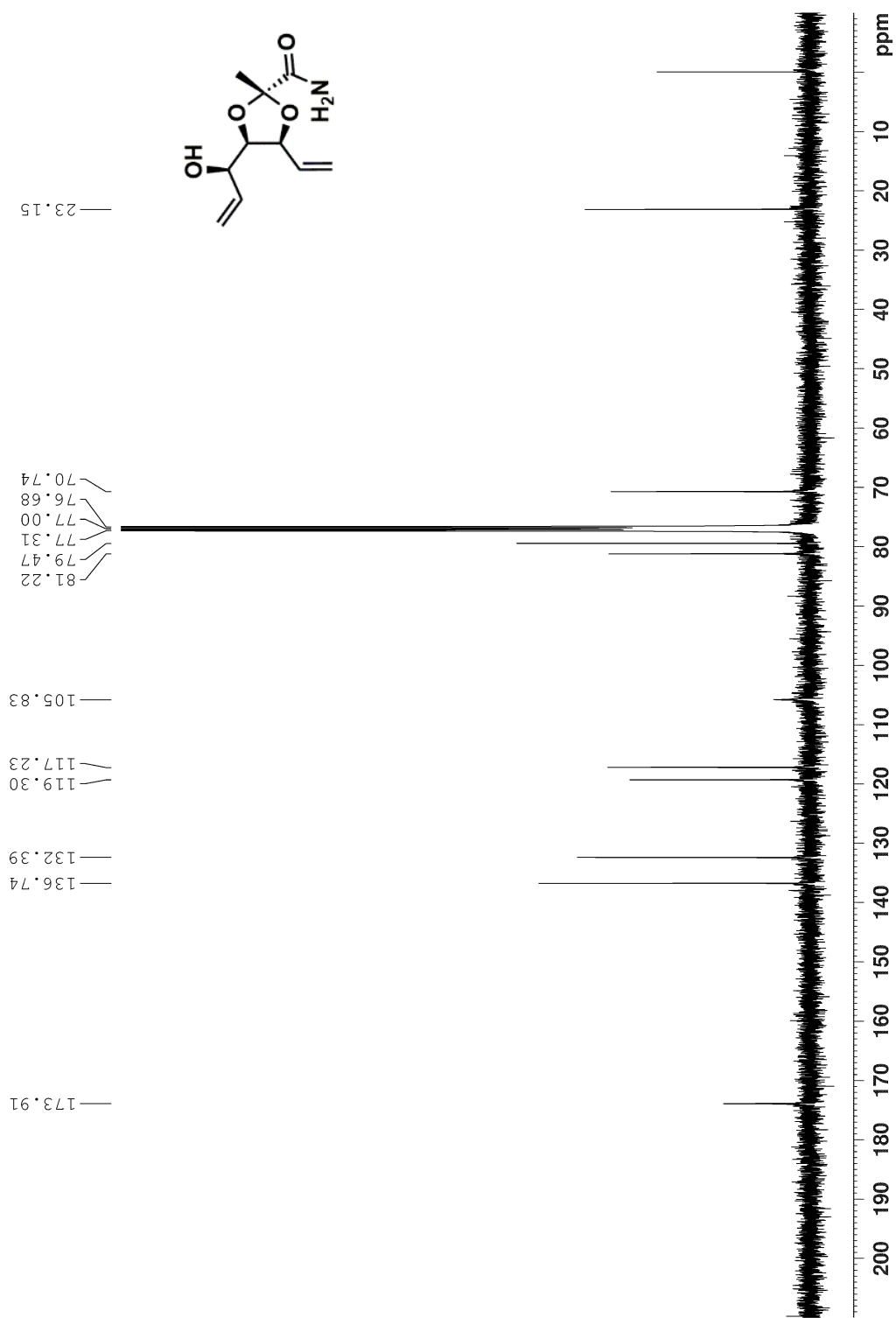
¹H NMR Spectrum of 1-89 (400 MHz, Acetone-d₆, 298 K)
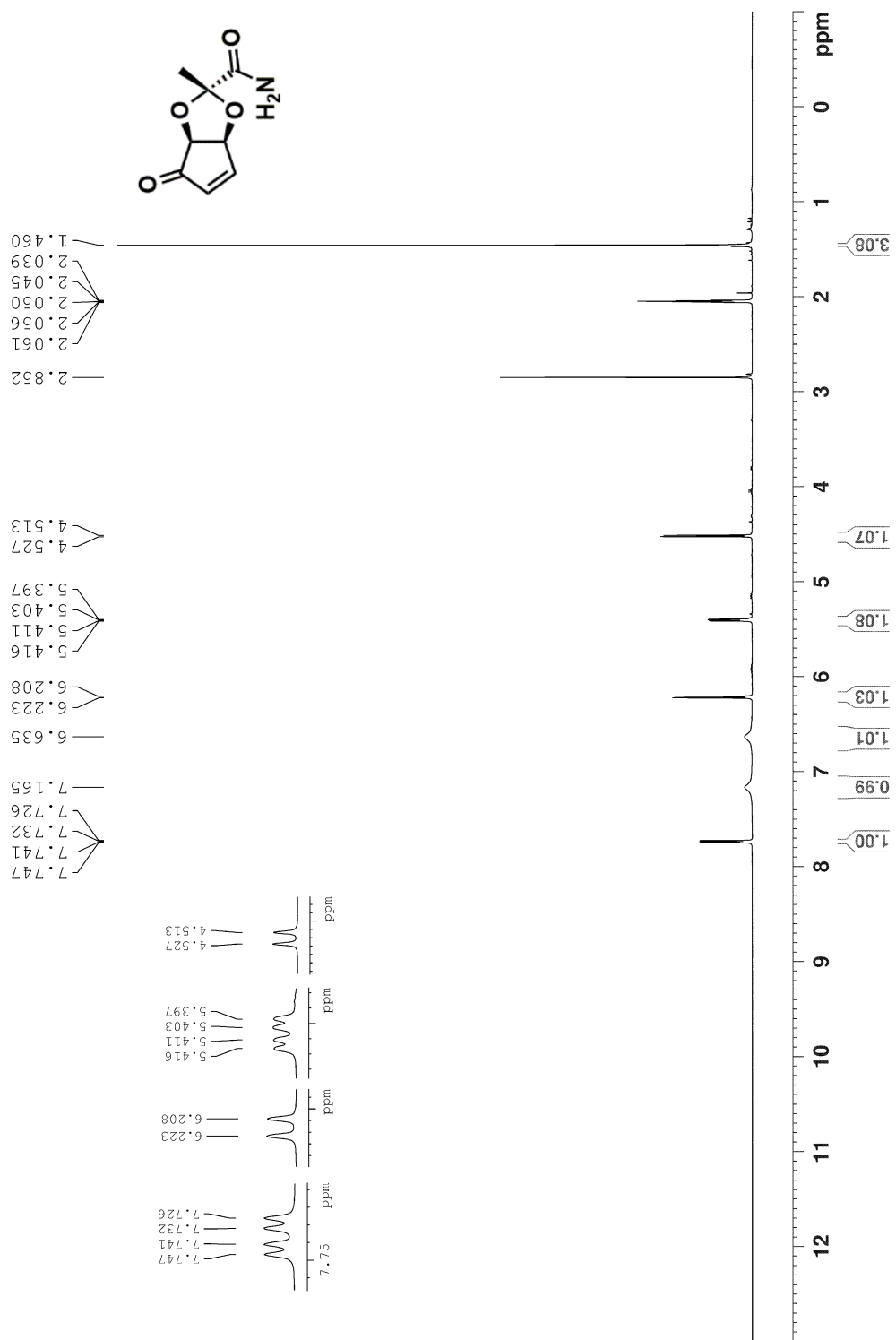
¹³C NMR Spectrum of 1-89 (100 MHz, Acetone-d₆, 298 K)

23.42
29.22
29.41
29.61
29.80
29.99
30.19
30.38

77.63
80.36

112.05

134.63

159.90

171.98

201.90

ppm
10
20
30
40
50
60
70
80
90
100
110
120
130
140
150
160
170
180
190
200
210

284
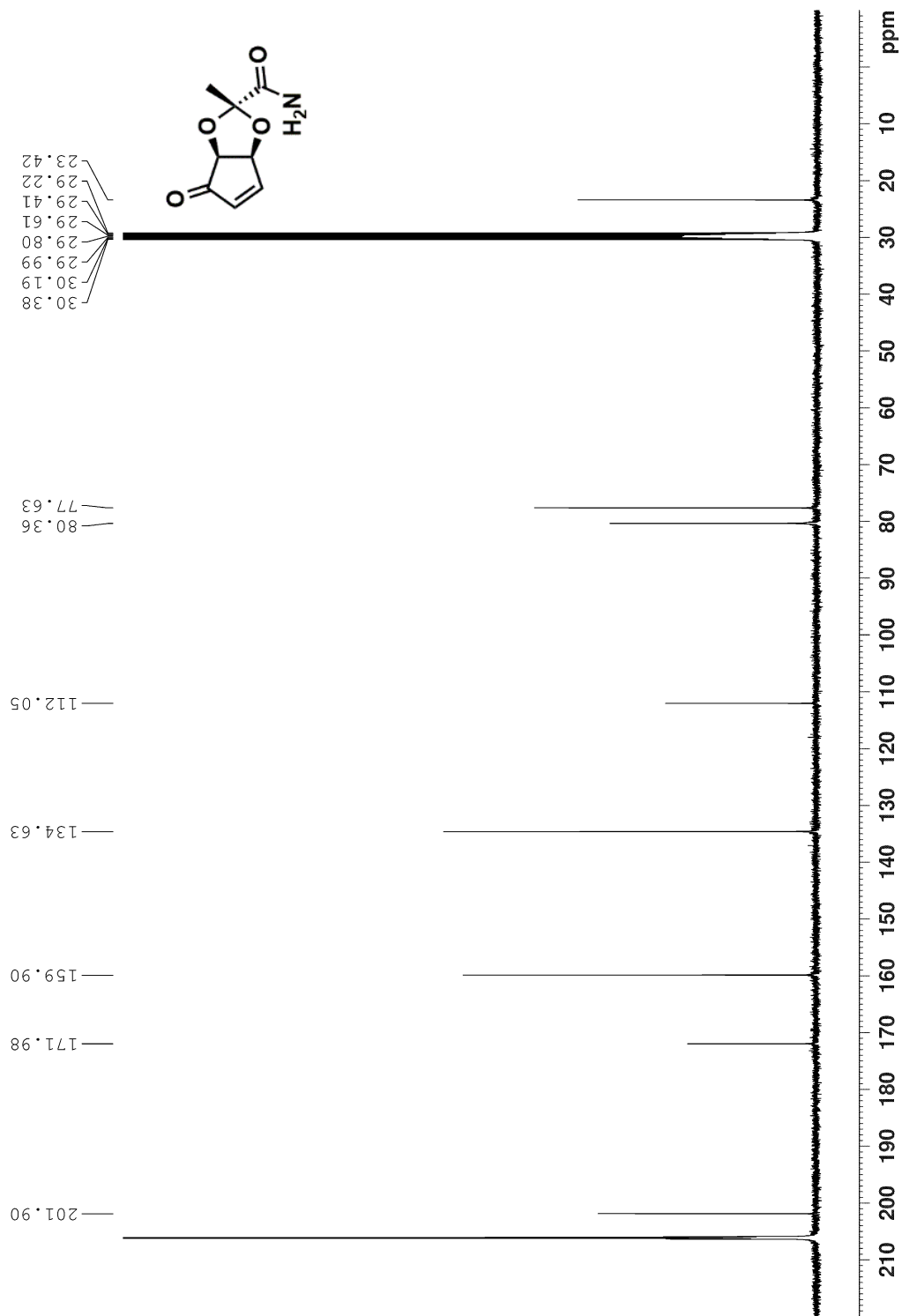
¹H NMR Spectrum of 1-90 (500 MHz, CDCl₃, 298 K)
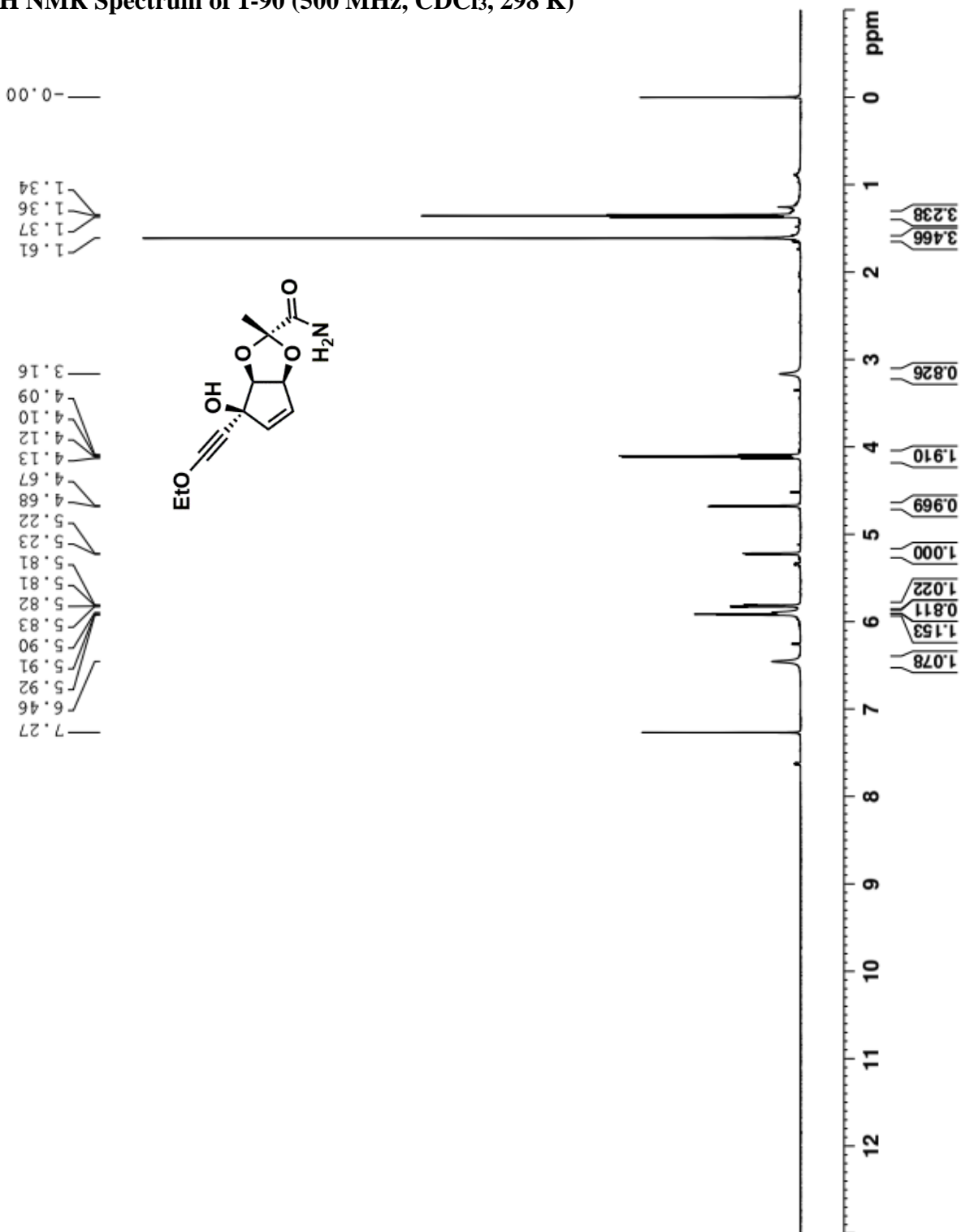
^{13}C NMR Spectrum of 1-90 (125 MHz, CDCl$_3$, 298 K)

14.31
23.63
38.49
75.00
75.15
76.74
77.00
77.25
84.56
84.79
94.72
109.18
129.08
139.24
172.66
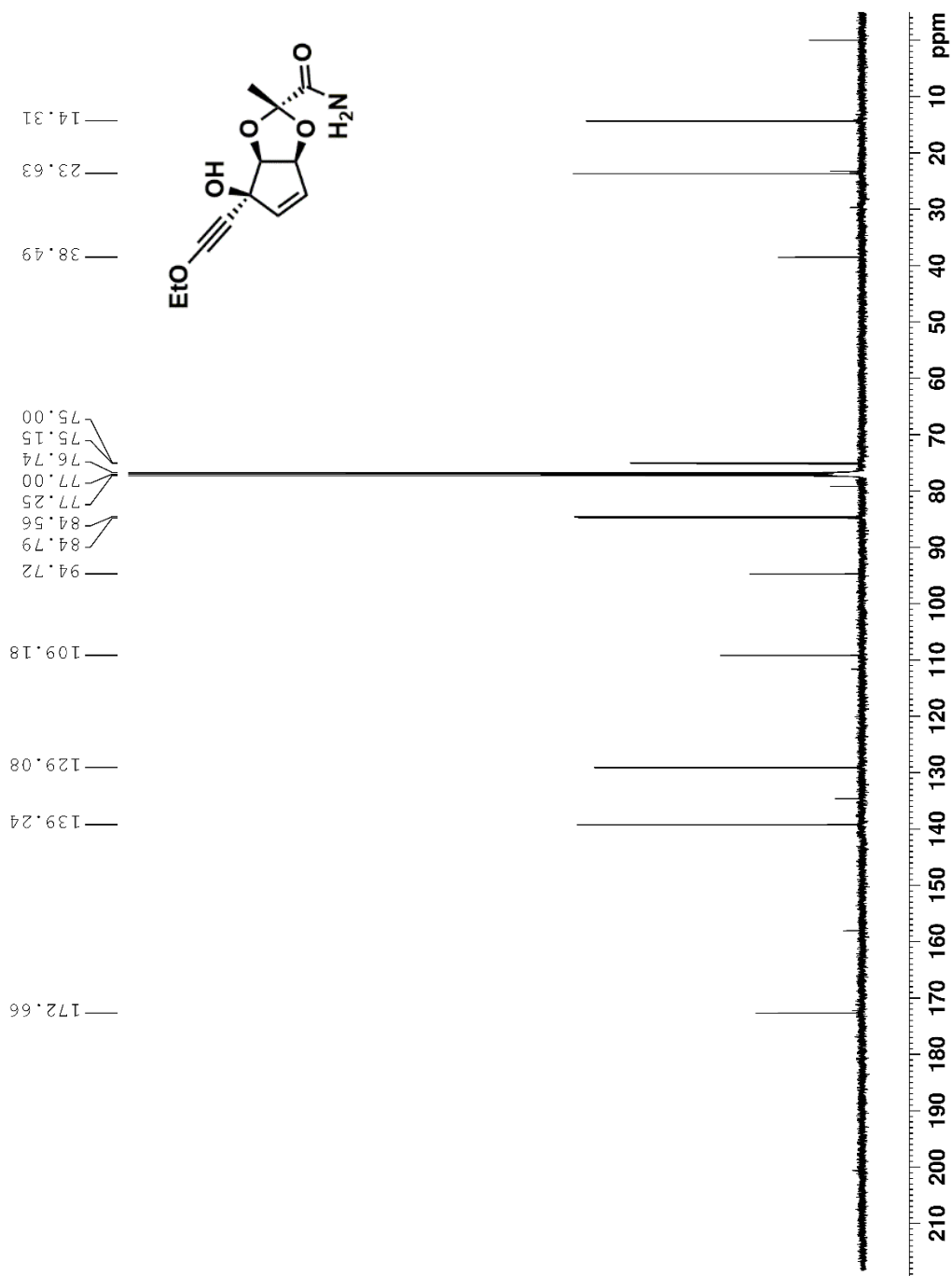
¹H NMR Spectrum of 1-81a (500 MHz, CDCl₃, 298 K)

-0.00

1.57

3.76

5.01
5.02
5.19
5.20
5.20
5.21
5.86
6.01
6.45
6.48
6.49
7.27
7.39
7.40

3.381

3.189

1.021
1.066

1.025
0.936
1.157

1.000
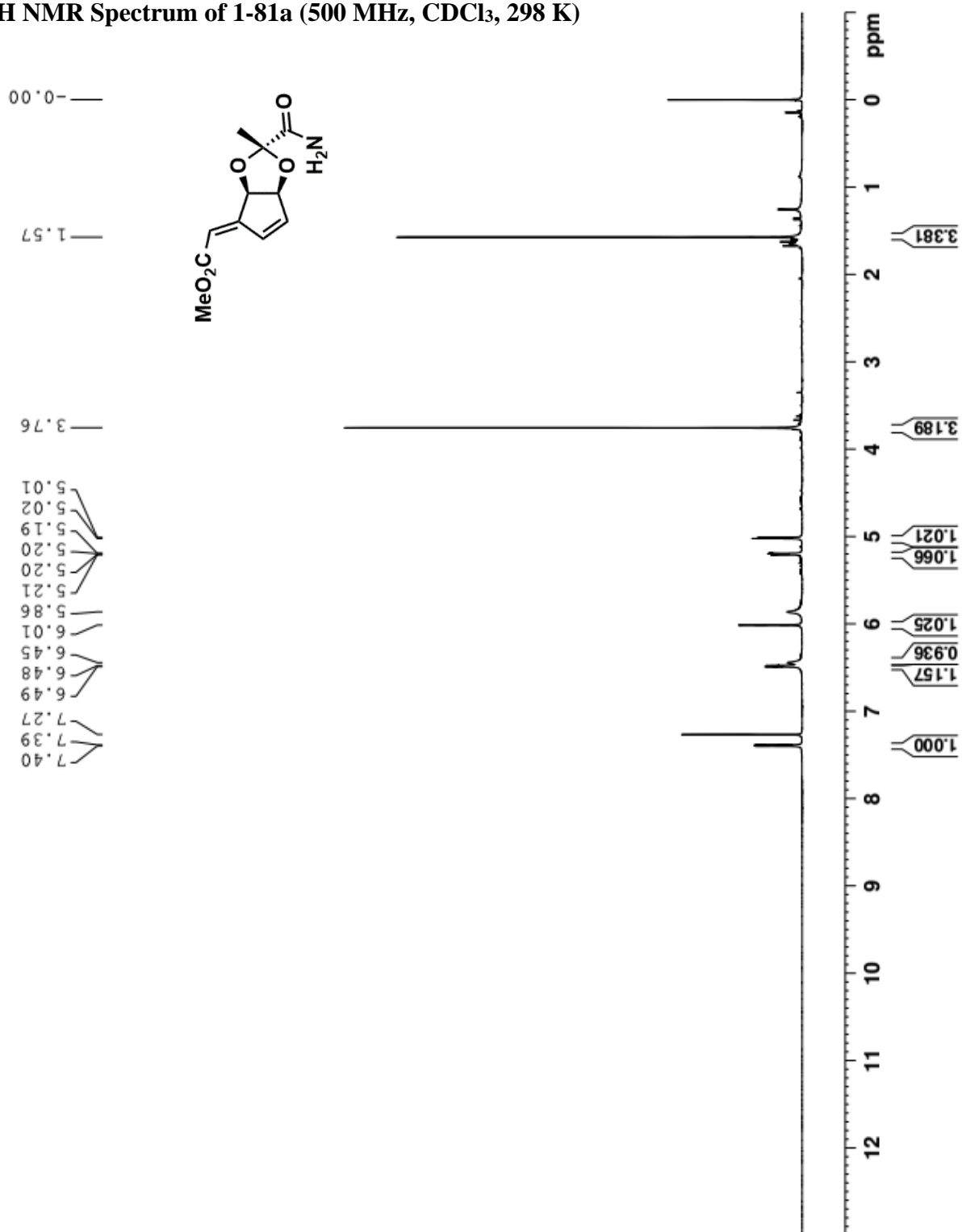
^{13}C NMR Spectrum of 1-81a (125 MHz, CDCl$_3$, 298 K)

23.36

51.50

76.74
77.00
77.25
80.31
82.52

109.00

115.19

133.57

141.51

156.01

166.36

173.05

ppm
10
20
30
40
50
60
70
80
90
100
110
120
130
140
150
160
170
180
190
200
210
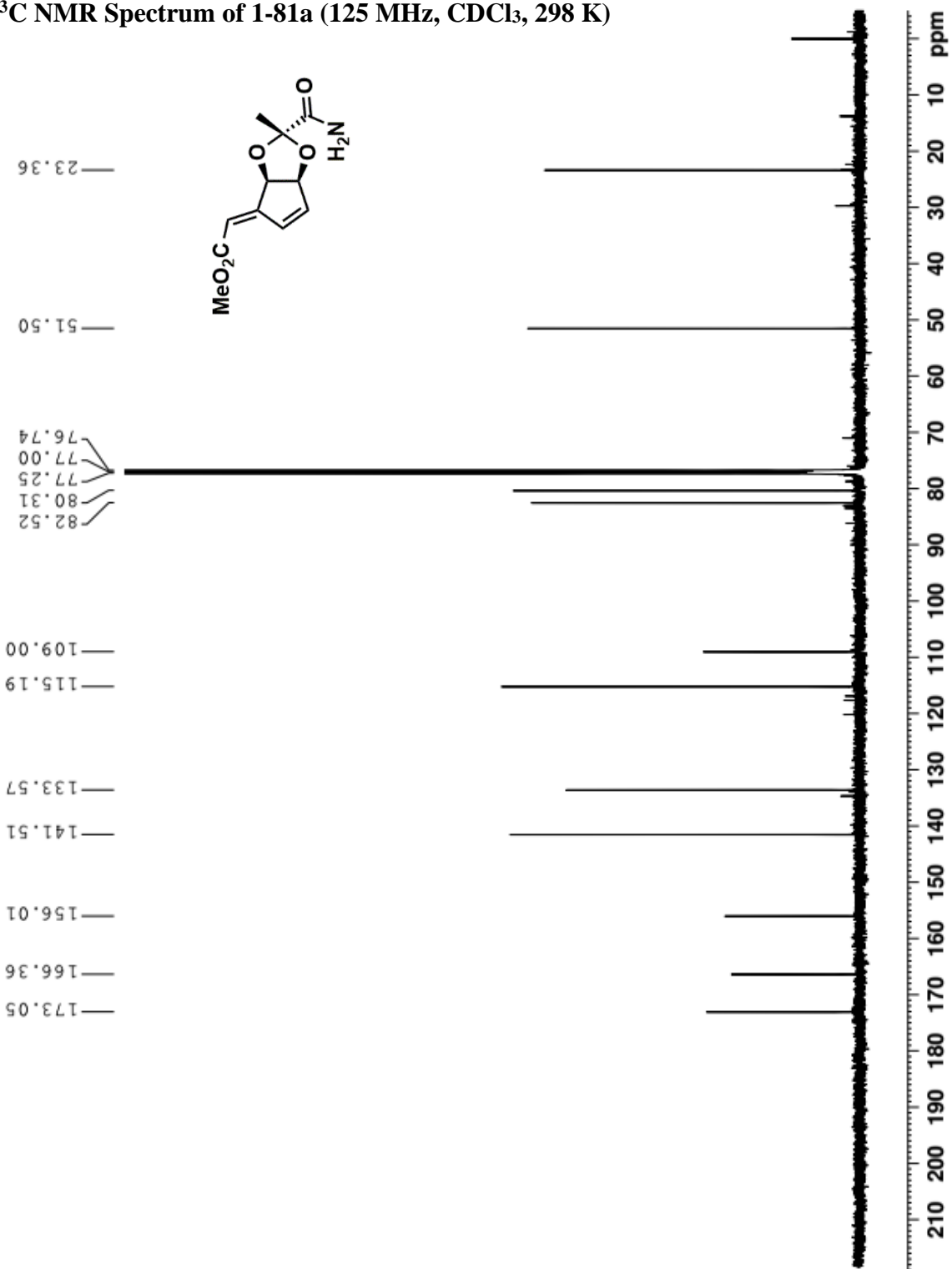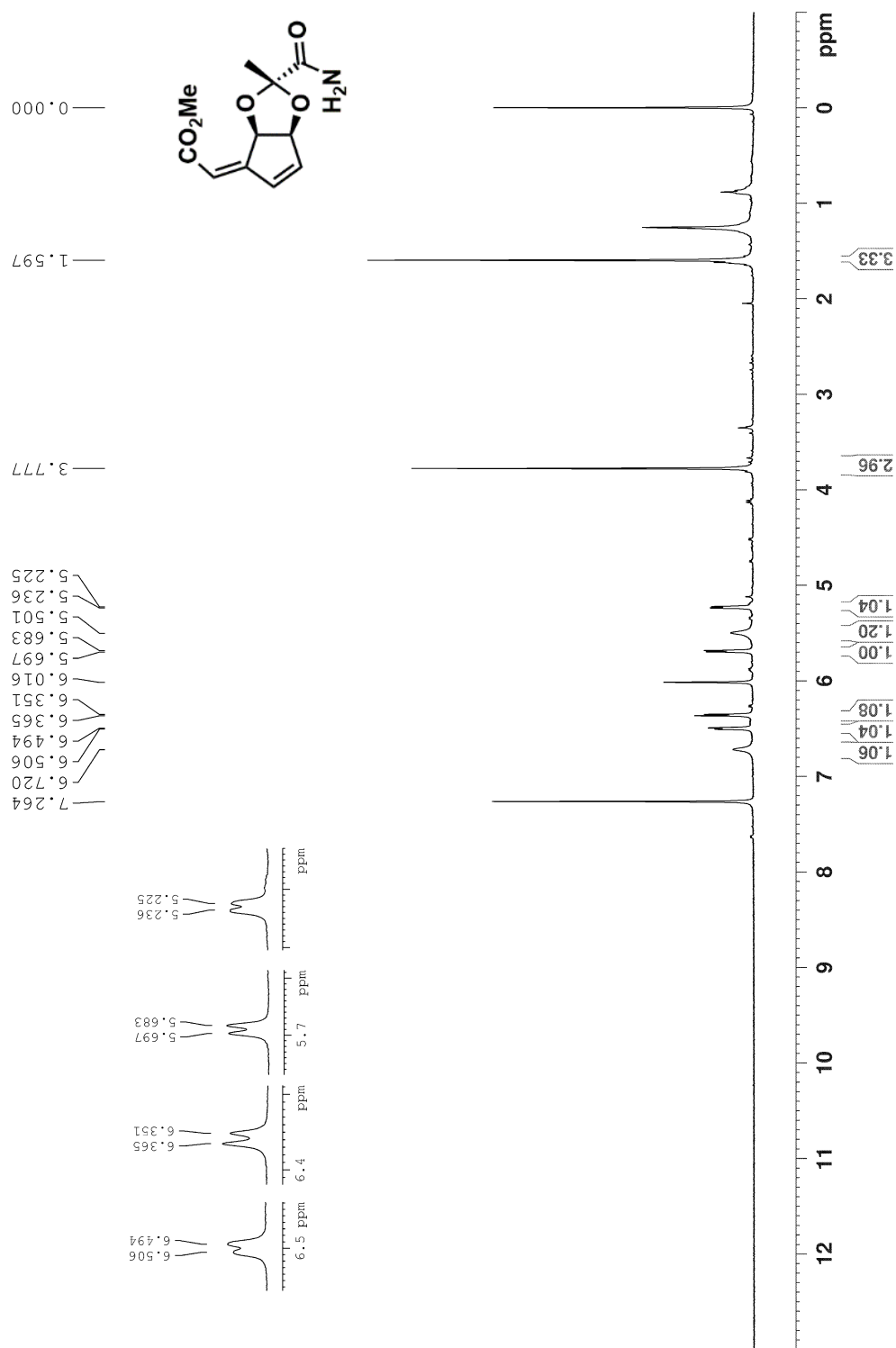
^{13}C NMR Spectrum of 1-81b (100 MHz, CDCl$_3$, 298 K)

23.11

51.64

76.68
77.00
77.20
77.31
83.61

108.60

115.56

134.89

142.32

156.62

166.28

173.05

ppm
200 190 180 170 160 150 140 130 120 110 100 90 80 70 60 50 40 30 20 10

¹H NMR Spectrum of 2-147 (500 MHz, CDCl₃, 298 K)
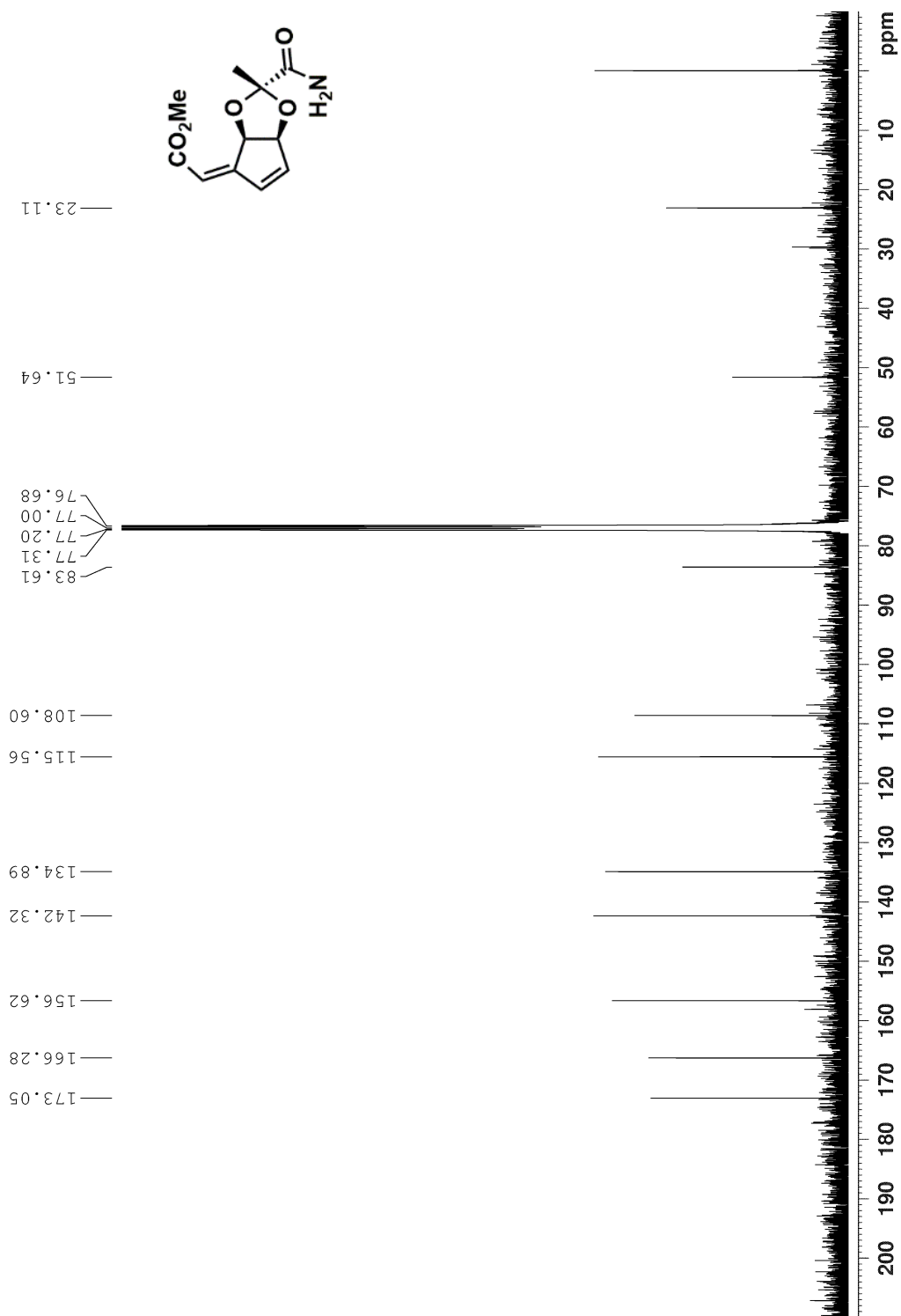
^{13}C NMR Spectrum of 2-147 (125 MHz, CDCl3, 298 K)

41.90

52.17
52.38
52.65

65.04
65.10

76.74
77.00
77.25

103.89
115.29
115.47
123.83
123.86
123.89
124.00
128.93
129.00
130.01
130.04

160.02
161.98
167.65
168.27

ppm
210 200 190 180 170 160 150 140 130 120 110 100 90 80 70 60 50 40 30 20 10

¹H NMR Spectrum of 2-148 (500 MHz, CDCl₃, 298 K)

^{13}C NMR Spectrum of 2-148 (125 MHz, CDCl$_3$, 298 K)

48.62
52.46
52.63
52.72

65.15
65.24

76.75
77.00
77.25

104.21

127.59
127.67
129.39
129.48
133.98
138.69

167.68
168.24

ppm
210 200 190 180 170 160 150 140 130 120 110 100 90 80 70 60 50 40 30 20 10

¹H NMR Spectrum of 2-149 (500 MHz, CDCl₃, 298 K)

48.41
52.48
52.62
52.73

65.15
65.22

76.74
77.00
77.25

104.19

121.57

131.07
131.33
135.63

167.72
168.26

ppm
10 20 30 40 50 60 70 80 90 100 110 120 130 140 150 160 170 180 190 200 210

296

¹H NMR Spectrum of 2-150 (500 MHz, CDCl₃, 298 K)
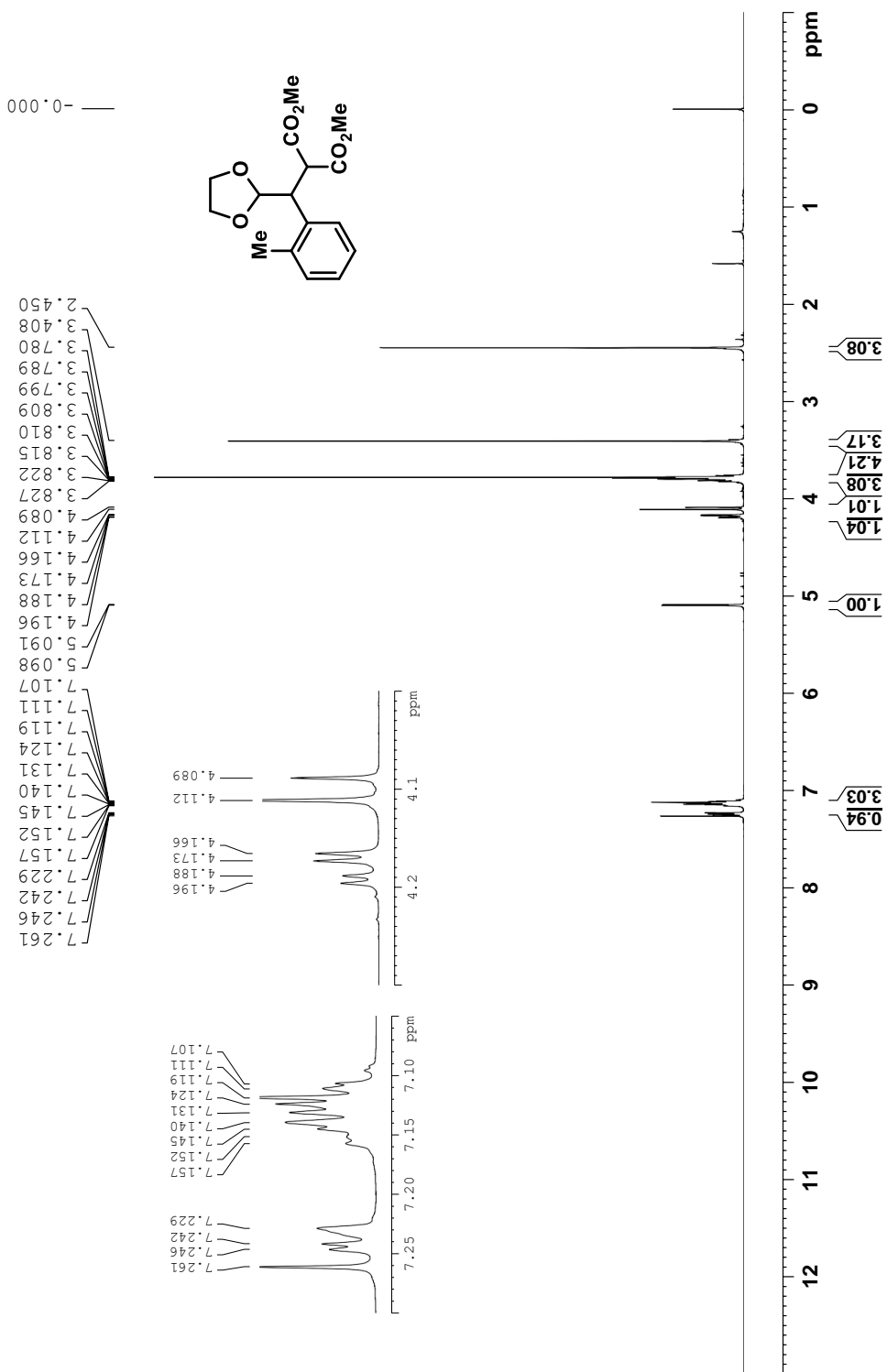
¹³C NMR Spectrum of 2-150 (125 MHz, CDCl₃, 298 K)

20.13

43.59
52.31
52.95
53.03
65.09
65.20
76.74
77.00
77.25
104.80
125.74
127.09
127.43
130.34
135.25
137.65
167.94
168.71
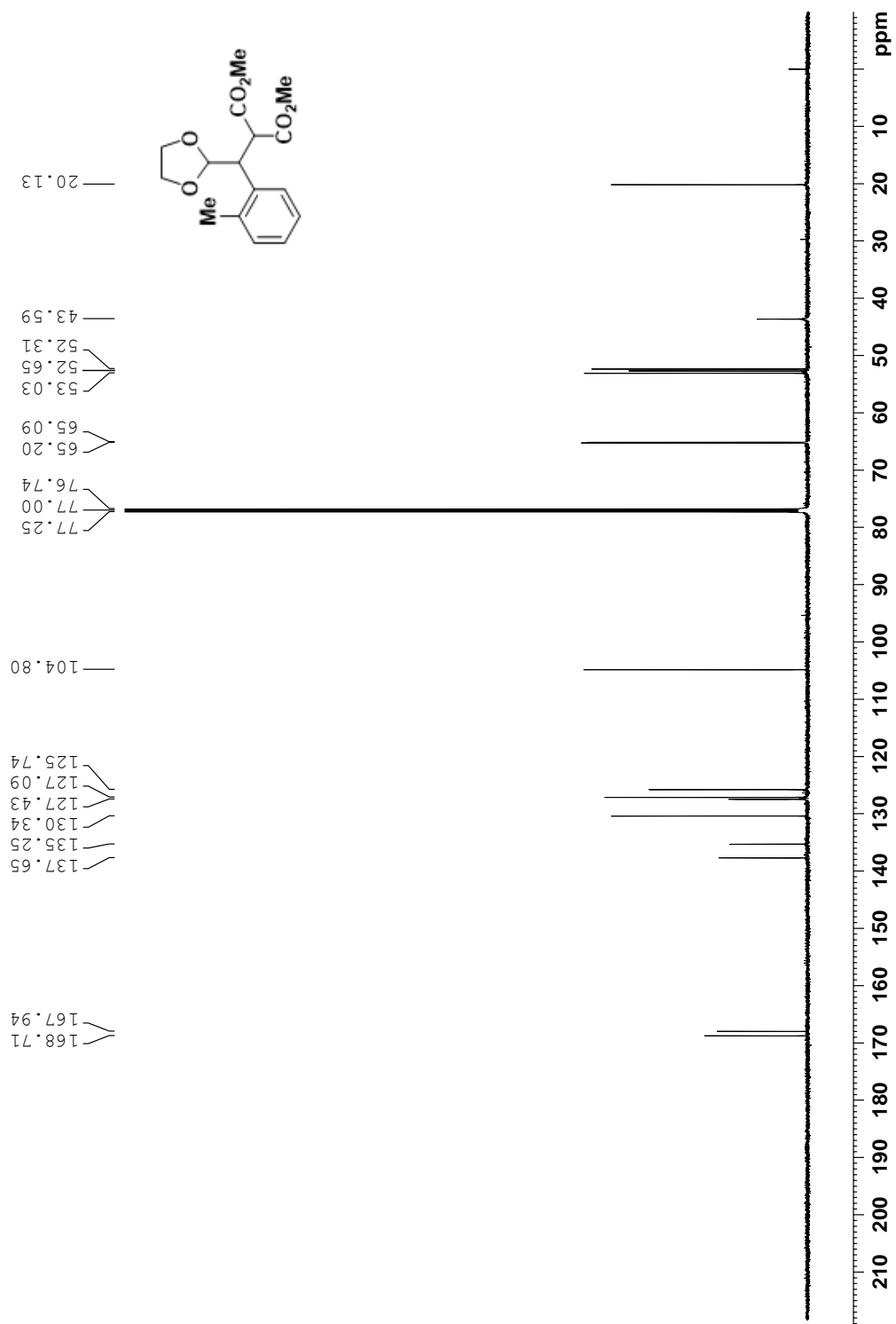
¹H NMR Spectrum of 2-121 (CDCl₃, 300 MHz, 298 K)
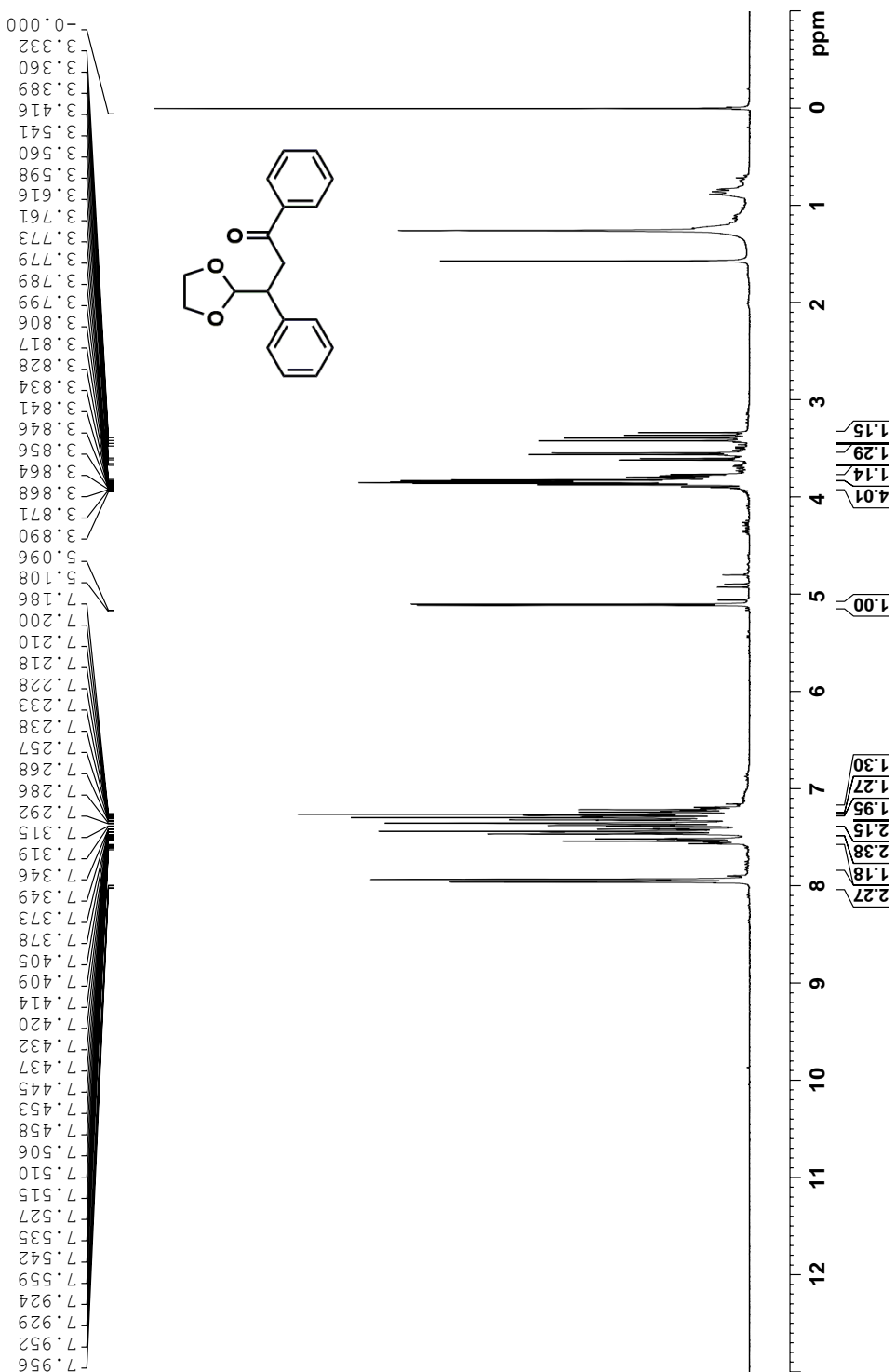
^{1}H NMR Spectrum of 2-121 (300 MHz, CDCl$_3$, 298 K)
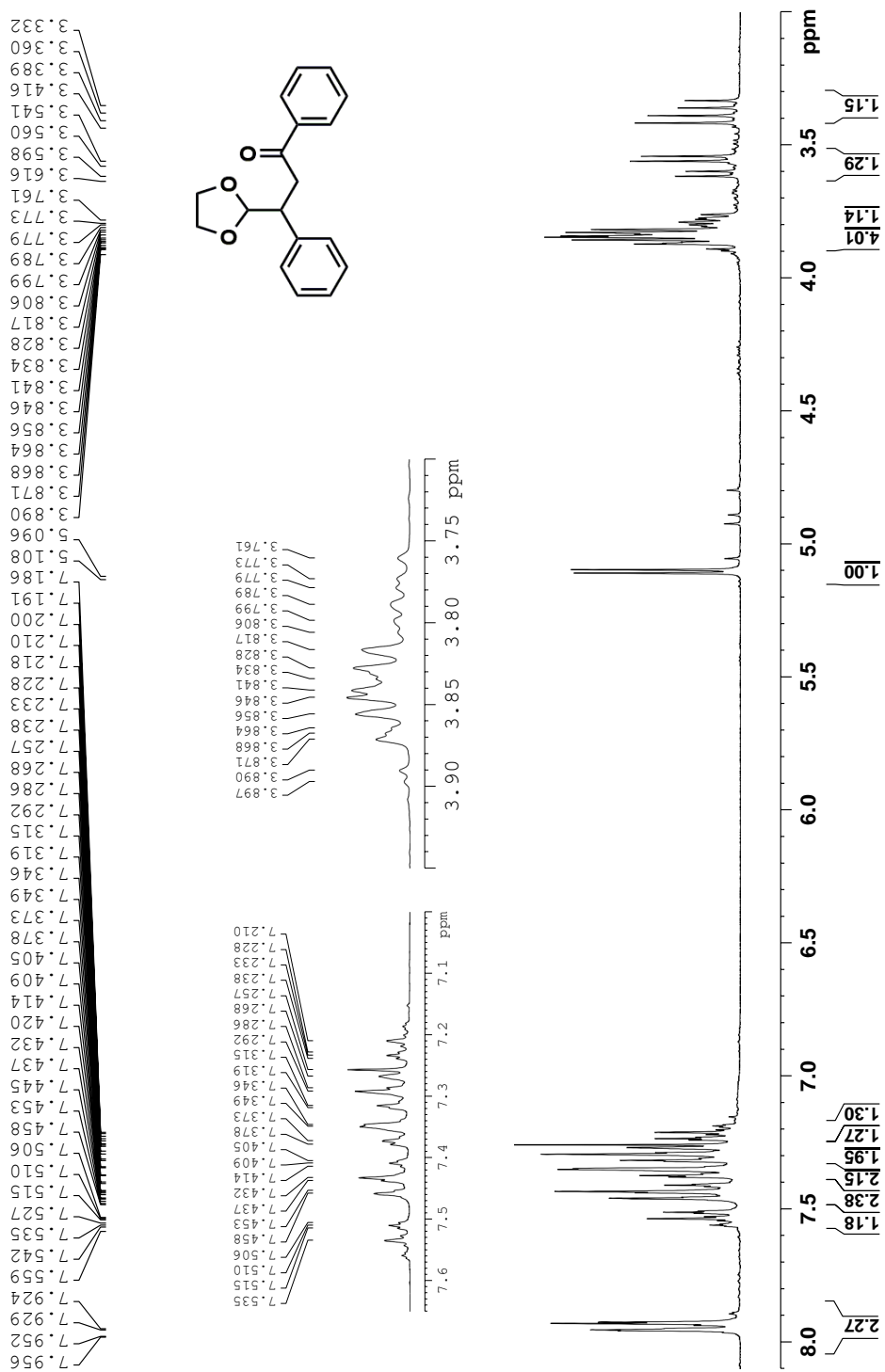
¹³C NMR Spectrum of 2-121 (75 MHz, CDCl₃, 298 K)

29.68

38.80

44.69

65.00
65.24

76.57
77.00
77.42

106.04

126.93
128.06
128.32
128.48
128.77
132.86
137.19
139.82

198.30

WCC-7231-13C-CDCl3-300MHz

ppm
10
20
30
40
50
60
70
80
90
100
110
120
130
140
150
160
170
180
190
200
210
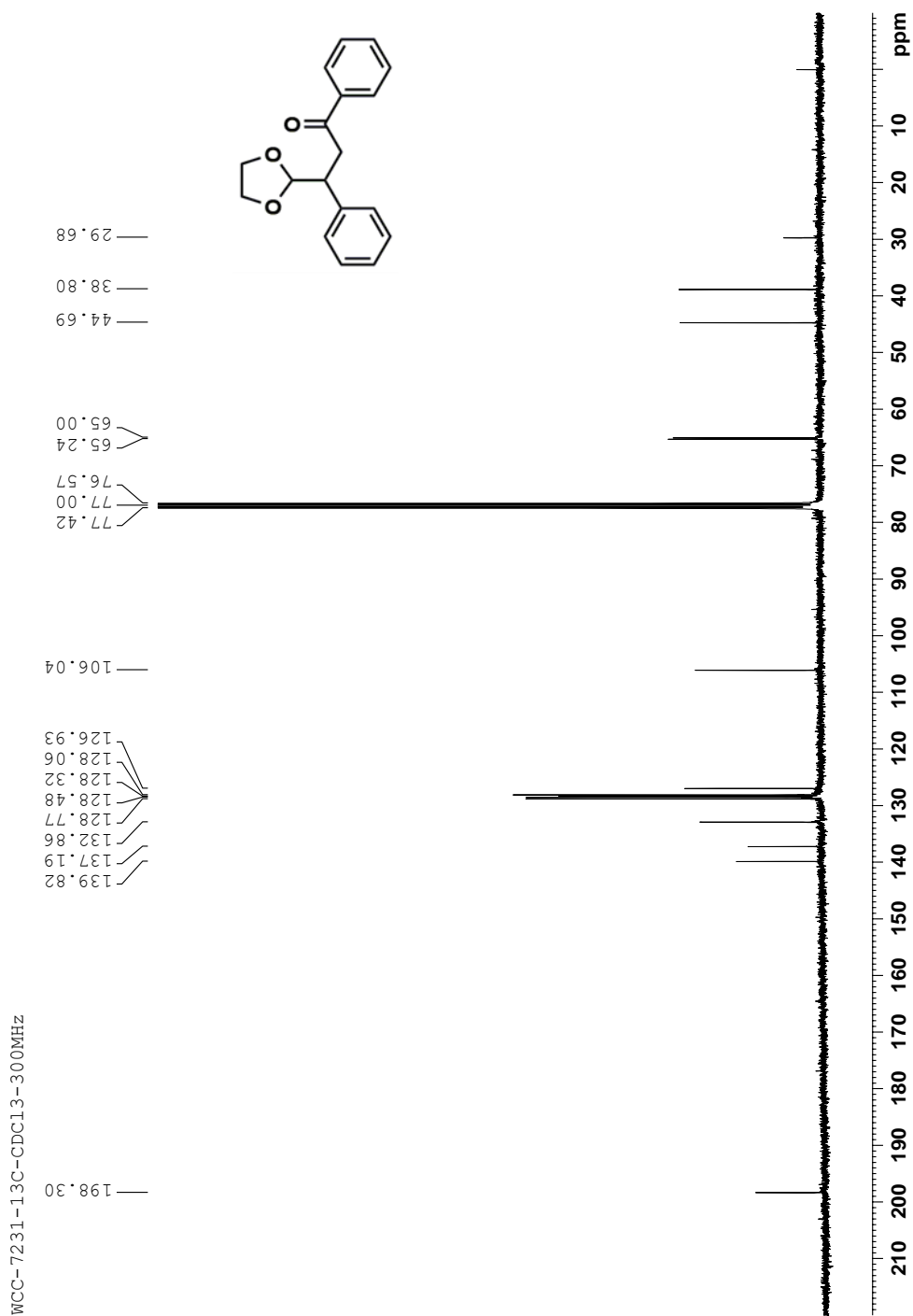
¹H NMR Spectrum of 2-151 (500 MHz, CDCl₃, 298 K)
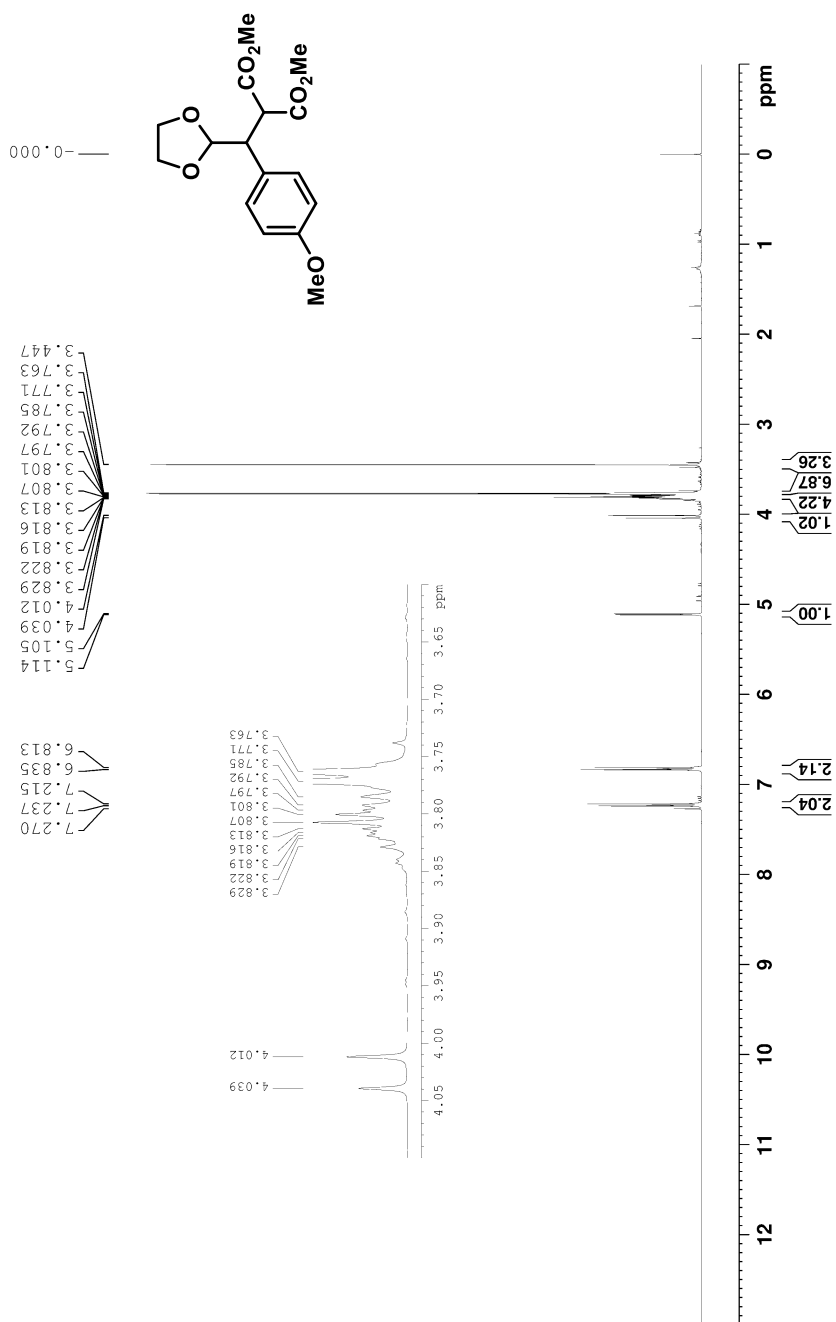
^{13}C NMR Spectrum of 2-151 (125 MHz, CDCl$_3$, 298 K)

48.22
52.32
52.58
52.90
55.05
65.05
65.13

76.68
76.99
77.31

104.74

113.59

128.49
130.23

158.76

167.94
168.55

ppm
10
20
30
40
50
60
70
80
90
100
110
120
130
140
150
160
170
180
190
200
210
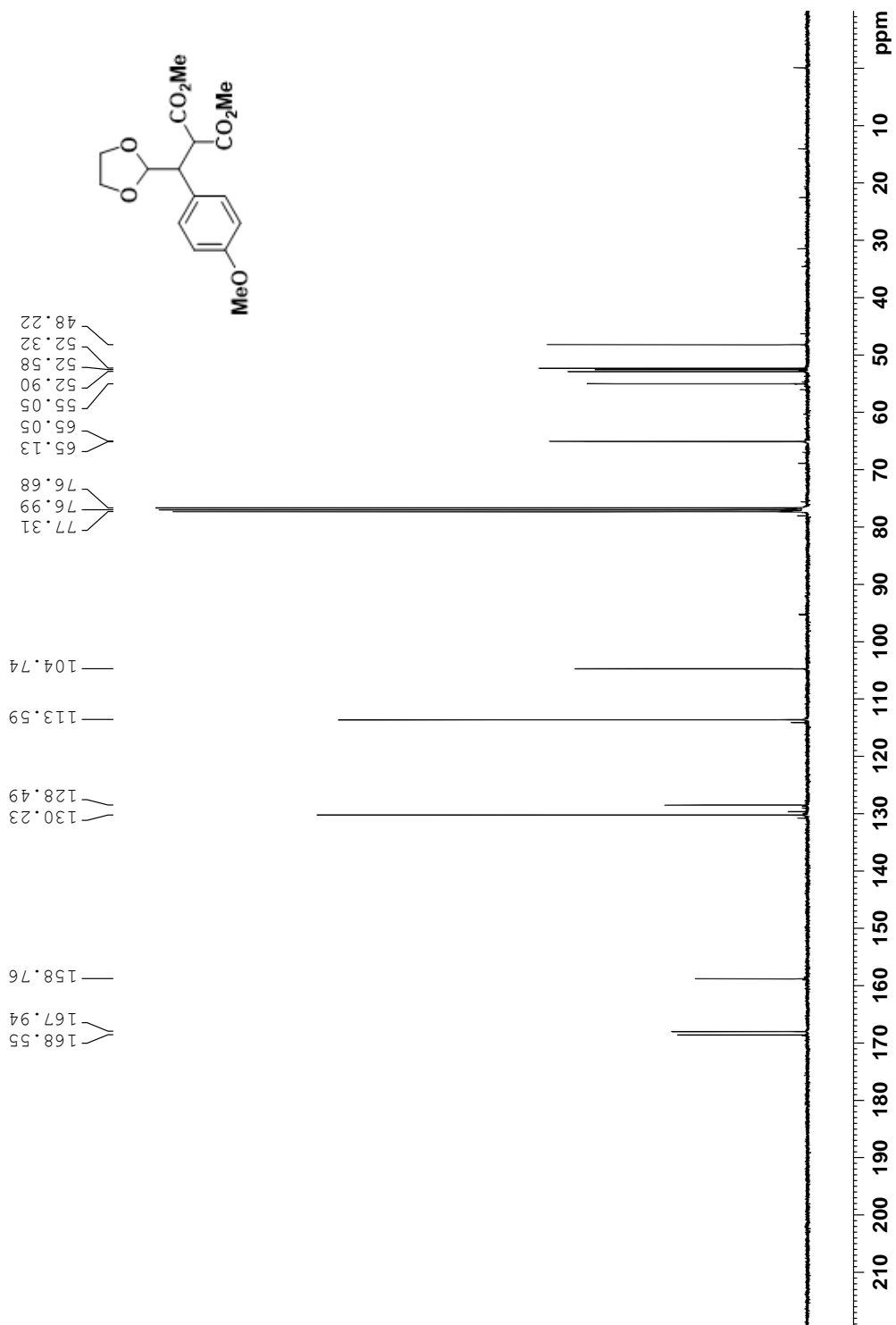
¹H NMR Spectrum of 2-152 (500 MHz, CDCl₃, 298 K)
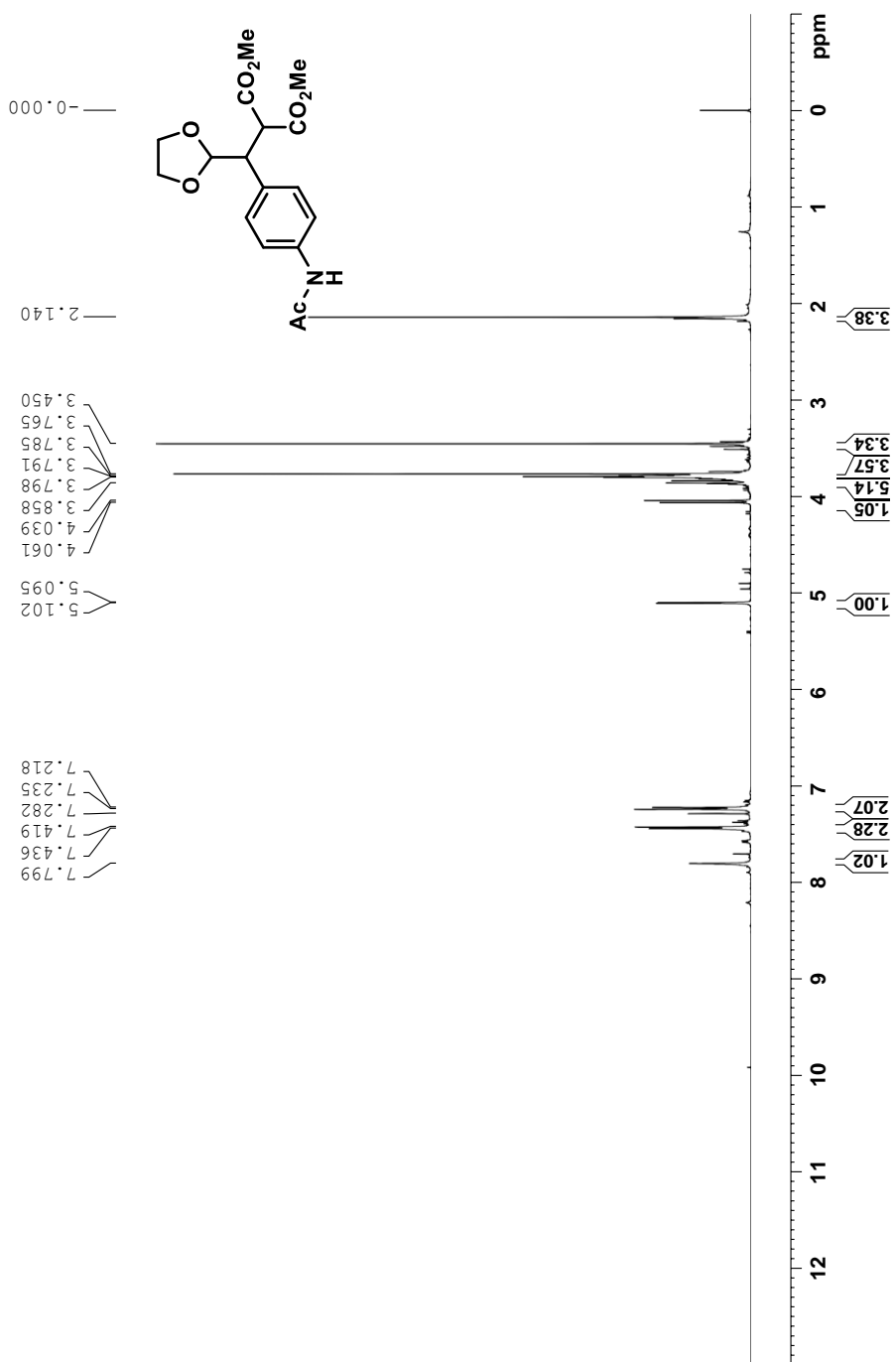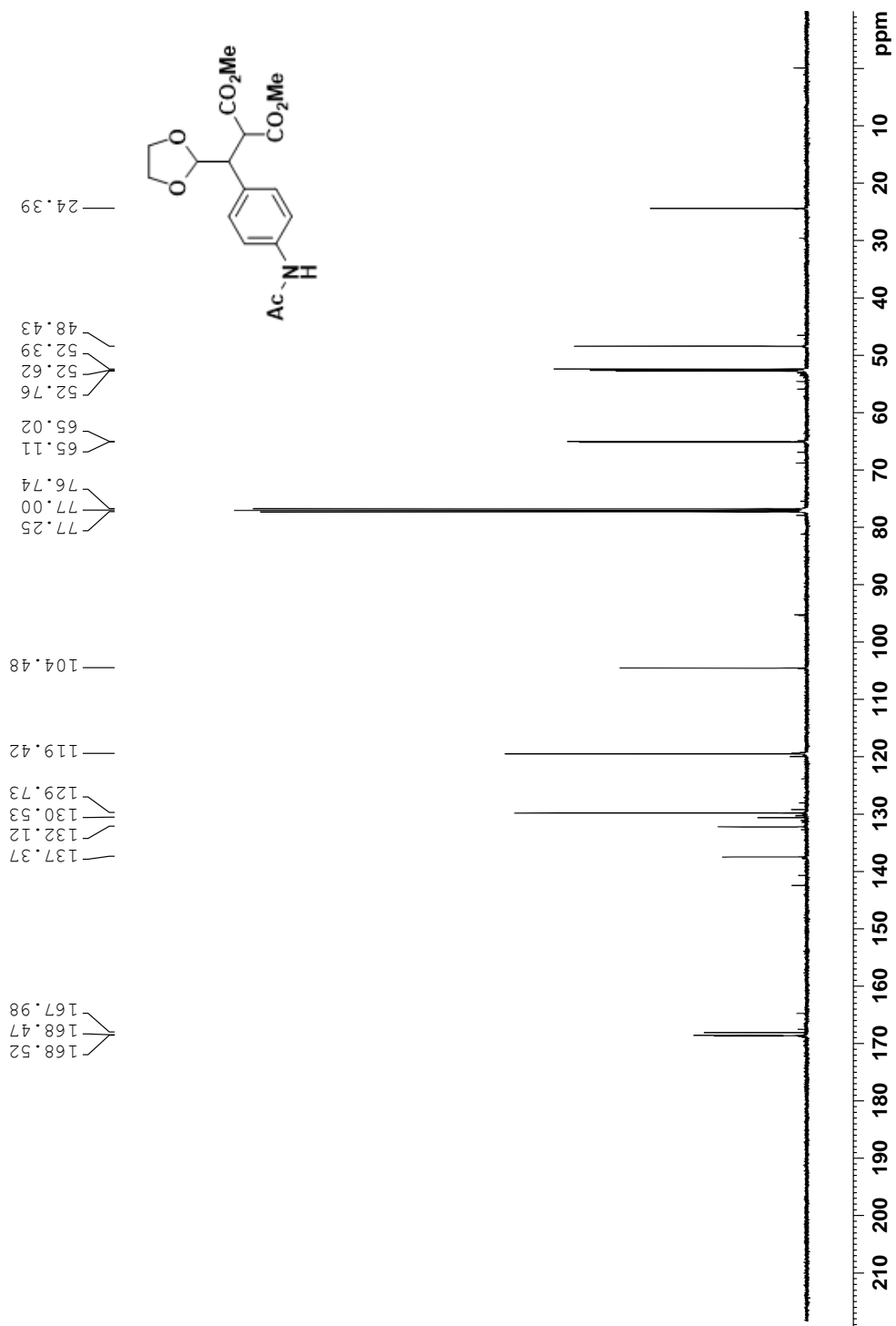
¹³C NMR Spectrum of 2-152 (125 MHz, CDCl₃. 298 K)

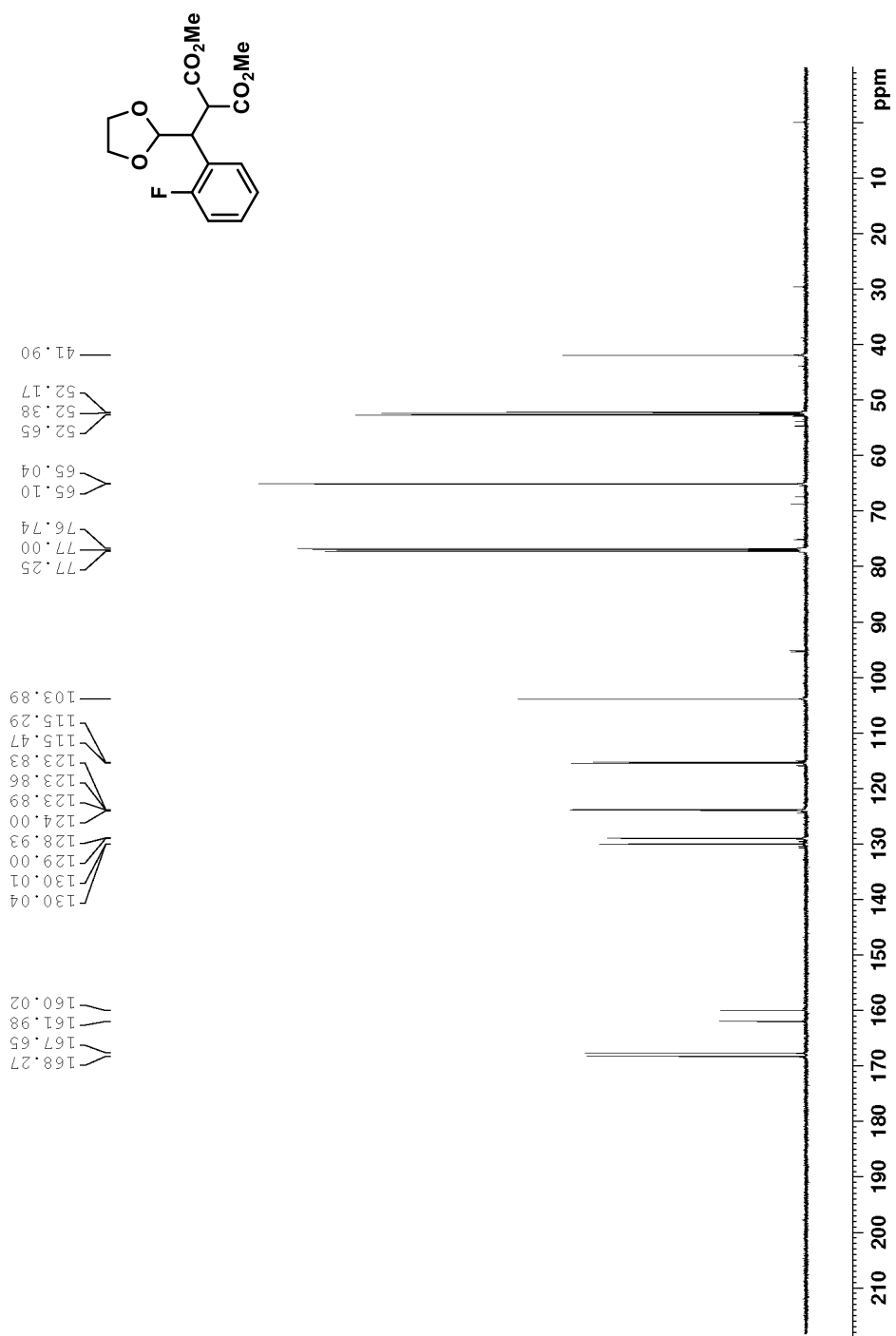**¹³C NMR Spectrum of 2-152 (125 MHz, CDCl₃. 298 K)**

24.39

48.43
52.39
52.62
52.76

65.02
65.11

76.74
77.00
77.25

104.48

119.42

129.73
130.53
132.12
137.37

167.98
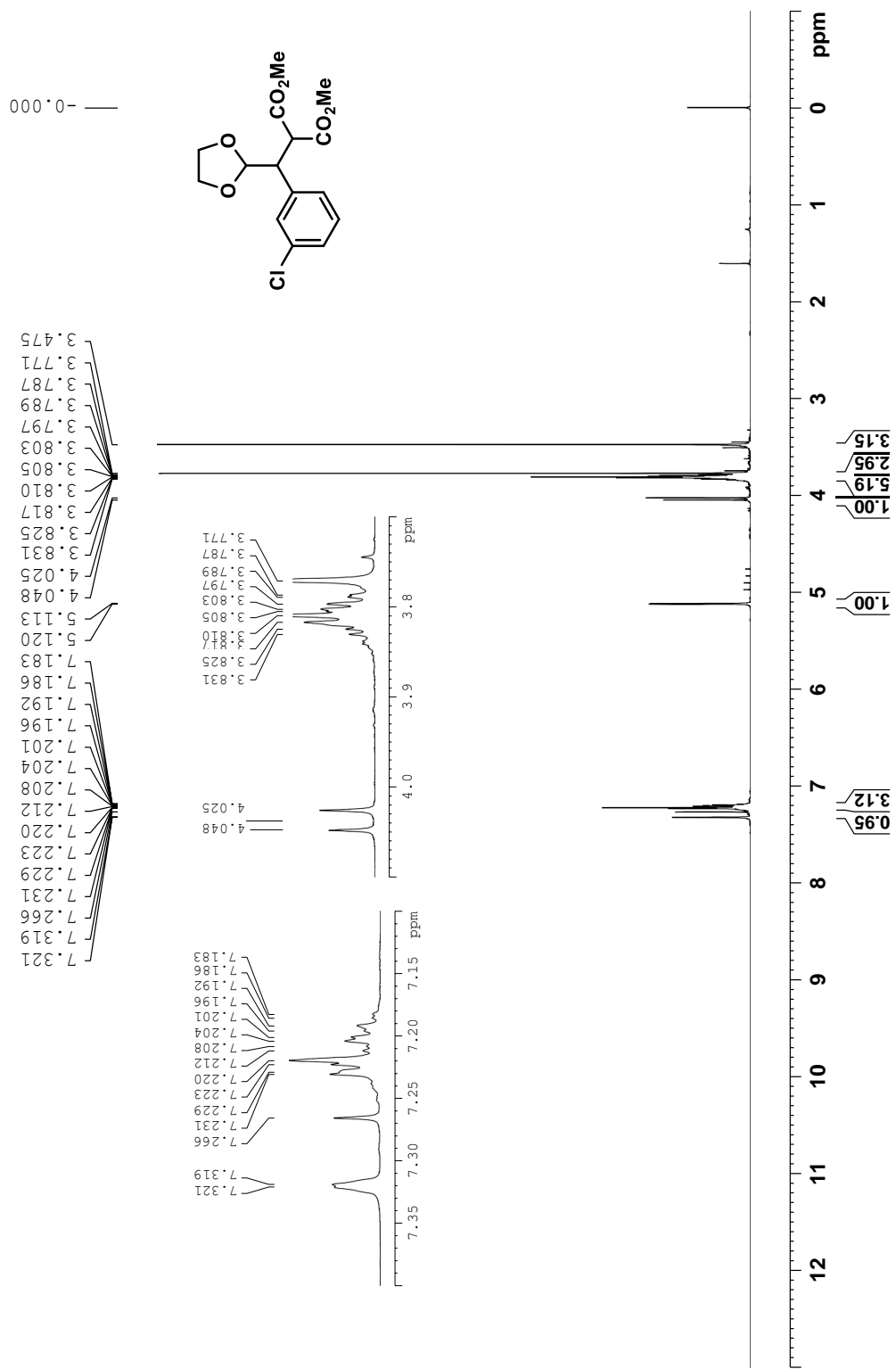168.47
168.52
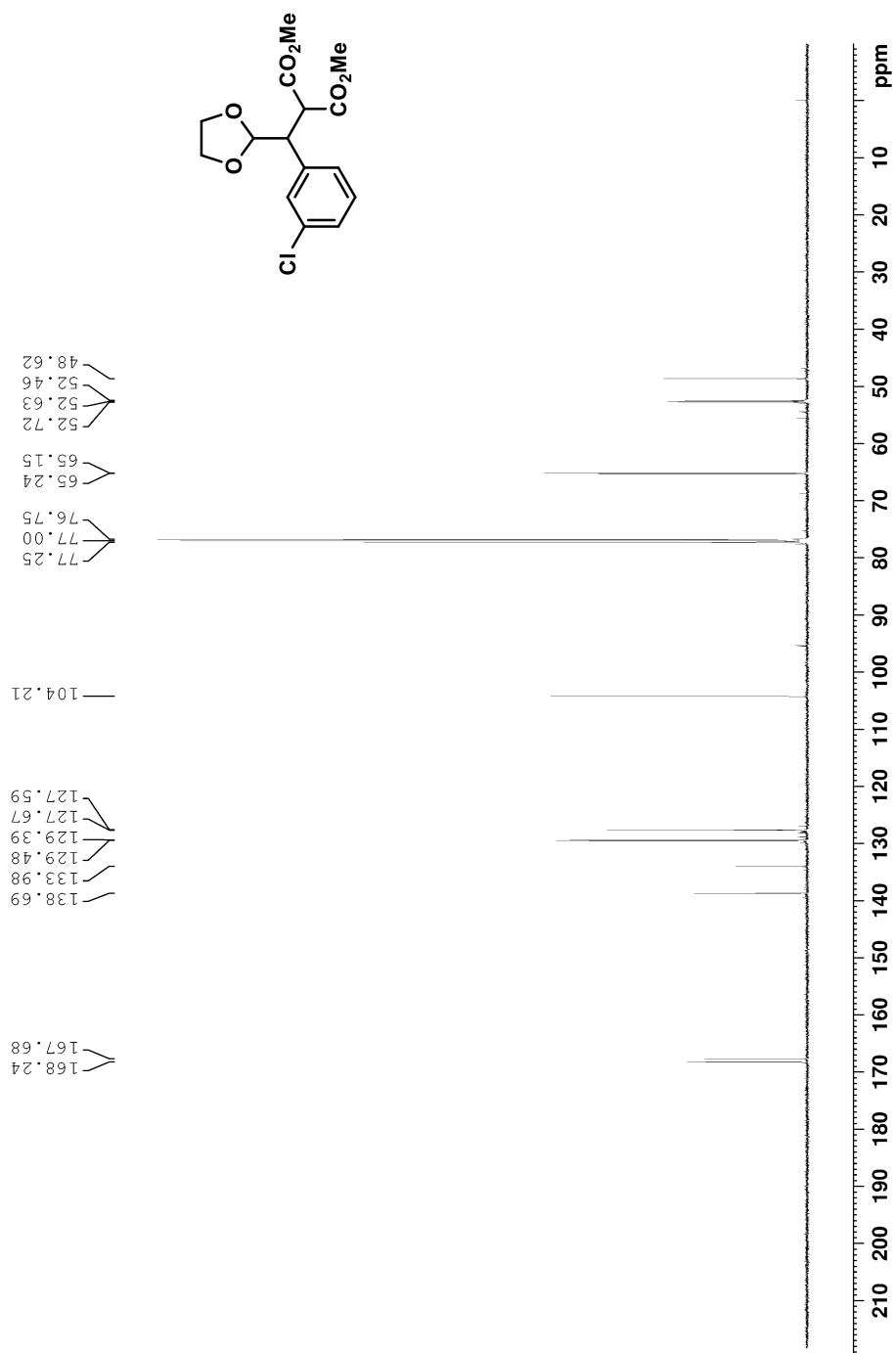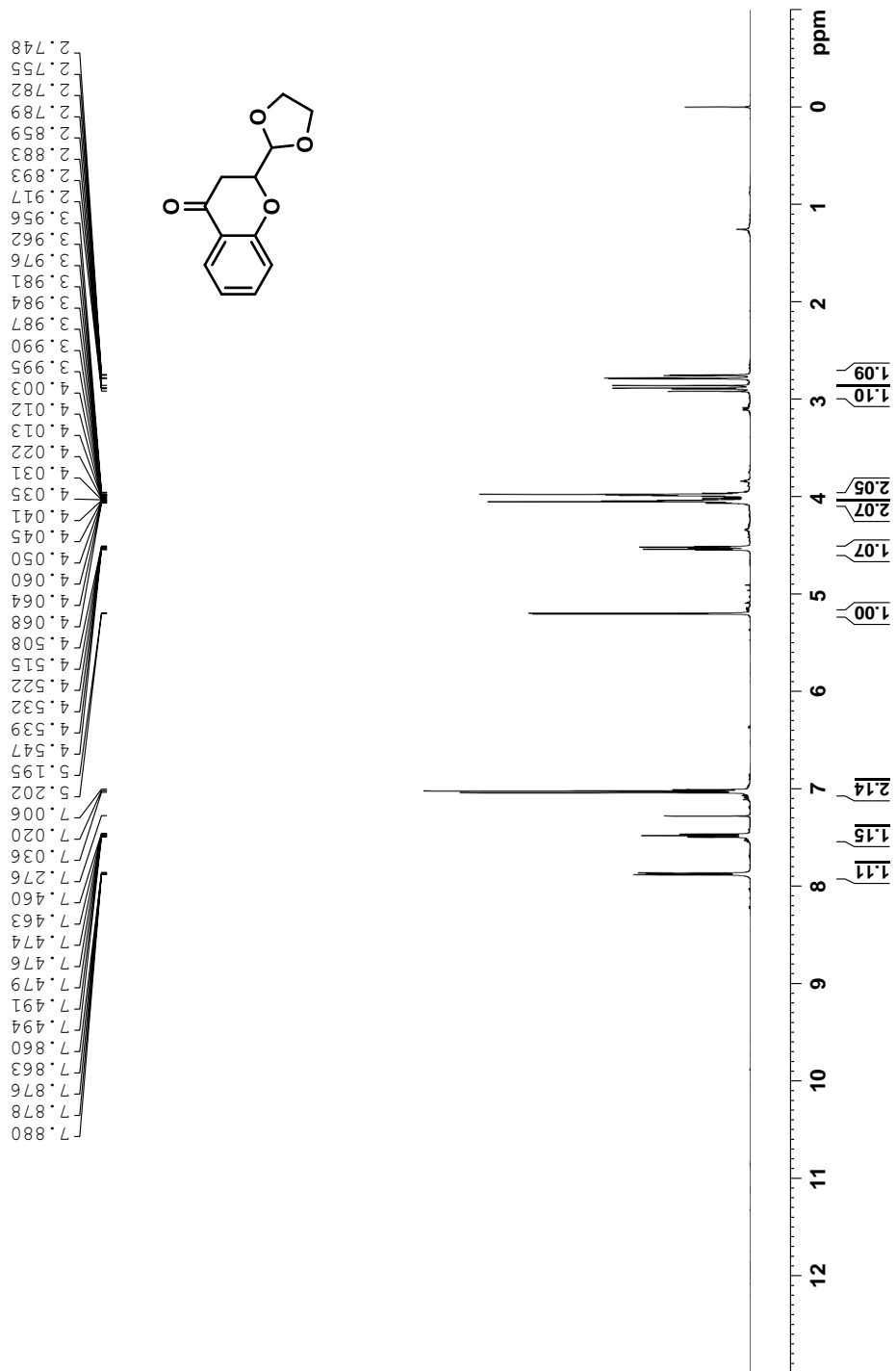
¹H NMR Spectrum of 2-115 (500 MHz, CDCl₃, 298 K)

¹H NMR Spectrum of 2-115 (500 MHz, CDCl₃, 298 K)

¹³C NMR Spectrum of 2-115 (125 MHz, CDCl₃, 298 K)

37.05

65.41
65.72
76.74
77.00
77.25
77.57

102.96

117.87
121.05
121.51
126.73

136.00

160.68

191.31

ppm
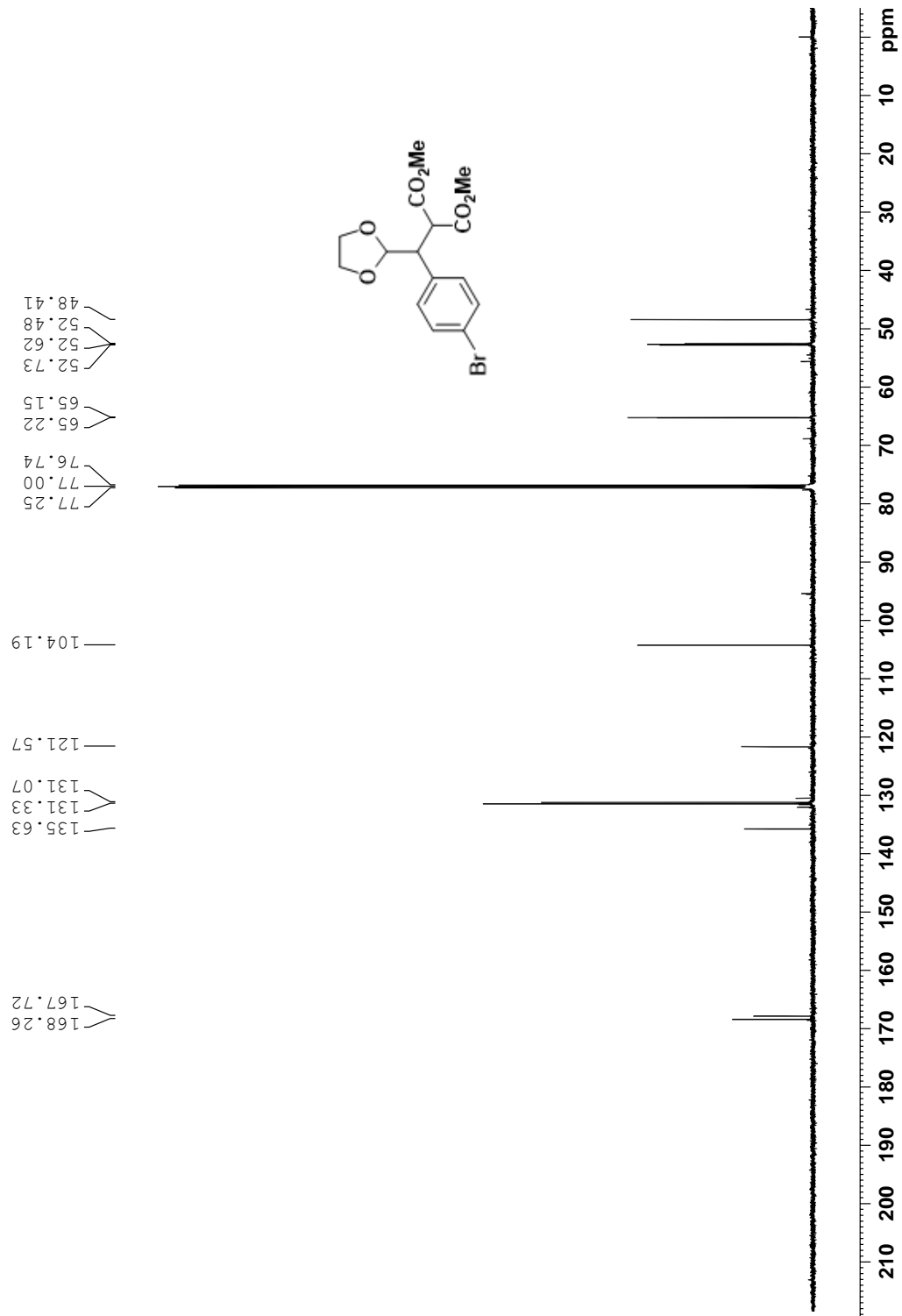210 200 190 180 170 160 150 140 130 120 110 100 90 80 70 60 50 40 30 20 10

309

^{1}H NMR Spectrum of 2-153 (500 MHz, CDCl$_3$, 298 K)

¹³C NMR Spectrum of 2-153 (125 MHz, CDCl₃, 298 K)

26.35
26.70
26.86
29.87
31.56
37.92

47.57
49.72
52.29

64.54
64.86

76.74
77.00
77.25

103.33

169.56
169.64

CO₂Me
CO₂Me

ppm
10
20
30
40
50
60
70
80
90
100
110
120
130
140
150
160
170
180
190
200
210

311

^{1}H NMR Spectrum of Crude 2-154 (300 MHz, CDCl$_3$ with 25.2 mg of Mesitylene, 298 K)

Peak labels (ppm):
1.267, 1.283, 1.291, 2.272, 2.554, 2.568, 2.578, 2.592, 2.603, 2.617, 2.627, 2.641, 2.650, 2.665, 3.505, 3.531, 3.811, 3.827, 3.831, 3.834, 3.840, 3.849, 3.852, 3.874, 3.885, 3.906, 3.910, 3.919, 3.925, 3.928, 3.932, 3.949, 4.147, 4.155, 4.171, 4.179, 4.195, 4.203, 4.219, 4.227, 4.878, 4.892, 6.796, 7.252

Integration labels:
1.37, 3.24, 7.43, 10.54, 0.96, 2.34, 2.29, 4.69, 1.00, 3.32

x-axis (ppm): 0, 1, 2, 3, 4, 5, 6, 7, 8, 9, 10, 11, 12
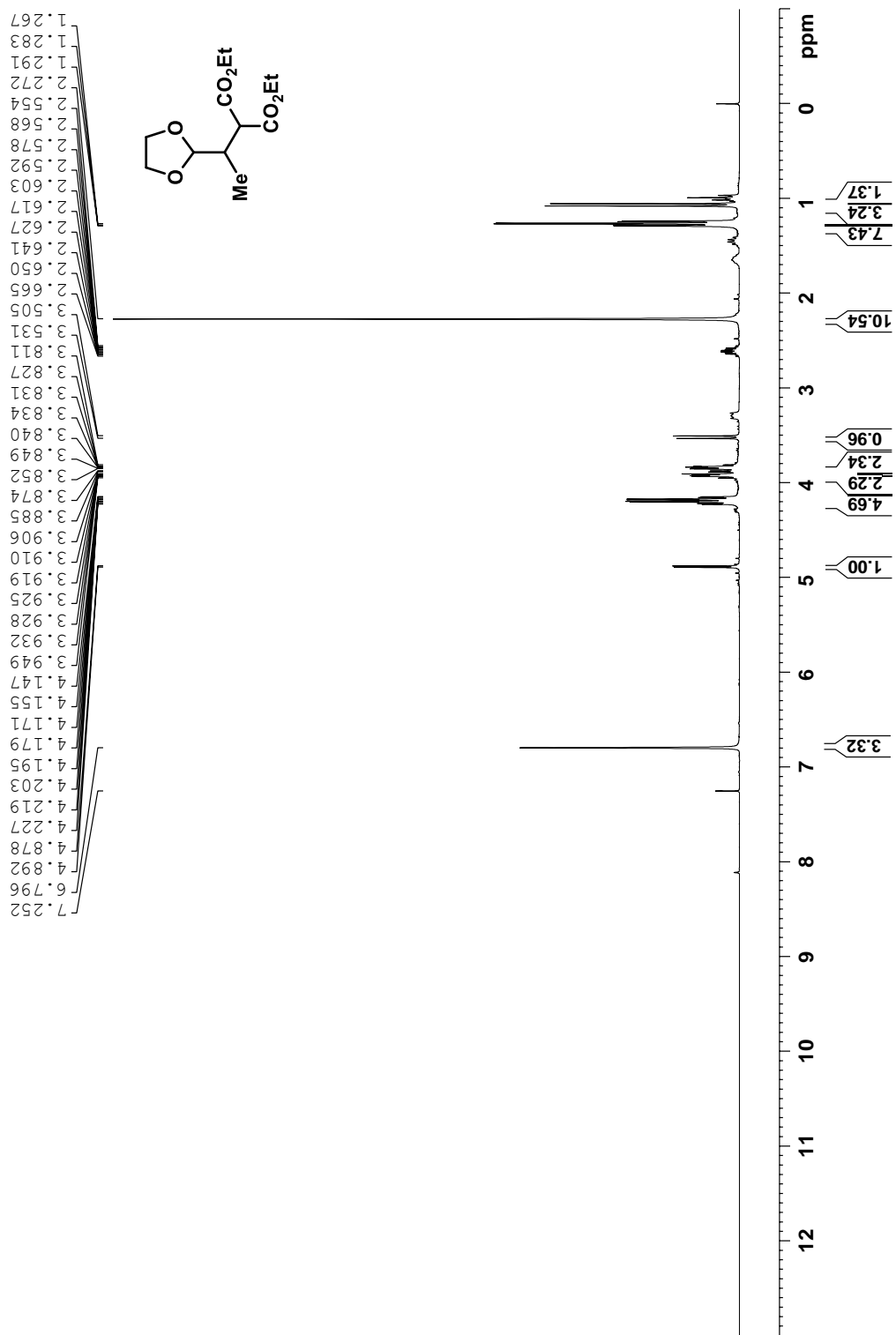
¹H NMR Spectrum of 2-155 (500MHz, CDCl₃, 298 K)
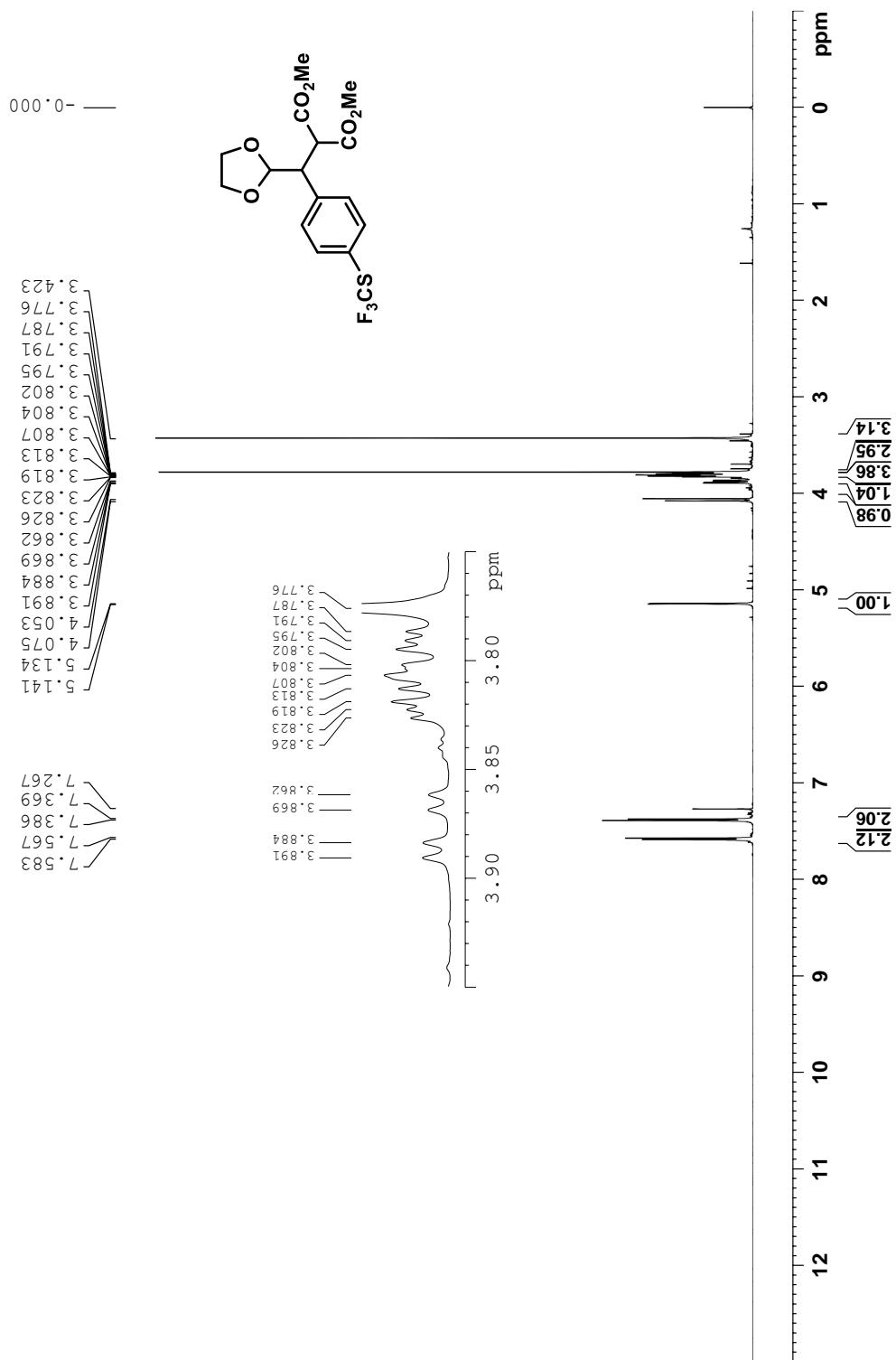
^{13}C NMR Spectrum of 2-155 (125 MHz, CDCl₃, 298 K)

48.65
52.38
52.57
52.75

65.16
65.23

76.74
77.00
77.25

104.08

130.56

135.98

139.88

167.67
168.16

ppm
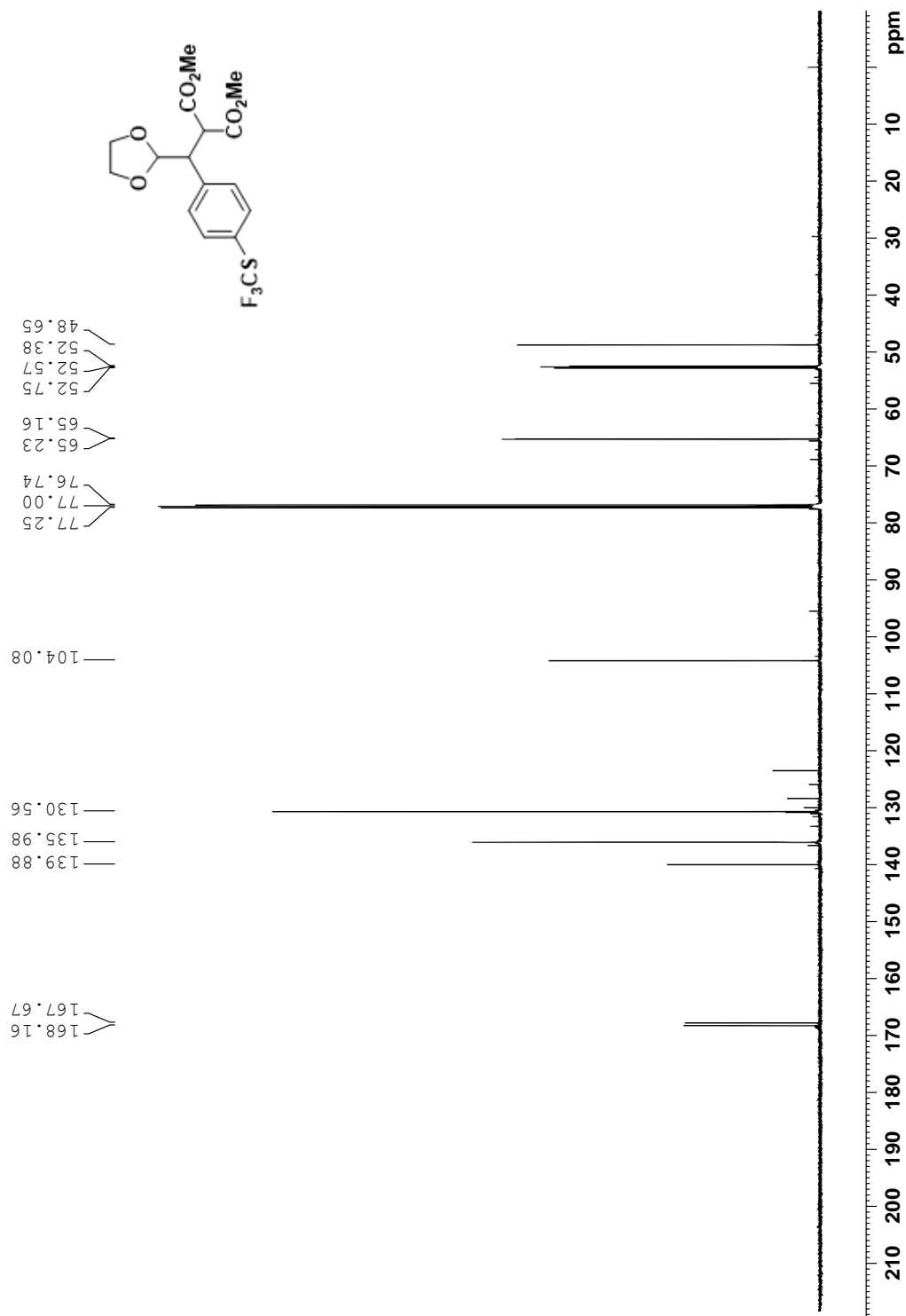
^{1}H NMR Spectrum of 2-156 (500 MHz, CDCl$_3$, 298 K)

−0.000

2.450
3.408
3.780
3.789
3.799
3.809
3.810
3.815
3.822
3.827
4.080
4.112
4.166
4.173
4.188
4.196
5.091
5.098
7.107
7.111
7.119
7.124
7.131
7.140
7.145
7.152
7.157
7.229
7.242
7.246
7.261

3.08

3.17
4.21
3.08
1.01
1.04

1.00

3.03
0.94

ppm

4.089
4.112
4.166
4.173
4.188
4.196

4.05
4.10
4.15
4.20
4.25
ppm

0 1 2 3 4 5 6 7 8 9 10 11 12 ppm

48.70
52.46
52.54
52.75

65.15
65.22

76.75
77.00
77.25

104.06

125.04
125.06
129.76

140.78

167.62
168.14

ppm

^{1}H NMR Spectrum of 2-157 (500 MHz, CDCl$_3$, 298 K)

0.000
3.170
3.310
3.675
3.677
3.687
3.695
3.709
3.715
3.721
3.724
3.730
3.734
3.739
3.747
3.751
3.758
3.760
3.766
3.770
3.809
3.818
3.848
3.854
3.872
3.879
3.896
3.901
4.679
4.697
4.787
4.808
4.944
4.949
5.726
5.731
6.702
6.720
6.989
7.007
7.127
7.141
7.151
7.154
7.165
7.169
7.176
7.182
7.206
7.210
7.217
7.221
7.227
7.230
7.235
7.239
7.246
7.248
7.268
7.282
7.286
7.838
7.856

2.56
0.90
6.06
6.88
4.83
1.05
0.91
1.00
0.85
2.09
1.78
5.12
4.40
2.68
1.80

ppm

12 11 10 9 8 7 6 5 4 3 2 1 0

317

¹H NMR Spectrum of 2-157 (500 MHz, CDCl₃, 298 K)

^{13}C NMR Spectrum of 2-157 (125 MHz, CDCl$_3$, 298 K)

47.73
48.60
52.32
52.88
55.59
55.67
65.07
65.11
65.27
65.39
71.37
72.26
76.74
77.00
77.25

102.60
104.61
113.76
114.15
127.56
127.71
127.83
127.91
129.38
130.12
130.35
130.66
131.48
133.81
134.76

163.38
164.15
165.42
166.06

ppm
210 200 190 180 170 160 150 140 130 120 110 100 90 80 70 60 50 40 30 20 10

319

¹H NMR Spectrum of 2-158 (400 MHz, CDCl₃, 298 K)

¹³C NMR Spectrum of 2-158 (100 MHz, CDCl₃)

27.33

45.01
45.19
47.34
47.51

65.28
69.07
72.63
76.68
76.99
77.31

95.23

100.69

190 180 170 160 150 140 130 120 110 100 90 80 70 60 50 40 30 20 10 0 ppm

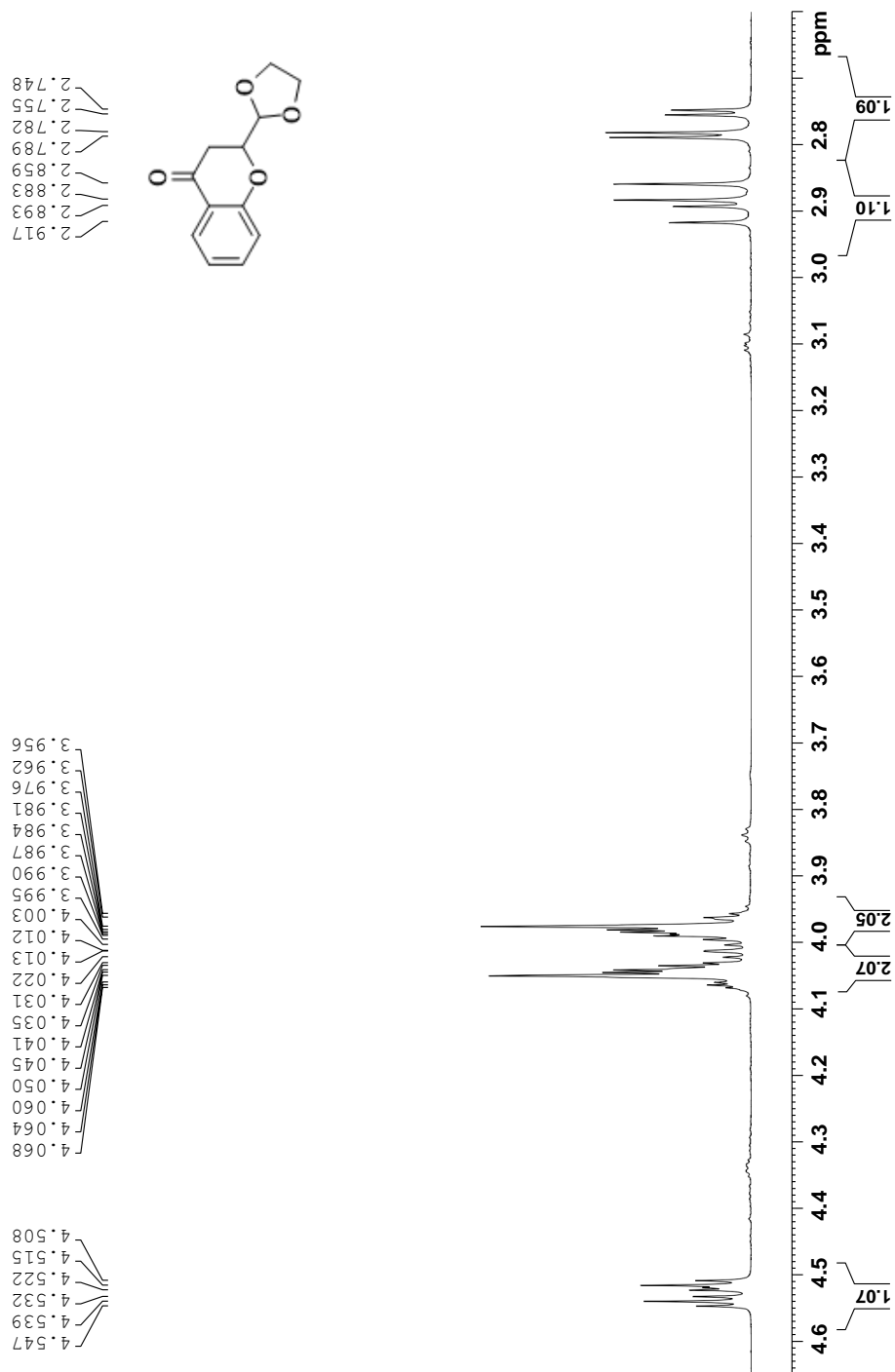**¹⁹F NMR Spectrum of 2-158 (371 MHz, CDCl₃, 298 K)**
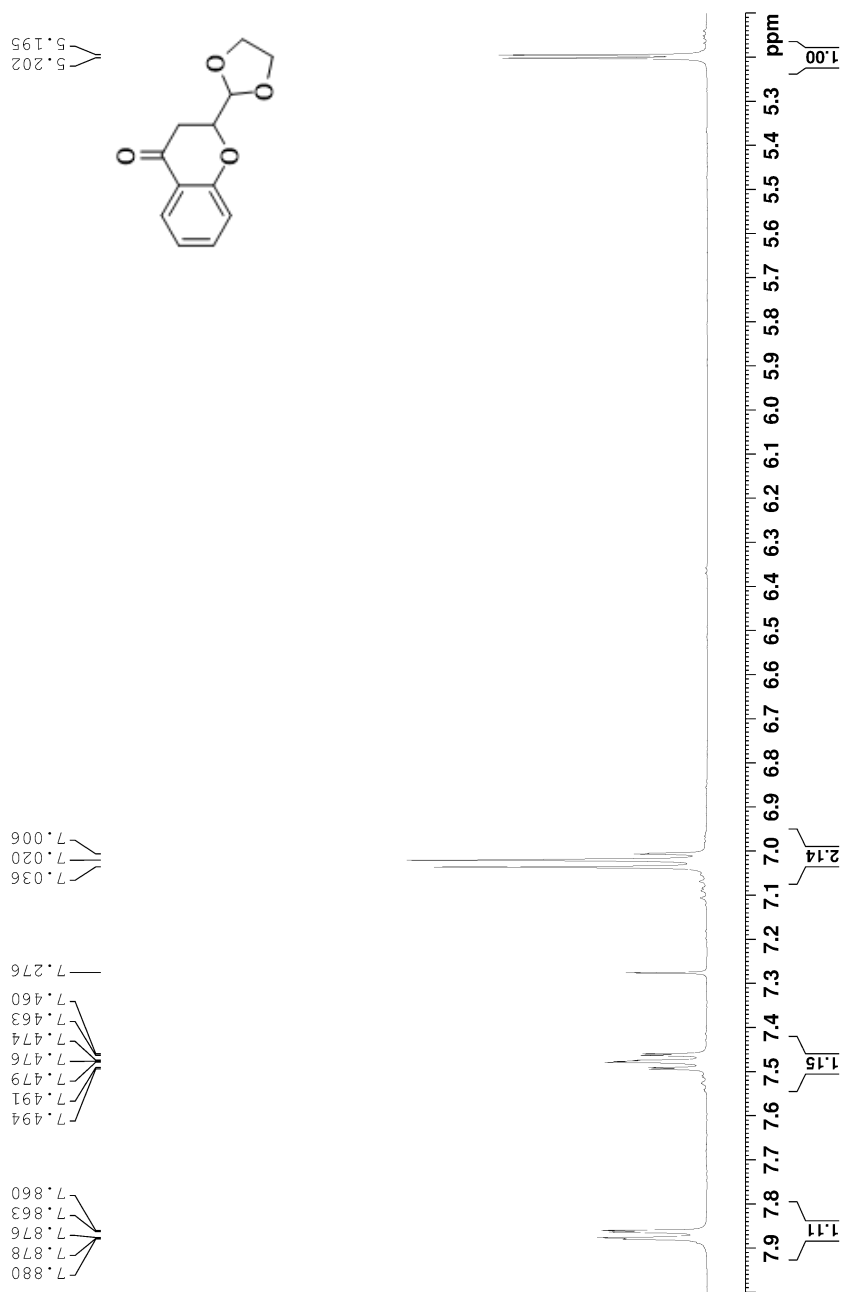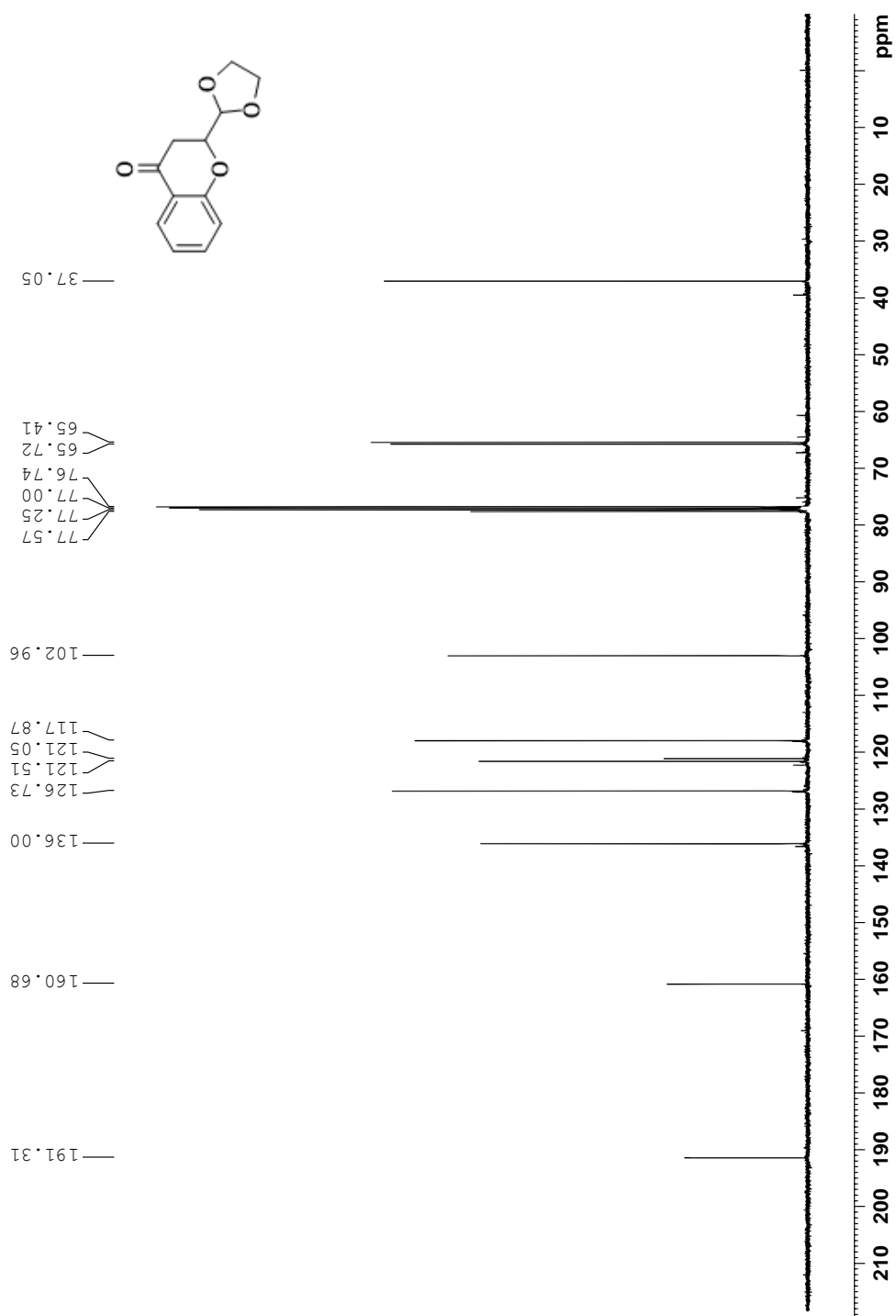
−151.93

¹H NMR Spectrum of 2-159 (500 MHz, CDCl₃, 298 K)

¹H NMR Spectrum of 2-159 (500 MHz, CDCl₃, 298 K)

¹H NMR Spectrum of 2-159 (500 MHz, CDCl₃, 298 K)
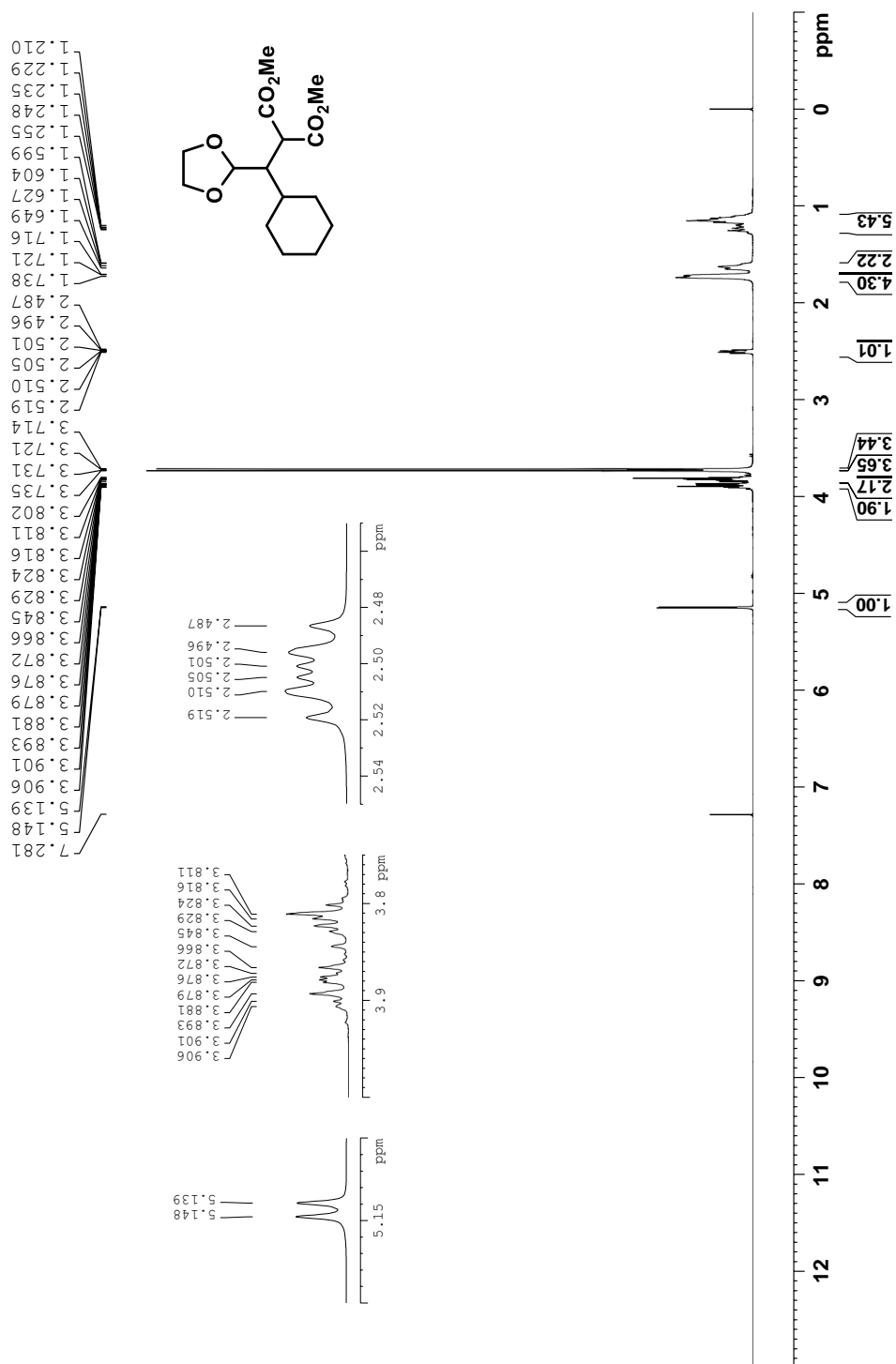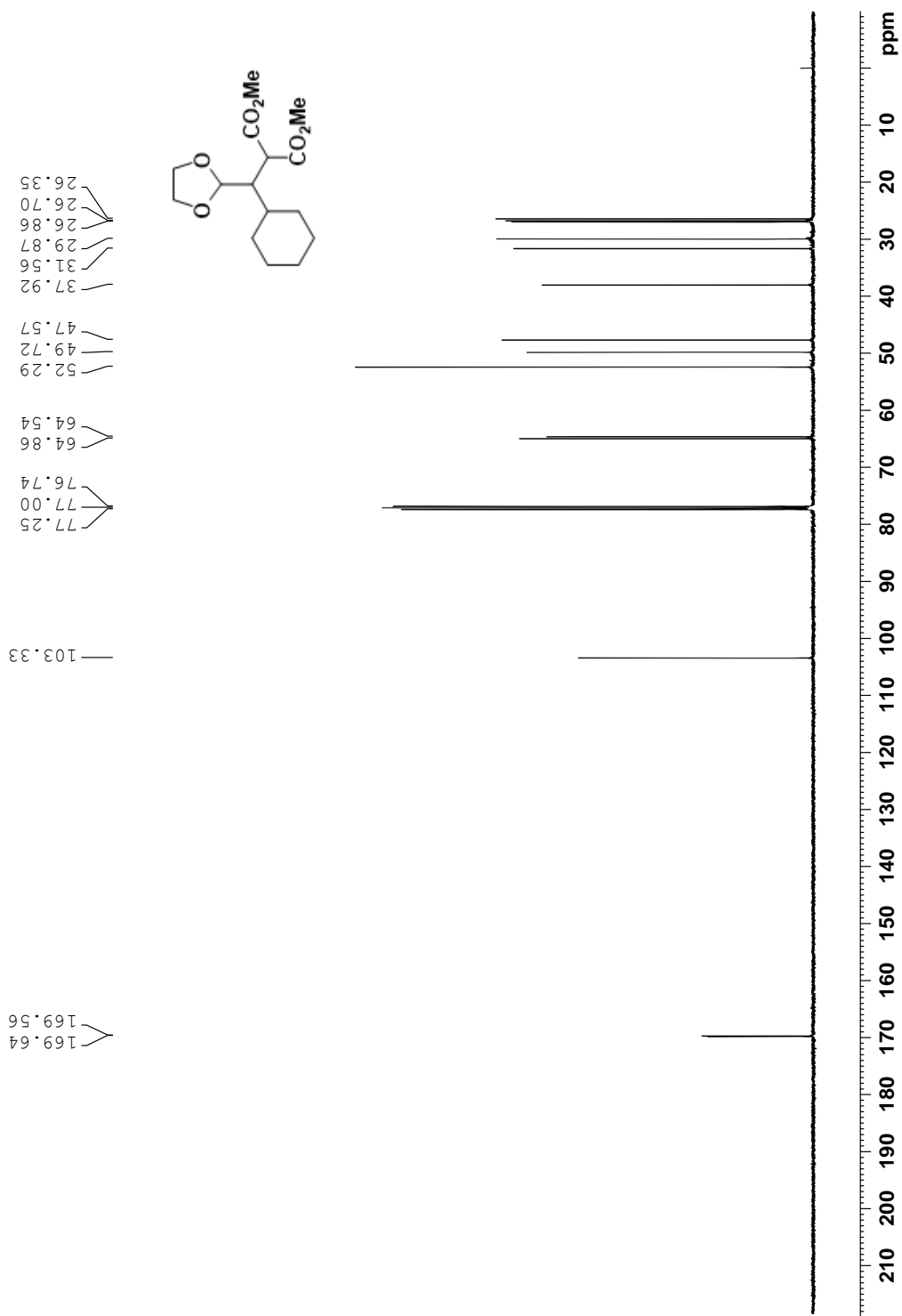

3.215
3.224
3.231
3.238
3.247
3.272
3.282
3.294
3.301
3.304
3.310
3.322
3.332

3.493
3.505
3.510
3.521

3.815
3.829
3.833
3.837
3.843
3.863
3.875
3.896
3.901
3.905
3.910
3.923
3.938
3.952
3.954
3.968
4.080
4.088
4.093
4.100
4.105
4.110
4.117
4.121
4.130

SO₂Ph

+

SO₂Ph

1.96

1.82

1.80

ppm 3.1 3.2 3.3 3.4 3.5 3.6 3.7 3.8 3.9 4.0 4.1 4.2 4.3

^{13}C NMR Spectrum of 2-159 (125 MHz, CDCl₃, 298 K)

^{13}C NMR Spectrum of 2-159 (125 MHz, CDCl₃, 298 K)

26.41
26.98

+

50.58
52.70

65.07
69.10
73.57
76.74
77.00
77.25

94.99

101.67

127.93
127.99
129.25
129.31
133.68
133.78
138.87

SO₂Ph

SO₂Ph

ppm
10
20
30
40
50
60
70
80
90
100
110
120
130
140
150
160
170
180
190
200
210

¹³C NMR Spectrum of 2-161 (125 MHz, CDCl₃, 298 K)

50.57
51.84
52.36
52.60
64.99
65.08
76.74
76.99
77.25
104.89
122.04
124.86
136.12
148.95
157.32
168.35
168.99

ppm
10 20 30 40 50 60 70 80 90 100 110 120 130 140 150 160 170 180 190 200 210
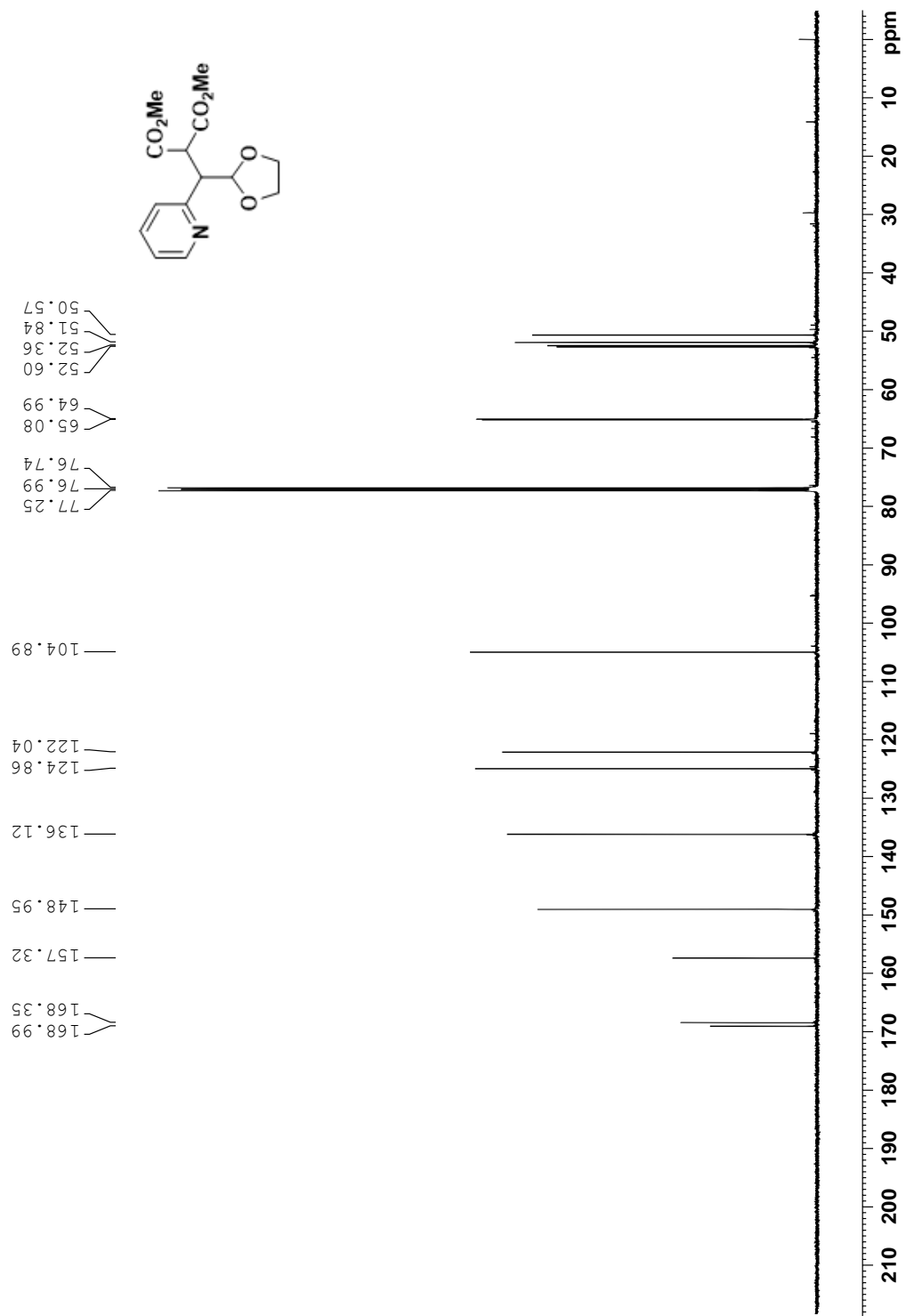
¹H NMR Spectrum of 2-162 (500 MHz, CDCl₃, 298 K)
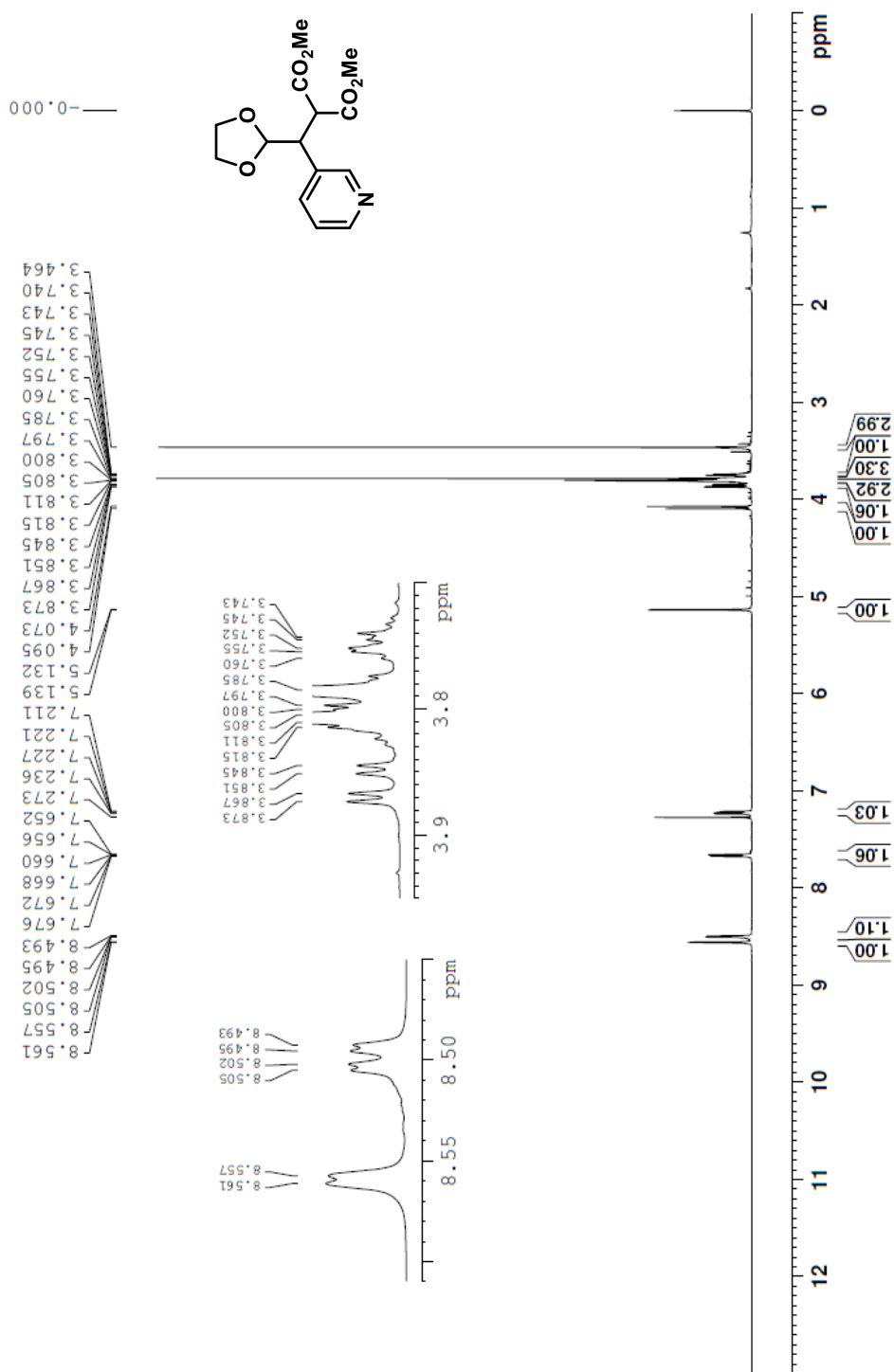
^{13}C NMR Spectrum of 2-162 (125 MHz, CDCl₃, 298 K)

46.56
52.38
52.51
52.80

65.22
65.25

76.74
77.00
77.25

103.78

122.98

132.13
136.86

148.81
150.89

167.58
168.09

ppm
10 20 30 40 50 60 70 80 90 100 110 120 130 140 150 160 170 180 190 200 210
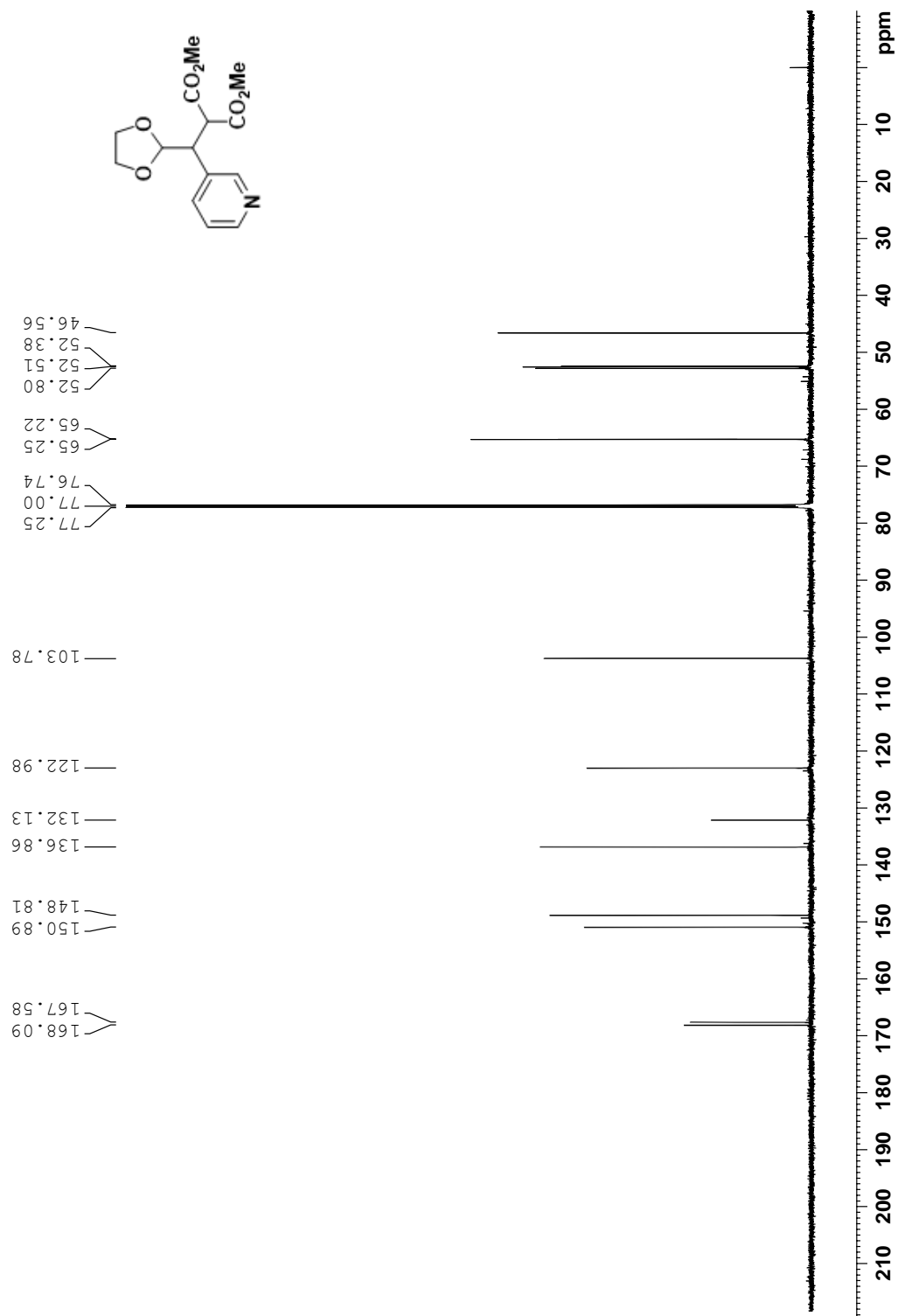
¹H NMR Spectrum of 2-163 (500 MHz, CDCl₃, 298 K)
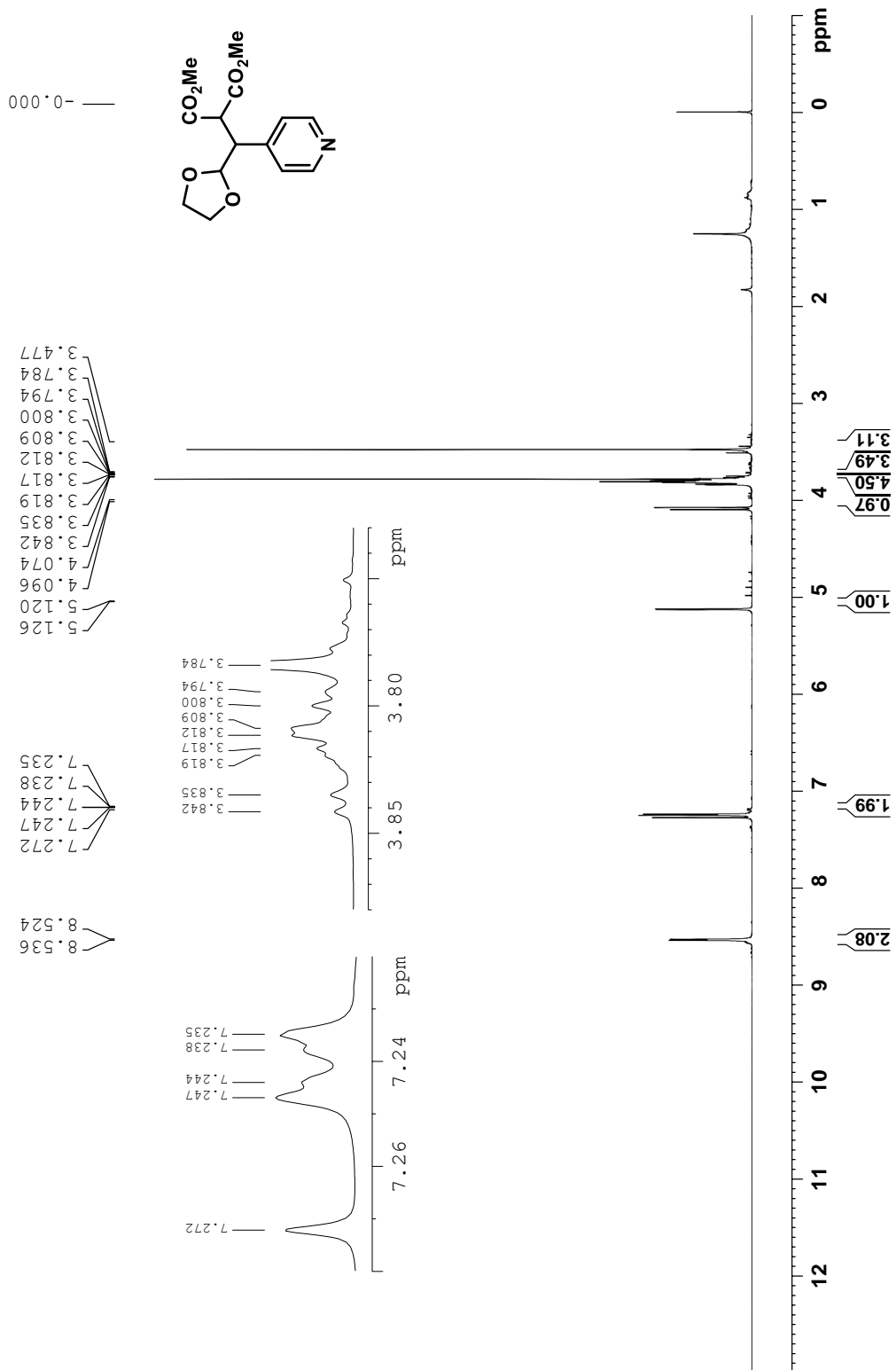
^{13}C NMR Spectrum of 2-163 (125 MHz, CDCl$_3$, 298 K)

48.31
52.15
52.56
52.84
65.20
65.26
76.74
77.00
77.25
103.67
124.60
145.71
149.64
167.47
167.96

ppm
10
20
30
40
50
60
70
80
90
100
110
120
130
140
150
160
170
180
190
200
210
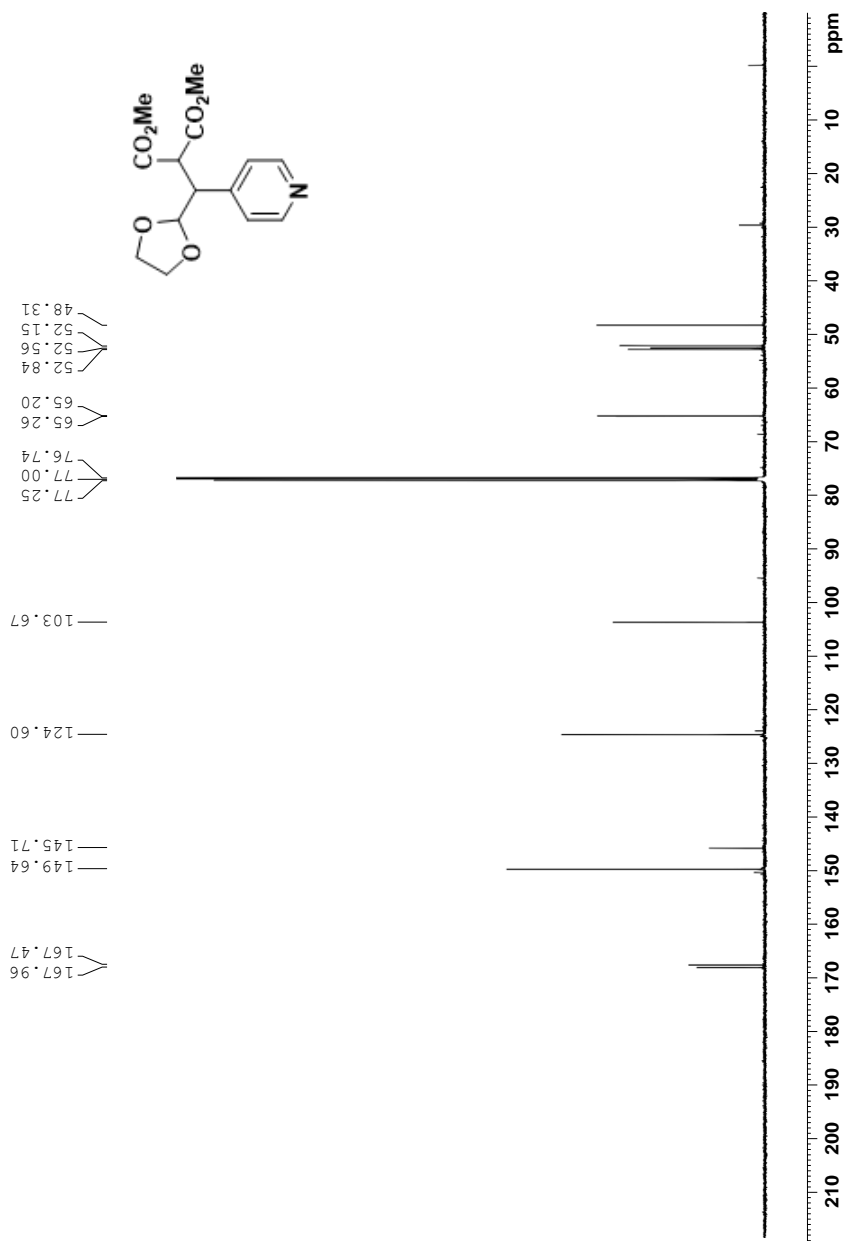
¹H NMR Spectrum of 2-164 (500 MHz, CDCl₃, 298 K)
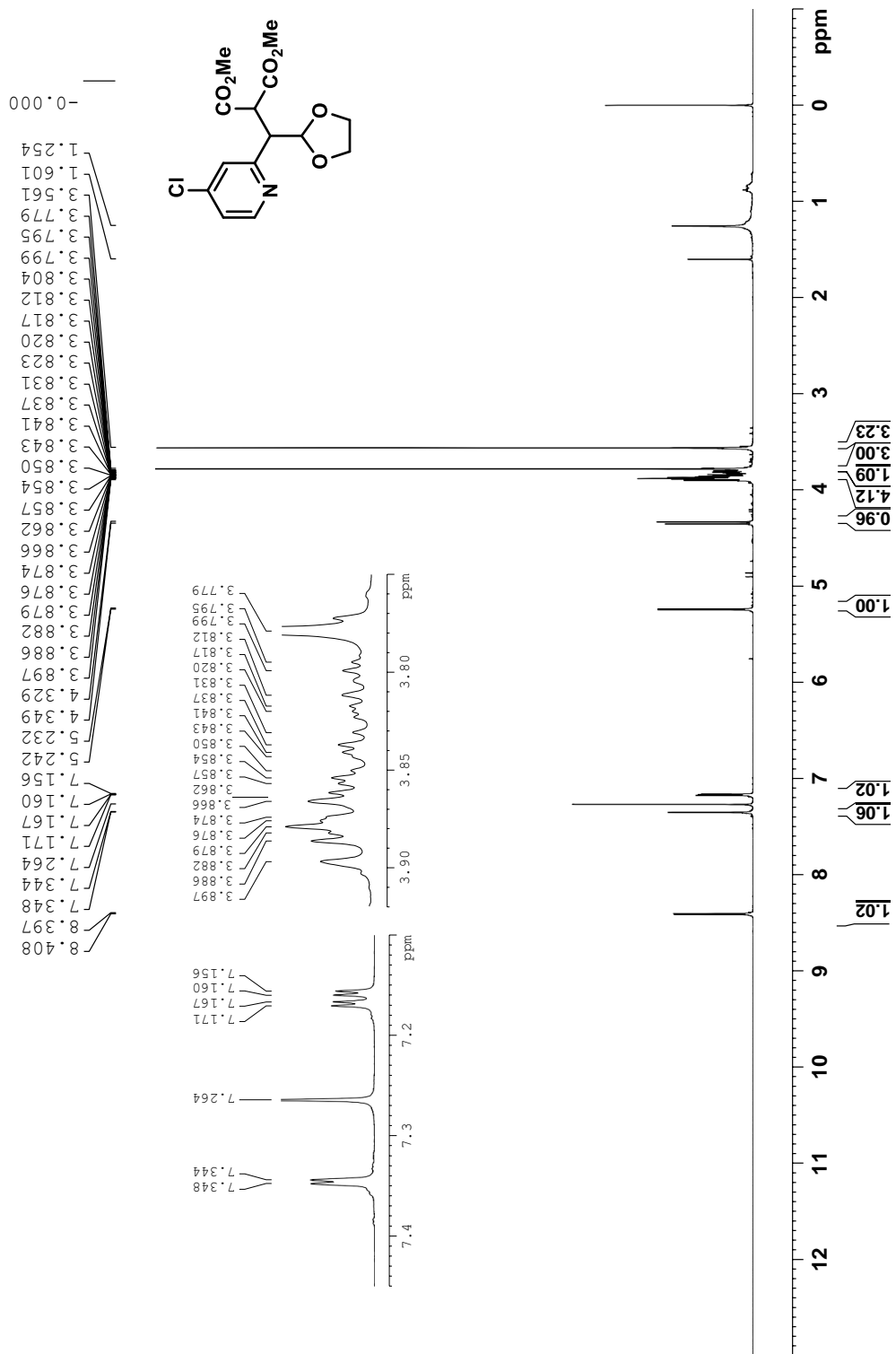
$$^{13}C \text{ NMR Spectrum of 2-164 (125 MHz, CDCl}_3, 298 \text{ K)}$$

50.41
51.70
52.52
52.71

65.07
65.16

76.74
76.99
77.25

104.54

122.57
125.27

144.07

149.70

159.04

168.24
168.78

ppm
210 200 190 180 170 160 150 140 130 120 110 100 90 80 70 60 50 40 30 20 10
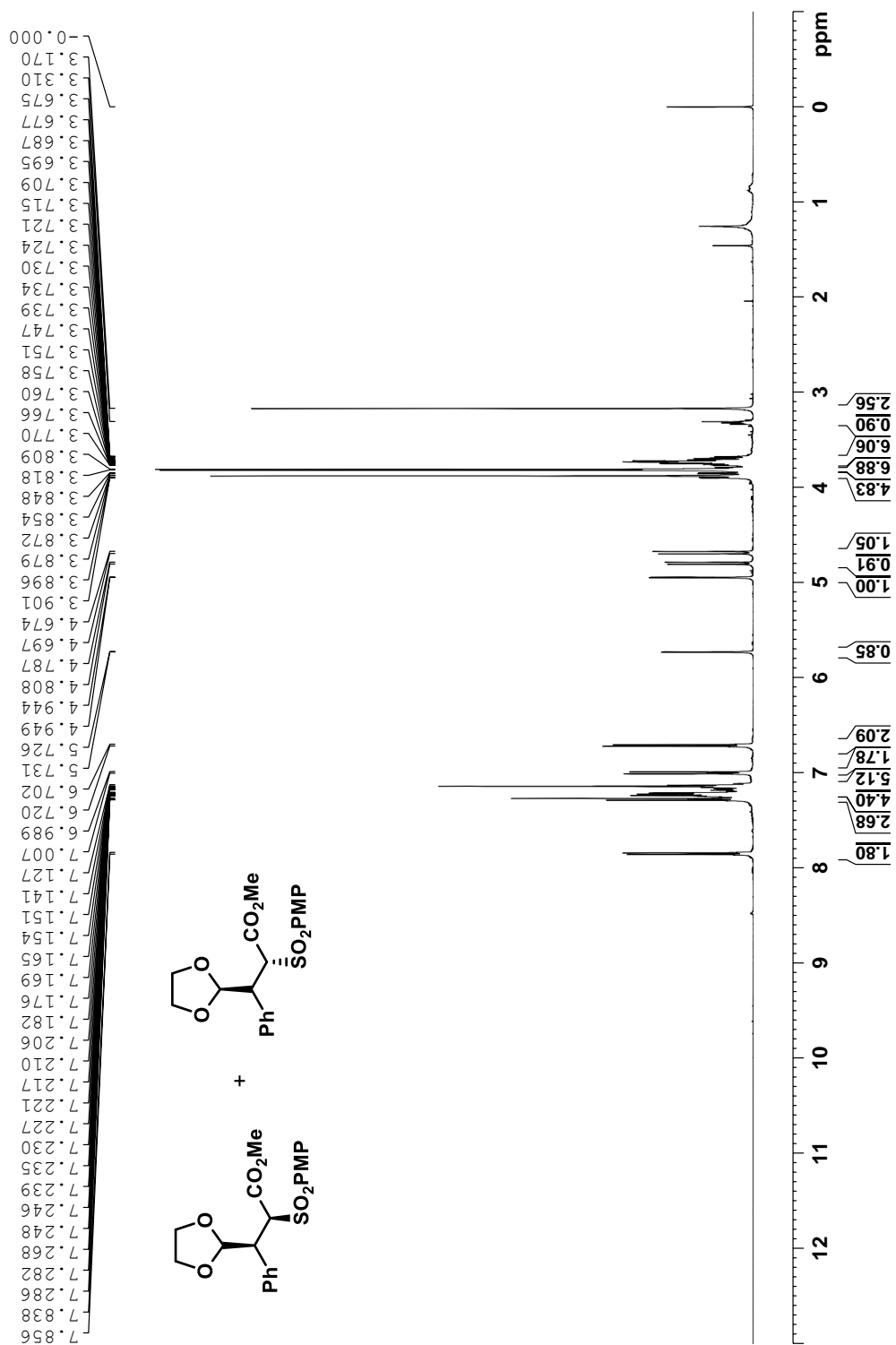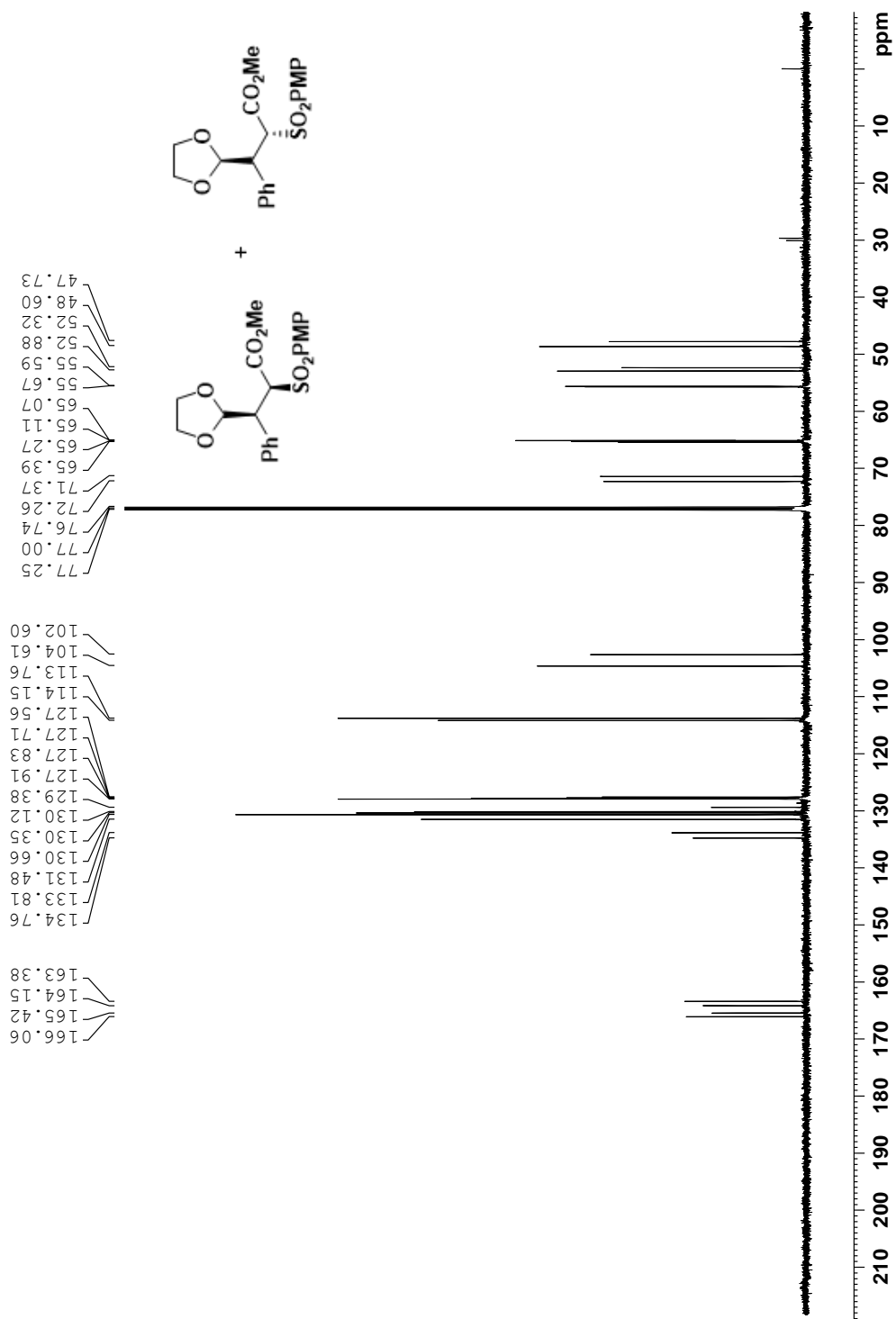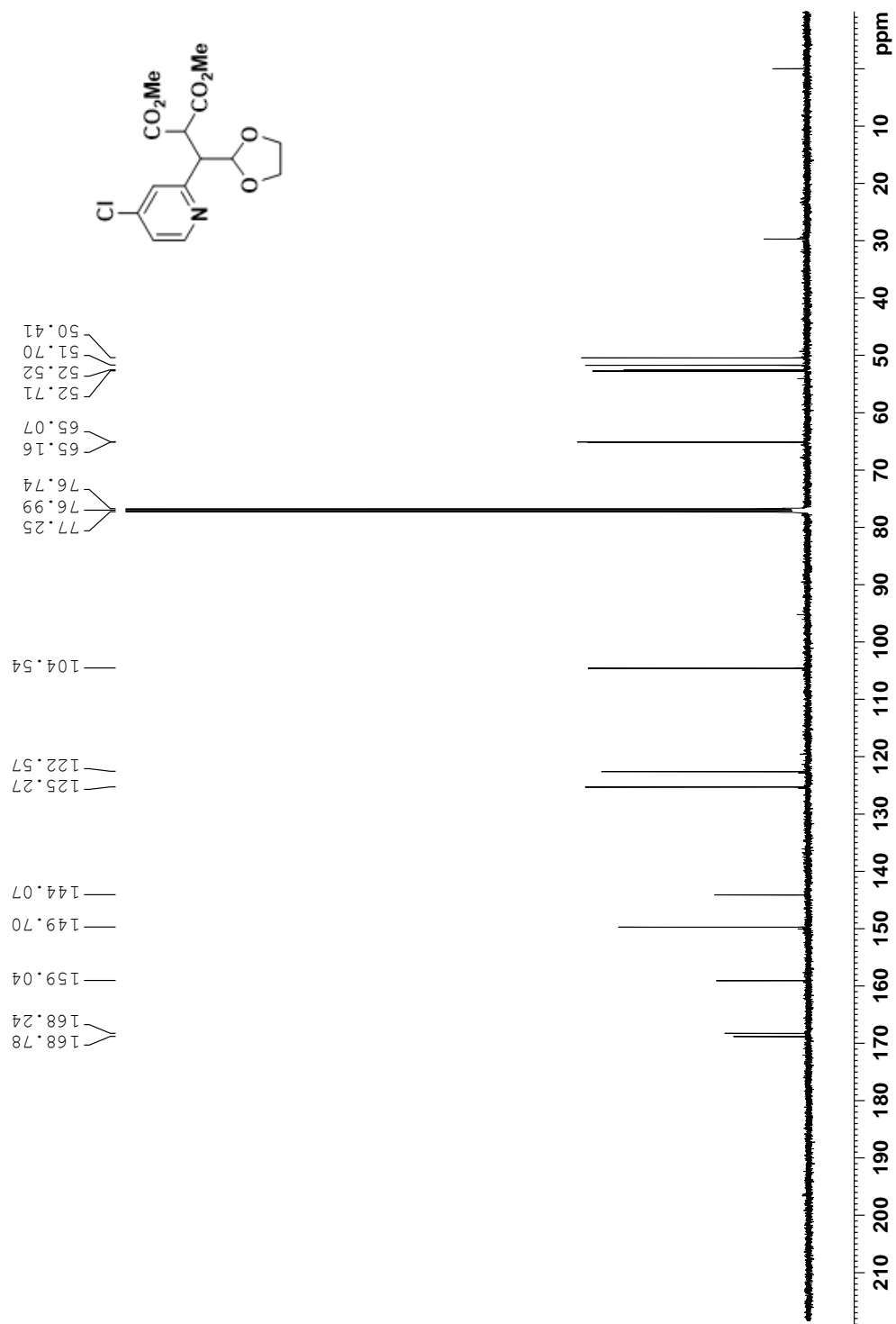
¹H NMR Spectrum of 2-165 (500 MHz, CDCl₃, 298 K)
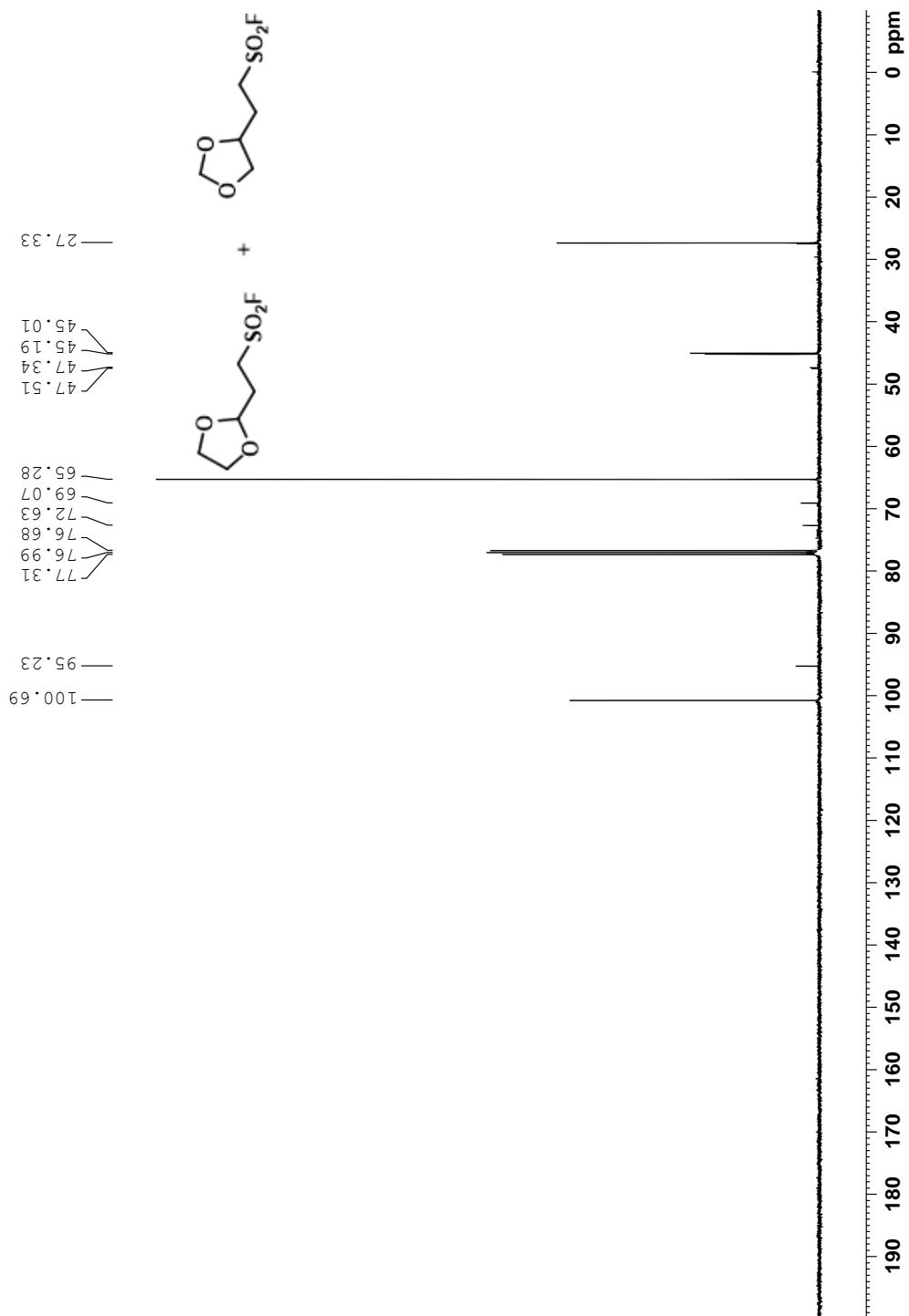
¹³C NMR Spectrum of 2-165 (125 MHz, CDCl₃, 298 K)

¹³C NMR Spectrum of 2-165 (125 MHz, CDCl₃, 298 K)

51.19
52.09
52.44
52.64
65.06
65.10
76.74
77.00
77.25
105.10
122.80
126.18
127.15
127.47
129.18
129.31
135.87
147.58
157.88
168.65
169.23

ppm
10 20 30 40 50 60 70 80 90 100 110 120 130 140 150 160 170 180 190 200 210
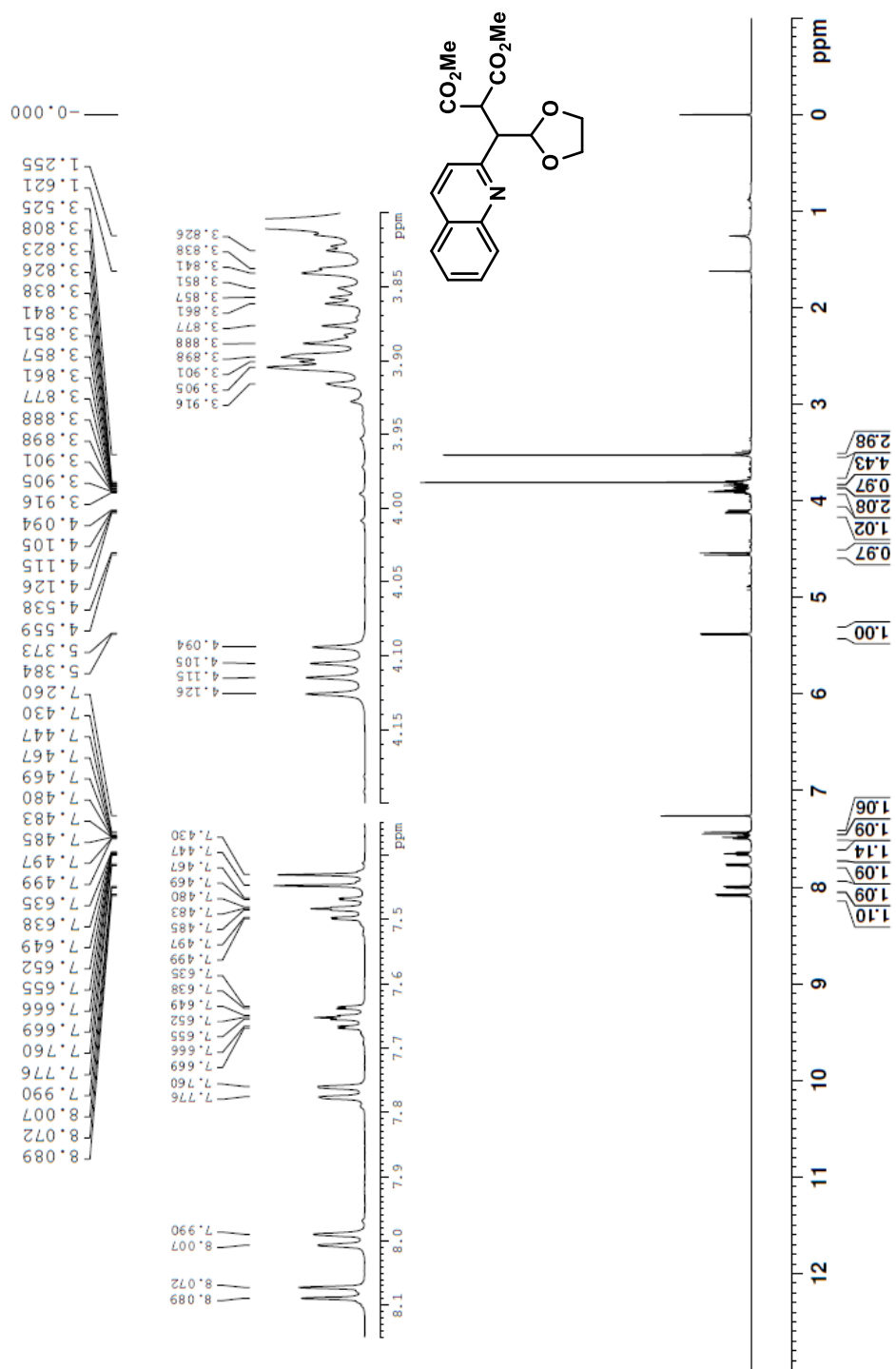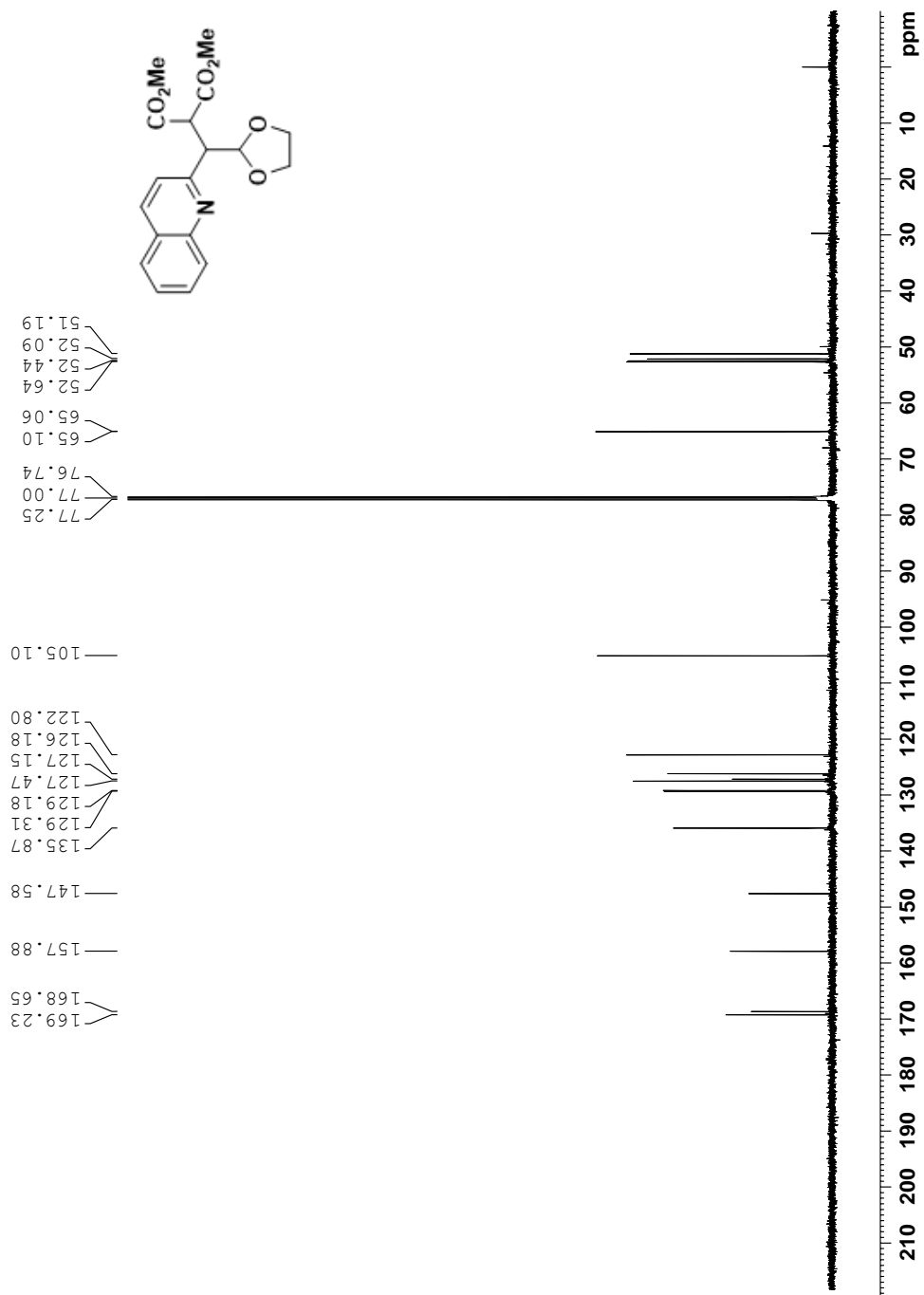
¹H NMR Spectrum of Crude Reaction of 2-136 (300 MHz, CDCl₃ with 26 mg Mesitylene, 298 K)

¹H NMR Spectrum of 2-174 (400 MHz, CDCl₃, 298 K)
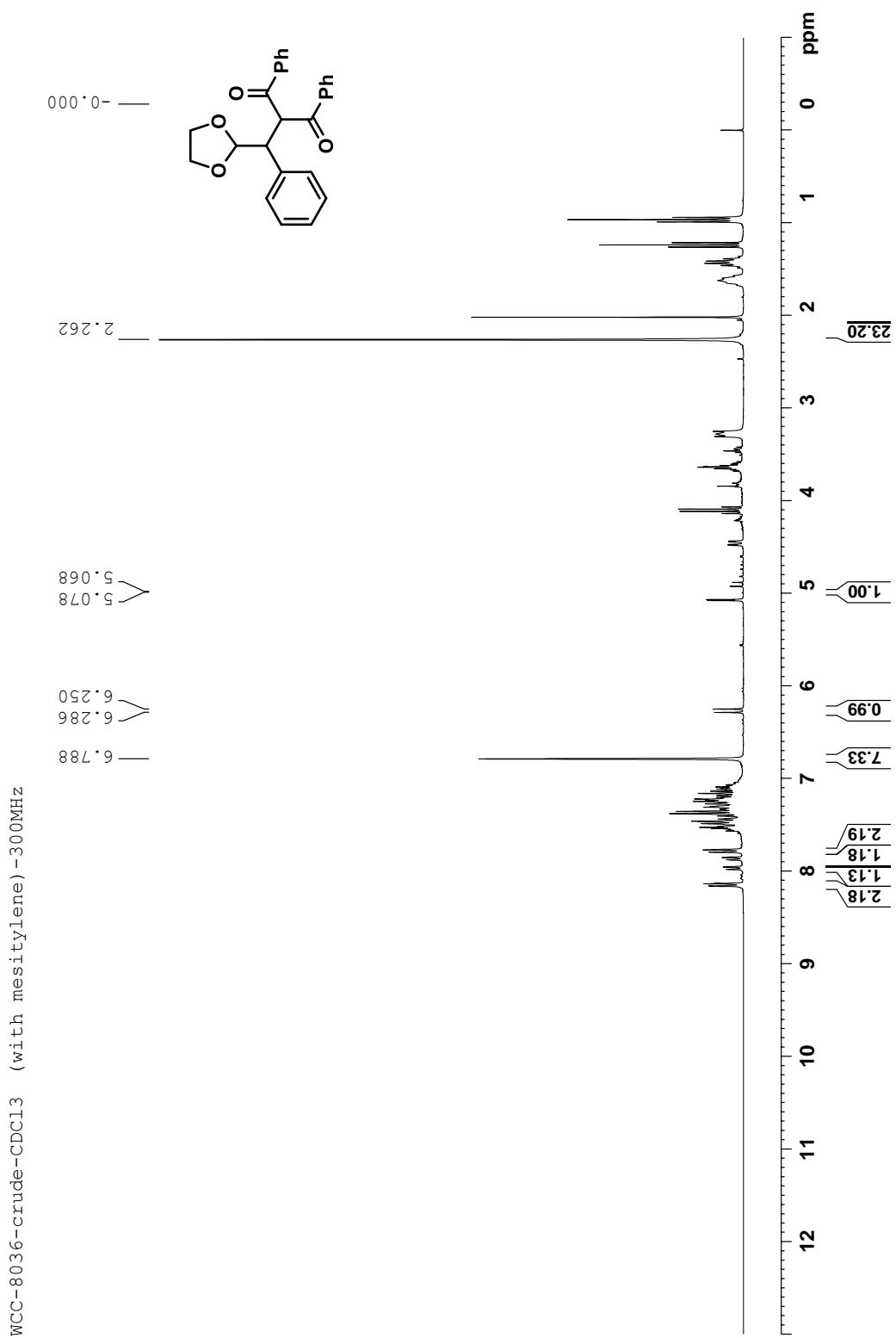
¹H NMR Spectrum of 2-174 (400 MHz, CDCl₃, 298 K)

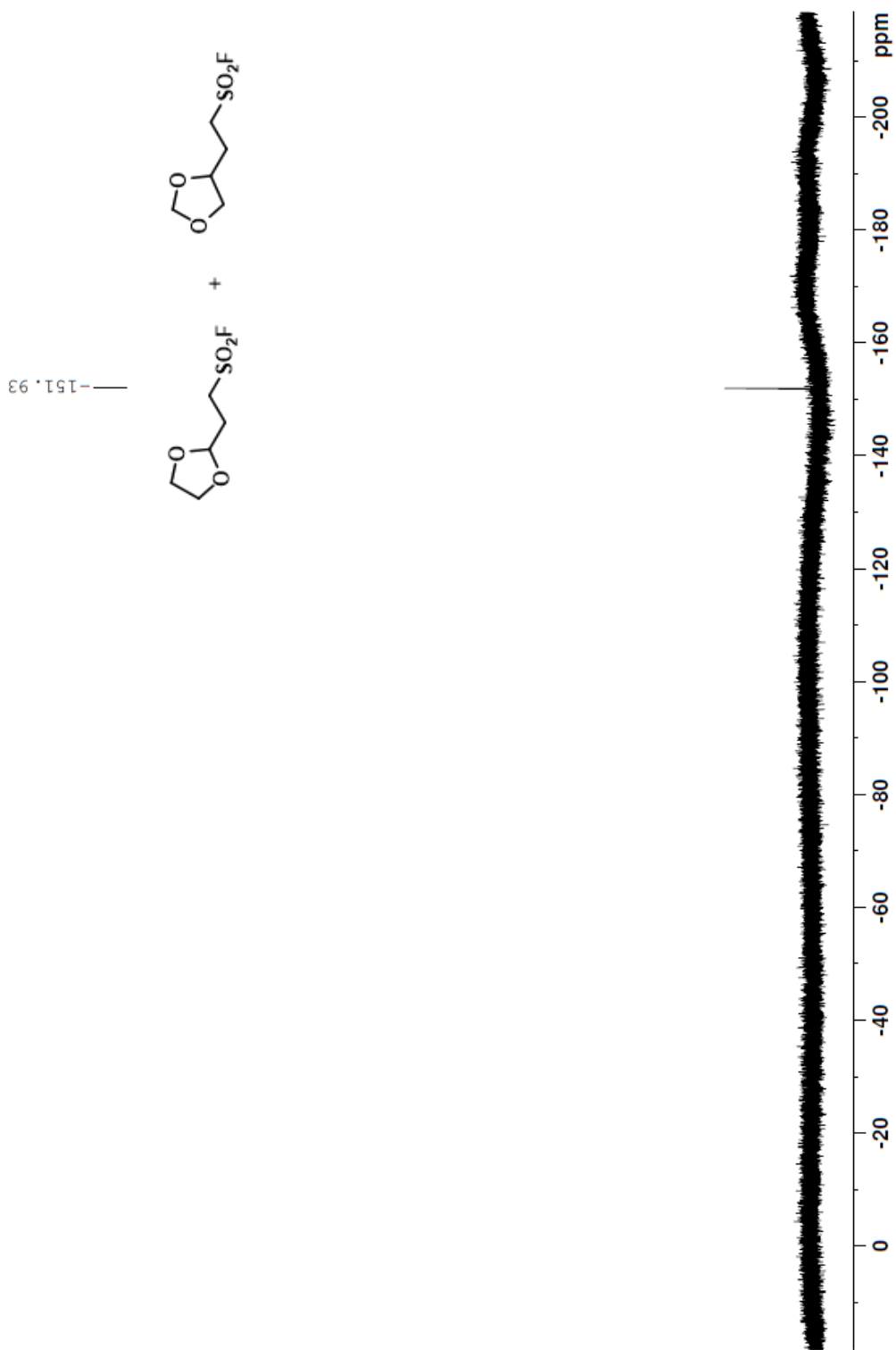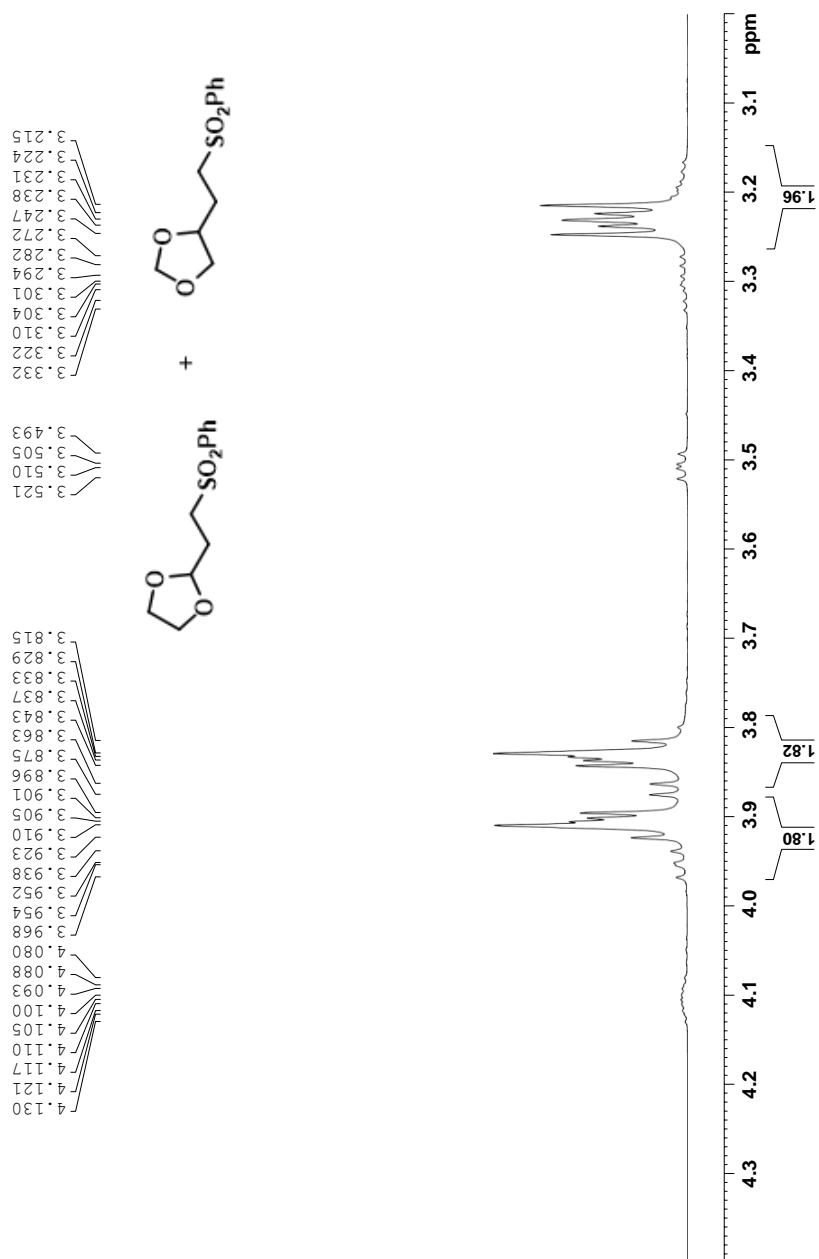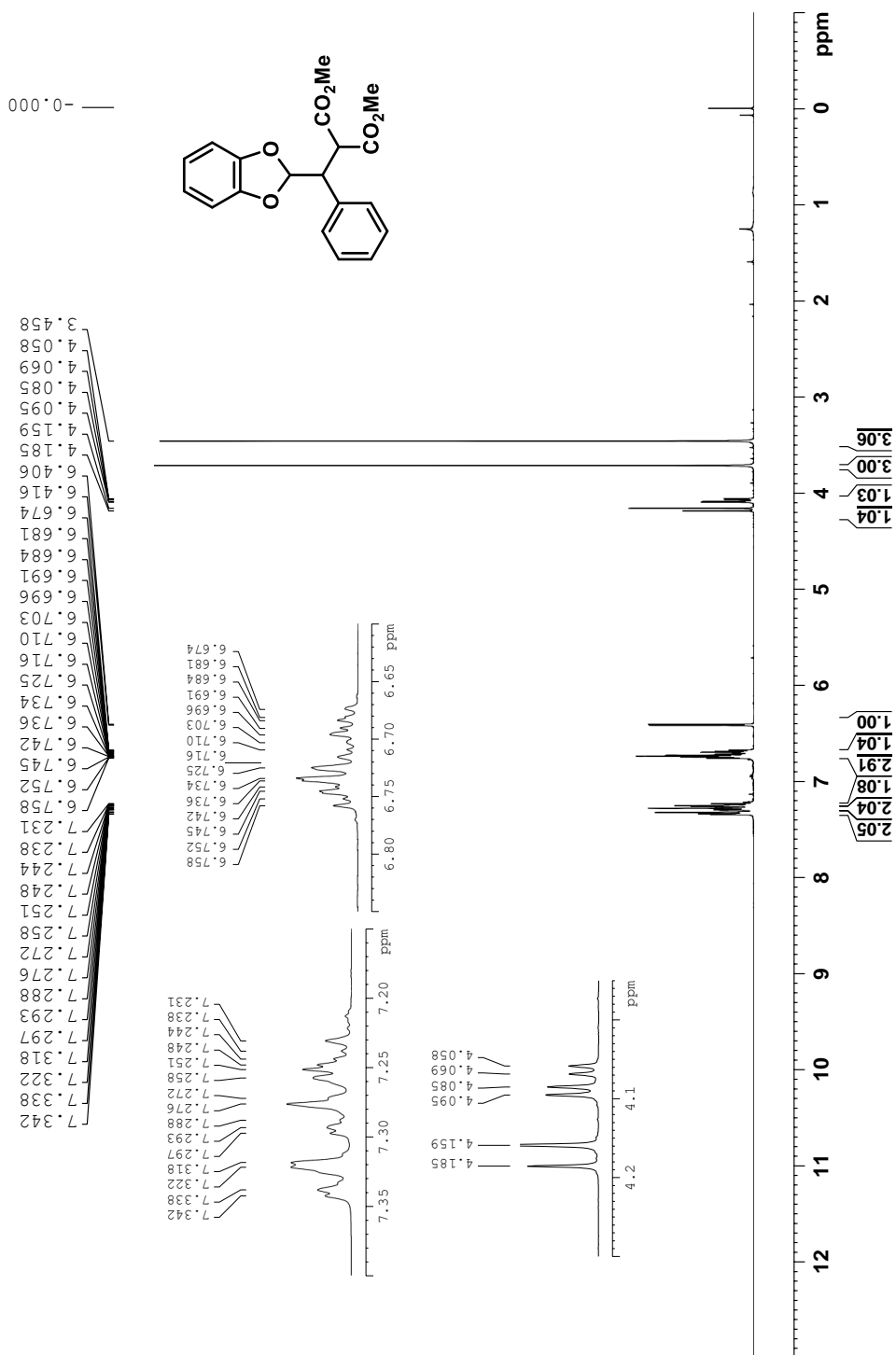**¹³C NMR Spectrum of 2-174 (100 MHz, CDCl₃, 298 K)**

49.31
52.52
52.79

76.68
77.00
77.31

108.36
108.47
110.75

121.51
121.58
127.89
128.38
129.38
134.73

147.06
147.20

167.44
168.15

210 200 190 180 170 160 150 140 130 120 110 100 90 80 70 60 50 40 30 20 10 ppm
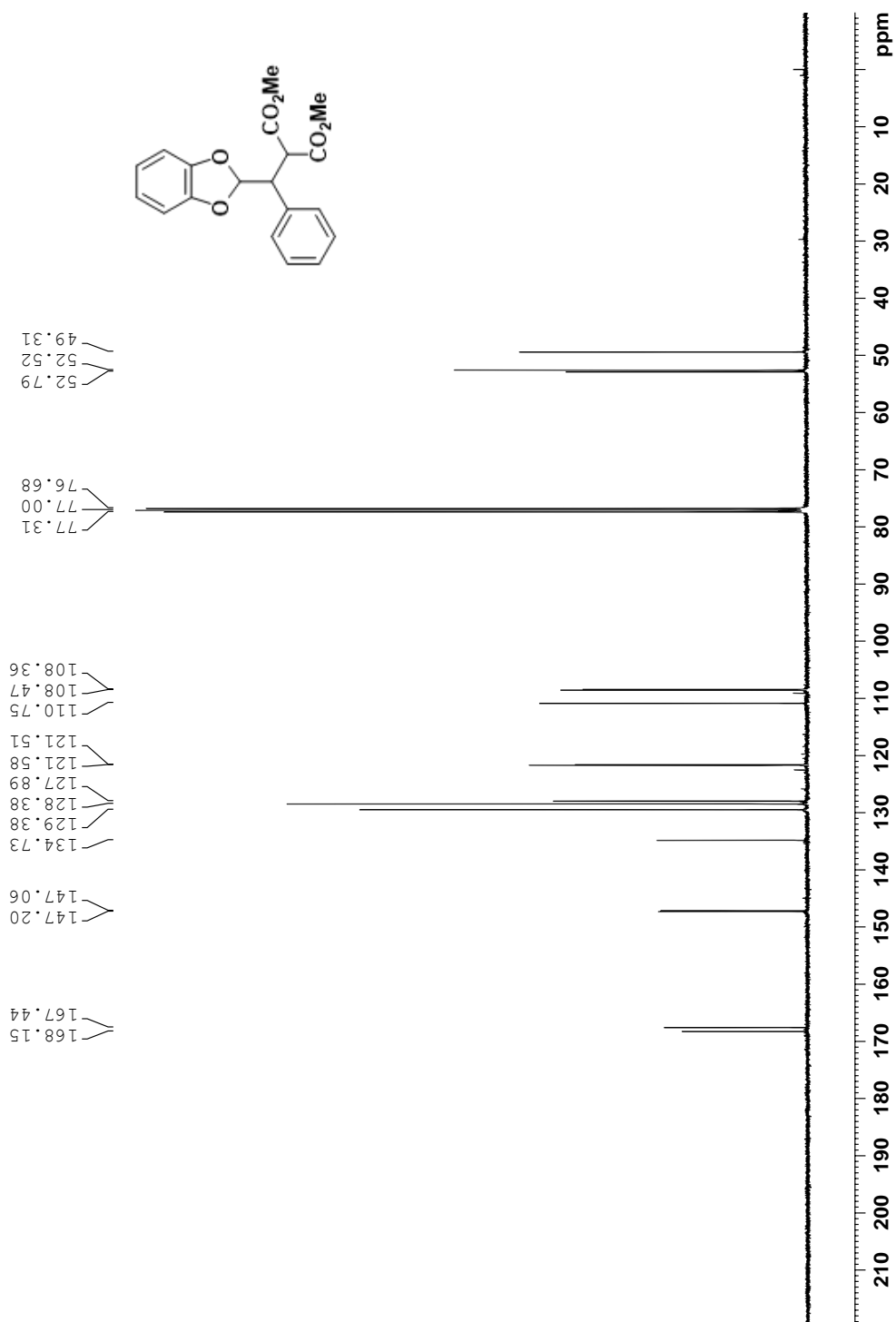
X-ray Crystal Structures
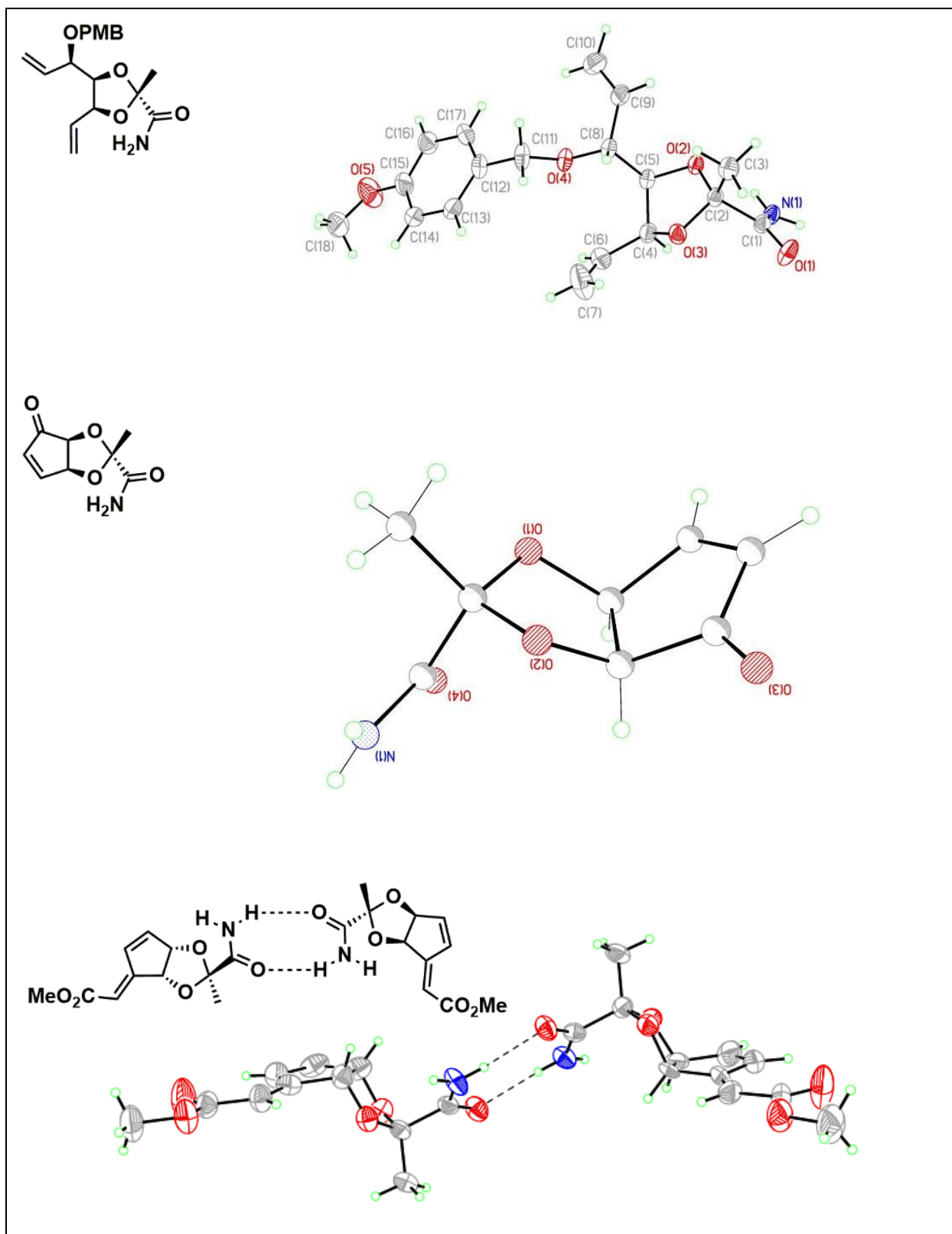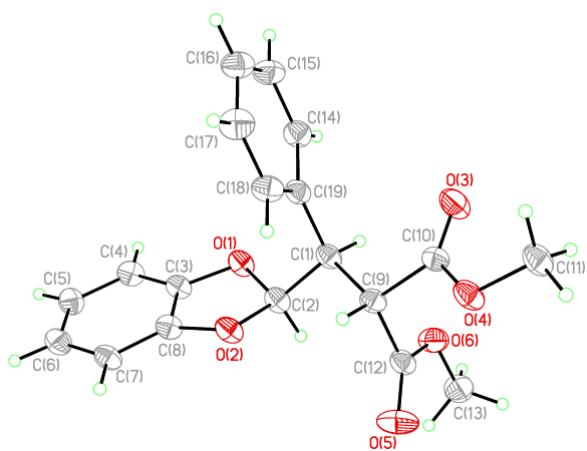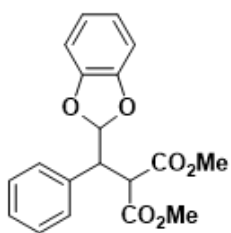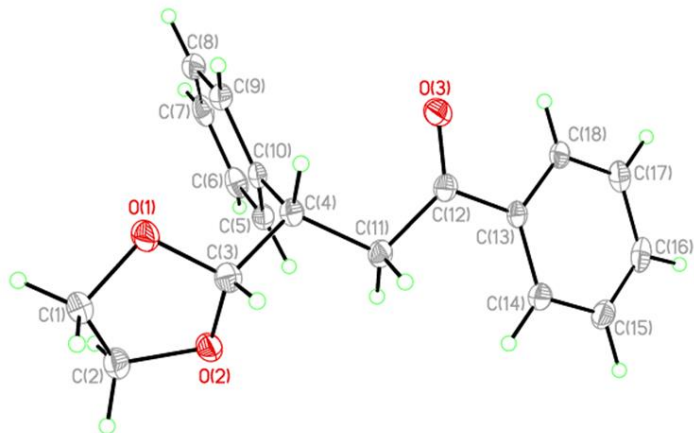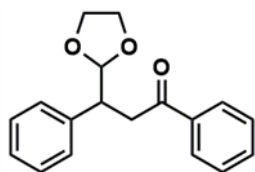
Bibliography

1. Calderwood, S. K.; Gong, J. Heat Shock Proteins Promote Cancer: It's a Protection Racket. *Trends Biochem. Sci.* **2016**, *41*, 311-323.

2. Wu, J.; Liu, T.; Rios, Z.; Mei, Q.; Lin, X.; Cao, S. Heat Shock Proteins and Cancer. *Trends Pharmacol. Sci.* **2017**, *38*, 226-256.

3. Ciocca, D. R.; Calderwood, S. K. Heat Shock Proteins in Cancer: Diagnostic, Prognostic, Predictive, and Treatment Implications. *Cell Stress & Chaperones.* **2005,** *10,* 86-103.

4. Butler, L. M.; Ferraldeschi, R.; Armstrong, H. K.; Centenera, M. M.; Workman, P. Maximizing the Therapeutic Potential of HSP90 Inhibitors. *Mol. Cancer Res.* **2015**, *13*, 1445-1451.

5. Barrott, J. J.; Haystead, T. A. J. Hsp90, an Unlikely Ally in the War on Cancer. *FEBS Journal*, **2013**, *280*, 1381-1396.

6. Armstrong, H. K.; Koay, Y. C.; Irani, S.; Das, R.; Nassar, Z. D. The Australian Prostate Cancer Bioresource, Selth, L. A.; Centenera, M. M.; McAlpine, S. R.; Butler, L. M. A Novel Class of Hsp90 C-Terminal Modulators Have Pre-Clinical Efficacy in Prostate Tumor Cells Without Induction of a Heat Shock Response. *Prostate* **2016**, *76*, 1546-1559.

7. Parimi, S.; Tsang, R. Y. Hsp90 Inhibitors in Oncology: Ready for Prime Time? *Curr. Oncol.* **2014,** *21,* e663-667.

8. Jhaveri, K.; Ochiana, S. O.; Dunphy, M. P. S.; Gerecitano, J. F.; Corben, A. D.; Peter, R. I.; Janjigian, Y. Y.; Gomes-DaGama, E. M.; Koren III, J.; Modi, S.; Chiosis, G. Heat Shock Protein 90 Inhibitors in the Treatment of Cancer: Current Status and Future Directions. *Expert Opin Investig Drugs,* **2014,** *23,* 611-628.

9. De Billy, E.; Powers, M. V.; Smith, J. R.; Workman, P. Drugging the Heat Shock Factor 1 Pathway: Exploitation of the Critical Cancer Cell Dependence on the Guardian of the Proteome. *Cell Cycle,* **2009,** *8:23,* 3806-3808.

10. Kumar, S.; Tamar, M. S.; Acharya, A. HSF1-Mediated Regulation of Tumor Cell Apoptosis: A Novel Target for Cancer Therapeutics. *Future Oncol.* **2013,** *9*, 1573-1586.

11. Zou, J.; Guo, Y.; Guettouche, T.; Smith, D. F.; Voellmy, R. Repression of Heat Shock Transcription Factor HSF1 Activation by HSP90 (HSP90 complex) that Forms a Stress-Sensitive Complex with HSF1. *Cell*, **1998,** *94,* 471-480.

12. Goloudina, A. R.; Demidov, O. N.; Garrido, C. Inhibition of HSP70: a Challenging Anti-Cancer Strategy. *Cancer Letters,* **2012**, *325*, 117-124.

13. Koay, Y. C.; Wahyudi, H.; McAlpine, S. R. Reinventing Hsp90 Inhibitors: Blocking C-Terminal Binding Events to Hsp90 by Using Dimerized Inhibitors. *Chem. Eur. J.* **2016,** *22,* 18572-18582.

14. Akagawa H.; Takano, Y.; Ishii, A.; Mizuno, S.; Izui, R.; Sameshima, T.; Kawamura, N.; Dobashi, K.; Yoshioka, T. tresgenin B, an Inhibitor of Heat-induced Heat Shock Protein Gene Expression, Produced by Streptomyces sp. AS-9. *J. Antibiot.* **1999**, *52*, 960-970.

15. Akagawa, H.; Mizuno, S. in Japanese Patent, P2000-197498, **2000**.

16. Lim, W.; Kim, J., Rhee, Y. H. Pd-Catalyzed Asymmetric Intermolecular Hydroalkoxylation of Allene: An Entry to Cyclic Acetals with Activating Group-Free and Flexible Anomeric Control. *J. Am. Chem. Soc.* **2014,** *136,* 13618-13621.

17. Jiang, L.; Jia, T.; Wang, M.; Liao, J.; Cao, P. Pd-Catalyzed Enantioselective Hydroalkoxylation of Alkoxyallenes with Phenol for Construction of Acyclic O,O-Acetals. *Org. Lett,* **2015,** *17,* 1070-1073.

18. Kawamura, Y.; Kawano, Y.; Matsuda, T.; Ishitobi, Y.; Hosokawa, T. Palladium(II)-Catalyzed Asymmetric Coupling of Allylic Alcohols and Vinyl Ethers: Insight into the Palladium and Copper Bimetallic Catalyst. *J. Org. Chem.* **2009,** *74,* 3048-3053.

19. Feng, Z.-G.; Bai, W.-J.; Pettus, T. R. R. Unified Total Syntheses of (−)-Medicarpin,(−)-Sophoracarpan A, and (±)-Kushecarpin A with Some Structural Revisions. *Angew. Chem., Int. Ed.,* **2015,** *54,* 1864-1867.

20. Davies, S. G.; Correia, L. M. A. R. B. Asymmetric Syntheses of Benzaldehyde and o-Anisaldehyde Methyl Isopropyl Acetals. *Chem. Commun.,* **1996,** 1803-1804.

21. Coric, I.; Vellalath, S.; List, B. Catalytic Asymmetric Transacetalization. *J. Am. Chem. Soc.,* **2010,** *132*, 8536-8537.

22. Coric, I.; Muller, S.; List, B. Kinetic Resolution of Homoaldols via Catalytic Asymmetric Transacetalization. *J. Am. Chem. Soc.* **2010,** *132,* 17370-17373.

23. Chen, Z.; Sun, J. Enantio- and Diastereoselective Assembly of Tetrahydrofuran and Tetrahydropyran Skeletons with All-Carbon-Substituted Quaternary Stereocenters. *Angew. Chem., Int. Ed.,* **2013,** *52,* 13593-13596.

24. Rubush, D. M.; Rovis, T. Stereoselective Synthesis of Dioxolanes and Oxazolidines via a Desymmetrization Acetalization/Michael Cascade. *Synlett,* **2014,** 713-717.

25. Matsumoto, A.; Asano, K.; Matsubara, S. A Chiral Phosphoric Acid Catalyst for Asymmetric Construction of 1,3-Dioxanes. *Chem. Commun.* **2015,** *51,* 11693-11696.

26. Qiu, L.; Guo, X.; Ma, C.; Qiu, H.; Liu, S.; Yang, L.; Hu, W. Efficient Synthesis of Chiral Cyclic Acetals by Metal and Brønsted Acid co-Catalyzed Enantioselective Four-Component Cascade Reactions. *Chem. Commun.* **2014,** *50,* 2196-2198.

27. Kim, J. H.; Coric, I.; Vellalath, S.; List, B. The Catalytic Asymmetric Acetalization. *Angew. Chem., Int. Ed.,* **2013,** *52,* 4474-4477.

28. Kim, J. H.; Cori, I.; Palumbo, C.; List, B. Resolution of Diols via Catalytic Asymmetric Acetalization. *J. Am. Chem. Soc.* **2015,** *137,* 1778-1781.

29. Coric, I.; List, B. Asymmetric Spiroacetalization Catalyzed by Confined Brønsted Acids. *Nature,* **2012,** *483,* 315-319.

30. (a) Armstrong, R. W.; Beau, J.-M.; Cheon, S. H.; Christ, W. J.; Fujioka, H.; Ham, W.-H.; Hawkins, L. D.; Jin, H.; Kang, S. H.; Kishi, Y.; Martinelli, M. J.; McWhorter, W. W. Jr.; Mizuno, M.; Nakata, M.; Stutz, A. E.; Talamas, F. X.; Taniguchi, M.; Tino, J. A.; Ueda, K.; Uenishi, J.-I.; White, J. B.; Yonaga, M. Total Synthesis of a Fully Protected Palytoxin Carboxylic Acid. *J. Am. Chem. Soc.* **1989,** *111,* 7525-7530; Total synthesis of Palytoxin Carboxylic Acid and Palytoxin Amide. *J. Am. Chem. Soc.* **1989,** *111,* 7531-7533; (b) Suh, E. M.; Kishi, Y. Synthesis of Palytoxin from Palytoxin Carboxylic Acid. *J. Am. Chem. Soc.,* **1994,** *111,* 11205-11206.

31. (a) Araoz, R.; Servent, D.; Molgo, J.; Iorga, B. I.; Fruchart-Gaillard, C.; Benoit, E.; Gu, Z.; Stivala, C. E.; Zakarian., A. Total Synthesis of Pinnatoxins A and G and Revision of the Mode of Action of Pinnatoxin A. *J. Am. Chem. Soc.,* **2011,** *133,* 10499-10511; (c) Matsuura, F.; Hao, J.; Kishi, Y. Total Synthesis and Stereochemistry of Pinnatoxins B and C. *Org. Lett.* **2006,** *8,* 3327-3330; (d) Selwood, A. I.; Miles, C. O.; Wilkins, A. L.; Ginkel, R. V.; Munday, R.; Rise, F.; McNabb, P. Isolation, Structural Determination and Acute Toxicity of Pinnatoxins E, F and G. *J. Agric. Food. Chem.,* **2010,** *58,* 6532-6542.

32. Matsuura, F.; Peters, R.; Anada, M.; Harried, S. S.; Hao, J.; Kishi, Y. Unified Total Synthesis of Pteriatoxins and Their Diastereomers. *J. Am. Chem. Soc.,* **2006,** *128,* 7463-7465.

33. Tian, W.-J.; Qiu, Y.-Q.; Yao, X.-J.; Chen, H.-F.; Dai, Y.; Zhang, X.-K.; Yao, X.-S. Dioxasampsones A and B, Two Polycyclic Polyprenylated Acylphloroglucinols with Unusual Epoxy-Ring-Fused Skeleton from *Hypericum sampsonii. Org. Lett.,* **2014,** *16,* 6346-6349.

34. Whitesell, J. K.; Buchanan, C. M. Synthesis of (-)- and (+)-Frontalin. *J. Org. Chem.,* **1986,** *51,* 5443–5445.

35. Yadav, J. S.; Baishya, G.; Dash, T. Synthesis of (+)-Amberketal and its Analog from L-Abietic Acid. *Tetrahedron,* **2007,** *63,* 9896-9902.

36. Paquette, L. A.; Wang, T.-Z.; Sivik, M. R. Enantioselective Synthesis of Natural (-)-Austalide B, an Unusual Ortho Ester Metabolite Produced by Toxigenic Cultures of Aspergillus ustus. *J. Am. Chem. Soc.* **1994,** *116,* 2665-2666.

37. Zhang, C.-R.; Yang, S.-P.; Liao, S.-G.; Fan, C.-Q.; Wu, Y.; Yue, J.-M. Chuktabularins A−D, Four New Limonoids with Unprecedented Carbon Skeletons from the Stem Bark of *Chukrasia tabularis*. *Org Lett.* **2007,** *9,* 3383-3386.

38. Tomono, Y.; Hirota, H.; Fusetani, N. Isogosterones A−D, Antifouling 13,17-Secosteroids from an Octocoral Dendronephthya sp. *J. Org. Chem.* **1999,** *64,* 2272-2275.

39. Loukaci, A.; Kayser, O.; Bindseil, K.-U.; Siems, K.; Frevert, J.; Abreu, P. M. New Trichothecenes Isolated from *Holarrhena floribunda*. *J. Nat. Prod.,* **2000,** *63,* 52-56.

40. Riveira, M. J.; La-Venia, A.; Mischne, M. P. New Strategy for the Construction of Epoxy-Bridged Tetrahydropyran Frameworks from Trioxane Precursors: Application to a Concise Synthesis of a Riesling Acetal. *J. Org. Chem.* **2008,** *73,* 8678-8681.

41. Raghavan, S.; Joseph, S. C. A Novel and Stereospecific Synthesis of (+)-exo-Brevicomin. *Tetrahedron Lett.* **2003,** *44,* 8237;8239; (b) Prasad, K. R.; Anbarasan, P. Asymmetric Synthesis of Unsaturated α-Benzyloxyaldehydes: an Enantioselective Synthesis of (+)-exo-Brevicomin. *Tetrahedron: Asymmetry,* **2005,** *16,* 3951–3953; (c) Burke, S. D.; Muller, N.; Beaudry, C. M. Desymmetrization by Ring-Closing Metathesis Leading to 6,8-Dioxabicyclo[3.2.1]octanes: A New Route for the Synthesis of (+)-exo- and endo-Brevicomin. *Org. Lett.* **1999,** *1,* 1827-1829.

42. Zhu, B.; Morioka, M.; Nakamura, H.; Naganawa, H.; Muroaka, Y.; Okami, Y.; Umezawa, H. A New Antitumor Antibiotic, Dioxolamycin. *J. Antibiot.* **1984**, *37*, 673-674.

43. Clinton, D; Rapoport, H. Stereochemistry of Quinate-Shikimate Conversions. Synthesis of (-)-4-epi-Shikimic acid. *J. Am. Chem. Soc.* **1973,** *95,* 7821-7828.

44. Oh, C. H.; Park, D. I.; Jung, S. H.; Reddy, R.; Gupta, A. K.; Kim, Y. M. Chemodiversity in the Palladium-Catalyzed Cyclizations of Allenynecarboxylates. *Synlett,* **2005,** *13,* 2092–2094.

45. Egorov, V. A.; Gimalova, F. A.; Khalikova, G. M.; Miftakhov, M. S. Design and Synthesis of Novel Polyheterofunctionalyzed Cyclopentenones. *Tetrahedron,* **2012,** *68,* 7122-7128.

46. Novák, L.; Rohály, J.; Gálik, G.; Fekete, J.; Varjas, L.; Szántay, C. A Convenient Method for the Synthesis of Insect Growth Regulators Cyclopentene Analogs of Alkyl (2E,4E)-Dodecadienoates. *Liebigs Ann. Chem.,* **1986,** 509–524.

47. (a) Swaminathan, S.; Narayanan, K. V. Rupe and Meyer-Schuster Rearrangements. *Chem. Rev.* **1971,** *71*, 429–438; (d) Rieder, C. J.; Winberg, K. J.; West, F. G. Olefination of α, α′-Divinyl Ketones through Catalytic Meyer-Schuster Rearrangement. *J. Org. Chem.* **2011,**

76, 50-56; (c) Rieder, C. J.; Winberg, K. J.; West, F. G. Cyclization of Cross-Conjugated Trienes: The Vinylogous Nazarov Reaction. *J. Am. Chem. Soc.* **2009,** *131,* 7504-7505.

48.　Bryan, C. S.; Lautens, M. A Tandem Catalytic Approach to Methyleneindenes: Mechanistic Insights into gem-Dibromoolefin Reactivity. *Org. Lett.* **2010,** *12,* 2754–2757.

49.　Wardrop, D. J.; Velter, A. I.; Forslund, R. E Template-Directed C−H Insertion: Synthesis of the Dioxabicyclo [3.2. 1] Octane Core of the Zaragozic Acids. *Org. Lett.* **2001**, *3*, 2261-2264.

50.　Wardrop, D. J.; Forslund, R. E. Synthesis of (±)-7-Episordidin. *Tetrahedron Lett.* **2002**, *43*, 737-739.

51.　Wardrop, D. J.; Forslund, R. E.; Landrie, C. L.; Velter, A. I.; Wink, D.; Surve, B. Template-directed C–H activation: development and application to the total synthesis of 7-episordidin*Tetrahedron: Asymmetry* **2003,** *14,* 929-940.

52.　Chen, M. S.; Prabagaran, N.; Labenz, N. A.; White, M. C. Serial Ligand Catalysis: A Highly Selective Allylic C−H Oxidation. *J. Am. Chem. Soc.* **2005,** *127,* 6970-6971.

53.　Fraunhoffer, K. F.; Prabagaran, N.; Sirois, L. E.; White, M. C. Macrolactonization via Hydrocarbon Oxidation. *J. Am. Chem. Soc.* **2006,** *128,* 9032-9033.

54.　Delcamp, J. H.; White, M. C. Sequential Hydrocarbon Functionalization: Allylic C−H Oxidation/Vinylic C−H Arylation. *J. Am. Chem. Soc.* **2006,** *128,* 15076-15077.

55.　Brill, Z. G.; Condakes, M. L.; Ting, C. P.; Maimone, T. J. Navigating the Chiral Pool in the Total Synthesis of Complex Terpene Natural Products. *Chem. Rev.* **2017,** *117,* 11753-11795.

56.　Srihari, P.; Kumaraswamy, B.; Yadav, J. S. A Carbohydrate Approach for the Synthesis of Tetrahydropyran Containing C16–C29 Fragment of Sorangicin A. *Tetrahedron* **2009**, *65*, 6304-6309.

57.　Smith, L. H. S.; Coote, S. C.; Sneddon, H. F.; Procter, D. J. Beyond the Pummerer Reaction: Recent Developments in Thionium Ion Chemistry. *Angew. Chem., Int. Ed.*, **2010,** *49*, 5832-5844.

58.　Bal, B. S.; Childers, W. E., Jr.; Pinnick, H. W. Oxidation of α,β-Unsaturated Aldehydes. *Tetrahedron*, **1981,** *37*, 2091–2096.

59.　(a) Grela, K.; Harutyunyan, S.; Michrowska, A. A Highly Efficient Ruthenium Catalyst for Metathesis Reactions. *Angew. Chem., Int. Ed.* **2002,** *41,* 4038-4040; Michrowska, A.; (b) Bujok, R.; Harutyunyan, S.; Sashuk, V.; Dolgonos, G.; Grela, K. Nitro-Substituted Hoveyda−Grubbs Ruthenium Carbenes: Enhancement of Catalyst Activity through Electronic Activation. *J. Am. Chem. Soc.* **2004,** *126,* 9318-9325.

60. Julia, M.; Paris, J.-M. Syntheses a l'aide de Sulfones v(+)- Methode de Synthese Generale de Doubles Liaisons. *Tetrahedron Lett.* **1973,** *14,* 4833-4836.

61. Kocienski, P. J.; Lythgoe, B.; Ruston, S. Scope and Stereochemistry of an Olefin Synthesis From β-Hydroxysulphones. *J. Chem. Soc., Perkin Trans.* 1 **1978,** 829-834.

62. Julia, M.; Verpeaux, J.-N. Synthèse d'oléfines et de Polyènes par Doublement d'anions α-Sulfonylés en Présence de sels de Nickel (XXII). *Tetrahedron Lett.* **1982,** *23,* 2457-2460.

63. Shriner, R. L. *Org. React.* **1942,** 1, 1-37.

64. Rathke, M. W. *Org. React.* **1975,** 22, 423-460.

65. Peterson, D. J. Carbonyl Olefination Reaction Using Silyl-Substituted Organometallic Compounds. *J. Org. Chem.* **1968,** *33,* 780-784.

66. Van Staden, L. F.; Gravestock, D.; Ager, D. J. New developments in the Peterson olefination reaction. *Chem. Soc. Rev.* **2002,** *31,* 195-200.

67. Wadsworth, W. S., Jr. *Org. React.* **1977**, 25, 73-253.

68. Arai, T.; Sasai, H.; Yamaguchi, K.; Shibasaki, M. Regioselective Catalytic Asymmetric Reaction of Horner−Wadsworth−Emmons Reagents with Enones: The Odyssey of Chiral Aluminum Catalysts. *J. Am. Chem. Soc.* **1998,** *120,* 441-442.

69. Alcaraz, L.; Cridland, A.; Kinchin, E. Novel Conversion of 1,2-Disubstituted cis-Epoxides to One-Carbon Homologated Allylic Alcohols Using Dimethylsulfonium Methylide. *Org. Lett.* **2001**, *3*, 4051-4053.

70. Bode, J. W.; Carreira, E. M. Stereoselective Syntheses of Epothilones A and B via Nitrile Oxide Cycloadditions and Related Studies. *J. Org. Chem.* **2001**, *66*, 6410-6424.

71. Hunter, C. A.; Sanders, J. K. M. The Nature of .pi.-.pi. Interactions. *J. Am. Chem. Soc.* **1990,** *112,* 5525-5534.

72. F.; Cinquini, M.; Annunziata, er, T.; Siegel, J. S. Polar/.pi. Interactions Between Stacked Aryls in 1,8-Diarylnaphthalenes. *J. Am. Chem. Soc.* **1992,** *114,* 5729-5733.

73. Ringer, A. L.; Sinnokrot, M. O.; Lively, R. P.; Sherrill, C. D. The Effect of Multiple Substituents on Sandwich and T-Shaped π–π Interactions. *Chem. - Eur. J.* **2006,** *12,* 3821-3828.

74. Wheeler, S. E.; Houk, K. N. Substituent Effects in the Benzene Dimer are Due to Direct Interactions of the Substituents with the Unsubstituted Benzene. *J. Am. Chem. Soc*. **2008,** *130,* 10854-10855.

75.   Wheeler, S. E. Local Nature of Substituent Effects in Stacking Interactions. *J. Am. Chem. Soc.* **2011,** *133,* 10262-10274.

76.   Liu, L.; Floreancig, P. E. Stereoselective Synthesis of Tertiary Ethers through Geometric Control of Highly Substituted Oxocarbenium Ions. *Angew. Chem., Int. Ed.* **2010,** *49*, 5894-5897.

77.   For the seminal work, see Molander, G. A.; Haar, J. P. Novel approach to remote asymmetric induction in carbonyl addition and related reactions. *J. Am. Chem. Soc.* **1993**, *115*, 40-49

78.   Krumper, J. R.; Salamant, W. A.; Woerpel, K. A. Continuum of Mechanisms for Nucleophilic Substitutions of Cyclic Acetals. *Org. Lett.* **2008**, *10*, 4907-4910.

79.   Garcia, A.; Otte, D. A. L.; Salamant, W. A.; Sanzone, J. R.; Woerpel, K. A. Influence of Alkoxy Groups on Rates of Acetal Hydrolysis and Tosylate Solvolysis: Electrostatic Stabilization of Developing Oxocarbenium Ion Intermediates and Neighboring-Group Participation To Form Oxonium Ions. *J. Org. Chem.* **2015**, *80*, 4470-4480

80.   Lavinda, O.; Tran, V. T.; Woerpel, K. A. Effect of Conformational Rigidity on the Stereoselectivity of Nucleophilic additions to Five-Membered Ring Bicyclic Oxocarbenium Ion Intermediates. *Org. Biomol. Chem.* **2014**, *12*, 7083-7091.

81.   Garcia, A.; Otte, D. A. L.; Salamant, W. A.; Sanzone, J. R.; Woerpel, K. A. Acceleration of Acetal Hydrolysis by Remote Alkoxy Groups: Evidence for Electrostatic Effects on the Formation of Oxocarbenium Ions. *Angew. Chem., Int. Ed.* **2015**, *54*, 3061-3064.

82.   Garcia, A.; Sanzone, J. R.; Woerpel, K. A. Participation by Alkoxy Groups in Reactions of Acetals: Violation of the Reactivity-Selectivity Principle in a Curtin–Hammett Kinetic Scenario. *Angew. Chem., Int. Ed.* **2015**, *54,* 12087-12090.

83.   Tran, V. T.; Woerpel, K. A. Nucleophilic Addition to Silyl-Protected Five-Membered Ring Oxocarbenium Ions Governed by Stereoelectronic Effects. *J. Org. Chem.* **2013**, *78*, 6609-6621.

84.   Mukaiyama, T.; Murakami, M. Cross-Coupling Reactions Based on Acetals. *Synthesis* **1987**, 1043-1054; (b) Hayashi, Y.; Wariishi, K.; Mukaiyama, T. Oxidative Carbon–Carbon Bond Forming Reaction via a 1,3-Dioxolan-2-ylium Cation. *Chem. Lett.* **1987**, 1243-1246.

85.   For a review on the applications of Parkins' catalyst, see: V. Cadierno. Synthetic Applications of the Parkins Nitrile Hydration Catalyst [PtH{(PMe2O)2H}(PMe2OH)]: A Review. *Appl. Sci.* **2015**, *5*, 380-401.

86.   For a recent application of Parkins' catalyst (substoichiometric) in total syntesis, see: Richter, M. J. R.; Schneider, M.; Brandstätter, M.; Krautwald, S.; Carreira, E. M. Total Synthesis of (−)-Mitrephorone A. *J. Am. Chem. Soc.* **2018,** 140, 16704-16710.

87.   Lee, J.; Kim, M.; Chang, S. B.; Lee, H. Y. Anhydrous Hydration of Nitriles to Amides using Aldoximes as the Water Source. *Org. Lett.* **2009**, *11*, 5598-5601.

88.   For a recent application of this method using Wilkinson's catalyst in total synthesis, see: Kou, K. G. M.; Kulyk, S.; Marth, C. J.; Lee, J. C.; Doering, N. A.; Li, B. X.; Gallego, G. M.; Lebold, T. P.; Sarpong, R. A Unifying Synthesis Approach to the C18-, C19-, and C20-Diterpenoid Alkaloids. *J. Am. Chem. Soc.* **2017**, *139*, 13882-13896.

89.   For recent reviews, see (a) Al-Huniti, M. H.; Croatt, M. P. Metal-Catalyzed Dehydration of Primary Amides to Nitriles. *Asian J. Org. Chem.* **2019**, *8*, 1791-1799; (b) Naka, H.; Naraoka, A. Recent Advances in Transfer Hydration of Nitriles with Amides or Aldoximes. *Tetrahedron Lett.* **2019,** *60,* 151557.

90.   Naraoka, A.; Naka, H. Transfer Hydration of Dinitriles to Dicarboxamides. *Synlett* **2019,** *30,* 1977-1980.

91.   Kanda, T.; Naraoka, A.; Naka, H. Catalytic Transfer Hydration of Cyanohydrins to α-Hydroxyamides. *J. Am. Chem. Soc.* **2019,** *141,* 825-830.

92.   Okabe H.; Naraoka, A.; Isogawa, T.; Oishi, S.; Naka, H. Acceptor-Controlled Transfer Dehydration of Amides to Nitriles. *Org. Lett.* **2019,** *21,* 4767-4770.

93.   Fuji, K.; Ichikawa, K.; Node, M.; Fujita, E. Hard Acid and Soft Nucleophile System. New Efficient Method for Removal of Benzyl Protecting Group. *J. Org. Chem.* **1979**, *44*, 1661-1664.

94.   Imamoto T.; Sugiura, Y. Selective 1,2-Addition of Organocerium(III) Reagents to α,β-Unsaturated Carbonyl Compounds. *J. Phys. Org. Chem.* **1989**, *2*, 93-102.

95.   Imamoto, T.; Sugiura, Y. Selective 1,2-Addition of Organocerium(III) Reagents to α,β-Unsaturated Carbonyl Compounds. *J. Organomet. Chem.* **1985**, *285*, C21-C23.

96.   Imamoto, T.; Kusumoto, T.; Tawarayama, Y.; Sugiura, Y.; Mita, T.; Hatanaka, Y.; Yokoyama, M. Carbon-Carbon Bond-Forming Reactions Using Cerium Metal or Organocerium(III) Reagents. *J. Org. Chem.* **1984**, *49*, 3904-3912.

97.   Liu, H. J.; Shia, K. S.; Shang, X.; Zhu, B. Y. Organocerium Compounds in Synthesis. *Tetrahedron* **1999**, *55*, 3803-3830.

98.   For a recent review, see: Engel, D. A.; Dudley, G. B. The Meyer–Schuster Rearrangement for the Synthesis of α,β-Unsaturated Carbonyl Compounds. *Org. Biomol. Chem.* **2009**, *7*, 4149-4158.

99.   Engel, D. A.; Lopez, S. S.; Dudley, G. B. Lewis Acid-Aatalyzed Meyer–Schuster Reactions: Methodology for the Olefination of Aldehydes and Ketones. *Tetrahedron* **2008**, *64*, 6988–6996.

100. For a review on the role of total synthesis in structural revision, see: Nicolaou, K. C.; Snyder, S. A. Chasing Molecules That Were Never There: Misassigned Natural Products and the Role of Chemical Synthesis in Modern Structure Elucidation. *Angew. Chem., Int. Ed.* **2005**, *44*, 1012-1044.

101. For a review on the role of total synthesis in structural revision, see: Nicolaou, K. C.; Snyder, S. A. *Angew. Chem., Int. Ed.* **2005**, *44*, 1012-1044.

102. For a structurally related natural product, see: Zhu, B.; Morioka, M.; Nakamura, H.; Naganawa, H.; Muraoka, Y.; Okami, Y.; Umezawa, H. A new antitumor antibiotic, dioxolamycin. *J. Antibiot.* **1984,** *37*, 673-674.

103. (a) Lodewyk, M. W.; Siebert, M. R.; Tantillo, D. J. Computational Prediction of 1H and 13C Chemical Shifts: A Useful Tool for Natural Product, Mechanistic, and Synthetic Organic Chemistry. *Chem. Rev.* **2012,** *112,* 1839-1862; (b) http://cheshirenmr.info/recommendations.

104. For a practical guide to computations of NMR chemical shifts, see Willoughby, P. H.; Jansma, M. J.; Hoye, T. R. A Guide to Small-Molecule Structure Assignment through Computation of (^{1}H and ^{13}C) NMR Chemical Shifts.. *Nature Protocols* **2014**, *9*, 643-660.

105. (a) For Gaussian 09 version D.01: M. J. Frisch, G. W. Trucks, H. B. Schlegel, G. E. Scuseria, M. A. Robb, J. R. Cheeseman, G. Scalmani, V. Barone, B. Mennucci, G. A. Petersson, H. Nakatsuji, M. Caricato, X. Li, H. P. Hratchian, A. F. Izmaylov, J. Bloino, G. Zheng, J. L. Sonnenberg, M. Hada, M. Ehara, K. Toyota, R. Fukuda, J. Hasegawa, M. Ishida, T. Nakajima, Y. Honda, O. Kitao, H. Nakai, T. Vreven, J. A. Montgomery, Jr., J. E. Peralta, F. Ogliaro, M. Bearpark, J. J. Heyd, E. Brothers, K. N. Kudin, V. N. Staroverov, T. Keith, R. Kobayashi, J. Normand, K. Raghavachari, A. Rendell, J. C. Burant, S. S. Iyengar, J. Tomasi, M. Cossi, N. Rega, J. M. Millam, M. Klene, J. E. Knox, J. B. Cross, V. Bakken, C. Adamo, J. Jaramillo, R. Gomperts, R. E. Stratmann, O. Yazyev, A. J. Austin, R. Cammi, C. Pomelli, J. W. Ochterski, R. L. Martin, K. Morokuma, V. G. Zakrzewski, G. A. Voth, P. Salvador, J. J. Dannenberg, S. Dapprich, A. D. Daniels, O. Farkas, J. B. Foresman, J. V. Ortiz, J. Cioslowski, and D. J. Fox, Gaussian, Inc., Wallingford CT, 2013; (b) for visualization software used in chapter 1: CYLview, 1.0b; Legault, C. Y., Université de Sherbrooke, 2009 (http://www.cylview.org)

106. Vollhardt, K. P. C.; Shore, N. *Organic Chemistry: Structure and Function, 7th ed.* Freeman: New York, NY, **2014;** p97-128.

107. Laevee, J.; Fouassier, J. P., *Encyclopedia of Radicals in Chemistry, Biology and Materials*. Wiley: New York, NY, 2012; p 37-56.

108. Kita, Y.; Matsugi, M., *Radicals in Organic Synthesis*. Wiley-VCH: Weinheim, 2001; p 1-10.

109. Brown, H. C.; Suzuki, A.; Nozawa, S.; Harada, M.; Itoh, M.; Midland, M. M. Oxygen-induced reaction of trialkylboranes with alkyl iodides. Facile coupling of benzylic and allylic iodides via triethylborane. *J. Am. Chem. Soc.* **1971,** *93,* 1508-1509.

110. Brown, H. C.; Midland, M. M. Convenient general synthesis of alkyl hydroperoxides via autoxidation of organoboranes. *J. Am. Chem. Soc.* **1971,** *93,* 4078-4080.

111. Mirviss, S. B. The Air Oxidation of Trialkylboranes. *J. Am. Chem. Soc.* **1961,** *83,* 3051-3056.

112. Mirviss, S. B. Mechanism of the oxidation of trialkylboranes. *J. Org. Chem.* **1967,** *32,* 1713-1717.

113. Nozaki, K.; Oshima, K.; Utimoto, K. Synthesis of α-Methylene-γ-butyrolactones via Addition of Tin Hydride to Enynes Induced by Triethylborane. *Bull. Chem. Soc. Jpn.* **1987,** *60,* 3465-3467.

114. Nozaki, K.; Oshima, K.; Uchimoto, K. Et3B-Induced Radical Addition of R3SnH to Acetylenes and its Application to Cyclization Reaction. *J. Am. Chem. Soc.* **1987,** *109,* 2547-2549.

115. Nozaki, K.; Oshima, K.; Utimoto, K. Et3B induced radical addition of Ph3SnH to Acetylenes and its Application to Cyclization Reaction. *Tetrahedron* **1989,** *45,* 923-933.

116. Oderinde, M. S.; Organ, M. G. Pronounced Solvent Effect on the Hydrostannylation of Propargylic Alcohol Derivatives with nBu3SnH/Et3B at Room Temperature. *Chem. Eur. J.* **2013,** *19,* 2615-2618.

117. Oderinde, M. S.; Froese, R. D. J.; Organ, M. G. 2,2′-Azobis(2-methylpropionitrile)-Mediated Alkyne Hydrostannylation: Reaction Mechanism. *Angew. Chem., Int. Ed.* **2013,** *52*, 11334-11338.

118. Beeler, A. B. Introduction: Photochemistry in Organic Synthesis. *Chem. Rev.* **2016,** *116,* 9629-9630.

119. Roth, H.D. The Beginnings of Organic Photochemistry. *Angew. Chem., Int. Ed. Engl.* **1989**, *28*, 1193-1207

120. Ramamurthy, V.; Turro, N. J. Photochemistry: Introduction. *Chem. Rev.* **1993**, *93,* 1-2.

121. Zimmerman, H. E. Five Decades of Mechanistic and Exploratory Organic Photochemistry. *Pure Appl. Chem.* **2006**, *78,* 2193–2203

122. Prier, C. K.; Rankic, D. A.; MacMillan, D. W. C. Visible Light Photoredox Catalysis with Transition Metal Complexes: Applications in Organic Synthesis. *Chem. Rev.* **2013,** *113,* 5322-5363.

123. Kärkäs, M. D.; Porco, J. A. Jr.; Stephenson, C. R. J. Photochemical Approaches to Complex Chemotypes: Applications in Natural Product Synthesis. *Chem. Rev.* **2016,** *116,* 9683-9747.

124. For reviews on organic photocatalysts and photosensitizers, see: (a) Sideri, I.; Voutyritsa, R.; Kokotos, C. G. Photoorganocatalysis, Small Organic Molecules and Light in the Service of Organic Synthesis: the awakening of a Sleeping Giant. *Org. Biomol. Chem.* **2018,** *16,* 4596-4614; (b) Miranda, M. A.; Garcia, H. 2,4,6-Triphenylpyrylium Tetrafluoroborate as an Electron-Transfer Photosensitizer. *Chem. Rev.* **1994,** *94,* 1063-1089; (c) Romero, N. A.; Nicewicz, D. A. Organic Photoredox Catalysis. *Chem. Rev.* **2016,** *116,* 10075-10166.

125. Sarabia, F. J.; Ferreira, E. M. Radical Cation Cyclopropanations via Chromium Photooxidative Catalysis. *Org. Lett.* **2017,** *19,* 2865-2868.

126. Higgins, R. F.; Fatur, S. M.; Damrauer, N. H.; Ferreira, E. M.; Rappe, A. K.; Shores, M. P. Detection of an Energy-Transfer Pathway in Cr-Photoredox Catalysis. *ACS Catal.* **2018,** *8,* 9216-9225.

127. Hu, A.; Guo, J. -J..; Pan, H.; Zuo, Z. Selective Functionalization of Methane, Ethane, and Higher alkanes by Cerium Photocatalysis. *Science,* **2018,** *361,* 668-672.

128. Hu, A.; Chen, Y.; Guo, J. -J.; Yu, N.; An, Q.; Zuo, Z. Cerium-Catalyzed Formal Cycloaddition of Cycloalkanols with Alkenes through Dual Photoexcitation. *J. Am. Chem. Soc.* **2018,** *140,* 13580-13585.

129. Zhang, K.; Chang, L.; An, Q.; Wang, X.; Zuo, Z. Dehydroxymethylation of Alcohols Enabled by Cerium Photocatalysis. *J. Am. Chem. Soc.* **2019,** *141,* 10556-10564.

130. Chen. Y; Du, J.; Zuo, Z. Selective C-C Bond Scission of Ketones via Visible-Light-Mediated Cerium Catalysis. *Chem.* **2020,** *6,* 266-279.

131. Skubi, K. L.; Blum, T. R.; Yoon, T. P. Dual Catalysis Strategies in Photochemical Synthesis. *Chem. Rev.* **2016,** *116,* 10035-10074.

132. Liu, D.; Liu, C.; Li, H.; Lei, A. Direct Functionalization of Tetrahydrofuran and 1,4-Dioxane: Nickel-Catalyzed Oxidative C(sp3)-H Arylation. *Angew. Chem., Int. Ed.* **2013,** *52,* 4453-4456.

133. Jin, J; MacMillan, D. W. C. Direct α-Arylation of Ethers through the Combination of Photoredox-Mediated C–H Functionalization and the Minisci Reaction. *Angew. Chem., Int. Ed.* **2015,** *54,* 1565-1569.

134. Shields, B. J.; Doyle, A. G. Direct C(sp^3)–H Cross Coupling Enabled by Catalytic Generation of Chlorine Radicals. *J. Am. Chem. Soc.* **2016,** *138,* 12719-12722; (b) Nielsen, M. K.; Shields, B. J.; Liu, J.; Williams, M. J.; Zacuto, M. J.; Doyle, A. G. Mild, Redox-Neutral Formylation of Aryl Chlorides through the Photocatalytic Generation of Chlorine Radicals. *Angew. Chem., Int. Ed.* **2017,** *56,* 7191-7194.

135. Ganley, J. M.; Christensen, M.; Lam, Y.-H.; Peng, Z.; Angeles, A. R.; Yeung, C. S. Metal- and Acid-Free C–H Formylation of Nitrogen Heterocycles: Using Trioxane as an Aldehyde Equivalent Enabled by an Organic-Soluble Oxidant. *Org. Lett.* **2018,** *20,* 5752-5756.

136. Fan, X. -Z.; Rong, J. -W.; Wu, H. -L.; Zhou, Q.; Deng, H. -P.; Tan, J. D.; Xue, C. -W.; Wu, Z. -L.; Tao, H. -R.; Wu, J. Eosin Y as a Direct Hydrogen-Atom Transfer Photocatalyst for the Functionalization of C-H Bonds. *Angew .Chem. Int. Ed.,* **2018,** *57,* 8514-8518.

137. Kuang, Y.; Wang, K.; Shi, X.; Huang, X.; Meggers, E.; Wu, J. Asymmetric Synthesis of 1,4-Dicarbonyl Compounds from Aldehydes by Hydrogen Atom Transfer Photocatalysis and Chiral Lewis Acid Catalysis. *Angew. Chem., Int. Ed.* **2019,** *58,* 16859-16863.

138. Zhu, K.; Ohtani, T.;Tripathi, C. B.; Uraguchi, D.; Ooi, T. Formal Hydroformylation of α,β-Unsaturated Carboxylic Acids under Photoexcited Ketone Catalysis. *Chem. Lett.* **2019,** *48,* 715-717.

139. Ravelli, D.; Albini, A.; Fagnoni, M. Smooth Photocatalytic Preparation of 2-Substituted 1,3-Benzodioxoles. *Chem. Eur. J.* **2011,** *17,* 572-579.

140. Manfrotto, C.; Mella, M.; Freccero, M.; Fagnoni, M.; Albini, A. Photochemical Synthesis of 4-Oxobutanal Acetals and of 2-Hydroxycyclobutanone Ketals. *J. Org. Chem.* **1999,** *64,* 5024-5028.

141. Mosca, R.; Fagnoni, M.; Mella, M.; Albini, A. Synthesis of Monoprotected 1,4-Diketones by Photoinduced Alkylation of Enones with 2-Substituted-1,3-Dioxolanes. *Tetrahedron,* **2001,** *57,* 10319-10328.

142. Dondi, D.; Caprioli, I.; Fagnoni, M.; Mella, M.; Albini, A. A Convenient Route to 1,4-Monoprotected Dialdehydes, 1,4-Ketoaldehydes, γ-Lactols and γ-Lactones through Radical Alkylation of α,β-Unsaturated Aldehydes in Organic and Organic-Aqueous Media. *Tetrahedron* **2003,** *59,* 947-957.

143. Dondi, D.; Protti, S.; Albini, A.; Carpio, S. M.; Fagnoni, M. Synthesis of γ-Lactols, γ-Lactones and 1,4-Monoprotected Succinaldehydes Under Moderately Concentrated Sunlight. *Green Chem.* **2009,** *11,* 1653-1659.

144. (a) Jung, J. C.; Kim, Y. H.; Lee, K. Practical β-Masked Formylation and Acetylation of Electron-Deficient Olefins Utilizing Tetra(n-butyl)ammonium Peroxydisulfate. *Tetrahedron Lett.* **2011,** *52,* 4662-4664; (b). Jung, J.C.; Choi, H. C.; Kim, Y. H. Direct facile tetrahydrofuranylation of alcohols through radical coupling with $(Bu_4N)_2S_2O_8$. *Tetrahedron Lett.* **1993,** *34,* 3581-3584.

145. Capaldo, L.; Merli, D.; Fagnoni, M.; Ravelli, D. Visible Light Uranyl Photocatalysis: Direct C–H to C–C Bond Conversion. *ACS Catal.* **2019,** *9,* 3054-3058.

146. Ou, W.; Zhang, G.; Wu, J.; Su, C. Photocatalytic Cascade Radical Cyclization Approach to Bioactive Indoline-Alkaloids over Donor–Acceptor Type Conjugated Microporous Polymer. *ACS Catal.* **2019,** *9,* 5178-5183.

147. Yang, S.; Zhu, S.; Lu, D.; Gong, Y. Formylation of Fluoroalkyl Imines through Visible-Light-Enabled H-Atom Transfer Catalysis: Access to Fluorinated α-Amino Aldehydes. *Org. Lett.* **2019,** *21,* 2019-2024.

148. Zeng, H.; Yang, S.; Li, H.; Lu, D.; Gong, Y.; Zhu, J. -T. Site-Specific Functionalization of 1,3-Dioxolane with Imines: A Radical Chain Approach to Masked α-Amino Aldehydes. *J. Org. Chem.* **2018,** *83,* 5256-5266.

149. Xu, R.; Xu, T.; Yang, M.; Cao, T.; Liao, S. A Rapid Access to Aliphatic Sulfonyl Fluorides. *Nat. Commun.* **2019,** *10,* 3752-3758.

150. Roberts, J. C. Naturally Occurring Xanthones. *Chem. Rev.* **1961,** *61,* 591-605.

151. Bräse, S.; Encinas, A.; Keck. J.; Nising, C. F. Chemistry and Biology of Mycotoxins and Related Fungal Metabolites. *Chem. Rev.* **2009,** *109,* 3903-3990.

152. Masters, K-S.; Bräse, S. Xanthones from Fungi, Lichens, and Bacteria: The Natural Products and Their Synthesis. *Chem. Rev.* **2012,** *112,* 3717-3776.

153. Wezeman, T.; Bräse, S.; Masters, K-S. Xanthone Dimers: A Compound Family Which is Both Common and Privileged. *Nat. Prod. Rep.* **2015,** *32,* 6-28.

154. Parish, C. A.; Smith, S. K.; Calati, K.; Zink, D; Wilson, K.; Roemer, T.; Jiang, B.; Xu, D.; Bills, G.; Platas, G.; Palaez, F.; Diez, M. T.; Tsou, N.; McKeown, A. E.; Ball, R. G.; Powles. M. A.; Yeung, L.; Liberator, P.; Harris, G. Isolation and Structure Elucidation of Parnafungins, Antifungal Natural Products that Inhibit mRNA Polyadenylation. *J. Am. Chem. Soc.* **2008,** *130,* 7060-7066.

155. (a) Albert, B. J.; Sivaramkrishnan, A.; Naka, T.; Koide, K. Total Synthesis of FR901464, an Antitumor Agent that Regulates the Transcription of Oncogenes and Tumor Suppressor Genes. *J. Am. Chem. Soc.* **2006,** *128,* 2792-2793; (b) Albert, B. J.; Sivaramakrishnan, A.; Naka, T.; Czaicki, N. L.; Koide, K. Total Syntheses, Fragmentation Studies, and Antitumor/Antiproliferative Activities of FR901464 and Its Low Picomolar Analogue. *J. Am. Chem. Soc.* **2007,** *129*, 2648-2659.

156. Zhou, Q.; Snider, B. B. Synthesis of Hexacyclic Parnafungin A and C Models. *J. Org. Chem.* **2010,** *75,* 8224-8233.

157. Zhou, Q.; Snider, B. B. Synthesis of the Isoxazolo[4,3,2-de]phenanthridinone Moiety of the Parnafungins. *Org. Lett.* **2009,** *11,* 2936-2939.

158. Qin, T.; Johnson, R. P.; Porco, J. A., Jr. Vinylogous Addition of Siloxyfurans to Benzopyryliums: A Concise Approach to the Tetrahydroxanthone Natural Products. *J. Am. Chem. Soc.* **2011,** *133,* 1714-1717.

159. Qin, T.; Porco, J. A. Jr. Total Syntheses of Secalonic Acids A and D. *Angew. Chem., Int. Ed.* **2014,** *53,* 3107-3110.

160. Qin, T.; Iwata, T.; Ransom, T. T.; Beutler, J. A.; Porco, J. A., Jr. Syntheses of Dimeric Tetrahydroxanthones with Varied Linkages: Investigation of "Shapeshifting" Properties. *J. Am. Chem. Soc.* **2015,** *137,* 15225-15233.

161.   Wu, X.; Iwata, T.; Scharf, A.; Qin, T.; Reichl, K. D.; Porco, J. A., Jr. Asymmetric Synthesis of Gonytolide A: Strategic Use of an Aryl Halide Blocking Group for Oxidative Coupling. *J. Am. Chem. Soc.* **2018,** *140,* 5969-5975.

162.   Hsung, R. P. First Stereoselective [4 + 2] Cycloaddition Reactions of 3-Cyanochromone Derivatives with Electron-Rich Dienes: An Approach to the ABC Tricyclic Frame of Arisugacin. *J. Org. Chem.* **1997,** *62,* 7904-7905.

163.   Hsung, R. P. Concentration Effect on the Stereoselectivity of [4+2] Cycloaddition Reactions of 3-Cyano-γ-benzopyrone Derivatives with Electron Rich Dienes. *Heterocycles* **1998,** *48,* 421-425.

164.   Danda, A.; Kesava-Reddy, N.; Golz, C.; Strohmann, C.; Kumar, K. Asymmetric Roadmap to Diverse Polycyclic Benzopyrans via Phosphine-Catalyzed Enantioselective [4 + 2]-Annulation Reaction. *Org. Lett.* **2016,** *18,* 2632-2635.

165.   Jung, M. E.; Gervay, J. gem-Dialkyl Effect in the Intramolecular Diels-Alder Reaction of 2-Furfuryl Methyl Fumarates: the Reactive Rotamer Effect, the Enthalpic Basis for Acceleration, and Evidence for a Polar Transition State. *J. Am. Chem. Soc.* **1991,** *113,* 224-232.

166.   Jung, M. E.; Piizzi, G. gem-Disubstituent Effect: Theoretical Basis and Synthetic Applications. *Chem. Rev.* **2005,** *105,* 1735-1766.

167.   Gigant, N.; Bäckvall, J. -E. Synthesis of Conjugated Dienes via a Biomimetic Aerobic Oxidative Coupling of Two C_{vinyl}–H Bonds. *Chem. -Eur. J.* **2013,** *19,* 10799-10803.

168.   Kang, D.; Ahn, K.; Hong, S. Site-Selective C−H Bond Functionalization of Chromones and Coumarins. *Asian J. Org. Chem.* **2018,** *7,* 1136-1150.

169.   Engle, K. M.; Mei, T. -S.; Wasa, M.; Yu, J. -Q. Weak Coordination as a Powerful Means for Developing Broadly Useful C–H Functionalization Reactions. *Acc Chem. Res.* **2012,** *45,* 788-802.

170.   Smith, J. M.; Harwood, S. J.; Baran, P. S. Radical Retrosynthesis. *Acc. Chem. Res.* **2018,** *51,* 1807-1817.

171.   De Vleeschouwer, F.; Van Speybroeck, V.; Waroquier, M.; Geerlings, P.; De Proft, F. Electrophilicity and Nucleophilicity Index for Radicals. *Org. Lett.* **2007,** *9,* 2721-2724.

172.   Miyake, Y.; Nakajima, K.; Nishibayashi, Y. Visible-Light-Mediated Utilization of α-Aminoalkyl Radicals: Addition to Electron-Deficient Alkenes Using Photoredox Catalysts. *J. Am. Chem. Soc.* **2012,** *134,* 3338-3341.

173.   Jones, G. *Organic Reactions*, 2011, pp. 204-599.

174.   Noble, A.; MacMillan, D. W. C. Photoredox α-Vinylation of α-Amino Acids and N-Aryl Amines. *J. Am. Chem. Soc.* **2014,** *136,* 11602-11605.

175.   Dong, J.; Krasnova, L.; Finn, M. G.; Sharpless, K. B. Sulfur(VI) Fluoride Exchange (SuFEx): Another Good Reaction for Click Chemistry. *Angew. Chem., Int. Ed.* **2014,** *53,* 9430-9448.

176.   Barrow, A. S.; Smedley, C. J.; Zheng, Q.; Li, S.; Dong, J.; Moses, J. E. The growing applications of SuFEx click chemistry. *Chem. Soc. Rev.* **2019,** *48,* 4731-4758.

177.   Tedder, J. M. Which Factors Determine the Reactivity and Regioselectivity of Free Radical Substitution and Addition Reactions? *Angew. Chem., Int. Ed. Engl.* **1982,** *21,* 401.

178.   Porter, N. A.; Giese, B.; Curran, D. P. Acyclic Stereochemical Control in Free-Radical Reactions. *Acc. Chem. Res.* **1991,** *24,* 296.

179.   Staveness, D. R.; Bosque, I.; Stephenson, C. R. J. Free Radical Chemistry Enabled by Visible Light-Induced Electron Transfer. *Acc. Chem. Res.* **2016,** *49,* 2295-2306.

180.   Curran, D. P.; Chang, C. T. Atom Transfer Cyclization Reactions of .alpha.-iodo Esters, Ketones, and Malonates: Examples of Selective 5-exo, 6-endo, 6-exo, and 7-endo Ring Closures. *J. Org. Chem.* **1989,** *54,* 3140-3157.

181.   Curran, D. P.; Bosch, E.; Kaplan, J.; Newcomb, M. Rate Constants for Halogen Atom Transfer from Representative .alpha.-halo Carbonyl Compounds to Primary Alkyl Radicals. *J. Org. Chem.* **1989,** *54,* 1826-1831.

182.   Li, Q.; Yin, Y.; Li, Y.; Zhang, J.; Huang, M.; Kim, J. K.; Wu, Y. A Simple Approach to Indeno-coumarins via Visible-Light-Induced Cyclization of Aryl Alkynoates with Diethyl Bromomalonate. *Org Chem. Front.* **2019,** *6,* 3238-3243.

183.   Alpers, D.; Brasholz, M.; Rehbein, J. Photoredox-Induced Radical 6-exo-trig Cyclizations onto the Indole Nucleus: Aromative versus Dearomative Pathways. *Eur. J. Org. Chem.* **2017,** 2186–2193.

184.   Muhmel, S.; Alpers, D.; Hoffmann, F.; Brasholz, M. Iridium(III) Photocatalysis: A Visible-Light-Induced Dearomatizative Tandem [4+2] Cyclization to Furnish Benzindolizidines. *Chem. Eur. J.* **2015**, *21,* 12308–12312.

185.   Teegardin, K.; Day, J. I.; Chan, J.; Weaver, J. Advances in Photocatalysis: A Microreview of Visible Light Mediated Ruthenium and Iridium Catalyzed Organic Transformations. *Org. Process. Res. Dev.* **2016,** *20,* 1156-1163.

186.   For chapter 2, computations were performed using Gaussian 16, version B.01: M. J. Frisch, G. W. Trucks, H. B. Schlegel, G. E. Scuseria, M. A. Robb, J. R. Cheeseman, G. Scalmani, V. Barone, G. A. Petersson, H. Nakatsuji, X. Li, M. Caricato, A. V. Marenich, J. Bloino, B. G. Janesko, R. Gomperts, B. Mennucci, H. P. Hratchian, J. V. Ortiz, A. F. Izmaylov, J. L. Sonnenberg, D. Williams-Young, F. Ding, F. Lipparini, F. Egidi, J. Goings, B. Peng, A. Petrone, T. Henderson, D. Ranasinghe, V. G. Zakrzewski, J. Gao, N. Rega, G. Zheng, W. Liang, M. Hada, M. Ehara, K. Toyota, R. Fukuda, J. Hasegawa, M. Ishida, T. Nakajima, Y. Honda, O. Kitao, H. Nakai, T. Vreven, K. Throssell, J. A. Montgomery, Jr.,

J. E. Peralta, F. Ogliaro, M. J. Bearpark, J. J. Heyd, E. N. Brothers, K. N. Kudin, V. N. Staroverov, T. A. Keith, R. Kobayashi, J. Normand, K. Raghavachari, A. P. Rendell, J. C. Burant, S. S. Iyengar, J. Tomasi, M. Cossi, J. M. Millam, M. Klene, C. Adamo, R. Cammi, J. W. Ochterski, R. L. Martin, K. Morokuma, O. Farkas, J. B. Foresman, and D. J. Fox, Gaussian, Inc., Wallingford CT, 2016.

187. Http://www.intermediates.basf.com/chemicals/web/en/brand/1_3_DIOXOLANE.

188. For a recent example on N–O bond cleavage via energy transfer, see: Patra, T.; Mukherjee, S.; Ma, J.; Strieth-Kalthoff, F.; Glorius, F. Visible-Light-Photosensitized Aryl and Alkyl Decarboxylative Functionalization Reactions. *Angew. Chem. Int. Ed.* **2019,** *58,* 10514-10520.

189. Dervery, J. J., III.; Nguyen, J. D.; Dai, C.; Stephenson, C. R. J. Light-Mediated Reductive Debromination of Unactivated Alkyl and Aryl Bromides. *ACS Catal.* **2016,** *6*, 5962-5967.

190. Rathnayake, M. D.; Weaver, J. D. Alkyl Halides via Visible Light Mediated Dehalogenation. *Org. Lett.* **2019,** *21,* 9681-9687.

191. Montesinos-Magraner, M.; Costantini, M.; Ramirez-Contreras, R.; Muratore, M. E.; Johansson, M. J.; Mendoza, A. *Angew. Chem., Int. Ed.* **2019,** *58,* 5930-5935.

192. Dimitrov, V.; Kostova, K.; Genov, M. Anhydrous Cerium(III) Chloride — Effect of the Drying Process on Activity and Efficiency. *Tetrahedron Lett.* **1996**, *37*, 6787-6790.

193. (a) Raghavan, S.; Samanta, P. K. Stereoselective Synthesis of the Macrolactone Core of (+)-Neopeltolide. *Org. Lett.* **2012,** *14,* 2346-2349; (b) Lee, B. W. K.; Sun, H. G.; Zang, T.; Kim, B. J.; Alfaro, J. F.; Zhou, Z. S. Enzyme-Catalyzed Transfer of a Ketone Group from an S-Adenosylmethionine Analogue: A Tool for the Functional Analysis of Methyltransferases. *J. Am. Chem. Soc.* **2010,** *132,* 3642-3643; (c) Yan, G.; Borah, A. J.; Wang, L.; Pan, Z.; Chen, S.; Shen, X.; Wu, X. α-Arylchalcogenation of Acetone with Diaryl Dichalcogenide via Metal-Free Oxidative C(sp3)–H Bond Functionalization. *Tetrahedron Lett.* **2015,** *56,* 4305-4307.

194. (a) Gaoni, Y.; Tomažič, A.; Potgieter, E. Stereochemistry of Addition of Organocopper Reagents and of the Hydride Ion to 1-(Arylsulfonyl)bicyclo[1.1.0]butanes. *J. Org. Chem.* **1985,** *50,* 2943-2947; (b) Holmbo, S. D.; Pronin, S. V. A Concise Approach to Anthraquinone–Xanthone Heterodimers. *J. Am. Chem. Soc.* **2018,** *140,* 5065-5068.